



COALTECH

Task 6.1.6

**LARGE SCALE STABILITY AND
NEUTRALISATION CAPACITY OF
POTENTIAL MINE BACKFILL MATERIAL
FORMED BY NEUTRALISATION OF FLY ASH
AND ACID MINE DRAINAGE**

by

Leslie F Petrik

1 February 2007

© Copyright COALTECH 2020

This document is for the use of COALTECH 2020 only, and may not be transmitted to any other party, in whole or in part, in any form without the written permission of COALTECH.

TASK TEAM:

**Leslie Felicia Petrik,
Viswanath Ravi Kumar Vadapalli,
Wilson Gitari,
Olivier Etchebers,
Kelly Reynolds,
Damini Surender,
Veruscha Fester,
Paul Slatter and
Gervais Sery**

LARGE SCALE STABILITY AND NEUTRALISATION CAPACITY OF POTENTIAL MINE BACKFILL MATERIAL FORMED BY NEUTRALISATION OF FLY ASH AND ACID MINE DRAINAGE

Executive Summary

The study focus was on an assessment of the feasibility for large scale treatment of AMD from coal mines and recovery of water including:

- Preliminary planning and consultation for large scale studies including, neutralisation, ash walling, ash lining, water recovery and mineralogical studies. Subtasks of this aspect were:
 - Determination of logistical parameters for application of fly ash as ameliorant for treatment of acid mine drainage
 - Engineering study of the requirements for large scale neutralisation process utilizing fly ash as treatment for acid mine drainage
 - Techno economic study of utilisation of fly ash for treatment of acid mine drainage as replacement for current limestone treatment options
- An evaluation of historical ash placement studies, to gain access and determine the mineralogical and other environmental impacts and changes associated with historical placements of ash previously used as fill materials
- A determination of the overall suitability of solid residues for extending the life of coal mines and increasing the amount of extractable coal from each mine
- The potential for control of surface AMD by employment of FA as ash walls within coal mine spoil heaps to establish performance as an in-situ barrier for passive treatment of AMD flows

Introduction

Utilisation of fly ash (FA) as ameliorant for the neutralisation of acid mine drainage (AMD) has proved to be feasible and was reported to the Water Research Commission by UWC in 2003 (WRC Final report K5/1242). The free alkalinity imparted by CaO and other ash components and the fact that FA has a very high surface area and small particle size make South African FA a good neutralisation agent and AMD ameliorant. High sulphate, major and trace element removal rates were also achieved. The two waste products (i.e. AMD and FA), usually formed in close proximity to each other, were reacted together and produced much cleaner effluent waters, comparable with lime and limestone treated AMD effluent, and suitable for discharge as mentioned in the WRC Final report K5/1242.

Moreover, pH neutral, insoluble solid residues obtained as a result of reaction between AMD and FA were successfully demonstrated as a suitable backfill material (WRC Final Report K5/1458, 2005). This previous study (2003-2005) that was funded by both the WRC, Coaltech2020 and co-funded by ESKOM covered the determination of process parameters and the extent of removal of toxic heavy metals from acid mine drainage as well as long term stability of bulk solid residues. In particular, the focus was on

comparing the stability, leaching characteristics and performance of backfill materials useful for underground placement that were prepared from fly ash residues or ash with various additives. The physical and chemical properties that were ascertained included characteristics such as hardness, strength as well as the chemistry, and long term phase transition kinetics of solid fill materials that may in future be in contact with acid mine drainage or waters of seepage.

By further processing the solid residues, high capacity zeolites were produced (WRC Final Report K5/1546). The zeolites were produced by fusing the solid residues with NaOH either at high (600°C) or low (100°C) temperatures. After the synthesis pure phases of Zeolite Y, Zeolite A and Zeolite P were identified by XRD. Zeolites are high value, micro porous, open structure crystalline aluminosilicates with a void volume of nearly 50%. The zeolites that were obtained from the solid residues were successfully used to treat post-neutralization waters, which complements the primary neutralization treatment. The zeolites have shown high adsorption capacity and have removed significant amounts of Hg, Se, B, As, Fe, Mn, and Ni from the post-neutralization waters.

This report covers research in 2006 that extended the scope of WRC K5/1458 and Coaltech2020 Task 6.1.6, and aimed to verify the protocols necessary for the industrial application of the treatment of AMD with FA. The study investigated the feasibility of industrial application, the parameters for large scale neutralization and utilisation of both FA and the solid residues remaining after neutralisation as mine backfill. Furthermore various aspects of the protocols necessary for large scale implementation such as slurry pumping were explored. Environmental impact assessment is imperative prior to licensing and implementation of this very promising, low cost neutralisation process.

Coaltech2020's decision to withdraw funding because of THRIP difficulties for this study during the latter part of 2006 had an impact on some of the deliverables. Historical ash placement studies could not be completed because of difficulty in accessing the sites and the slurry pumping tests are incomplete. Some of deliverables relating to the large scale neutralization were also hindered by the delay in decision making by Anglo to fund the pilot scale plant at Navigation.

An overview of the progress made in 2006 is presented in the next section.

Large Scale Neutralization of AMD with FA

This follow on project (WRC 662) for the large scale utilisation of fly ash (FA) as ameliorant for the neutralisation of acid mine drainage was initiated by negotiations to collaborate with Anglocoal as an industrial partner. Initial discussions indicated that Anglo would be interested in the large scale process and would consider building a continuous FA Pilot Scale plant at Navigational Mine to treat AMD. On the basis of this understanding, three comparison studies were accordingly carried out that involved a cost comparison between the current limestone treatment at Navigation and the FA treatment. These studies were carried out using limestone that is used at Navigation mine to treat AMD and comparing its efficacy with different types of FA derived from different power stations. The AMD/waste waters that were used for the study were from Navigation Mine and Schoongezicht AMD. On their request, UWC submitted a detailed project proposal

to Anglo for approval of the pilot scale plant that included results obtained from the three case studies. Despite many efforts to collaborate with Anglo, it took about 18 months for Anglocoal to come to a decision, which hindered the progress of some of the deliverables as these were linked with the pilot scale plant either directly or indirectly. Finally a negative answer was received from them. Thereafter, a further partner search was made and bhpbilliton was identified. After various negotiations and the submission of a proposal bhpbilliton has shown interest to build a pilot scale plant at Middleberg mine. Negotiations with bhpbilliton are ongoing and confirmation of the project is expected. The plant will hopefully be up and running by March'2007. We anticipate finishing off the outstanding deliverables of this part of the study in future by making use of the facilities at Middleberg mine should Coaltech review their decision based on THRIP funding in 2007.

As a part of assessing the feasibility of large scale neutralization, meetings were held with people from academic and industrial or institutional backgrounds. These meetings were held with different objectives in mind. A detailed explanation of all the meetings that were held is given under the chapter "Feasibility for large scale treatment of AMD from coal mines". Some of the people with whom we had meetings were: J. Maree (CSIR), Dr. P.Gunther and F.Nkosi (Anglo), Dr.H.Ilgner (CSIR), Prof.P.Slatter, Dr.R. Haldenwang, V.Fester and Gervais Sery (CPUT) and Jacob Clifford (Steel Utilities).

An engineering study was performed to understand the technical requirements for the large scale plant with the help of Steel Utilities (Jacob Clifford), an engineering company located in Pretoria. Designs were drawn and quotations were obtained for building a pilot scale plant that uses FA to treat AMD. The quotes obtained included the costs of building a pilot scale plant either of 1 cubic meter, 5 cubic meter or 250 cubic meter (to treat 1, 5 and 250 cubic meters of water/hour). It was estimated that a cost of R908 500, R1 326 641 and R4 238 220 will respectively be incurred to build 1 cubic metre, 5 cubic metre or 250 cubic metre pilot scale treatment plants. The proposed design and breakdown of costs are discussed in detail in the report.

A techno economic study was carried out using limestone and different type of FA derived from different power stations to compare the costs incurred to neutralize AMD using either limestone or FA. This techno economic study was carried out in three phases. In the first phase, the theoretical value of Fly Ash or Limestone neutralization was used to obtain a preliminary cost estimate. This was done with the help of CSIR. In the second phase, instead of using theoretical values, experimentally calculated values such as alkalinity and acidity of Fly Ash and Limestone were used to reach a more meaningful cost estimate. These experiments were carried out using different Fly Ash types and Navigation AMD. The phase three experiments were similar to phase two but with the difference that less contaminated Schoongezicht waters were used instead of Navigation AMD. The cost estimate took several factors into account, namely: Neutralization Capacity (% CaCO_3); Material Usage; Recovered Water; and Residual Sludge etc. Based on the current investigations, the FA treatment is competitive with the lime stone treatment. Moreover, there are a number of advantages that are gained from FA neutralization of AMD. For example, unlike lime stone treatment, the treatment with FA involves neither addition of flocculants and other additives, nor a costly biological sulphate reduction step as a secondary treatment step. The residual solids that are

obtained can be used as a suitable backfill material. Furthermore, these solids can be transformed via hydrothermal synthesis to obtain high quality zeolites, which can be used to treat either raw AMD or process waters. This compliments the primary treatment. Moreover, if one can negotiate on the transportation cost to transport FA to the treatment site then FA treatment would be considerably cheaper than the limestone treatment in terms of cost effectiveness and is more efficient.

Historical Ash Placement Studies

Access to the historical underground ash placement sites was not granted thus the deliverables envisaged in this task could not be accomplished despite much interaction with different people from governmental and the non-governmental sector. Many efforts were made to access existing sites but in vain except for one site visit to the ash placement sites at “Ermelo” with Willie Kruger in June 2006. In this case, quite a number of people were contacted to find out whether they knew anything about the ash placement in that area. There were no remaining signs of ash placement in that area since it was done many years ago. A consolidated sample was collected at the site indicated by Willie Kruger and sent for chemical analysis but results indicated that it was not an ash sample. Eskom has indicated that it may be possible to sample old ash dumps at Vaal and Kragbron in the Meyerton district. No further efforts were made to access these sites after UWC was informed by Coaltech2020 that the project had come to an end in September 2006.

Solid Residues for extending life of Coal Mines

The suitability of Solid Residues (SR), recovered after the neutralization of AMD with FA was evaluated for backfill and extending the life of coal mines. This was ascertained by investigating their long term physical and chemical behaviour. Moreover, the rheological behaviour of ash and solid residues was investigated to understand the slurry pumping requirements for any future transport or backfill operations.

Columns experiments were carried out to understand the long term chemical behaviour of solid residues if placed as backfill and exposed to AMD in the mining environment. SR were obtained by reacting Navigation AMD and Arnot FA in 3:1 ratio. Columns containing FA by itself, SR by itself, SR+5% of FA, SR+25% of FA, SR+40% of FA and SR+6% of OPC were leached using synthetic AMD. Leachates were analyzed for pH, EC and Eh, major elements, cations and anions and the results were compared. Modelling studies were carried out to understand the mineral phases that control the chemistry of the solutions at a particular pH.

Initial and progressive neutralization of SAMD was achieved with all blends and removal of sulphate and most elements from the SAMD was excellent during a significant period of the time of exposure applied. The SR alone and SR blended with fly ash appeared to have a significant buffering capacity, maintaining neutral to alkaline pH for an extended period of time (97-110 days) with high sulphate, Al and Fe removal rates as opposed to OPC blended SR which acidified relatively rapidly. The SR was found to have a higher capacity than other columns for removal of Al. Overall the FA, SR + 25 % FA, SR + 6 %

OPC columns were found to have a somewhat higher capacity than unblended SR column to remove SO_4 , Fe and Mn from SAMD over an extended period.

The results indicated that the column solid cores acidified in a stepwise fashion over the time period investigated under a repetitive flow of highly concentrated SAMD, and exhibited three buffer zones. As the exposure of the solid residue to acidic flows progressed there was a steady but small increase of most of the major elements (Mn, Al, Fe, Mg) and SO_4^- in unreacted fly ash and solid residues blended with fly ash once the pH of the leachate decreased to the acidic buffer region. A phenomenon was observed where slight increases in concentrations for some elements were observed that do not correspond to a decrease in pH and this was attributed to probable re-solubilization of previously formed precipitates. This phenomenon was observed by other researchers using limestone and red mud to remove inorganic contaminants from synthetic solutions simulating acid mine drainage.

If placed in a mining area generating AMD, these solid residues or blends thereof could provide a passive method of treatment of polluted water with the neutralization of AMD taking place in situ over an extended period of time.

The strength testing of SR was carried out on the solids obtained from the neutralization reactions that were carried out using different AMD to FA ratios. AMD from Navigation mine and FA from Arnot power station were reacted in 1:3, 1:4 and 1:6 ratios (FA: AMD) and at circumneutral pH, and solids were recovered from the reactions. These solids were tested for strength development over a period of 410 days at CSIR, Johannesburg. Strength development tests were performed with and without additional binder (cement). Strength development was investigated for 14, 28, 90, 180 and 410 days. The solids to which no cement was added showed no strength development for the first 28 days (for both unconfined compressive strength and elastic modulus). Thereafter these materials slowly started gaining strength after 28 days, and after 410 days the SR recovered from the 1: 3 ratio gained an unconfined strength of 0.201Mpa and Elastic modulus of 70.1 Mpa. These values are quite good and show that SR itself can be used as a backfill material. On the other hand SR with binder started gaining strength from day 14. After 14 days, the SR recovered from the 1:3 ratio with additional binder gained a strength that was more or less equal to the strength gained by the SR (without adding binder) after 410 days. After 14 days, only solids recovered from the 1: 4 ratio were tested further. After 410 days SR with binder gained an unconfined compressive strength of 0.301 Mpa and Elastic Modulus of 149.6 Mpa, which is considerably higher than in the case without adding the binder. The results indicated that solid residues will develop considerable strength over time with or without adding the binder which makes them suitable for backfilling of mines.

The importance of amorphous precipitates in the attenuation of contaminants was demonstrated in the high concentrations retained in the amorphous fraction of solid cores in the sequential extractions performed. Gypsum precipitation was also observed to be a significant SO_4 retention pathway as also evidenced by the high concentrations of Ca observed in the water soluble fraction and also in the amorphous fraction. High retention of contaminants Fe, Mn, Al, Ca and Si was observed in the amorphous fraction in the SR + 6 % OPC solid core which renders credence to the fact that formation of amorphous

calcium silicate hydrate, calcium ferrite hydrate and possibly calcium aluminate hydrate gels were contributing to the increased contaminants retention in this solid core.

The rheological study performed in collaboration with the Flow Processing Unit at CPUT concentrated on two aspects. The first dealt with the rheological behaviour of the SR obtained after neutralization of AMD using different ratios of FA and AMD. The second investigated the influence of FA- Particle Size Distribution (PSD) on the rheological behaviour. All the solids recovered from different FA: AMD reactions showed a typical shear thinning behaviour, with a decrease in viscosity upon an increase in shear rate. The residual solids that were recovered from the reactions were tested for their flow behaviour. It was observed that the higher the solids to liquid ratio the greater the viscosity for all the solids recovered from reactions. The data that was obtained using a rheometer should be validated by means of evaluating the viscosity of solid residues in pipe tests. Unfortunately due to unforeseen problems the larger scale experiments at Eskom were postponed and the project was terminated before these validation tests could be performed. It is hoped that these experiments will be carried out in March 2007 at Middleberg mine.

Particle Size Distribution (PSD) of FA varies from time to time depending on the coal burning conditions in the power station. Such variability in PSD of FA could influence its capability to neutralize AMD as well as the flow behaviour of residual solids that have to be transported to the backfilling site by means of pipes. A set of experiments were performed to study the influence of variability of PSD on the above mentioned properties.

The FA from Arnot power station in South Africa was used for this study. The % of fine and coarse particles (in the context of this study) could influence the neutralization capacity of FA and also influence the rheological behaviour of residual solids. Therefore the original FA was compared to samples that were prepared by fine or coarse particle addition to contain double the amount (%) with respect to either the <25 µm or the 75-150µm fractions. Thus the AMD from Landau mine was reacted with un-altered FA and two altered FA that were doubled with respect to either their fine or coarse fractions.

It was found that pH and EC trends differed significantly for each size fraction. The time that was taken to achieve a neutral pH, as well as major and trace element removal efficiencies of each reaction was compared. It was observed that the reaction was more rapid (to achieve neutral pH) for the sample containing a higher % of fines with better removal rates. The rheological behaviour of residual solids obtained from the reactions using un-altered and altered FA was compared and it was found that the sample enriched with fines showed the highest slurry viscosity. Thus particle size has an influence on the neutralization capacity of FA and the rheological behaviour of residual solids.

Ash walling studies

Passive treatment of AMD through contact with FA from power stations is possible and was evaluated in columns studies to simulate ashwalling or ashlining applied in order to create reactive barriers. Columns of different length were prepared and packed using FA from Kendal, Matla and Duhva. AMD from Middleburg, Landau and Navigation mines was continuously percolated through these columns respectively. These column studies

were performed to simulate conditions in which FA is in contact with AMD over long periods (280 days). The aim was to model the placement of ash in acidic environments, to establish suitable monitoring criteria, to understand the mineralogical characteristics and to verify the chemical interactions taking place in ash in contact with AMD over the longer term. These columns showed good neutralizing and amelioration capacity over an extended period of time.

The analysis of the leachates that were collected at the bottom of the columns was presented in final WRC report (WRC K5/1458 and Coaltech2020 Task 6.1.6: Petrik et al., 2005). The XRD and XRF analyses of all the FA columns were also presented in the previous final WRC report. This report includes the FTIR, Raman and SEM-EDS analyses of Matla FA columns.

After the percolation of AMD, samples were collected from each section of the columns and analyzed. These FA samples were investigated for any mineralogical changes that occurred due to the contact with AMD for longer periods of time. According to FTIR, distinct changes in the chemistry were observed, when compared with the unreacted FA. The asymmetric stretching of Si-O-Si and Al-O-Si at 1096 cm^{-1} shifted to higher wave numbers, by 56 cm^{-1} and can be attributed to the structural reorganisation of aluminosilicate glassy phases. Two new peaks appeared at 660 cm^{-1} and 600 cm^{-1} that can be attributed to the depolymerisation of the original aluminosilicate phase, indicating dissolution of this phase. The vibrations of Al-O-Si and Si-O-Si at 560 cm^{-1} and 460 cm^{-1} became weaker. The Raman analysis of the samples collected suggested changes in the ash chemistry when compared to the unreacted FA. The precipitation of calcite, Na_2SO_4 and depolymerisation of the original graphitic structure of the remaining carbon was observed. The precipitation of Na_2SO_4 was not observed in any of the layers of the short 0.25m column. By comparing the EDS and SEM results of the three layers it is evident that the degree of metal precipitation and subsequent adsorption on the surface of FA particles was higher at the first contact point between FA and AMD, at the top layer, and became lower by the time the water had percolated through the column to reach the bottom layer.

These results indicate that FA has a considerable capacity to treat and ameliorate contaminants in AMD and that contaminants are precipitated as mineral phases in the ash. Thus because of the physical and chemical durability of solid residues as a backfill material, backfilling with solid residues is feasible with or without adding binders. The ash walling treatment also seems to be very promising and ash can be effectively used as passive barrier to treat AMD.

Recommendations

Because of the potential commercial opportunities presented by exploiting the use of fly ash and its derivatives/by-products in remediation or applying fly ash in active or passive acid mine drainage treatment systems, it is recommended that Coaltech2020 consider continuing the funding of this project. The funding discontinuation in 2006 was not in any way related to the project's performance or objectives, which remain viable and valid and of significant interest to the mining and power generation industries. This funding decision was taken because of the regulations imposed by THRIP for the participation of

SMME and BEE in all the Coaltech2020 projects, which meant that the THRIP funding expected in 2006 was not realized.

It is recommended for column or in-situ studies to be carried out over the longer term probably for one year or longer to ascertain the final break-up of the alkalinity of these solid cores and also confirm to what extent the re-dissolution of the previously formed precipitates will occur.

Another recommendation would be to assess whether the SR can be used as passive treatment barriers, this would require probably the drainage of the SR with AMD under a dynamic flow regime to quantify the amount of coal mines waste water that can be treated over a given period of time.

Currently both ESKOM and bhpbilliton are seriously considering investing in the full scale implementation of active and passive neutralization systems using fly ash. Coaltech2020's continued participation in the project would ensure that the investment made by Coaltech2020 and WRC to date in this research accrues to the benefit of all contributors.

Acknowledgements

Funder project mentors

WRC Project leader: Meiring du Plessis

Coaltech 2020 Project leader: Johann Beukes

ESKOM Project mentors: Gerhard Gericke, Siven Naidoo

Research leader: L. Petrik, Dept Chemistry, UWC

Project mentors: R. Meyer, H. Ilgner J. Maree (CSIR); R. Kruger (Ash Resources); G. Gericke (Eskom)

Team Members: V.R. Kumar Vadapalli, O. Etchebers, A.Ellendt, D. Key, E. Iwuoha, C. Okujeni, and D. Cowan (UWC).

Students: W.Gitari (PhD), K.Reynolds (PhD), D.Surender (MSc), M.Ndaba, M.Antonie

Table of Contents	Page No
<u>1 February 2007.....</u>	<u>i</u>
<u>Executive Summary.....</u>	<u>A</u>
<u>Acknowledgements.....</u>	<u>I</u>
<u>List of Figures.....</u>	<u>5</u>
<u>List of Tables.....</u>	<u>10</u>
<u>2 Background.....</u>	<u>12</u>
<u>2 Aims.....</u>	<u>14</u>
<u>3 Deliverables.....</u>	<u>14</u>
2.1 Deviations from the Schedule	14
<u>3 Large Scale Remediation of Acid Mine Drainage with Fly Ash.....</u>	<u>15</u>
3.1 Introduction	15
3.2 Background	15
3.3 Preliminary planning and consultation and determination of logistical Parameters for large scale studies	17
3.4 Engineering study of the requirements for large scale neutralisation process	17
3.4.1 Objectives	17
3.4.2 Installation of Plant	18
3.4.3 Process Description	18
3.5 Techno economic study of utilisation of fly ash for treatment of acid mine drainage	19
3.5.1 Neutralizing Potential and Cost Analysis (Phase-I)	20
3.5.1.1 Materials and Methods	20
3.5.1.2 Results	20
3.5.1.3 Cost analysis	21
3.5.2 Neutralizing Potential and Cost Analysis (Phase-II)	22
3.5.2.1 Materials and Methods	22
3.5.2.2 Results	23
3.5.2.3 Cost Analysis	24
3.5.3 Neutralizing Potential and Cost Analysis (Phase-III)	25
3.5.3.1 Materials and Methods	25
3.5.3.2 Results and Cost Analysis	26
<u>4 Historical Ash Placement Studies.....</u>	<u>28</u>
<u>5 Suitability of Solid Residues for Extending the Life of Coal Mines.....</u>	<u>29</u>
5.1 Introduction	29
5.2 Chemical Suitability of solid residues as a backfill material	29
5.2.1 Materials and Methods	30
5.2.1.1 Sample collection, preparation of SR and column assembly set-up	30
5.2.1.2 Simulated acid mine drainage preparation and drainage	31
5.2.1.3 Analysis of the leached solid residue cores	34
5.2.1.4 Sequential Chemical Extractions	34
5.2.1.5 Geochemical Modelling	35
5.2.2 Results and Discussion	35
5.2.2.1 Composition of Fly Ash, Solid residues (SR) and Ordinary Portland Cement (OPC)	36
5.2.2.2 Evolution of pH in the leachate	37
5.2.2.1 Acidity Attenuation by the Column Cores	38

5.2.2.1.1 Fly ash and solid residue (SR), solid residue (SR) + FA column cores.....	38
5.2.2.1.2 Solid residues (SR) + 6 % Ordinary Portland Cement (OPC) column cores.....	54
5.2.2.1.3 Conclusions.....	58
5.2.2.2 Contaminants Attenuation by Fly Ash (FA), Solid Residues (SR), Solid Residues (SR) + 25 % FA and Solid Residues (SR) + 6 % Ordinary Portland Cement (OPC) column blends	58
5.2.2.2.1 Attenuation in Fly ash column cores.....	59
a. Sulphate and calcium.....	60
b. Total iron, manganese and aluminium	60
60	
5.2.2.2.2 Solid residue (SR) column cores.....	61
a. Sulphate and calcium.....	61
b. Total iron, manganese and aluminium.....	63
5.2.2.2.3 Solid residues (SR) + 25 % FA.....	63
a. Sulphate and calcium.....	63
b. Total iron, manganese and aluminium.....	65
5.2.2.2.4 Solid residues (SR) + 6 % Ordinary Portland Cement (OPC).....	66
a. Sulphate and calcium.....	67
b. Total iron, manganese and aluminium.....	67
5.2.2.3 Decontamination efficiency of each column solid core	68
5.2.2.4 Contaminants attenuation mechanisms and solubility controls	69
69	
5.2.2.4.1 Sulphate and calcium.....	70
5.2.2.4.2 Sulphate, Aluminium and Iron.....	77
5.2.2.4.3 Fe (oxy) hydroxides and Al (oxy) hydroxides.....	78
5.2.2.4.4 Manganese.....	89
5.2.2.5 X-ray diffraction (XRD), Fourier Transform infra-red (FTIR), Scanning electron microscopy(SEM) and Scanning Electron microscopy-Energy dispersive X-ray spectroscopy (SEM-EDX) analysis of the leached column solid cores	91
5.2.2.5.1 Visualization of the sectioned leached solid cores.....	92
5.2.2.5.2 X-ray diffraction (XRD) analysis of the leached solid cores.....	92
5.2.2.5.3 Fourier Transform infra-red analysis (FTIR) of the leached solid residue cores	94
5.2.2.5.4 Scanning electron microscopy (SEM) and Scanning Electron microscopy-Energy dispersive X-ray spectroscopy (SEM-EDX) analysis of the leached column solid cores.....	98
5.2.3 pH profile of the column residue cores	104
5.2.4 Sequential chemical extraction (SSE) of the leached solid residue (SR) cores	106
5.2.4.1 Water soluble fraction	106
5.2.4.1.1 Fly Ash (FA) leached solid core.....	107
5.2.4.1.2 Solid residue (SR) leached solid core.....	112
5.2.4.1.3 Solid residue + 6 % Ordinary Portland Cement (SR + 6 % OPC) leached solid core.....	112

5.2.4.2 Amorphous fraction	112
5.2.4.2.1 Fly Ash (FA) leached solid core.....	112
5.2.4.2.2 Solid residue (SR) leached solid core.....	113
5.2.4.2.3 Solid residue + 6 % Ordinary Portland Cement (SR + 6 % OPC) leached solid core.....	113
5.2.4.3 Reducible Fraction	114
5.2.4.3.1 Fly ash (FA) leached solid core.....	114
5.2.4.3.2 Solid residue (SR) leached solid core.....	115
5.2.5 Conclusions	115
5.3 Strength Testing of Solid Residues	116
5.3.1 Materials and methods	117
5.3.1.1 FA and AMD	117
5.3.1.2 Preparation of SR from the neutralisation of AMD with FA	117
5.3.1.3 Determination of moisture content	119
5.3.1.4 Determination of specific gravity	119
5.3.1.5 Flow test using marsh cone	119
5.3.1.6 Materials supplied to CSIR for strength testing	120
5.3.1.7 Preparation of the cylinders and curing for strength tests	120
5.3.2 Results	121
5.3.2.1 Moisture content	121
5.3.2.2 Specific gravity	121
5.3.2.4 Flow test using marsh cone	122
5.3.2.5 Stability of SR without binder	124
5.3.2.6 Stability of SR with cement binder	126
5.4 Hydraulic transport of SR precipitated from AMD treatment	128
5.4.1 Rheological behaviour of SR obtained from different FA and AMD reactions	128
5.4.1.1 Introduction	128
5.4.1.2 Literature	128
5.4.1.2.1 Rheological Modelling.....	129
5.4.1.2.2 Correlation of rheological parameters with concentration.....	130
5.4.1.2.3 Pipe Flow Models.....	131
5.4.1.3 Objectives	132
5.4.1.4 Measuring apparatus and procedure	132
5.4.1.5 Results	133
5.4.1.5.1 Rheological Investigation.....	133
5.4.1.5.2 Application of rheology to pumping conditions.....	138
5.4.1.6 Discussion and recommendations	142
5.4.2 Influence of FA-Particle Size Distribution (PSD) on the rheological behaviour of SR	142
5.4.2.1 Introduction	142
142	
5.4.2.2 Literature	142
5.4.2.2.1 Particle concentration.....	142
5.4.2.2.2 Dilute Suspensions.....	143
5.4.2.2.3 Medium suspension.....	144
5.4.2.2.4 High concentrations.....	144
5.4.2.3 Objectives	146

5.4.2.4 Sample Preparation	147
5.4.2.4.1 Measuring Apparatus and Procedure	148
5.4.2.5 Results	149
5.4.2.5.1 Rheological Investigation	149
5.4.2.5.2 Effect of concentration	150
5.4.2.5.3 Pumping Predictions	154
5.4.2.5.4 Deposition Behaviour	155
5.4.2.6 Discussion	155
5.4.2.7 Conclusions	156
6 Ash walling studies to control surface AMD	157
6.1 Introduction	157
6.2 Materials and Methods	158
6.2.1 Fourier Transformed Infra Red Spectroscopy	159
6.2.2 Raman Spectroscopy	159
6.2.3 Scanning Electron Microscopy (SEM) and Energy Dispersive X-Ray Spectroscopy (EDS)	160
6.3 Results and Discussions	160
6.3.1 FTIR Analysis	160
6.3.1.1 Conclusions	163
6.3.2 Raman Analysis	164
6.3.2.1 Conclusions	167
6.3.3 Characterisation of FA columns leached with AMD using scanning electron microscopy coupled with energy dispersive X-ray spectroscopy	167
6.3.4 Conclusions from the fly ash column studies	172
7 General Conclusions	174
8 References	176
Appendix A. Revised WRC deliverables compared to Coaltech2020 and original WRC deliverables	clxxxviii
Appendix B. Academic and Industrial Interactions	cxix
Appendix C. Budget capital project cost estimate	cxvii
Appendix D1. Cost analysis of lime, Limestone and Fly Ash treatments (Phase I)	cci
Appendix D2. Utilisation of Fly Ash to Neutralize and Remediate Acid Mine Drainage at Navigation	ccii
Appendix E. Column leachate concentration for elements	ccviii
Appendix F. Influence of Particle Size Distribution (PSD) of FA on the Neutralization Reaction Kinetics	ccxxx
Appendix G. IR vibration modes of Matla fly ash and various layers of Matla fly ash columns	ccxxxv
Appendix H. Capacity Development and Technology Transfer	ccxxxvi

List of Figures

Figure 4.1: Schematic of the proposed large scale treatment plant.....	19
Figure 4.2: pH and EC during the neutralisation of Schoongezicht AMD with limestone.....	26
Figure 4.3: pH and EC during the neutralisation of Schoongezicht AMD with Kriel FA.....	26
Figure 6.4: The 150 litre capacity agitator used to generate the SR used for the drainage experiments.....	30
Figure 6.5: Column assembly used for the leaching experiments.....	31
Figure 6.6(a-c): Evolution of pH in the leachate with cumulative volume for the FA, SR (SR), SR + 5 % FA, SR + 25 % FA, SR + 40 % FA and SR + 6 % OPC.	37
Figure 6.7: SEM-backscattered micrograph of gypsum crystals in FA column cores with the EDX pattern superimposed.....	39
Figure 6.8: SEM-backscattered micrograph of gypsum crystals in solid residue (SR) column cores with the EDX pattern superimposed.....	40
Figure 6.9: Plot of pH versus $2\text{Log } \alpha\text{Al}^{3+} + \text{Log } \alpha\text{H}_4\text{SiO}_4$ over the pH range 6.5-9.0 for solid residue (SR) core leachates (SR column core).....	42
Figure 6.10: Plot of pH versus $2 \text{Log } \alpha\text{Al}^{3+} + \text{Log } \alpha\text{H}_4\text{SiO}_4$ over the pH range 6.5-9.0 for solid residue (SR) + 25 % FA core leachates (column 5).....	42
Figure 6.11: Sillimanite solubility equilibria for solid residue (SR) core leachates	43
Figure 6.12: Mullite solubility equilibria for solid residue (SR) core leachate.....	44
Figure 6.13: Sillimanite solubility equilibria for solid residue (SR) + 25 % FA core leachates.....	44
Figure 6.14: Mullite solubility equilibria for solid residue (SR) + 25 % FA core leachates.....	45
Figure 6.15: Sillimanite solubility equilibria for FA column core leachates.....	45
Figure 6.16: Mullite solubility equilibria for FA column core leachates.....	46

Figure 6.17: Amorphous silica solubility equilibria for solid residue (SR) column core leachates.	47
Figure 6.18: Amorphous silica solubility equilibria for solid residue (SR) + 25 % FA column core leachates.....	48
Figure 6.19: Amorphous silica solubility equilibria for FA column core leachates.	48
Figure 6.20: XRD spectra of the FA column solid cores showing the change in the mullite: quartz peak ratio from top to bottom.....	49
Figure 6.21: XRD spectra of the solid residue cores showing the change in the mullite: quartz peak ratio from top to bottom of core.....	50
Figure 6.22: XRD spectra of the solid residue (SR) + 40 % FA cores showing the change in the mullite: quartz peak ratio from top to bottom.....	50
Figure 6.23: Equilibrium pH for precipitating basic aluminium hydroxy sulphates for the SR solid cores compared to measured pH of leachate	53
Figure 6.24: Equilibrium pH for precipitating basic aluminium hydroxy sulphates for the FA solid cores compared to measured pH of leachate	53
Figure 6.25: Equilibrium pH for the dissolution of jarosite-K for the SR and FA solid cores compared to measured pH of leachate.....	54
Figure 6.26: SEM micrograph showing ettringite crystals embedded in CSH gel matrix, the EDX pattern is superimposed showing the Ca/Al ratio which approximates that of ettringite.	55
Figure 6.27: Saturation indices for ettringite with pH change as the drainage progressed for the SR + 6 % OPC solid cores.....	55
Figure 6.28: SEM micrograph showing the C-S-H gel that embedded the ettringite crystals, the EDS pattern superimposed showing Ca/Si ratio which approximates that of C-S-H gel (Taylor, 1997).....	56
Figure 6.29: SEM micrograph showing extensive aggregation of the solid residue particles in the SR + 6 % OPC column cores.....	57
Figure 6.30: SEM micrograph showing encapsulation of the solid residue particles in the SR + 6 % OPC column cores by a Si-rich gel.	57
Figure 6.31: Equilibrium pH for the precipitation of jurbanite in SR + 6 % OPC solid cores compared to measured pH of leachate	58
Figure 6.32: Fe, Mn and Al concentration in leachates versus cumulative volume (L/kg) of SAMD for FA solid cores.	59
Figure 6.33: Ca and SO ₄ ²⁻ concentration in leachates versus cumulative volume (L/kg) of SAMD for FA solid cores.	60
Figure 6.34: Fe, Mn and Al concentration in leachates versus cumulative volume (L/kg) of SAMD for SR solid cores.	62
Figure 6.35: Ca and SO ₄ ²⁻ concentration in leachates versus cumulative volume (L/kg) of SAMD for SR solid cores.	62
Figure 6.36: Fe, Mn and Al concentration in leachates versus cumulative volume (L/kg) of SAMD for SR + 25 % FA solid cores.	64
Figure 6.37: Ca and SO ₄ ²⁻ concentration in leachates versus cumulative volume (L/kg) of SAMD for SR + 25 % FA solid cores.....	64
Figure 6.38: Fe, Mn and Al concentration in leachates versus cumulative volume (L/kg) of SAMD for SR + 6 % OPC solid cores.	66
Figure 6.39: Ca and SO ₄ ²⁻ concentration in leachates versus cumulative volume (L/kg) of SAMD for SR + 6 % OPC solid cores.	66

Figure 6.40: % removal of contaminants from the total SAMD feed solution applied.....	69
Figure 6.41: Plots of log SO ₄ ²⁻ activity versus log Ca activity showing control of SO ₄ ²⁻ and Ca by gypsum solubility in the leachates for FA and SR solid cores...	71
Figure 6.42: Plots of log SO ₄ ²⁻ activity versus log Ca activity showing control of SO ₄ ²⁻ and Ca by gypsum solubility in the leachates for SR + 25 % FA column solid cores.....	71
Figure 6.43: SEM micrographs of leached SR from column 1(FA) and column 5 (SR + 25 % FA) showing gypsum crystals.....	72
Figure 6.44: SEM micrographs of leached SR from column 2(SR) showing gypsum crystals.	73
Figure 6.45: Regression analysis of log Fe activity versus log SO ₄ ²⁻ activity for the FA, SR and SR + FA solid cores leachates.	74
Figure 6.46: SEM micrographs of leached SR from column 8(SR + 6 % OPC) showing gypsum crystals.	76
Figure 6.47: Plots of log SO ₄ ²⁻ activity versus log Ca activity showing control of SO ₄ ²⁻ and Ca by gypsum solubility in the leachates for SR + 6 % OPC column solid cores.....	76
Figure 6.48: Plots of saturation indices for precipitating Fe-bearing mineral phases during the leaching study period for FA and SR solid core leachates.....	78
Figure 6.49: Plots of saturation indices for precipitating Fe-bearing mineral phases during the leaching study period for SR + 25 % FA and SR + 6 % OPC solid core leachates.....	79
Figure 6.50: Logarithmic activity plot of the dissolved Fe ³⁺ versus pH in the leachates for FA, SR, SR + 25 % FA and SR + 6 % OPC solid cores.....	80
Figure 6.51: Plot of log Fe ³⁺ activity against pH for the FA solid core leachates with solubility lines.....	81
Figure 6.52: Plot of log Fe ³⁺ activity against pH for the SR solid core leachates with solubility lines.....	81
Figure 6.53: Plot of log Fe ³⁺ activity against pH for the SR + 25 % FA solid core leachates with solubility lines.....	82
Figure 6.54: Plot of log Fe ³⁺ activity against pH for the SR + 6 % OPC solid core leachates with solubility lines.....	82
Figure 6.55: Plots of saturation indices for precipitating Al-(oxy) hydroxide and Al-hydroxysulphates mineral phases during the leaching study period for FA solid core leachates.....	84
Figure 6.56: Plots of saturation indices for precipitating Al-(oxy) hydroxide and Al-hydroxysulphates mineral phases during the leaching study period for SR solid core leachates.....	85
Figure 6.57: Plots of saturation indices for precipitating Al-(oxy) hydroxide and Al-hydroxysulphates mineral phases during the leaching study period for SR + 25 % FA solid core leachates.....	85
Figure 6.58: Plots of saturation indices for precipitating Al-(oxy) hydroxide and Al-hydroxysulphates mineral phases during the leaching study period for SR + 6 % OPC solid core leachates.....	85
Figure 6.59: Plot of log Al ³⁺ activity against pH for the FA, SR, SR + 25 % FA and SR + 6 % OPC solid core leachates with solubility lines.....	86

Figure 6.60: Leachate ion activities relative to stability lines for Al-hydroxysulphate minerals.....	88
Figure 6.61: Saturation indices versus pH for selected Mn-bearing mineral phases for FA, SR, SR + 25 % FA and SR + 6 % OPC solid residue cores.....	89
Figure 6.62: Leachate Mn ²⁺ activities versus CO ₃ ²⁻ activities for FA, SR, SR + 25 % FA and SR + 6 % OPC showing the pH ranges at which rhodochrosite controls Mn ²⁺ activity.....	90
Figure 6.63: Logarithm of the activity of Mn ²⁺ ion plotted against pH with equilibrium solubility lines.....	91
Figure 6.64: Digital photos of the sectioned FA and SR leached solid cores.....	93
Figure 6.65: Digital photos of the SR + 25 % FA and SR + 6 % OPC leached solid cores.....	94
Figure 6.66: Infra-red spectra for the top, middle and bottom slices of the fly ash (FA) leached SR cores with the spectra of a pure unhydrous ferric sulphate imposed for comparison.....	95
Figure 6.67: Infra-red spectra for the top, middle and bottom slices of the leached SR (SR) cores with the spectra of ammonium oxalate extracted (ES) top slice imposed for comparison.....	96
Figure 6.68: Infra-red spectra for the top, lower top, upper bottom and bottom slices of the leached solid residue (SR) + 25 % FA cores.	96
Figure 6.69: Infra-red spectra for the top, middle and bottom slices of the leached solid residue (SR) + 6 % OPC cores.	97
Figure 6.70: SEM backscattered micrographs showing spots where EDX analysis was done for the solid residue (SR) cores.....	100
Figure 6.71: SEM backscattered micrographs showing spots where EDX analysis was done for the SR + 6 % OPC solid cores.....	102
Figure 6.72: Graphical pH profile of the pore waters of the leached FA and solid residue (SR) cores.	104
Figure 6.73: SEM micrograph showing numerous gypsum crystals in the top section of the leached solid residue (SR) cores.....	107
Figure 6.74: Backscattered SEM micrograph showing Fe, Mn, S rich Ca-Al-Si-O gel with accompanying EDX analysis.....	114
Figure 6.75: SEM micrograph showing Ca-Si-Al-O rich gel encapsulating precipitates and solid residue particles.....	114
Figure 6.76: Pilot-scale reactor used for the neutralisation of AMD with FA and preparation of SR.....	118
Figure 6.77: Graph showing difference in Elastic UCS of the materials derived from different FA: AMD reactions.....	126
Figure 6.78: General form of the flow curve (or rheogram) - linear axes.....	129
Figure 6.79: General form of the flow curve (or rheogram) - logarithmic axes...129	129
Figure 6.80: General form of the viscosity diagram for the rheological models on logarithmic axes.....	130
Figure 6.81: Viscosity versus time for the 1:6 residual solids slurry at RD 1.45 for various shear rates.....	134
Figure 6.82: Viscosity curves for various concentrations of the 1:3 residual solids slurry.....	134
Figure 6.83: Viscosity curves for various concentrations of the 1:4 residual solids slurry.....	135

Figure 6.84: Viscosity curves for various concentrations of the 1:6 residual solids slurry.....	135
Figure 6.85: Flow curves for various concentrations of the 1:3 residual solids slurry.....	136
Figure 6.86: Flow curves for various concentrations of the 1:4 residual solids slurry.....	136
Figure 6.87: Flow curves for various concentrations of the 1:6 residual solids slurry.....	137
Figure 6.88: Yield stress versus relative density for all residual slurries, each at various concentrations.....	138
Figure 6.89: Results of the rheological parameter correlation for the 1:3 slurry.	139
Figure 6.90: Pumping system curve for slurry A.....	140
Figure 6.91: Pumping system curve for slurry B.....	140
Figure 6.92: Pumping system curve for slurry C.....	141
Figure 6.93: Specific power consumption vs. concentration for the 1:3 slurry....	141
Figure 6.94: Graphs showing cumulative PSD and Volume % of PSD in the standard and modified ash.....	147
Figure 6.95: Volume fractions obtained for each suspension.....	149
Figure 6.96: Time dependant behaviour of fly ash.....	150
Figure 6.97: Effect of concentration on the viscosity for the standard suspension	150
Figure 6.98: Effect of concentration on the viscosity for the fines enriched suspension.....	151
Figure 6.99: Effect of concentration on the viscosity for the coarse enriched suspension.....	151
Figure 6.100: Yield stress dependence on concentration.....	152
Figure 6.101: The $1-\mu r^{1/2} - \phi$ relationship at shear rates of 10 and 100 s ⁻¹ for fines enriched sample.....	152
Figure 6.102: Comparison between model and experimental result for fines enriched sample.....	153
Figure 6.103: Comparison between model and experimental result for coarse enriched sample.....	154
Figure 6.104: Effect of fines at a volume fraction $\phi = 0.41$	154
Figure 6.105: Hydraulic gradient for various particle sizes.....	155
Figure 6.106: Slump tests for various suspensions fresh and after 1 day.....	156
Figure 7.107: Gravity fed AMD through ash columns.....	158
Figure 7.108: IR spectra of different layers of the 1.5 m Matla FA column.....	162
Figure 7.109: IR spectra of different layers of the 1 m Matla FA column.....	162
Figure 7.110: IR spectra of different layers of the 0.5 m Matla FA column.	163
Figure 7.111: IR spectra of different layers of the 0.25 m Matla FA column.....	163
Figure 7.112: Raman spectra of different layers of the 1.5 m Matla FA column.....	165
Figure 7.113: Raman spectra of different layers of the 1m Matla FA column.....	165
Figure 7.114: Raman spectra of different layers of the 0.5 m Matla FA column.....	166
Figure 7.115: Raman spectra of different layers of the 0.25 m Matla FA column.	166
Figure 7.116: SEM micrographs of Matla fly ash taken using a back scattered detector (a) and a secondary detector (b).....	168

Figure 7.117: SEM micrographs and EDS spectra of small spherical (a) and larger irregular (b) particles of Matla fly ash.....	168
Figure 7.118: SEM micrographs of the top layer of the 0.5 m ash column taken using a back scattered detector (a) and a secondary detector (b).....	169
Figure 7.119: SEM micrograph and EDS spectrum of the material that was observed in the top layer of the 0.5 m ash column	169
Figure 7.120: SEM micrograph and EDS spectrum of an agglomerated particle of the top layer of the 0.5 m ash column.	170
Figure 7.121: SEM micrographs of the middle layer of the 0.5 m ash column taken using a back scattered detector (a) and a secondary detector (b).....	170
Figure 7.122: SEM micrograph and EDS spectrum of particles from the middle layer of the 0.5 m column.....	171
Figure 7.123: SEM micrographs of the bottom layer of the 0.5 m ash column taken using a back scattered detector (a) and a secondary detector (b).....	171
Figure 7.124: SEM micrograph and EDS spectrum of sample from the bottom layer of the 0.5 m ash column.....	172

List of Tables

Table 4.1: Cost of different sized AMD treatment facilities.....	18
Table 4.2: Percentages of alkaline material (CaCO ₃ or CaO) for different fly ash types and limestone used at Navigation plant.....	21
Table 4.3: Alkaline content in different fly ashes and in limestone used at Navigation plant.....	23
Table 4.4: Comparison of limestone and Kriel FA for the neutralisation of Schoongezicht AMD.....	27
Table 6.5: Test conditions for the fly ash, SR, fly ash and Ordinary Portland Cement blended SR.....	31
Table 6.6: Composition of the Simulated Acid Mine Drainage (SAMD) solution used in the leaching experiments (mg/L).....	32
Table 6.7: Column compositions and total mass (kg, dry weight basis), leachate volumes (L) and liquid to solid ratios for each column.....	32
Table 6.8: The number of times SAMD was drained through the columns, and the corresponding time in days and cumulative volume of SAMD (L/kg).....	33
Table 6.9: Elemental composition of SR, Arnot fly ash and Ordinary Portland cement.....	36

Table 6.10: Total amount in mmol of ions drained through each column and calculated % contaminant removed by each column solid core.....	68
Table 6.11: Drainage time (days) and pH range over which the regression was calculated.....	75
Table 6.12: Characteristic absorption bands observed for FA, SR, SR + 25 % FA and SR + 6 % OPC leached solid residue cores.....	95
Table 6.13: EDS elemental analysis results (weight %) for the solid residue cores	101
Table 6.14: EDX elemental analysis results (weight %) for the SR + 6 % OPC solid cores.....	103
Table 6.15: pH profile of the column solid residue cores with depth.....	104
Table 6.16: Sequential extraction results for the FA solid core (results presented as mean±SD for n=3 extractions, DL-detection limits).....	108
Table 6.17: Sequential extraction results for the solid residue (SR) leached solid core (results presented as mean±SD for n=3 extractions).....	109
Table 6.18: Sequential extraction results for the SR + 25 % FA leached solid core (results presented as mean±SD for n=3.....	110
Table 6.19: Sequential extraction results for the SR + 6 % OPC leached solid core (results presented as mean±SD for n=3 extractions).....	111
Table 6.20: Composition of Navigation toe seep AMD used to prepare SR.....	117
Table 6.21: Experimental details of the preparation of SR from Arnot C1 FA and Navigation AMD at a FA:AMD ratio of 1:3.....	118
Table 6.22: Experimental details of the preparation of SR from Arnot C1 FA and Navigation AMD at a FA:AMD ratio of 1:4.....	119
Table 6.23: Experimental details of the preparation of SR from Arnot C1 FA and Navigation AMD at a FA:AMD ratio of 1:6.....	119
Table 6.24: Schedule of curing for strength testing of SR.....	121
Table 6.25: Moisture content of solid residues, Arnot C1 FA and Castle cement	121
Table 6.26: Specific gravity of solid residues, Arnot C1 FA and Castle cement..	122
Table 6.27: Marsh cone tests results for solid residues obtained from the reaction between Arnot C1 FA and Navigation AMD at a FA:AMD ratio of 1:3.....	123
Table 6.28: Marsh cone tests results for solid residues obtained from the reaction between Arnot C1 FA and Navigation AMD at a FA:AMD ratio of 1:4.....	123
Table 6.29: Marsh cone tests results for solid residues obtained from the reaction between Arnot C1 FA and Navigation AMD at a FA:AMD ratio of 1:6.....	123
Table 6.30: Marsh cone tests results for Arnot C1 FA.....	123
Table 6.31: Elastic unconfined compressive strength of SR without binder.....	124
Table 6.32: Elastic modulus of SR without binder.....	125
Table 6.33: Elastic unconfined compressive strength of SR with 3 % cement binder.....	126
Table 6.34: Elastic modulus of SR with 3 % cement binder.....	127
Table 6.35: Test matrix for residual solids suspensions.....	133
Table 6.36: Rheological parameters.....	137
Table 6.37: Results of the rheological parameter correlation for the 1:3 slurry..	138
Table 6.38: Details for the three pumping curve examples A, B and C.....	139
Table 6.39: Malvern Particle Sizer Results for standard and modified ash samples	147

Table 6.40: Rosin-Rammler parameters for standard and modified ash samples
148

Table 6.41: Reaction time and pH of suspensions..... 148

Table 6.42: Values of D, E and G constants from Eq. 7.50..... 153

Table 7.43: Assignments of infrared active bands that are detected for fly ash.. 161

2 Background

The initial study funded by both the WRC and Coaltech2020 during 2001-2003 (WRC Final report K5/1242; Coaltech2020 Task 6.1.4) provided proof of concept that neutralisation of coal mine derived acid mine drainage (AMD) with South African fly ash (FA) is a suitable method for the low cost treatment of wastewater, and allows recovery of water as well as the preparation of high quality zeolite adsorbents by post process conversion of solid waste residues using hydrothermal synthesis.

Larger scale testing of fly ash as an ameliorant to AMD and as in situ mine backfill was funded by both the WRC and Coaltech2020 in 2003 – 2005 (WRC final report K5/1458, Coaltech2020 Task 6.1.6). Pilot scale testing of the neutralisation of AMD with fly ash showed some differences compared to small beaker scale experiments but conclusively

proved that FA has the capacity to neutralise AMD, reduce sulphate, Fe, Al concentrations and remove a large amount of toxic elements from the water.

Utilization of FA as ameliorant for the neutralization of AMD has thus proved to be feasible. Alkalinity in the form of CaO, as well as high surface area and small particle size, make South African FA a good neutralisation material and AMD ameliorant. Various sources of AMD and FA, usually generated in close proximity, were reacted and resulted in cleaner effluent waters, comparable with lime and limestone treated AMD effluent, and suitable for discharge. The newly developed neutralization procedure worked best for treating high TDS AMD. Sulphate removal rates achieved were high while Fe, Al and toxic element removal was often total depending on the final pH. EC was seen to drop to a minimum at pH ~10. Post-process waters were significantly ameliorated compared to the raw AMD, with only relatively low concentration (parts per billion) of some species of toxic elements remaining in solution (e.g. As, B, W and Mo).

By further processing, the recovered bulk solid residues were successfully used to prepare high capacity adsorbents such as zeolites via a high temperature thermal fusion step and also via lower temperature hydrothermal synthesis routes (WRC 1546). Zeolites are high value, micro porous, open structure crystalline aluminosilicates with a void volume of nearly 50 %. High quality, high yield, clean phase (as indicated by XRD) zeolites that were formed included zeolite Y (faujasite), zeolite A, zeolite P, and sodalite. These zeolites have widespread potential application as adsorbents in water treatment or as catalysts. These high capacity zeolite adsorbents were applied for toxic element removal and showed that significant removal of toxic elements such as Hg, Se, B, As, Fe, Mn, Ni is possible, allowing recovery and purification of contaminated wastewater.

Long term performance and stability criteria determination were necessary to assess the feasibility of application of fly ash as liming substitute in active acid mine drainage treatment systems, or as an in-situ barrier suitable for ash walling in the passive treatment of acid mine drainage, or as backfill material in mines. Larger scale testing was also imperative prior to application of this very promising, low cost process that addresses remediation of two major wastes (acid mine drainage and fly ash) simultaneously.

In the second study (WRC K5/1458), the insoluble, pH neutral, bulk solid residues derived from the remediation process were shown to be suitable as neutral and stable fill material. Strength tests showed that both FA and the solid residues from the neutralisation of AMD with FA had positive strength development and slurry rates without the need for additives like cement or flow agents. Column tests showed that passive treatment of AMD (both real and simulated) is possible with the same reductions in dissolved constituents as is found in active treatment.

This current study, which is a follow up study that extends the scope of WRC K5/1458 and Coaltech2020 Task 6.1.6, aimed to verify the protocols necessary for the industrial application of the treatment of AMD with FA. The study included investigations into large scale neutralization and utilisation of both FA and the solid residues remaining after neutralisation as mine backfill. The aims of this study are described in the following section.

2 Aims

1. Investigate the feasibility of introducing the large scale treatment of acid mine drainage from coal mines and recovery of water from a logistical and engineering perspective.
2. Evaluate, at pilot scale, the suitability of solid residues derived from the full scale co-disposal process as chemically stable backfill material and determine their capacity to extend the life of coalmines and increase the amount of extractable coal.
3. Evaluate the large scale on site employment of fly ash as walls within coal mine spoil heaps to control surface acid mine drainage.
4. Conduct a techno-economic study of the full scale implementation of the treatment of acid mine drainage with fly ash.
5. Determine the environmental impact, mineralogical and other changes associated with historical ash placements underground.

3 Deliverables

The WRC deliverables that were originally submitted were later revised and modified according to the diminished budget that was allocated, in agreement with WRC and Coaltech2020. The revised WRC deliverables are presented in APPENDIX A. The reader is respectfully referred to the Appendix to consider the revision.

2.1 Deviations from the Schedule

The project has come to an abrupt end due to the unavailability of THRIP funds in 2006. Due to the abrupt termination of the project by Coaltech2020 in 2006 resulting from the discontinuation of THRIP funding, only 4 quarterly reports were submitted followed by the current final report. These regular quarterly research reports to the funders WRC and Coaltech2020 were presented to the Coaltech 2020 surface environment and to the WRC steering committee for review.

Coaltech2020 decided in September 2006 that it couldn't fund the project anymore due to lack of expected THRIP funding and advised the team to prepare the final report. The project has ended in September 2006 instead of March 2007. This led to the reporting of some unfinished deliverables that will be explained in detail in the later sections of the report. The deliverable relating to an evaluation of historical ash placement studies, to gain access and determine the mineralogical and other environmental impacts and changes associated with historical placements of ash previously used as fill materials was cancelled due to the lack of budget allocation.

3 Large Scale Remediation of Acid Mine Drainage with Fly Ash

3.1 Introduction

The project “Large Scale Remediation of Acid Mine Drainage with Fly Ash” is the continuation study of the project “Co-Disposal Method for Treatment of Acid Mine Drainage (AMD) with fly ash (WRC Report No: K5/1242/3).

The study focus was on an assessment of the feasibility for large scale treatment of AMD from coal mines and recovery of water including:

- Preliminary planning and consultation for large scale studies including, neutralisation, ash walling, ash lining, water recovery and mineralogical studies. Subtasks of this aspect was:
 - Determination of logistical parameters for application of fly ash as ameliorant for treatment of acid mine drainage
 - Engineering study of the requirements for large scale neutralisation process utilizing fly ash as treatment for acid mine drainage
 - Techno economic study of utilisation of fly ash for treatment of acid mine drainage as replacement for current limestone treatment options
- An evaluation of historical ash placement studies, to gain access and determine the mineralogical and other environmental impacts and changes associated with historical placements of ash previously used as fill materials
- A determination of the overall suitability of solid residues for extending the life of coal mines and increasing the amount of extractable coal from each mine
- An investigation of the potential of large scale ash walling to control surface AMD
- Investigate the potential for control of surface AMD by employment of FA as ash walls within coal mine spoil heaps at larger scale and establish performance as an in-situ barrier for passive treatment of AMD flows

After presenting the background in the next section, each of the above aspects will be presented, detailing the research approach with results and discussions.

3.2 Background

As shown in the previous studies utilization of fly ash for the neutralization of AMD from coal mines has proved to be feasible. Initial studies showed that the co-disposal process using fly ash as ameliorant is able to simultaneously neutralize the high acidity and remove a high % of sulphates and heavy metals from AMD without additional use of costly reagents. Moreover, in this process, insoluble, pH neutral solid residues will be precipitated which have been tested positively as a suitable backfill material for coalmines. The physical and chemical properties ascertained were characteristics such as hardness, strength, long term phase transition and seepage of water. By further processing these solid residues, adsorbents such as zeolites were prepared in bulk. These zeolites were successfully tested to treat post neutralization waters. This complements the primary active AMD treatment. During the initial phase studies it was possible to establish FA-AMD process parameters as well as long term stability, neutralization

capacity and the extent of potential leaching of toxic metals from ash or from the FA-AMD mixture materials. Moreover, optimization of co-disposal process parameters such as neutralization potential of different ashes for various acidic waters and other issues such as sludge settling time, handling and stability of solid residues, potential for leaching of heavy metals etc., were also investigated during this period. A novel treatment technology called ash walling was also successfully investigated during previous studies. Ash walling or lining is a passive treatment option, in which ash is placed in the mine voids as an in situ barrier. The ash barrier neutralizes the AMD that is produced in the mine voids and therefore reduces the threat of surface and ground water contamination. All these necessary process variables were examined in four case specific pilot studies: (1) Treatment of AMD waters generated at Bank Colliery by neutralizing with fly ash (Anglocoal); (2) Potential use of fly ash as an in-situ barrier for the treatment of AMD (ESKOM); (3) Site specific study of using FA as a measure to treat AMD at Arnot (ESKOM); (4) Potential use of solid residues as neutral and stable backfill material for mines.

The current project “Large Scale Remediation of Acid Mine Drainage using Fly Ash” is a continuation project (WRC 662) of the project “Co-Disposal Method for Treatment of Acid Mine Drainage (AMD) with fly ash”(WRC Report No: K5/1242/3). This study aimed to take place on site with an industrial partner since full scale testing and Environmental Impact Assessment (EIA) is imperative prior to licensing and implementation of the low cost co-disposal process. The previous phases of the study “Co-Disposal Method for Treatment of Acid Mine Drainage (AMD) with fly ash” was restricted to laboratory findings/observations and based on these studies a schematic of the treatment technology was developed.

This follow on project (WRC 662) was initiated by negotiations to collaborate with Anglocoal as an industrial partner. Initial discussions indicated that Anglo would be interested in the large scale process and would consider building a continuous FA Pilot Scale plant at Navigational Mine to treat AMD. On the basis of this understanding, three comparison studies were accordingly carried out that involved a cost comparison between the current limestone treatment at Navigation and the FA treatment. These studies were carried out using limestone that is used at Navigation mine to treat AMD and comparing its efficacy with different types of FA derived from different power stations. The AMD/waste waters that were used for the study were from Navigation Mine and Schoongezicht AMD. On their request, UWC submitted a detailed project proposal to Anglo for approval of the pilot scale plant that included results obtained from the three case studies. But, despite many efforts to motivate Anglo, it took about 18 months for Anglocoal to come to a decision, which hindered the progress of some of the deliverables as these were linked with the pilot scale plant either directly or indirectly. Finally a negative answer was received from them. Thereafter, a further partner search was made and bhpbilliton was identified. After various negotiations and the submission of a proposal bhpbilliton has shown interest to build a pilot scale plant at Middleberg mine. Negotiated with bhpbilliton are ongoing and confirmation of the project is expected. The plant will hopefully be up and running by March’2007. We anticipate finishing off the outstanding deliverables of part of the study by making use of the facilities at Middleberg mine should Coaltech review their decision based on THRIP funding in 2007.

3.3 Preliminary planning and consultation and determination of logistical Parameters for large scale studies

Preliminary planning and consultation and determination of logistical parameters for large scale studies involved interaction with people from academic and non-academic backgrounds. Quite a number of meetings were held to ensure that proper planning was done before the start of the project. The industrial interaction is specified in APPENDIX B.

3.4 Engineering study of the requirements for large scale neutralisation process

An engineering study was carried to understand the technical requirements for the large scale plant. This included preliminary design of the plant and assessing and understanding the process variables of the large scale plant. This study was performed with the help of CSIR and Steel Utilities, an engineering company that is located in Pretoria. Quotations were obtained to build a pilot plant for the active neutralisation of toeseep water at Navigation Mine utilizing fly ash instead of limestone. The reader is respectfully reminded that the studies relating to the installation of the large scale plant were done, keeping Navigation mine in mind as a potential place to build the plant. This was because of ongoing negotiations with Anglocoal. But, during the latter part of 2006 Anglo decided not to go ahead with building the plant. Since the studies were done keeping Navigation Mine in mind, most of the results and discussions will refer to Navigation Mine although the plant was not constructed.

The main objective of building a pilot plant at Navigation mine was to determine the practical feasibility and quantify the potential costs and benefits involved with a change to fly ash instead of lime or limestone as an ameliorant for treatment of acid mine drainage. Moreover, the correct treatment protocol needed to be developed based on the previous studies to ensure that the process parameters were fully optimised prior to full scale operation.

3.4.1 Objectives

The following objectives were set for this aspect of the project:

Civil, mechanical and electrical engineering design of a fly-ash handling and dosing system and neutralisation pilot plant.

Production of detailed drawings of all disciplines (civil, mechanical, and electrical).

Manufacture and/or installation of mechanical equipment and construction of civil components. Complete electrical installation as required.

Commissioning of Pilot Plant

3.4.2 Installation of Plant

It was proposed that the installation of the plant at Navigation is executed in two Stages.

Stage 1: Civil, Mechanical and Electrical Design and production of detailed drawings.

Stage 2: Manufacture and/or installation of equipment and construction of civil components and plant commissioning.

The costs of Stage 2 will be finalised after the completion and approval of Stage 1. The total estimated costs as prepared by Steel Utilities in 2006 for stage 1 and 2 are presented in Table 4.1

Table 4.1: Cost of different sized AMD treatment facilities

Volume of the AMD treatment mixing tank	No. of litres of AMD to be treated per day	Total cost for project* (stage1 & 2)
1 m ³	24 000	R908 500
5 m ³	120 000	R1 326 641
2 x 125m ³	1 000 000	R4 238 220

*Break down of the costs is provided in APPENDIX C

3.4.3 Process Description

Figure 4.1 is the schematic of the proposed large scale plant at Navigation Mine. The proposed design is based on treating 5 m³/h of Navigation toe seep AMD (highly contaminated effluent). FA is fed to the mixing tank on a continuous basis, either with the help of a screw conveyor or from a coal hopper. The residence time in the reaction tank is 4-6 hours. The FA settling rate is expected to be sufficiently high to allow for efficient separation of the solid and liquid phases by gravity. Three different mixing tank sizes were considered (1 m³, 5 m³ and 2*125 m³). The surface area occupied by a 1m³ plant is 15 x 5 m; by a 5m³ plant is 15 x 10 m. In each case the surface area can be doubled to ensure sufficient capacity in terms of storage, delivery, etc. The energy input for impeller mixing is 37 152 kW/hr per annum in the mixing tank and 164 160 kWhr per annum in the reaction tank. This is not expected to change if FA replaces limestone, unless the slurry take-up method is changed.

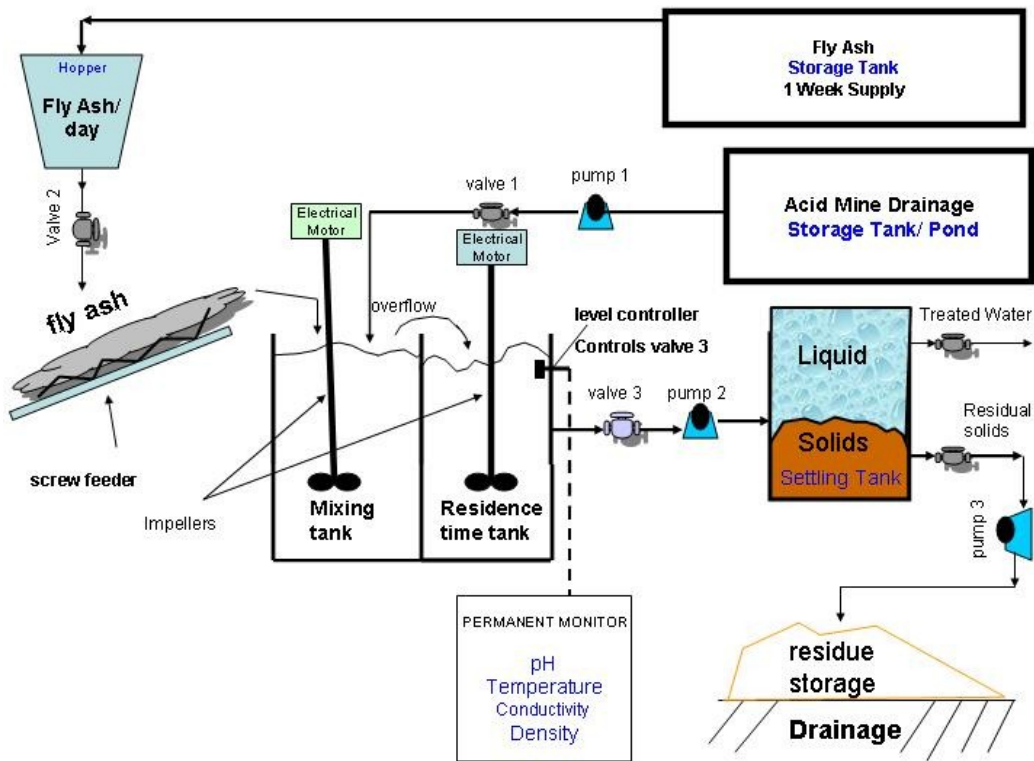


Figure 4.1: Schematic of the proposed large scale treatment plant

The design above is a draft. A more detailed final design would have been obtained from Steel Utilities but due to the discontinuity of the project and lack of Anglo's support to build the plant, no further communication was made with the Steel Utilities to obtain the technical drawings. However, although it is beyond the scope of this project, there is a high chance that this part of the project (building the large scale plant) may be taken over by bhpbilliton. Negotiations with bhpbilliton are very encouraging and there is a high possibility that the large scale operations will be done using the existing facilities at Middleburg mine. Currently, the lime treatment plant at Middleburg mine is inefficient to obtain the quality water and it is estimated that, with slight modifications, this plant could be used for AMD treatment using Fly Ash (2nd phase). The first phase of this project is envisaged to be testing the FA treatment technology using a continuous pilot scale plant that should be built during 2007 at the Middleburg mine.

3.5 Techno economic study of utilisation of fly ash for treatment of acid mine drainage

In order to understand the cost effectiveness of the Fly Ash treatment, a cost estimate was developed based on neutralization experiments in which the costs of the Fly Ash treatment were compared with that of limestone. This techno economic study was carried out in three phases. The first phase was done with the help of CSIR. The second phase was a continuation of phase one in which the experiments were repeated to reach a more meaningful cost estimate. These experiments were carried out using different Fly Ash types and Navigation AMD. The phase three experiments are similar to that of phase two

but with the only difference being that Schoongezicht waters were used instead of Navigation AMD. All the results are presented and discussed in the following section. Based on the results obtained, a detailed proposal was submitted to Anglo to consider funding for building a large scale plant at Navigation.

3.5.1 Neutralizing Potential and Cost Analysis (Phase-I)

Alkalinity is a measure of the neutralising capacity of a liquid or solid system towards an acid (Drever, 1997). In limestone, the alkalinity of CaCO_3 is responsible for the neutralising capacity of the material. In fly ash, it is generally assumed that the alkalinity is exclusively provided by CaO (this is in fact not the full picture). Various experiments were conducted to determine the CaCO_3 content in the limestone currently used at Navigation plant and the CaO content in Arnot, Hendrina and Kriel fly ash. Based on these comparative values, a cost estimate (APPENDIX-D1) was developed, in order to understand whether the fly ash treatment option would lead to an economic benefit compared to limestone. The cost estimate is based on R 55/ton for transporting Arnot FA to Navigation mine.

3.5.1.1 Materials and Methods

The experiments were conducted using a method derived from the method used at the CSIR for determination of CaCO_3 content in solid samples.

For limestone, the method was as follows:

1. Dry the limestone at 105 °C for 12 h.
2. Dissolve 5 g of dry limestone in 100 ml of a solution of HCl 1 N.
3. Titrate the obtained solution (100 ml) with a solution of NaOH 1 N, until pH 7.

The dissolution in HCl allows the calculation of the % of CaCO_3 in limestone, according to the following equation:

$$\begin{aligned} \text{Percentage CaCO}_3 &= (V_{\text{HCl}} \times C_{\text{HCl}} - V_{\text{NaOH}} \times C_{\text{NaOH}}) / m_{\text{limestone}} \times M_{\text{CaCO}_3} / 2 \times 100 \\ \text{Percentage CaCO}_3 &= (100 \times 1 - V_{\text{NaOH}} \times 1) / 5 \times 100 / 2 \times 100 \end{aligned}$$

For FA, the method was as follows:

1. Dry the FA at 105 °C for 12 h.
2. Dissolve 25 g of dry FA in 100 ml of a solution of HCl 1 N.
3. Titrate the obtained solution (100 ml) with a solution of NaOH 1 N, until pH 7.

The dissolution in HCl allows the calculation of the % of CaO in FA, according to the following equation:

$$\begin{aligned} \text{Percentage CaO} &= (V_{\text{HCl}} \times C_{\text{HCl}} - V_{\text{NaOH}} \times C_{\text{NaOH}}) / m_{\text{FA}} \times M_{\text{CaO}} / 2 \times 100 \\ \text{Percentage CaO} &= (100 \times 1 - V_{\text{NaOH}} \times 1) / 25 \times 56 / 2 \times 100 \end{aligned}$$

3.5.1.2 Results

The determination of the alkaline content of fly ash and limestone is presented in Table 4.2. Among the different fly ash types, Hendrina ash had the highest percentage of CaO (9.4 %), followed by Kriel and Arnot. Limestone has a CaCO_3 content of 90.4 % and is thus expected to have a higher neutralising capacity than FA. From these results it can be

anticipated that the amount of FA to be used to neutralise a given volume of AMD will be higher than the amount of limestone required treating the same volume of AMD.

Table 4.2: Percentages of alkaline material (CaCO₃ or CaO) for different fly ash types and limestone used at Navigation plant

Neutralising agent	Percentage of alkaline material
Arnot fly ash	6.87 % CaO
Hendrina fly ash	9.40 % CaO
Kriel fly ash	8.55 % CaO
Limestone	90.4 % CaCO ₃

3.5.1.3 Cost analysis

A cost estimate was developed with the help of J. Maree of CSIR, based on the alkaline content of each material. The full description of the cost estimate is presented in APPENDIX D1.

The cost analysis focused on three steps:

Step 1. Cost incurred to bring the pH of AMD up to 7 (primary treatment), using lime, limestone, Arnot FA, Hendrina FA and Kriel FA.

Step 2. Cost incurred to take the process water from pH 7 to pH 10 (secondary treatment) using lime, Arnot FA, Hendrina FA and Kriel FA.

Step 3. Cost incurred to reduce the sulphate concentrations to as low as 2000 mg/L using the biological sulphate removal plant (SRP), or Arnot FA, Hendrina FA and Kriel FA.

For lime and limestone treatments, the costs of additives such as flocculants were taken into account. For sulphate removal using the SRP, there is a necessary lime pre-treatment to be carried out, by raising the pH to 10 with lime (step 2). This pre-treatment aims at partially removing Mg, Mn and SO₄²⁻ from the solution. The treatment with lime seemed to be economically inappropriate and was eliminated from the overall cost estimate. At Navigation plant, lime has already been replaced by limestone a few years ago, with the objective of performing a cheaper treatment.

Among the three FA types that were tested, Hendrina FA seemed to be the most cost effective neutralising agent, due to a higher CaO content. Hence, Hendrina FA was selected for the overall cost comparison. The results are presented in Appendix D1. █

After calculating the cost for each of the three steps described above, a final cost estimate was obtained by summing the costs of three steps, with three distinct treatment options:

Option 1. Primary treatment of AMD with limestone and sulphate removal with biological SRP.

Option 2. Primary treatment of AMD with limestone and sulphate removal with Hendrina FA.

Option 3. Primary treatment of AMD and sulphate removal with Hendrina FA.

Among the three options that were given in the final estimate, option 2 (using limestone for primary treatment of AMD and Hendrina FA for sulphate removal) appeared to be the

most cost effective choice, with a cost of 5.05 R/m³ of AMD treated. Since the idea is to compare the cost effectiveness of FA treatment with the existing limestone treatment, emphasis was given on the complete use of these two treatment options. The calculations showed that the use of Hendrina FA for the treatment of AMD (neutralisation + sulphate removal) would work out cheaper than the limestone + biological SRP combination, by 0.3 R/m³.

By filling up FA in trucks or trains which carry coal to the power stations and return empty on their way back to the mines, the cost of the transportation of FA could be greatly reduced. As transport of material is the major cost involved in the FA option, this would mean a significant reduction in the cost involved for option 2 and 3. This has to be negotiated once the contract is signed with the industrial partner to set up the pilot plant. It offers the possibility to make the FA treatment option even more attractive.

3.5.2 Neutralizing Potential and Cost Analysis (Phase-II)

The phase II cost analysis is based on alkalinity experiments that are a continuation of experiments performed in phase I. In phase II, various experiments were again conducted to determine the alkalinity of Navigation limestone and Arnot, Kriel and Hendrina FA. The limestone and different FA types were reacted with Navigation toe seep AMD in different ratios and at different time intervals. The resultant pH, acidity and SO₄²⁻ content were used to prepare a comprehensive cost estimate to assess whether FA is economically beneficial in the neutralisation treatment and understand the intricacies involved in limestone treatment. The cost estimate is based on R 55/ton for transporting Arnot FA to Navigation mine.

3.5.2.1 Materials and Methods

The experiments were conducted using a method derived from the approach used at the CSIR for determination of CaCO₃ content in solid samples.

For limestone, the method was as follows:

1. Dry the limestone at 105 °C for 12 h.
2. Dissolve 5 g of dry limestone in 100 ml of a solution of HCl 1 N.
3. Titrate the obtained solution (100 ml) with a solution of NaOH 1 N, until pH 7.

The dissolution in HCl allows the % of CaCO₃ in limestone to be calculated, according to the following equation:

$$\text{Percentage CaCO}_3 = (V_{\text{HCl}} \times C_{\text{HCl}} - V_{\text{NaOH}} \times C_{\text{NaOH}}) / m_{\text{limestone}} \times M_{\text{CaCO}_3} / 2 \times 100$$

$$\text{Percentage CaCO}_3 = (100 \times 1 - V_{\text{NaOH}} \times 1) / 5 \times 100 / 2 \times 100$$

For FA, the method was as follows:

1. Dry the FA at 105 °C for 12 h.
2. Dissolve 25 g of dry FA in 100 ml of a solution of HCl 1 N.
3. Titrate the obtained solution (100 ml) with a solution of NaOH 1 N, until pH 7.

The dissolution in HCl allows the % of CaO in FA to be calculated, according to the following equation:

$$\text{Percentage CaO} = (V_{\text{HCl}} \times C_{\text{HCl}} - V_{\text{NaOH}} \times C_{\text{NaOH}}) / m_{\text{FA}} \times M_{\text{CaO}} / 2 \times 100$$

$$\text{Percentage CaO} = (100 \times 1 - V_{\text{NaOH}} \times 1) / 25 \times 56 / 2 \times 100$$

The pH of the solutions in the experiments was measured with a Hanna portable pH/EC/TDS multi meter and sulphate analysis was carried out at Eskom laboratories, Johannesburg using ion chromatography.

3.5.2.2 Results

The determination of the alkaline content of fly ash and limestone are presented in Table 4.3. Among the different fly ash types, Kriel ash had the highest percentage of alkalinity (18 % as CaCO₃), followed by Hendrina and Arnot. Hendrina and Arnot FA had the same percentage of alkalinity (13% as CaCO₃). Limestone had a CaCO₃ content of 98 % and is thus expected to have a higher neutralising capacity than FA. From these results it can be anticipated that the amount of FA to be used to neutralise a given volume of AMD will be higher than the amount of limestone required treating the same volume of AMD.

Table 4.3: Alkaline content in different fly ashes and in limestone used at Navigation plant

Neutralising agent	Alkaline content (% as CaCO ₃)
Arnot fly ash	13
Hendrina fly ash	13
Kriel fly ash	18
Limestone	98

The full description of the experiments conducted using different ratios of FA and AMD with different time intervals, and the resultant pH, SO₄²⁻ concentrations and amount of residual sludge is presented in Appendix D2. Appendix D2 also describes the cost incurred for various experiments using the parameters mentioned above. This simulation used only enough FA to bring water to a comparable pH as could be achieved with limestone. Based on these results a detailed project proposal was submitted to Anglo (Appendix D2). A summary of the experimental results is presented in this section:

In the case of FA, a larger mass must be used because of the lower alkaline material content of FA.

A pH of about 7.5 is the maximum that can be attained using limestone, whereas FA can increase pH to higher levels, depending on the quantity used and the contact time, as was previously proven.

Using limestone, neutralisation could be achieved after 6 hours; with the restricted amount of FA utilized, neutralisation was achieved with a similar time scale or in some cases within a shorter time frame.

The decrease in acidity and sulphate concentrations that was achieved by using a limestone dosage of 25 kg/m³ was also achieved with FA, but higher amounts of FA were needed. The amount of FA used to obtain similar results as limestone with respect to different FA types is as follows: 143 kg/m³ for Kriel FA, 250 kg/m³ for Hendrina and Arnot FA.

Kriel FA had the capacity to completely neutralise toe seep AMD, and remove sulphate to a high degree provided the reaction time was extended to 20 h (test 3). This result

showed that the FA treatment can be more competitive than limestone for reducing acidity and sulphate removal costs.

Limestone utilisation produced 10 kg of sludge per kg of material used, while with FA the sludge produced amounted to only 2.3 - 2.5 kg per kg of material used.

The sludge obtained after limestone treatment only contained 12 % solids, while the FA sludge contained 42 – 45 % solids,

3.5.2.3 Cost Analysis

A cost estimate was developed using different experimental results detailed in Appendix D2. The results and factors that were taken into consideration were:

- quantity of neutralising agent that was added to AMD
- pH achieved after the neutralisation reaction
- amount of sulphate removed
- amount of sludge remaining
- cost of additives such as flocculants
- purchase and transportation costs of the neutralising agent.

The cost that is incurred for different processes is divided into four categories:

1. Neutralisation cost (R/m³ of AMD) excluding transportation cost
2. Neutralisation cost (R/m³ of AMD) including transportation cost
3. Cost incurred for acidity removal (R/kg as CaCO₃) including transportation cost
4. Cost incurred for sulphate removal (R/kg) including transportation cost.

When including transportation costs, it appears that for all the categories except category 1, limestone seems to be the most cost effective neutralising agent. The cost estimate is based on R 55/ton for transporting Arnot FA to Navigation mine. The cost of transport is an uncertain variable at this stage, since it may be possible to reduce the transport cost significantly in most cases because of shorter distances between other mines and power stations, making FA the more cost effective option since its only cost is transport.

Furthermore the advantages of FA treatment can be summarized as follows:

As per the previous observations, a pH of about 7.5 is the maximum that can be attained using limestone, whereas FA can increase the pH to higher levels, depending on the quantity used and the contact time.

Kriel FA had the capacity to neutralise toe seep AMD and effectively reduced sulphate if allowed to react for more than 20 hours at the restricted dosage applied. This indicates that FA is competitive with limestone in terms of acidity and sulphate removal costs.

Using a larger amount of FA (250 kg/m³), a significant decrease in acidity and sulphate concentrations is observed. A neutral pH would have been reached, in the other FA dosage tested (143kg/m³) had more FA been added or a longer time of contact been applied as previously shown. Addition of higher amounts of FA may not be practically feasible in the large scale, but longer contact times with lower dosage are possible.

The settling time of the sludge that is formed with the limestone treatment is more than the settling time of the sludge that is formed with the FA treatment. Due to a better

separation of phases, much higher amounts of water are recovered from the FA treatment than from the limestone treatment.

Unlike limestone sludge, FA sludge settles fast and hence does not require the addition of flocculants.

The cost estimate is based on R 55/ton for transporting Arnot FA to Navigation mine. The FA transportation cost can be minimised, since Kriel and Hendrina power stations are closer to Navigation compared to Arnot. Then FA treatment will be highly competitive in terms of reducing AMD treatment costs. Alternative ways of transport, such as by train or return after coal delivery, should be considered to reduce costs

3.5.3 Neutralizing Potential and Cost Analysis (Phase-III)

In phase II, limestone and different FA types were reacted with highly contaminated Navigation toe seep AMD to prepare a comprehensive cost estimate. As the cost estimates based upon that study were not entirely conclusive, it was decided to run similar tests and cost analyses using Schoongezicht AMD instead. This effluent is less contaminated than toe seep AMD and because it is less contaminated, its treatment would require lower amounts of FA. Moreover, large volumes of this quality of AMD are typically treated in liming plants.

3.5.3.1 Materials and Methods

Neutralisation reactions, similar to those involved in the phase II study, were carried out to neutralise Schoongezicht AMD with Kriel FA or limestone at different solid/liquid ratios. The materials used were limestone from Navigation plant and Kriel FA, and were already employed and characterised during phase II of the study.

The experimental procedure was as follows:

- collection of raw untreated AMD (usually 400 to 500 ml) and the corresponding mass, depending on the ratio required, of neutralising agent (either ash or limestone)
- mixing of AMD and neutralising agent under agitation
- measurement of pH and EC at regular intervals over several hours
- when pH 7 is reached (whenever possible), stop agitation
- settling of solids for 60 min
- separation of phases

The acidity of the initial AMD and of the various treated solutions was determined using the standard method provided by the American Public Health Association, American Water Works Association and Water Environment Federation (1995).

A cost estimate was developed with the help of different experimental results. The results and factors that were taken into consideration were:

- quantity of neutralising agent added to AMD
- pH and residual acidity achieved after the neutralisation reaction
- purchase and transportation costs of the neutralising agent.

3.5.3.2 Results and Cost Analysis

Schoongezicht AMD is characterised by a relatively low acidity (< 1500 mg/L as CaCO₃) (Table 4.4), compared to Navigation toe seep AMD from the same mine (up to 18000 mg/L as CaCO₃). It can thus be treated with reduced amounts of limestone or FA. Limestone achieved neutralisation at a ratio of 1:370 with a contact time of 6 h (Figure 4.2). As expected, when more limestone was used the contact time necessary to reach a neutral pH was reduced. Neutralisation was achieved with Kriel fly ash within 4-6 h, depending on the ratio used (Figure 4.3). The treatment of the less contaminated Schoongezicht water used significantly less ash (ratio 1:70) than was required for neutralising highly contaminated toe seep acid mine drainage (typically ratio 1:6).

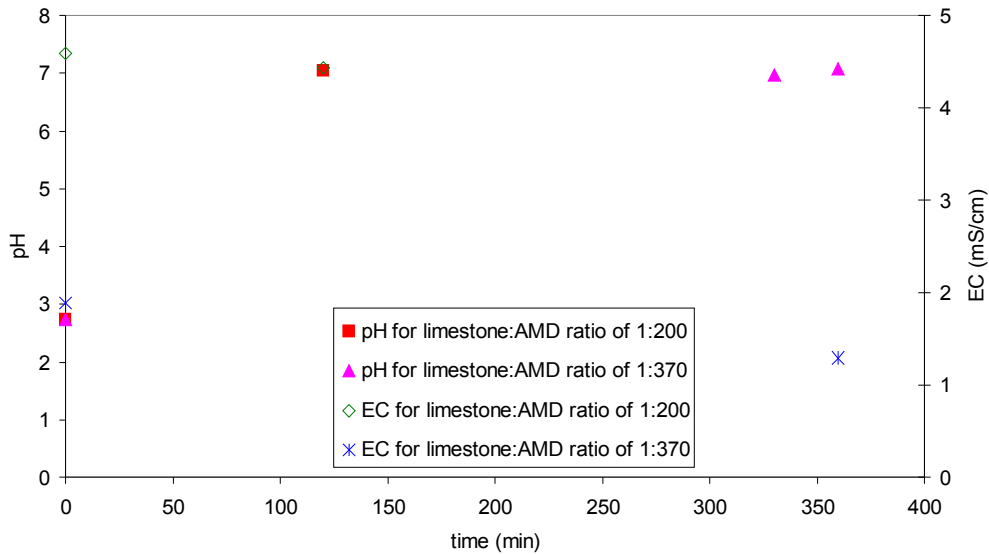


Figure 4.2: pH and EC during the neutralisation of Schoongezicht AMD with limestone

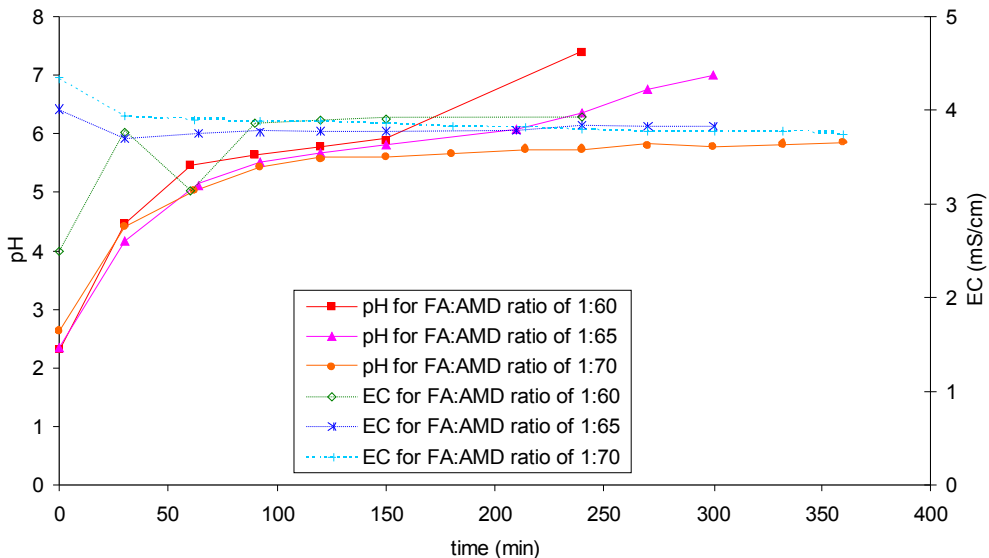


Figure 4.3: pH and EC during the neutralisation of Schoongezicht AMD with Kriel FA

Similar to the previous estimates, these results show that the initial neutralisation is achieved at a roughly similar cost to the limestone treatment, depending on the ratio used

and the reaction time (Table 4.4). Once again it should be remembered that limestone only achieves neutralisation and not a removal of toxic elements. In addition, unlike the case with fly ash, water recovered from the limestone neutralisation step would still need to be further processed by flocculation and biological sulphate reduction, which adds costs to the process. These costs are significant but are not included in this estimate. Moreover, the cost of fly ash (55 R/t) is based purely on projections of transport costs as previously determined and not on material costs. Hence these results further support the feasibility of using fly ash as replacement for limestone in the treatment of acid mine drainage.

Table 4.4: Comparison of limestone and Kriel FA for the neutralisation of Schoongezicht AMD

Neutralising agent	limestone	limestone	Kriel FA	Kriel FA	Kriel FA
Ratio (solid:liquid)	1:200	1:370	1:60	1:65	1:70
pH in feed	2.74	2.74	2.30	2.35	2.63
pH in effluent	7.04	7.07	7.39	7.01	5.85
Acidity in feed (mg/L)	1466	1466	1466	1466	1466
Acidity in effluent (mg/L)	9	11	81	15	89
Acidity removed (mg/L)	1458	1455	1386	1451	1377
Neutralising material usage (kg/m ³)	5.0	2.7	16.7	15.4	14.3
Neutralising material price (R/t)	170	170	55	55	55
Residence time (h)	2.0	6.0	4.0	5.0	6.0
Neutralisation cost (R/m ³)	0.85	0.46	0.92	0.85	0.79
Acidity removal cost (R/kg)	0.58	0.32	0.66	0.58	0.57

4 Historical Ash Placement Studies

Access to the historical underground ash placement sites was not granted thus the deliverables envisaged in this task could not be accomplished despite much interaction with different people from industry, governmental and the non-governmental sector. Many efforts were made to access existing sites but in vain except for one site visit to the ash placement sites at “Ermelo” with Willie Kruger in June 2006. In this case, quite a number of people were contacted to find out whether they knew anything about the ash placement in that area. There were no remaining signs of ash placement since it was done many years ago. A consolidated sample was collected at the site indicated by Willie Kruger and sent for chemical analysis but results indicated that it was not an ash sample. Eskom has indicated that it may be possible to sample old ash dumps at Vaal and Kragbron in the Meyerton district. No further efforts were made to access these sites since UWC was informed by Coaltech2020 that the project had come to an end in September 2006.

5 Suitability of Solid Residues for Extending the Life of Coal Mines

5.1 Introduction

Backfilling of mines with suitable grouting is used to avoid subsidence, provide support to pillars and walls and reduce the void volume (Barret *et al.*, 1978). Backfilling also plays a role in mitigating the environmental concerns of underground fires and the future production of AMD as well as neutralizing existing AMD (USEPA, 1999). South African FA has already been investigated as a backfill material and successfully applied on a few occasions (Ilgner, 2000; Ilgner, 2002). However no studies were found relating to the possible use of Solid Residues (SR) resulting from FA, obtained after reaction with AMD, for backfill. These SR are potentially suitable material for backfilling. Despite the prior reaction with AMD they still have alkaline properties which can be employed for passive treatment of AMD (M.W. Gitari *et al.*, 2005). However there is concern over the probable impact on the groundwater quality over time should these materials be exposed to acid flows.

Extensive literature on the backfilling of mines using different materials including Fly Ash and information on different backfilling techniques was provided in the previous WRC Report No: K5/1458. This particular section of the report covers three aspects of the backfilling using SR. The first aspect focuses on the chemical suitability of SR as a backfill material. The second aspect concentrates on the physical durability of SR such as strength testing over an extended period of time. The third deals with the rheology of SR. The rheological behaviour of SR is important because it defines the optimum pumping requirements and desired solid to water concentration to transport the SR and pump it underground for backfilling.

5.2 Chemical Suitability of solid residues as a backfill material

Results of a six months column study of the interaction of simulated acid mine water (SAMD) with the FA and its derivatives as the SAMD percolated through are presented. This column study was performed with a view to better understand the mechanisms of acidity attenuation by the SR, contaminant attenuation mechanisms and leaching characteristics. In addition the study also aimed to model the chemical and mineralogical changes that could be expected over time when SR are placed underground as fill or backfill material in possible contact with AMD flows.

It would be useful firstly to apply the FA to actively neutralize the AMD prior to its use as a backfill material so that the full benefit of the FA alkalinity is exploited (M.W. Gitari *et al.*, 2006). A comparison was thus necessary between the behaviour of fly ash by itself and that of SR and various combinations of these materials. In addition to passively treating the AMD percolating through, a potential backfill material should also develop compressive strength over time to support overburden in backfill areas. Investigations on the strength development of the material (SR) recovered from these experiments were carried out. The results (Petrik *et al.*, 2005) confirmed that the SR can be used for backfilling.

5.2.1 Materials and Methods

5.2.1.1 Sample collection, preparation of SR and column assembly set-up

Fly Ash samples were collected at Arnot power station in South Africa. AMD was sampled at Navigation plant toe seep dam (Landau colliery). The SR were generated by reacting Arnot fly ash and Navigation AMD in a ratio (FA: AMD) of 1:3 using a 150 litre capacity agitator at Centre for Scientific and Industrial Research (CSIR) in Pretoria (South Africa) (Figure 6.1).



Figure 6.4: The 150 litre capacity agitator used to generate the SR used for the drainage experiments

The mixture was stirred at a rate of 1000 RPM, the EC and pH was monitored during the course of the reaction. The reaction was stopped when a pH of 9.20 was attained. The mixture was allowed to settle and the liquid phase was drained. The solids were then air dried. The chemical composition of FA and SR was ascertained by X-ray fluorescence spectroscopy (XRF) by fusing with lithium metaborate. The SR were dried for 12 hours at 105°C and ground to a fine powder before analysis.

The bulk solids were crushed and mixed thoroughly to attain homogeneity and thereafter placed in columns. A whatman filter paper was cut to fit the PVC pipe used as a column material and was inserted at the top and bottom of the tube. A plastic grid with 8 evenly spread holes was placed on the filter paper. The filter papers and grids were meant to contain the fine particles and spread the leachate respectively. The column assembly used for the experiments is shown in Figure 6.2. All columns used were PVC pipes (diameter 101 mm). The diameter of the columns was constant at 101 mm (10.1 cm) but the height of packing for each blend in the columns varied. The height of packing in the columns were as follows: FA-13 cm, SR-11 cm, SR + 5 % FA-11.8 cm, SR + 25 % FA- 15 cm, SR + 40 % FA- 18.8 cm and SR + 6 % OPC-12.8 cm. The SR were packed into columns in small portions of 500 gms. After each addition the material was then gently pressed with a 1 L PVC bottle in order to pack sediments. Each column was duplicated for each different composition of solid material (Table 6.1 and 6.3). Calculation of the loading

weights in the columns was done taking into account the moisture content of the SR. The moisture content was determined by oven drying the wet SR at 105°C for 12 hours. The % moisture content was 12.09 ± 0.01 .



Figure 6.5: Column assembly used for the leaching experiments

Table 6.5: Test conditions for the fly ash, SR, fly ash and Ordinary Portland Cement blended SR.

Column code	Weight of co-disposal/ fly ash (kg)	Dry weight (kg)	Weight of fly ash/OPC added (g)	% fly ash/OPC added (dry weight)	Height of column solids (cm)	drainage volume (L) per experiment
C1a	1.000	1.000			13	0.35
C1b	1.000	1.000			13	0.35
C2a	1.000	0.879			11	0.35
C2b	1.000	0.879			11	0.35
C3a	1.000	0.925	46	5	11.8	0.35
C3b	1.000	0.925	46	5	11.8	0.35
C5a	1.000	1.172	293	25	15	0.45
C5b	1.000	1.172	293	25	15	0.45
C6a	1.000	1.465	586	40	18.8	0.555
C6b	1.000	1.465	586	40	18.8	0.555
C8a	1.000	0.935	56.1	6	12.8	0.35
C8b	1.000	0.935	56.1	6	12.8	0.35

5.2.1.2 Simulated acid mine drainage preparation and drainage

Simulated acid mine drainage (SAMD) was used in the column study because of logistical constraints and to exclude variability. The model SAMD solutions were formulated using soluble salts of the major elements in AMD (Fe, Al, Mn and SO_4^{2-}). The SAMD used in the column experiments contained 2000 mg/L Fe^{3+} , 3000 mg/L Fe^{2+} , 1000 mg/L Al^{3+} , 200 mg/L Mn^{2+} and 14407 mg/L SO_4^{2-} (Table 6.2). It was modelled to simulate Navigation AMD which was used in the initial experiments. SAMD was prepared at two levels of $\text{Fe}^{2+}/\text{Fe}^{3+}$ (1000:1000ppm) and (2000:3000 ppm) giving a total concentration of Fe similar to the natural AMD (Navigation AMD). It was prepared by dissolving the required amounts of Ferric sulphate anhydrous [$\text{Fe}_2 (\text{SO}_4)_3$], Ferrous

sulphate heptahydrate [FeSO₄·7H₂O], Aluminium sulphate 18-hydrate, [Al₂(SO₄)₃·18H₂O], Manganese (II) nitrate tetrahydrate [Mn(NO₃)₂·4H₂O]. All chemicals used were of analytical grade. The weighed salts were dissolved in 0.005 M H₂SO₄ solution prepared using milliQ water to prevent immediate precipitation of ferric iron. The final pH of the solution ranged from 1.82 –1.84. The actual concentration of the SAMD was ascertained by inductively coupled-mass spectrometry (ICP-MS) for major elements and ion chromatography (IC) for SO₄²⁻. The SAMD was prepared each time, a few minutes before the experiments.

Table 6.6: Composition of the Simulated Acid Mine Drainage (SAMD) solution used in the leaching experiments (mg/L)

Contaminant	calculated	SAMD1	SAMD2	Mean±SD
Al	1000	907.60	909.75	908.7±1.07
Mn	200	201.40	198.86	200.1±1.27
Fe (total)	5000	4657.01	4795.70	4726.4±69.3
SO ₄	14407			

(SD: standard deviation)

Table 6.3 details the column fill compositions and total mass (kg, dry weight basis), as well as the leachate volumes (L) and liquid to solid ratios for each column.

Table 6.7: Column compositions and total mass (kg, dry weight basis), leachate volumes (L) and liquid to solid ratios for each column.

Column number	Column fill composition	Mass solids (kg)	SAMD added per drainage (L)	Total SAMD added after 16 drainages (L)	Liquid:Solid ratio per drainage (L/kg)	Total Liquid:Solid ratio (L/kg)
1	Fly ash (FA)	1.000	0.350	5.60	0.350	5.600
2	Solid residue (SR)	0.897	0.350	5.60	0.390	6.243
3	SR + 5 % FA	0.925	0.350	5.60	0.378	6.054
5	SR + 25 % FA	1.172	0.450	7.20	0.384	6.143
6	SR + 40 % FA	1.465	0.555	8.88	0.379	6.061
8	SR + 6 % OPC	0.935	0.350	5.60	0.374	5.989

The specified volume of SAMD was added to each column over a period of several minutes and collected once it had percolated through the column. This is termed drainage. The SAMD neutralization kinetics was developed to confirm its buffering properties when compared to the natural AMD. Reactions were carried out for 24 hours and EC and pH was monitored over time. Columns 1, 2, 3 and 8 were leached with batches of 350 ml SAMD. Columns 5 and 6 containing different masses of solid material, were leached with 450 and 555 ml respectively, in order to maintain a consistent liquid to solid ratio between all the columns (Table 6.3). Drainage was done after each 7 day period for the first 53 days and thereafter with 14 day intervals until completion of the experiment at

165 days. The number of times SAMD was drained through the columns, and the corresponding time in days and cumulative volume of SAMD (L/kg) is shown in Table 6.4. Leachates from the previous drainage were collected before the next drainage commenced. Leachates were analyzed within 24 hours for pH, EC and Eh. Sub-samples were thereafter preserved with HNO₃ for analysis of metals by inductively coupled-mass spectrometry (ICP-MS) for major elements and un-acidified samples were diluted accordingly for SO₄²⁻ analysis by ion chromatography (IC). Samples were refrigerated at 4°C until analysis.

Table 6.8: The number of times SAMD was drained through the columns, and the corresponding time in days and cumulative volume of SAMD (L/kg).

Drainage No	Time (days)	Volume (L/kg) of SAMD added per column					
		Column 1	Column 2	Column 3	Column 5	Column 6	Column 8
1	1	0.35	0.40	0.38	0.38	0.38	0.37
2	7	0.70	0.79	0.76	0.77	0.76	0.74
3	15	1.05	1.18	1.13	1.15	1.14	1.11
4	22	1.40	1.57	1.51	1.54	1.52	1.48
5	29	1.75	1.95	1.89	1.92	1.90	1.85
6	36	2.10	2.34	2.27	2.30	2.27	2.22
7	44	2.45	2.73	2.65	2.69	2.65	2.59
8	53	2.80	3.12	3.02	3.07	3.03	2.96
9	67	3.15	3.51	3.40	3.46	3.41	3.33
10	81	3.50	3.90	3.78	3.84	3.79	3.70
11	97	3.85	4.29	4.16	4.22	4.17	4.07
12	110	4.20	4.68	4.54	4.61	4.55	4.44
13	124	4.55	5.07	4.91	4.99	4.93	4.81
14	138	4.90	5.46	5.29	5.38	5.31	5.18
15	152	5.25	5.84	5.67	5.76	5.69	5.55
16	165	5.60	6.23	6.05	6.14	6.06	5.92

At the end of the drainage experiment the columns were left intact for another three months to cure without being drained again. The columns were then cut lengthwise into two equal sections by using a saw. One of these sections was divided into three sections for column C1, C2, C3, C5 and C8 while column C6 was divided into four sections. Physical, chemical and mineralogical analysis was performed on the three or four sections of the solid cores.

The samples for pH determination of solids were sampled across the length of the surface of the half-section and blended to create a composite sample. Samples were taken every 2 cm down the solid residue column cores for columns C1, C2, C3, C8 and after every 2.5 cm for columns C5 and C6. pH was determined using 1:1(solid residue: water) ratio by following the method of Eckert (1988).

10 grams of the leached SR were weighed and put in a beaker and an equal amount (10 ml) of de-ionized water added. The mixture was then stirred thoroughly for 5 seconds,

allowed to settle for 15 minutes and the pH of the supernatant recorded. This was done in triplicate.

5.2.1.3 Analysis of the leached solid residue cores

X-ray diffraction, Scanning Electron microscopy, Scanning Electron microscopy-energy dispersive spectroscopy (SEM-EDX) and infra-red analysis of column solid cores was performed to evaluate the mineralogical changes resulting from the interaction of the SAMD with the various solid residue (SR) blends. Samples were taken from the sectioned solid residue cores. The solid samples were sampled from the sectioned column starting from the top of the column to the bottom. The samples were then crushed and oven-dried for 12 hours at 105°C to remove the interstitial water, and then crushed further to obtain a fine powder.

The XRD spectra were obtained by a PANalytical X-ray diffractometer (XRD) using Cu $K\alpha$ radiation generated at 20 mA and 40 KV. Specimens were step scanned as random powder mounts from 5 to 85° 2θ integrated at 0.02° 2θ per second. X-ray diffraction analysis can detect crystalline phases present at 5 % mass. Powder samples for SEM and SEM-EDX were loaded on copper stubs coated with carbon graphite glue mixture and then carbon coated for 30 minutes. Both backscatter and secondary electron modes were used for image acquisition. Dried powdered solid residue cores section samples were also analysed by Fourier Transform Infra-Red Spectroscopy (FTIR). The powder samples were mixed with 95 % dried analar grade KBr, ground with mortar and pestle and pressed into a transparent disc and thereafter scanned over the wave number range 4000 cm^{-1} to 200 cm^{-1} .

5.2.1.4 Sequential Chemical Extractions

To complement the data on mineralogical analysis and to be able to account for the contaminants profiles obtained in the leachates and the contaminant attenuation behaviour of the FA solid residues (SR) and the tested SR blends, the solid residue core sections were subjected to sequential chemical extraction based on the work of Ribet *et al.* (1995), Tessier *et al.* (1979) and Schwertmann *et al.* (1982). All the extraction experiments were carried out with wet samples scooped from the column sections starting from the top to the bottom of the column. These extractions were done to determine the water soluble fraction, amorphous fraction and reducible fraction. All experiments were carried out in triplicate.

i) Water soluble fraction: the distilled-water soluble fraction was determined by agitating 5 g of the wet solids in 50 ml of MilliQ water with a table shaker for 1 hour, the mixture was then centrifuged at 1000 rpm for 10 minutes, and filtered through a 0.45 μm nucleopore membrane. The obtained supernatant was then prepared for metal and SO_4^{2-} analysis. A parallel sub-sample of the insoluble fraction was dried for 12 hours at 105°C to determine the moisture content so as to be able to calculate the dry weight.

ii) Amorphous fraction: 1.0 gm of the wet SR from (a) were extracted with 200 ml of 0.2 M ammonium oxalate buffer at pH 3.0 in the dark. The buffer was prepared by adding 1100 ml of 0.2 M oxalic acid solution to 1500 ml of 0.2 M ammonium oxalate solution to

obtain a final pH of 3.07. The buffer was prepared fresh during each series of extraction for a given column section. The extraction was done by agitating the mixture in a table shaker for 4 hours. The mixture was then centrifuged at 1000 rpm for 10 minutes, filtered through a 0.45 μM nucleopore membrane and the supernatant prepared for metal and SO_4^{2-} analysis.

iii) Reducible fraction: 0.5 gm of the wet solids from (ii) were added to 15 ml of 1.0 M hydroxylamine hydrochloride ($\text{NH}_2\text{OH}\cdot\text{HCL}$) solution in 25 % (v/v) acetic acid solution and then heated to $95 \pm 5^\circ\text{C}$ for 6 hours to remove the crystalline Fe and Mn (hydrous) oxides (Tessier *et al.*, 1979). The 1.0 M hydroxylamine hydrochloride solution was made by dissolving 13.898 gm of hydroxylamine hydrochloride salt in 200 ml of 25 % acetic acid solution. The extraction was done by agitating the mixture in a table shaker with a water bath maintained at $95 \pm 5^\circ\text{C}$. The mixture was then centrifuged at 1000 rpm for 10 minutes after cooling, filtered through a 0.45 μM nucleopore membrane and the supernatant prepared for metal and SO_4^{2-} analysis.

5.2.1.5 Geochemical Modelling

Precipitation of solid phases may be the most important chemical process influencing the fate of major (SO_4^{2-} , Fe^{3+} , Fe^{2+} , Al, Mn, Ca) and minor elements (Zn, Cu, Mo, Ni, B, Sr) in acid mine waters. Activities of aqueous species and mineral saturation indices of selected mineral phases were calculated using PHREEQC software (Parkhurst, 1995) and the WATEQ4F database which was modified to include ettringite. FeOOH was added to the database with $\text{Log } K = 4.891$ for ferrihydrite. Sillimanite, a mineral similar to mullite (main aluminosilicate matrix in fly ash) was added since its thermodynamic data is available (Lindsay, 1979). The alkalinity reported as mg CaCO_3/L was recalculated to mg HCO_3^-/L as is required for input by PHREEQC. Data of the leachates from each drainage of the various column solid cores was the input for the software and was used to estimate the activities of the various species. The activities of the dissolved species were calculated with the Davies equation (Davies, 1962). All the dissolved Fe was assumed to be oxidized to Fe^{3+} thus redox reactions were eliminated from the modeling to simplify the equilibrium calculation. The data used for the calculations were pH, alkalinity, $\rho_e = 4$, solute concentrations for Al, Ca, Cu, Fe, Zn, SO_4^{2-} , Na, K, Si, Mn, Pb, B, Sr, Ba, and Mo. The saturation index (SI) is used when large deviations from equilibrium are observed. For $\text{SI}=0$, there is equilibrium between the mineral and the solution; $\text{SI}<0$ reflects under-saturation, and $\text{SI}>0$ super-saturation. For a state of under-saturation dissolution of the solid phase is expected and super-saturation suggests precipitation.

5.2.2 Results and Discussion

It is worth mentioning that the results obtained for SR+5% FA solid cores were similar to the results obtained for SR cores and likewise the results obtained for SR+40% FA solid cores were similar to the pure FA columns. Hence, some of the explanation does not cover results pertaining to SR+5% FA solid cores and SR+ 40% FA solid cores, unless and otherwise specifically mentioned in the case of different trends. The reader is requested to assume that wherever there is no explanation of SR+5% FA solid cores and

SR+40% FA solid cores, the results of these solid cores are similar to the results of SR and pure FA solid cores respectively.

5.2.2.1 Composition of Fly Ash, Solid residues (SR) and Ordinary Portland Cement (OPC)

Table 6.5 shows the chemical characteristics of the fly ash, SR and ordinary Portland cement used in the column studies.

Table 6.9: Elemental composition of SR, Arnot fly ash and Ordinary Portland cement.

SR				Ordinary portland cement		Arnot fly ash			
Element	wt %	Element	ppm	Element	wt %	Element	wt %	Element	ppm
SiO ₂	45.88	Mo	6.2	SiO ₂	35.26	SiO ₂	53.39	Mo	5.23
Al ₂ O ₃	24.57	Sr	1954.4	Al ₂ O ₃	12.83	Al ₂ O ₃	23.40	Sr	1463.9
TiO ₂	1.19	Pb	46.8	TiO ₂	0.80	TiO ₂	1.34	Pb	56.35
Fe ₂ O ₃	6.31	Co	29.5	Fe ₂ O ₃	1.44	Fe ₂ O ₃	4.72	Co	18.25
MnO	0.10	Mn	642.9	MnO	0.36	MnO	0.06	Cr	179.2
MgO	2.39	Cr	230.6	MgO	3.55	MgO	2.70	Zn	57.33
CaO	7.14	Zn	144.3	CaO	42.82	CaO	8.43	Cu	47.34
Na ₂ O	0.41	Cu	52.3	Na ₂ O	0.05	Na ₂ O	0.35	Ni	93.41
K ₂ O	0.51	Ni	83.3	K ₂ O	0.59	K ₂ O	0.49	Ba	928
P ₂ O ₅	0.68	Ba	136.9	P ₂ O ₅	0.15	P ₂ O ₅	0.35		
SO ₃	3.48			Cr ₂ O ₃	0.002	Cr ₂ O ₃	0.03		
Cr ₂ O ₃	0.04					NiO	0.011		
NiO	0.01								

The high weight % of Si, Al and Ca reflect the main components of Ordinary Portland Cement (OPC). OPC consists primarily of compounds of calcium and silicon with smaller amounts of iron and aluminium compounds (Taylor, 1997). Compared to fly ash and the SR, OPC had high amounts of Mn and Mg which could be mobilized during the leaching study. The SR and fly ash have a high weight % of SiO₂, Al₂O₃ which reflects the main components of fly ash, the aluminosilicate matrix. This has been established to be mainly quartz and mullite (Gitari *et al.*, 2004).

The decrease of 1.29% in CaO content in the SR compared to fly ash reflects the free alkalinity content (as CaO) of the FA that was utilized in the active neutralization of AMD and shows the significant residual alkalinity in the form of CaO (7.14%) remaining in the SR after the neutralization step. This residual alkalinity can be slowly released over time in passive treatment systems. A decrease in MgO is also observed which indicates its additional contribution to the neutralization capacity of the fly ash.

A decrease in SiO₂ is observed in the SR which is attributed to the dissolution of the alumino-silicate matrix during the neutralization process. An enrichment of Fe and Al is observed in the SR as a result of the removal of these elements from AMD as insoluble precipitates. Other elements observed to be enriched in the SR include Mo, Sr, Co, Cr and Zn.

5.2.2.2 Evolution of pH in the leachate

Figure 6.3(a-c) shows the evolution of pH as function of cumulative S/L ratio for the different solid cores.

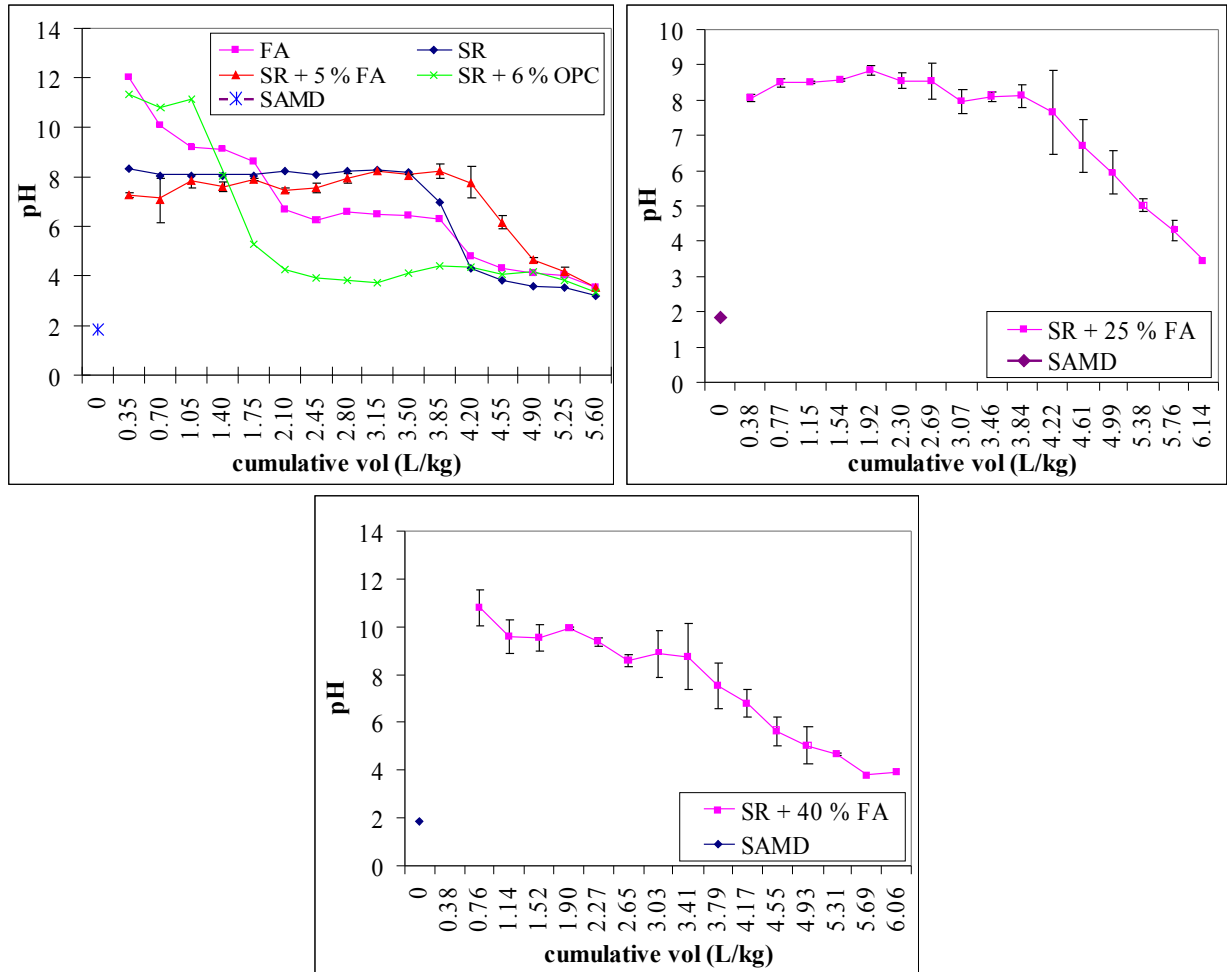


Figure 6.6(a-c): Evolution of pH in the leachate with cumulative volume for the FA, SR (SR), SR + 5 % FA, SR + 25 % FA, SR + 40 % FA and SR + 6 % OPC.

The FA cores, the solid residue (SR) + FA and solid residue (SR) + 6 % OPC cores exhibited stepwise acidification which indicates that several acidity attenuation mechanisms are involved as the drainage progresses (Fig 6.3a). FA cores exhibited three acidification steps, SR, SR+FA and SR+ 6 % OPC cores two acidification steps. The higher pH buffer region (pH 7.5-9) was sustained for a longer duration than the lower one (pH 3-4) in SR and SR+FA cores. SR+OPC cores reached the lower buffer region (pH 3.5-4) sooner and remained at this level for a longer duration of the experiment.

An observed similarity in pH profile of the SR + 40 % FA solid core with the FA column core probably indicates that at 40 % or higher blending rate, the dissolution kinetics and

free alkalinity of the fly ash will dominate. The solid residue cores (SR) appeared to have a significant buffering capacity, maintaining a neutral to slightly alkaline pH in the leachates for an extended period of time (97 days). Blending of the solid residue (SR) with fly ash of up to 25 % by weight increased the duration of the circum-neutral, or alkaline pH of the leachates and increased the time before breakthrough to the acidic zone to 110 days.

If placed in a mining area generating AMD, these SR could provide a passive method of treatment of polluted coal mine water. The alkaline properties of the original FA or the residual alkalinity of the SR would thus have the potential to passively treat any flows of AMD, with a neutralization reaction taking place in situ over an extended period of time. The use of Ordinary Portland Cement as a binder reduces this neutralization capacity to 22 days (Fig 6.3 and Table 6.4; the figure numbers need to be changed to correspond to figure numbers indicated in the figure caption). Results obtained in the case of addition of the OPC binder may indicate possible excessive aggregation of residue particles or physical encapsulation by the generated CSH gel in the Ordinary Portland Cement amendment that may have reduced the active surface area of particles resulting in less of the residual alkalinity being available for neutralization.

5.2.2.1 Acidity Attenuation by the Column Cores

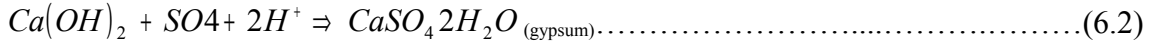
5.2.2.1.1 Fly ash and solid residue (SR), solid residue (SR) + FA column cores

Stepwise acidification of all the column residue cores was observed as the drainage progressed (Figure 6.3(a-c)). The presence of buffering regions suggests that different acidity attenuation mechanisms were responsible for the eventual clean-up of the SAMD percolating through the various column packings.

The pH profile for the entire drainage period indicates that FA and solid residue (SR) + 40 % FA column cores exhibited similar trends pointing to a probable similarity in the kinetics and evolving chemistry as the drainage progresses. Moreover for the period of the study the kinetics observed (pH and EC) strongly points to those of dissolution of the free alkalinity of the unreacted fly ash used to blend the SR. In this context more detailed discussion of the evolving chemistry in these two cases are confined to the fly ash column cores only. Similarly, the pH profile of the solid residue (SR), solid residue (SR) + 5 % FA and solid residue (SR) + 25 % FA column cores point to similar dissolution kinetics and chemistry. The significant difference noted for the three blends is that the time during which the leachate pH was sustained at approximately pH 8.0 was extended to 110 days for the solid residue (SR) + 5 % FA and solid residue (SR) + 25 % FA compared to the solid residue (SR) column cores, a longer period than for either unblended FA or SR column packings by themselves. Another notable difference is that the solid residue (SR) + 25 % FA cores sustained a pH higher than 8.0 in the leachates for 110 days as compared to the solid residue (SR) and solid residue (SR) + 5 % FA cores, again most probably due to the additional free alkalinity in the 25% FA fraction. Clearly there is a synergistic effect as the FA/SR blended materials performed better than either FA or SR by itself. Detailed discussion of the evolving chemistry is confined to solid residue (SR) and solid residue (SR) + 25 % FA column cores.

FA solid cores had the highest initial pH of the leachates (pH 9.2- 12.0) compared with the SR and SR + FA solid cores (Fig 6.3), which can be attributed to the unreacted free alkalinity which is readily soluble and immediately available for acidity attenuation.

The initial high pH of the leachates for the FA columns was attributed to the dissolution of free alkalinity in the form of surface CaO as the acidic mine water contacted the fly ash particles (Eq 6.1). The generated Ca (OH) ₂ is highly soluble at alkaline pH and interacts with SO₄ in the SAMD to form gypsum which precipitates.



Gypsum was identified by XRD and SEM-EDX in all the FA sectioned column solid cores (Figs 10 and 11) as a result of the contact with sulphate rich SAMD, indicating again the major role that gypsum precipitation plays in sulphate removal from AMD. That dissolution of CaO from the fly ash particles was responsible for the initial high pH of the leachates is supported by the fact that the initial decrease in Ca was only observed for the FA solid core leachates (Fig 6.4). The actual EDX mass % data is presented in the Tables 6.9 and 6.10.

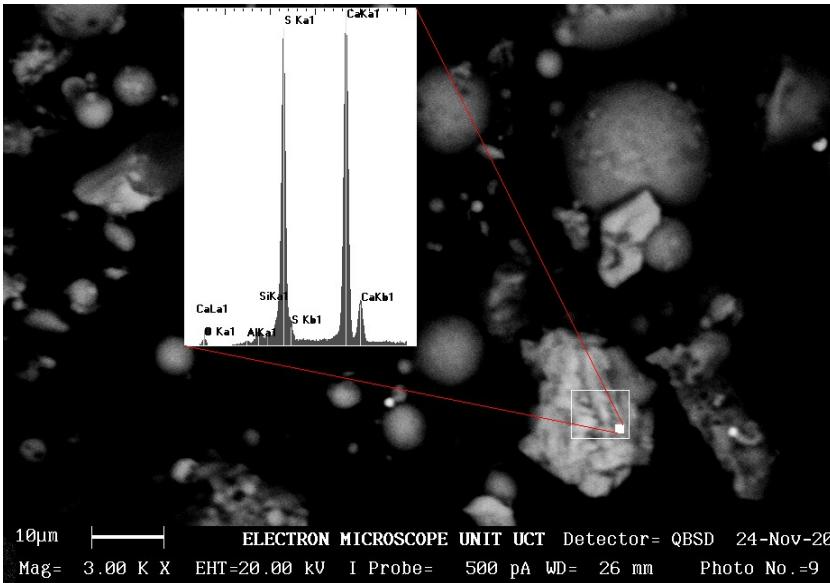


Figure 6.7: SEM-backscattered micrograph of gypsum crystals in FA column cores with the EDX pattern superimposed.

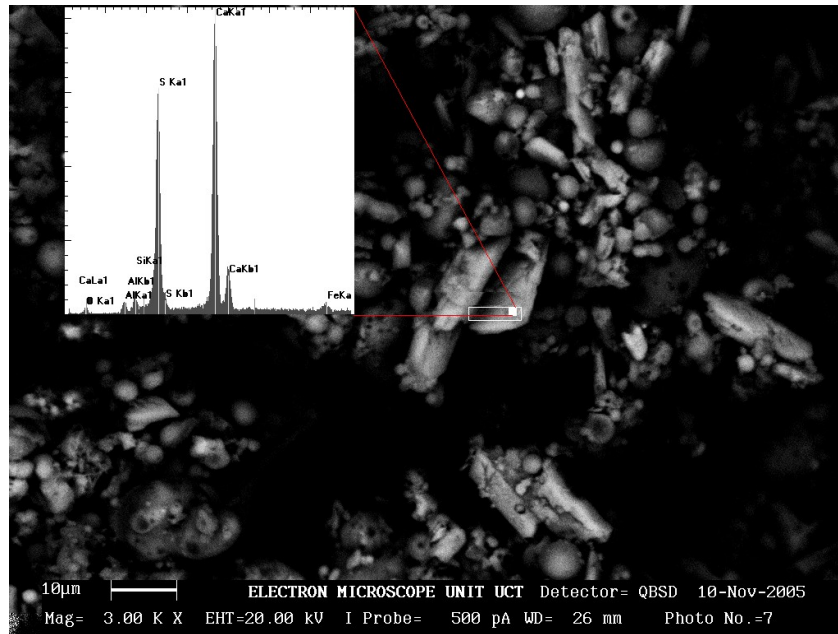
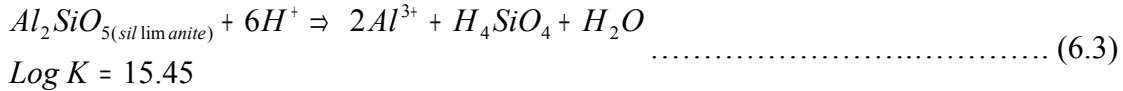


Figure 6.8: SEM-backscattered micrograph of gypsum crystals in solid residue (SR) column cores with the EDX pattern superimposed.

The decrease in Ca in the SR + FA blended solid cores leachates are not obvious (Fig 6.32 to 6.36) Part of the reason may be that the SR were loaded in the columns while wet (moisture content 12.1 %) and interaction of the wet SR with the blended FA initiated CaO dissolution and formation of $\text{Ca}(\text{OH})_2$ and on drainage with SAMD, reaction with SO_4 occurred leading to locking of Ca^{2+} as gypsum.

The SR cores as well as the SR + FA cores exhibited strong acidity attenuation at pH 7.5-9.0. This pH buffer zone was sustained for slightly over 110 days for solid residue (SR) + 5 % FA and solid residue (SR) + 25 % FA and 97 days for solid residue (SR) cores (Fig 6.3 and Table 6.4). The effect of FA addition to the SR is observed with the SR + 25 % FA solid cores where the pH front breakthrough to the acidic zone is steady as compared to the SR cores which exhibit a sharp breakthrough. Acidity attenuation at this pH range is also observed for the FA cores from 29-97 days of drainage while for the solid residue (SR) + 40 % FA cores it was observed at 15-97 days.

Several mechanisms can be proposed for the acidity attenuation at this pH range in these solid cores. After the initial rapid dissolution of CaO and other soluble salts coating the fly ash particles the aluminosilicate matrix, amorphous SiO_2 and quartz are exposed and can interact with the percolating SAMD and there is a possibility of their dissolution with time. Laboratory studies of quartz dissolution and precipitation kinetics indicate that quartz dissolution and precipitation are extremely slow at low temperatures (25°C) (Rimstidt and Barnes, 1980). The measured temperature of all the column leachates varied from $19.1\text{-}23.6^\circ\text{C}$ hence contribution of quartz to the dissolved silica would be insignificant. Seoanne and Leiros (2001) argued that the minerals most susceptible to weathering after the initial rapid dissolution of CaO and other soluble salts in fly ash were probably aluminosilicates. Dissolution of these minerals consumes hydrogen ions as indicated in Eq. (6.3) for sillimanite (Lindsay, 1979).



Sillimanite was chosen to confirm the contribution of aluminosilicate minerals in attenuation of acidity and buffering of pH at 7.5-9.0 for the solid residue (SR) and solid residue (SR) + FA solid column cores. Sillimanite is a mineral similar to mullite (Lindsay, 1979). Saturation indices (SI) were calculated over the pH range 7.5-9.0 for the solid residue (SR) and solid residue (SR) + 25 % FA solid cores. An observation of the calculated SI over this pH range for the solid residue (SR) core leachates (Table E8) indicates that sillimanite was over-saturated up to 44 days becoming under-saturated for the rest of the drainage time. The transition from over-saturation to under-saturation is not pH dependent over the said pH range and could mean two things: (i) its contribution to buffering at this pH range is confined within a certain initial period of the drainage experiment. (ii) its contribution to attenuation of acidity and hence buffering becomes indirect via conversion to a new mineral phase. For the solid residue (SR) + 25 % FA a slightly different scenario is observed where sillimanite remains near saturation for most of the drainage period (Table E10.) strongly indicating it was in an equilibrium state under the acidic conditions.

From Eq (6.3) the equilibrium for the dissolution of sillimanite can be written as

$$K = \frac{[Al^{3+}]^2 [H_4SiO_4]}{[H^+]^6} = 10^{15.45} \dots\dots\dots (6.4)$$

Taking logarithm to base 10 results in the following expression

$$15.45 = 2Log[Al^{3+}] + Log[H_4SiO_4] + 6pH \dots\dots\dots (6.5)$$

If sillimanite is contributing significantly to the attenuation of acidity over this pH range then a plot of pH versus $2Log^a$

$[Al] + Log^a [H_4SiO_4]$ should give a straight line graph with a slope of -6 and y-intercept of 15.45 over the pH range 7.5-9.0 corresponding to the stoichiometry of Eq (6.3). An observation of the plots over this pH range for solid residue (SR) (Fig 6.6) and solid residue (SR) + 25 % FA (Fig 6.7) core leachates indicates a stoichiometry corresponding to Eq (6.3) confirming the contribution of sillimanite in buffering the pH in this range.

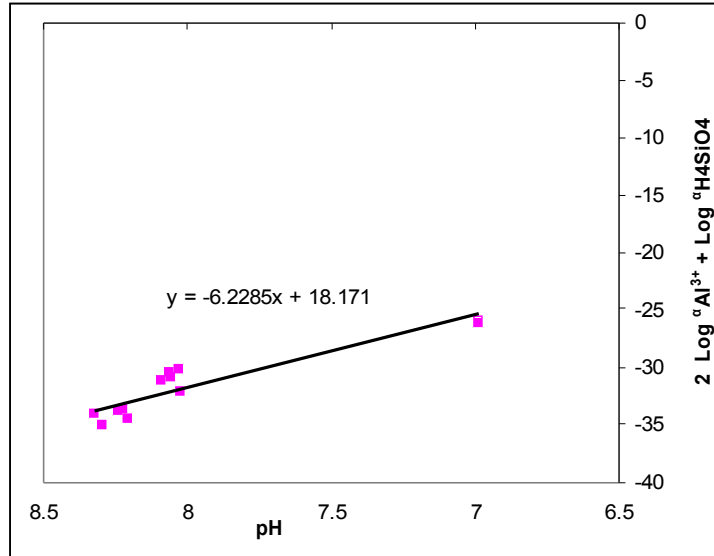


Figure 6.9: Plot of pH versus $2\text{Log } a_{\text{Al}^{3+}} + \text{Log } a_{\text{H}_4\text{SiO}_4}$ over the pH range 6.5-9.0 for solid residue (SR) core leachates (SR column core).

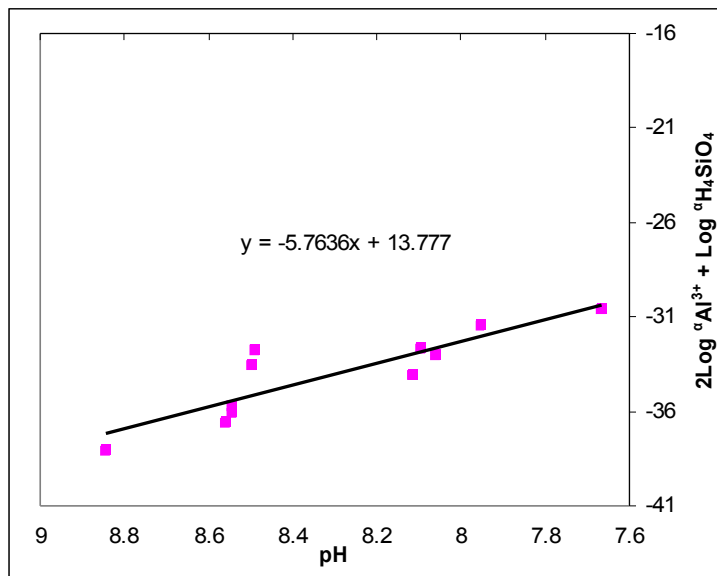
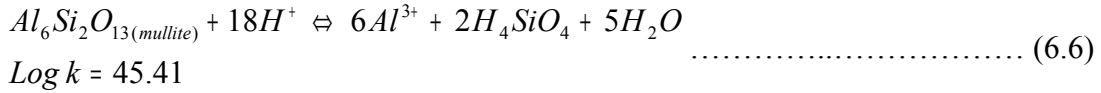


Figure 6.10: Plot of pH versus $2\text{Log } a_{\text{Al}^{3+}} + \text{Log } a_{\text{H}_4\text{SiO}_4}$ over the pH range 6.5-9.0 for solid residue (SR) + 25 % FA core leachates (column 5).

Plots of solubility equilibria for mullite and sillimanite, which are the main crystalline aluminosilicate phases in the investigated fly ash, were constructed and the calculated activities of Al^{3+} and H_4SiO_4 from the experimental data were used to derive the experimental solubility curves ($\text{Log } k = 45.41$ obtained from Roy and Griffin (1984). (Figs 6.8- 6.13).

The theoretical activities Al^{3+} and H_4SiO_4 for mullite were calculated by using the equilibrium expression derived from the following Eqs (6.6, 6.7 and 6.8).



From Eq (6.6) the equilibrium for the dissolution of mullite can be written as

$$k = \frac{[H_4SiO_4]^2 [Al^{3+}]^6}{[H]^{18}} = 10^{45.41} \quad \dots\dots\dots (6.7)$$

Taking logarithm to base 10 results in the following expression

$$45.41 = 2 \text{Log } H_4SiO_4 + 6 \text{Log } Al^{3+} + 18 \text{pH} \quad \dots\dots\dots (6.8)$$

Using the solubility constant for mullite and measured pH the activities of Al^{3+} and H_4SiO_4 at equilibrium with mullite for the leachates can be calculated.

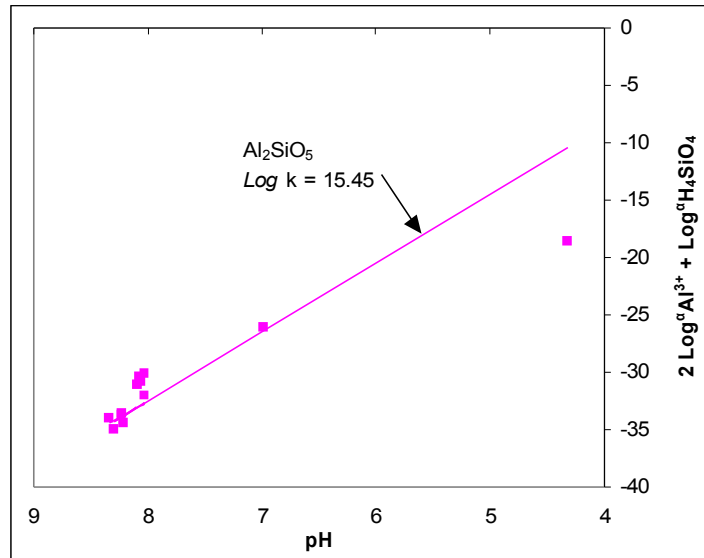


Figure 6.11: Sillimanite solubility equilibria for solid residue (SR) core leachates

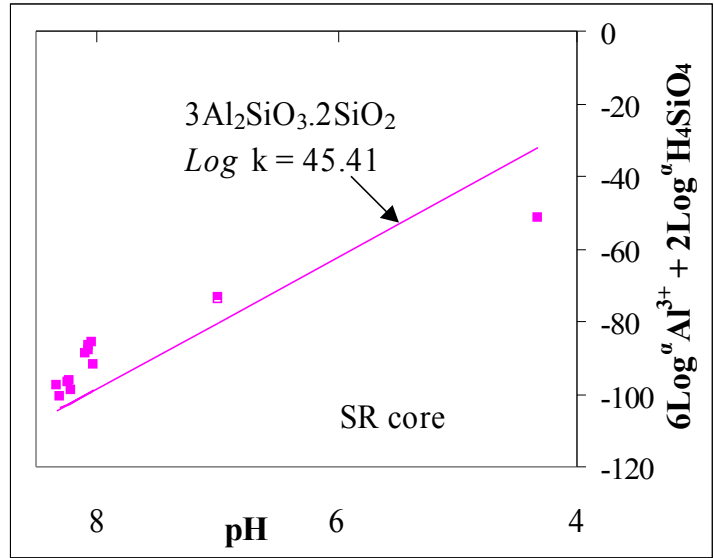


Figure 6.12: Mullite solubility equilibria for solid residue (SR) core leachate

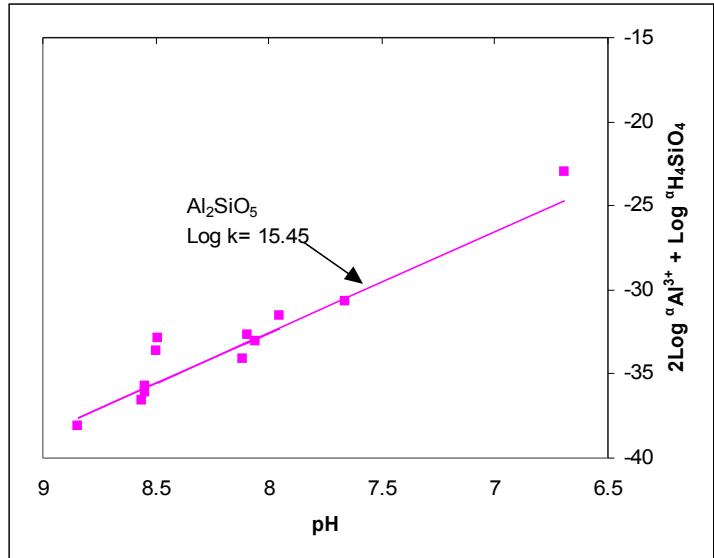


Figure 6.13: Sillimanite solubility equilibria for solid residue (SR) + 25 % FA core leachates.

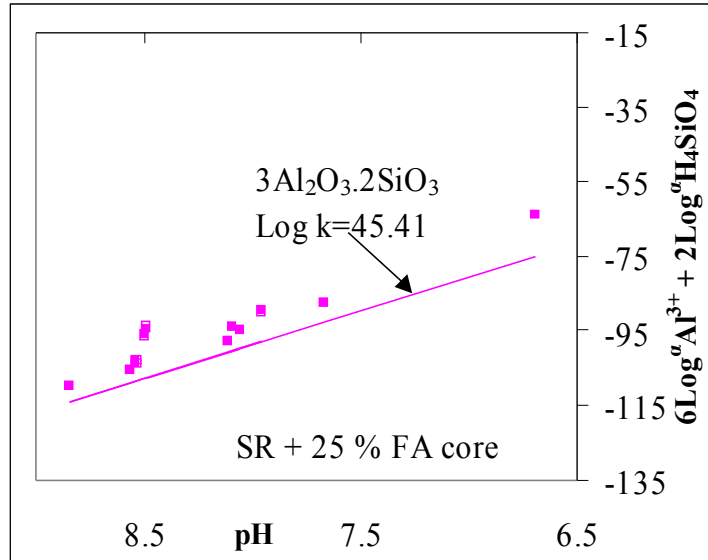


Figure 6.14: Mullite solubility equilibria for solid residue (SR) + 25 % FA core leachates.

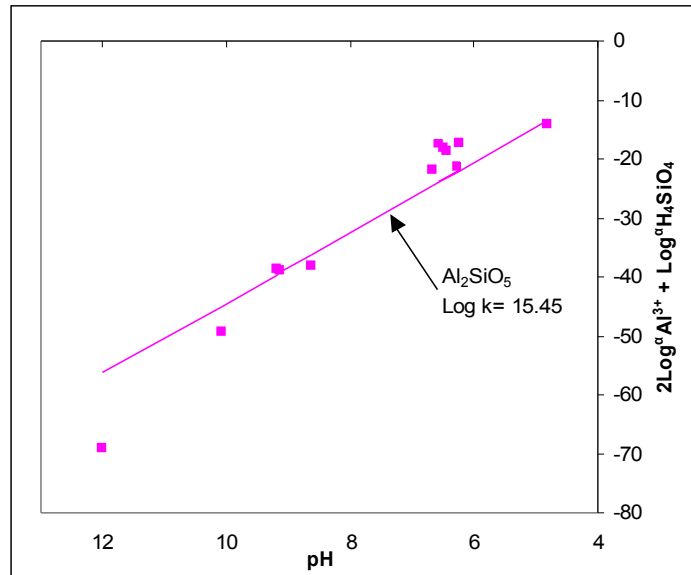


Figure 6.15: Sillimanite solubility equilibria for FA column core leachates.

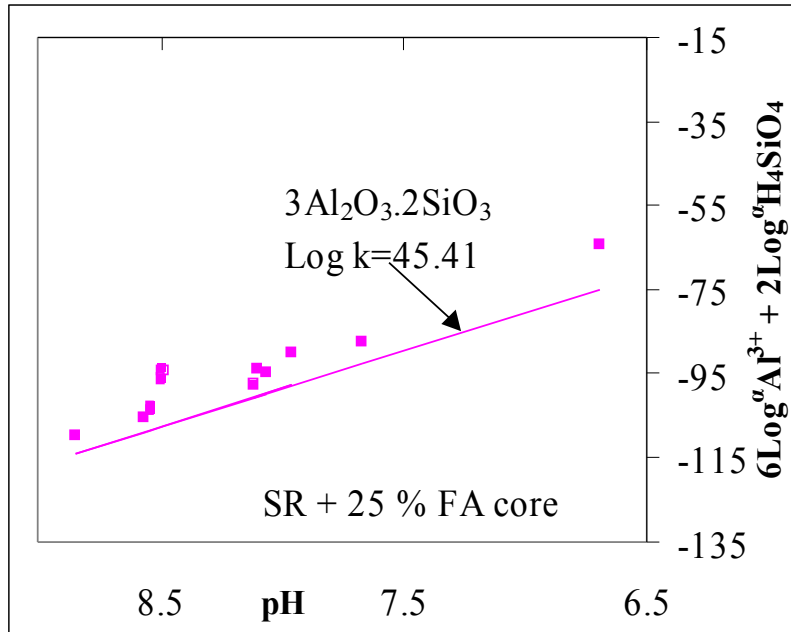


Figure 6.16: Mullite solubility equilibria for FA column core leachates.

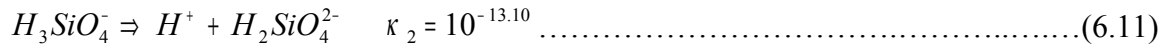
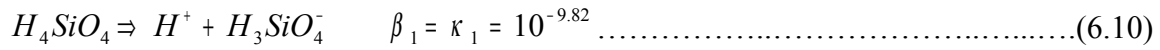
Aqueous solution modeling indicates that the solid residue (SR), solid residue (SR) + 25 % FA and FA core leachates were in equilibrium with sillimanite over the pH range 6.99-8.33. The FA core leachates were observed to be in equilibrium with mullite over the pH range 8.62-10.08 while the SR, SR + 25 % FA core leachates remained over-saturated over the pH range 6.5-8.85. This could be interpreted to mean that sillimanite and mullite were controlling both Al^{3+} and H_4SiO_4 concentration in the leachates over the pH range 6.5-8.85. The strong equilibrium observed with sillimanite for the SR and SR + 25 % FA points to the importance of this amorphous aluminosilicate matrix in controlling the chemistry of the leachates over this pH range. A peculiar phenomenon is observed with FA cores' leachates becoming over-saturated with both mullite and sillimanite at pH 6.22-6.68. Roy and Griffin (1984) observed equilibrium with mullite for acidic fly ash extracts at pH 4.1 and after equilibration for a long time with water (up to 140 days), the fly ash extracts became over-saturated with mullite as the pH approached 6.0.

Apart from the amorphous aluminosilicate minerals, fly ash also consists of mineral phases such as quartz and amorphous SiO_2 . Solubility of quartz is very low (Brownlow, 1979) hence would not dissolve rapidly under the acidic leaching conditions at low temperature. Langmuir (1997) points out that the most soluble form of SiO_2 is the amorphous silica. Therefore dissolution of amorphous silica is expected to contribute to the control of leachate chemistry over this pH range. To confirm this, equilibrium diagrams for amorphous silica were plotted for the FA, SR, SR + 25 % solid cores which exhibited extended buffering at pH 6.5-8.9.

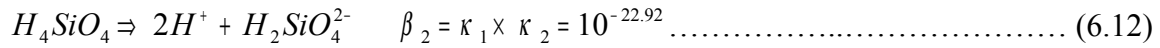
Equilibrium for amorphous silica can be written as for quartz (Eq. 6.9)



The silicic acid being a weak acid dissociates in two steps (constants used are for 25°C).



The cumulative constant for the reaction:



From Eq(6.12) the equilibrium for equilibration of silicic acid resulting from dissolution of amorphous silica can be expressed as

$$\kappa = \frac{[H^+]^2[H_2SiO_4^{2-}]}{[H_4SiO_4]} = 10^{-22.92} \dots\dots\dots (6.13)$$

Taking logarithms to base 10 on both sides of equation (6.13) gives:

$$22.92 = 2pH - [Log H_2SiO_4^{2-} - Log H_4SiO_4] \dots\dots\dots (6.14)$$

Equation (6.14) was then used to derive the plots for silicic acid equilibria over the pH range of 6.5- 8.85. The plots are shown in Figures 6.14, 6.15 and 6.16.

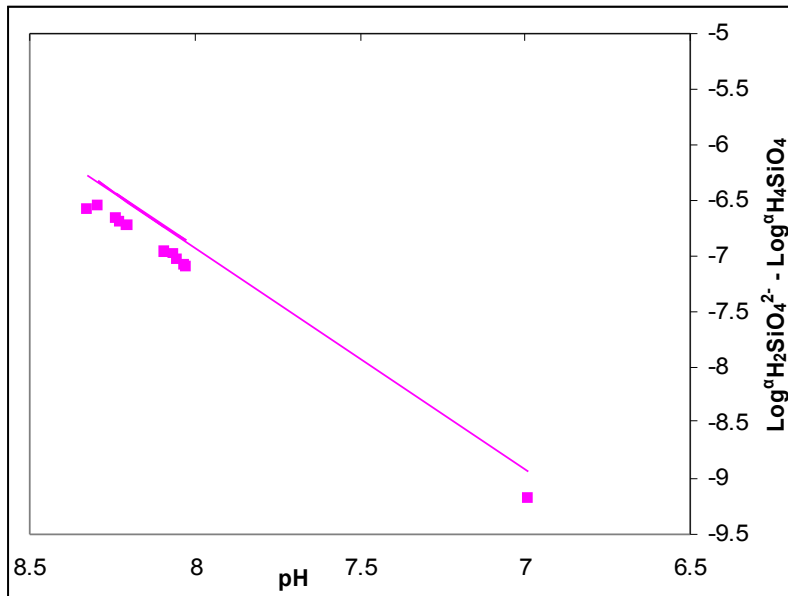


Figure 6.17: Amorphous silica solubility equilibria for solid residue (SR) column core leachates.

(solid line represents SiO_{2(amorphous)} equilibria)

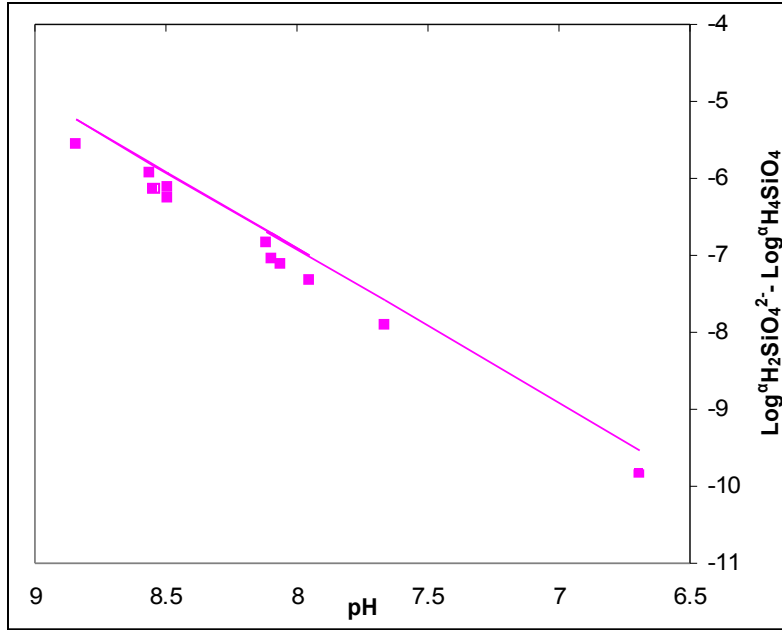


Figure 6.18: Amorphous silica solubility equilibria for solid residue (SR) + 25 % FA column core leachates.

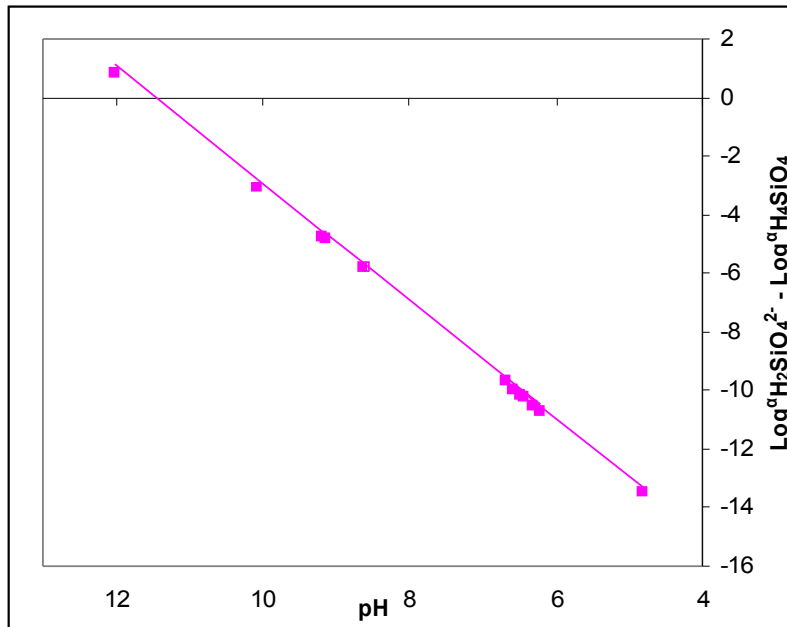


Figure 6.19: Amorphous silica solubility equilibria for FA column core leachates.

An observation of the amorphous silica equilibria as a function of pH indicates that the leachates were near equilibrium with amorphous silica over the pH range 6.5-8.85. The equilibration is less for the solid residue (SR) core leachates than for the solid residue (SR) + 25 % FA core leachates. This is probably due to the slightly higher pH generated in this column. This is confirmed further by the total equilibrium observed in the FA

cores. This strongly indicates that amorphous silica largely controlled solubility of aqueous H_4SiO_4 in the leachates at this pH range. An observation of the calculated saturation indices for amorphous silica indicates that it was under-saturated for the entire drainage period confirming that it was undergoing dissolution in the FA, solid residue (SR) and solid residue (SR) + 25 % FA cores.

Evidence that part of the glassy phase was soluble and was contributing to the consumption of acidity as the drainage progressed is seen in the change in the ratio of the mullite: quartz peak in the XRD patterns for FA, SR and SR + FA column solid cores (Figs 6.17, 6.18 and 7.19). The change in the ratio of the diffraction peak intensities for mullite and quartz indicates that dissolution of the glassy material from the ash particles occurred and varied with depth. This led to increase in intensity of the mullite peak relative to quartz. This is a possible indication that the $SiO_2(a)$ in the SR or coatings on the mullite were dissolving relative to quartz. This is feasible since at the bottom of the column the precipitates most likely derived from constituents in the upper parts of the column were deposited on the lower section. Warren and Dudas (1984) observed that Al and Si, leached from the ash under acidic conditions, appeared to be derived from the glassy matrix of the fly ash particles. The change in the ratio of diffraction peak intensities for mullite: quartz indicated that dissolution of the glassy material decreased with depth in the ash core according to the chemical dissolution gradient. The upper and middle parts of the solid cores in this study experienced the greatest chemical dissolution and probably this explains the increased relative intensity of mullite. Analysis of the leached solid residue cores indicated a chemical gradation with the top section of each column showing the highest load of precipitates and low pH and the last section showing the highest pH indicating least chemical reactivity (Figs 6.60, 6.61 and 6.66). Chemical extraction results indicated an increase of Al, Si and Fe in the solid cores from top section to the bottom section for the amorphous fraction (Tables 6.12, 6.13, 6.14 and 6.15).

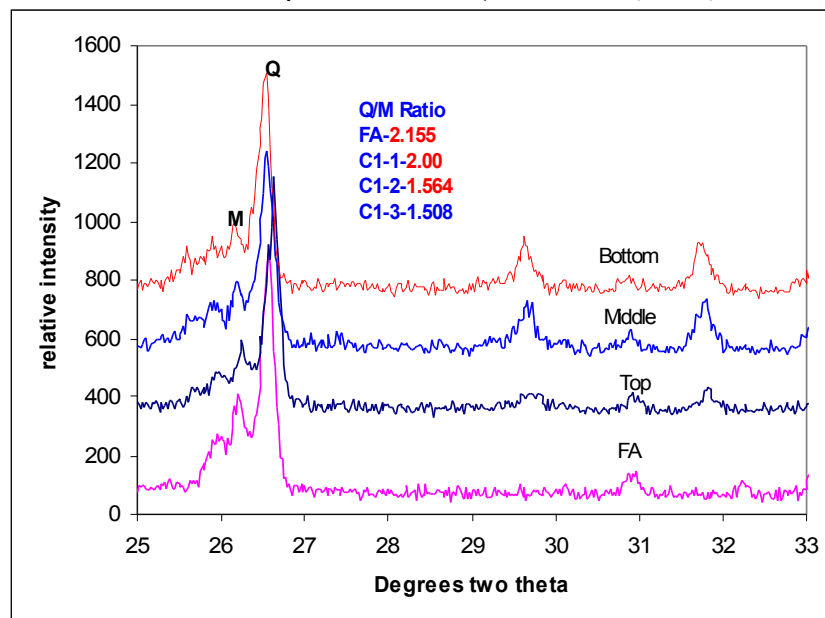


Figure 6.20: XRD spectra of the FA column solid cores showing the change in the mullite: quartz peak ratio from top to bottom.

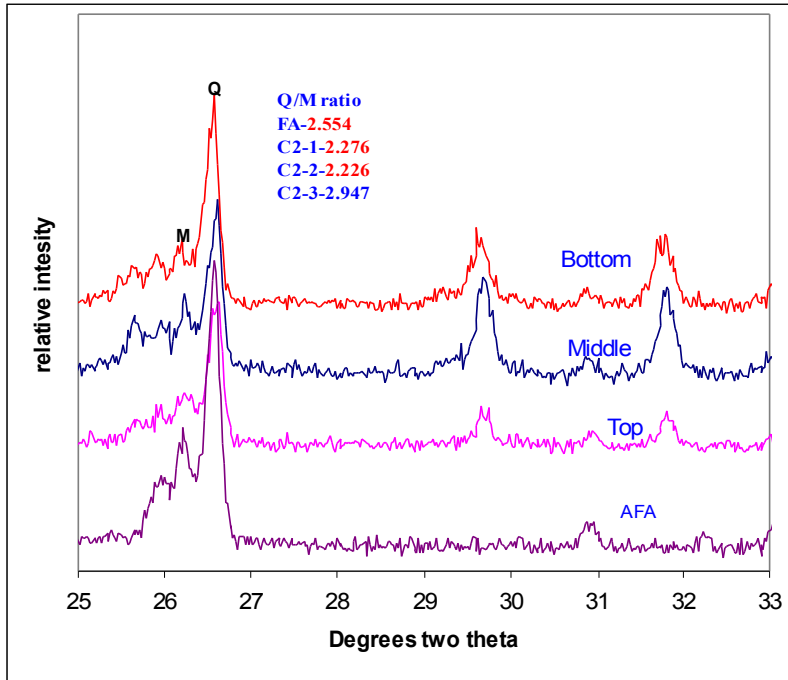


Figure 6.21: XRD spectra of the solid residue cores showing the change in the mullite: quartz peak ratio from top to bottom of core.

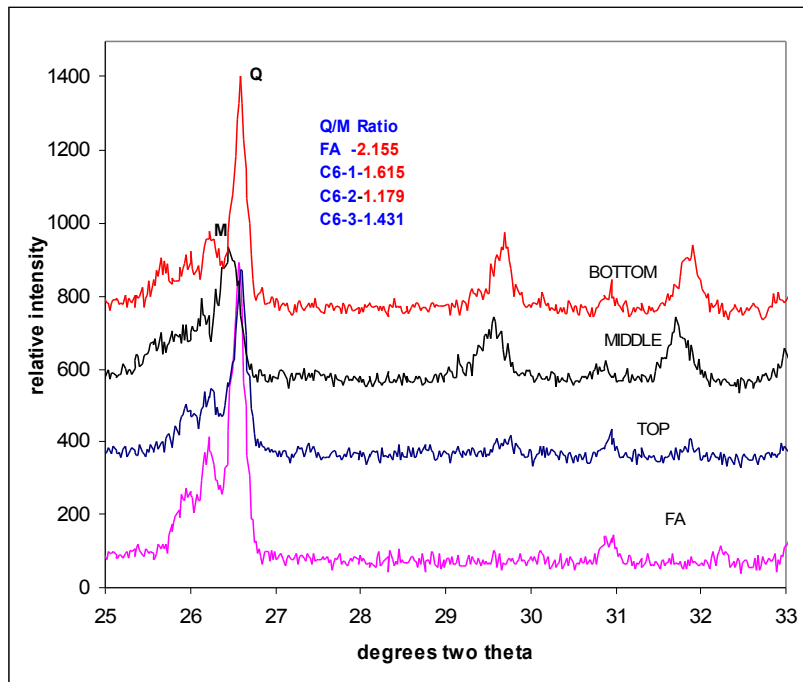


Figure 6.22: XRD spectra of the solid residue (SR) + 40 % FA cores showing the change in the mullite: quartz peak ratio from top to bottom.

This confirms that the highest degree of chemical activity was at the top where the highly acidic SAMD was greatly neutralized, with decreasing reaction because of prior neutralization as the SAMD percolated to the bottom of the solid core of SR.

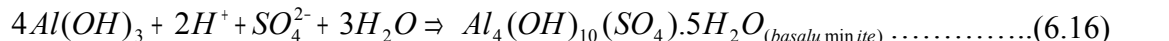
At this point it can be tentatively concluded that at pH 6.5-8.5 the silicic acid system is controlling the pH in the leachate analogous to the control of pH in natural waters by the carbonate system (Drever, 1997). The buffering of the leachate pH by the silicic acid system will only hold as long as there is SiO_{2 (amorphous)} dissolution from SR, SR + FA solid cores or generation of silicic acid by the dissolution of the aluminosilicate matrix, otherwise the buffering is overwhelmed when the SiO_{2 (amorphous)} is completely dissolved from the fly ash matrix. Yong *et al.* (2001) determined heavy metal (Cu, Zn, Pb) retention capacity of some estuarine alluvia soils using column tests by draining with a landfill leachate at pH 1.5. The resulting effluent was buffered at pH 7.5-9.5. The soils mainly consisted of kaolinite, illite and chlorite. This corroborates the results obtained in this study which observed that after the initial rapid hydration of CaO resulting in alkaline pH the leachates were thereafter buffered at pH 7.5-9.5 for a greater duration of the experiment by the slow dissolution of amorphous silica and aluminosilicates.

PHREEQC simulation indicates that the leachates for the FA solid cores were over saturated or at equilibrium with Al(OH)_{3(amorphous)} at 36-97 days of drainage (pH 8-8.5) (Fig 6.51 and Table E7). An observation of the Al trends in the leachates (Fig 6.29) show a decrease in Al concentration at 29 days of drainage. Except for the peak at 53 days which was attributed to resolubilization of previously formed precipitates the concentration remained below 6 mg/L until 97 days of drainage. Precipitation of Al(OH)_{3(a)} can occur through the following reaction consuming acidity and contributing to buffering of pH in the region of pH 8-8.5.



Calculation of equilibrium pH ($\log K_{eq} = 5.6$) using activities of Al(OH)₄⁻ over the pH range did not reveal a correlation with the measured pH. The equilibrium alone could not account for the pH observed. This could partly be due to the fact that Al(OH)_{3(a)} could also be generated directly from the hydrolysis of Al³⁺ from the fresh SAMD feed.

After the buffer zone at pH 7.5-9, the FA, SR and solid residue (SR) + FA solid cores were observed to enter the acidic buffer zone (pH 3-4) as the drainage progressed. The transition to the acidic buffer zone occurred at different drainage times for each solid core. Several researchers (Adams and Rawajifih, 1977; Bigham and Nordstrom, 2000 and Nordstrom, 1982) have pointed out that precipitation of basic aluminum sulfate minerals occur in acid sulphate waters. They point out that basaluminite is the first to occur if the solution is sufficiently enriched in sulphate and at pH below 4.5 jurbanite becomes the most stable while alunite is stable at pH range 3.3-5.7. The mineral formation may follow the reactions below:



Log $K_{eq} = 17.3$



Log K_{eq} = 28.3



Log K_{eq} = 12.0

PHREEQC simulation (Figs 6.37 and 6.38 and Table E7 and E8) indicates that the leachates from the FA and SR, were under-saturated with respect to basaluminite, alunite and jurbanite at pH > 8 but became saturated as the pH dropped below 6. The SR + 25 % FA solid cores had not entered the acidic buffer zone at the time of stopping the drainage experiment. Amorphous Al(OH)₃ and gibbsite were postulated to be precipitating at pH range 4-11 but became under-saturated in the leachates as the pH dropped to below 4. Precipitation of the basic aluminium sulphate minerals therefore could contribute to acid attenuation according to equations 6.16- 6.17 and contribute to buffering of pH in the acidic zone. To test this hypothesis, equilibrium pH for these reactions were calculated and compared with the measured pH. The results showed that the equilibrium pH for basaluminite and alunite was out of range of the measured pH hence could not be contributing to buffering in this range but jurbanite was within the range (pH 3.5-5) (Figs 6.20 and 6.21). Khanna *et al*, (1987) suggested that retention and release of sulphate in acidic forest soils was by the successive precipitation and dissolution of jurbanite. They suggested that jurbanite formed from the dissolution of gibbsite. In this study jurbanite could be forming from amorphous Al (OH)_{3(a)} since no crystalline Al phase was identified. Equilibrium pH for alunite in the FA solid cores is within the range of the measured pH (6.5) for days 36-97 of drainage indicating that it was a strong pH buffer at circum-neutral values. PHREEQC simulation indicates that alunite was over saturated over the same pH range and drainage period (Fig 6.21 and Table E7).

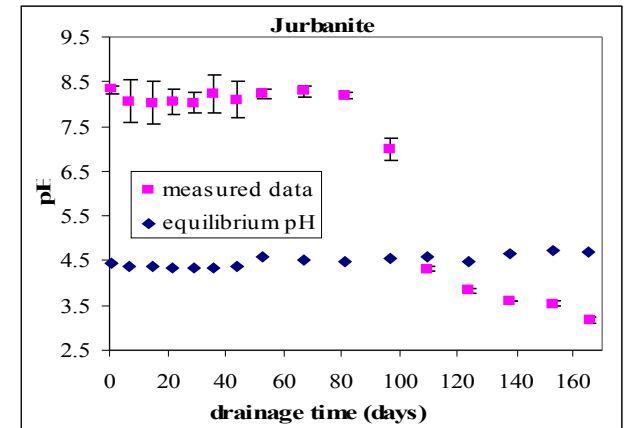
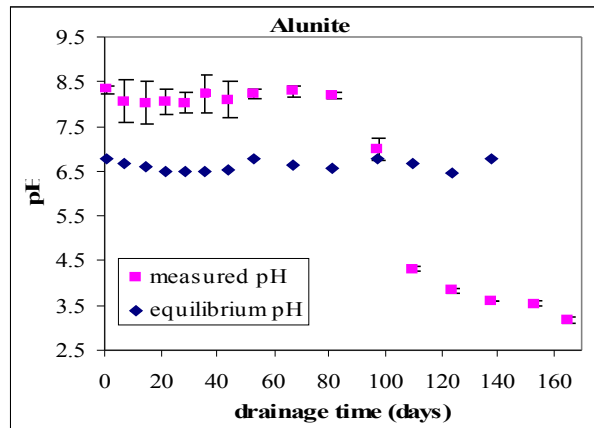
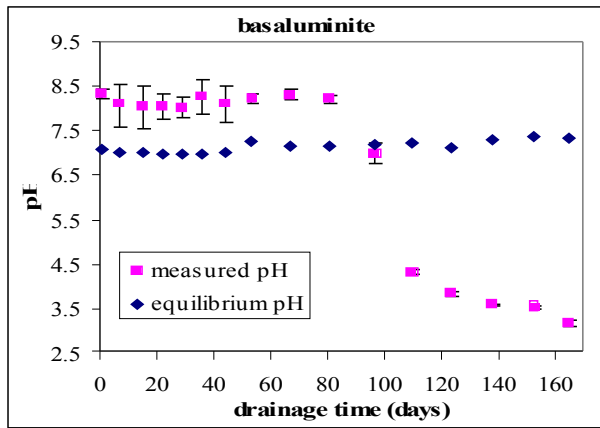


Figure 6.23: Equilibrium pH for precipitating basic aluminium hydroxy sulphates for the SR solid cores compared to measured pH of leachate (error bars represent 1 SD above and below the mean, n=4)

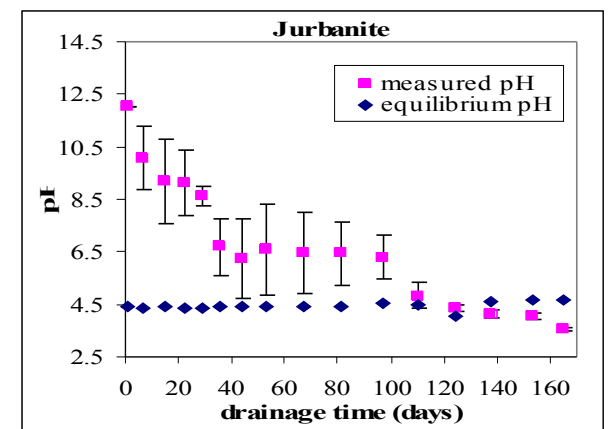
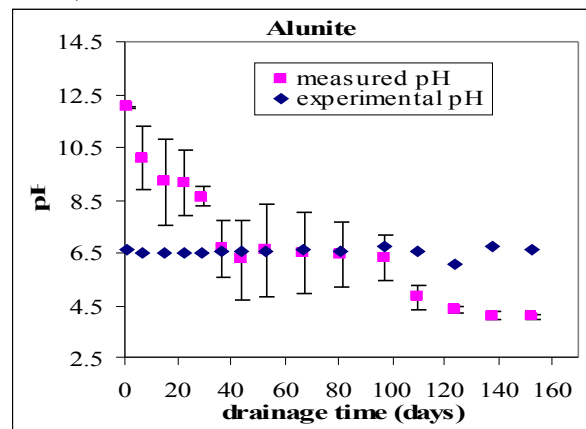
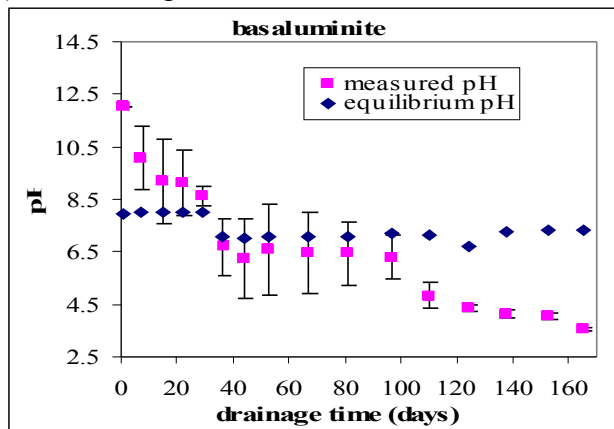
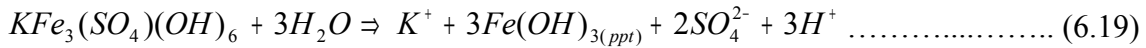


Figure 6.24: Equilibrium pH for precipitating basic aluminium hydroxy sulphates for the FA solid cores compared to measured pH of leachate (error bars represent 1 SD above and below the mean, n=4)

Langmuir (1997) observes that ferric and ferrous sulphates (e.g. coquimbite, jarosites, melanterite and szomolnokite) are strong acid buffers that keep the pH values at or below 3 until they are dissolved. PHREEQC simulation shows that leachates collected over the pH range 6.5-7 were over-saturated with respect to jarosite-K but became under-saturated as the pH dropped to below 5. For the SR cores the leachates were over-saturated with respect to jarosite-K at the pH range of 8-8.3 becoming highly under-saturated as the pH dropped to below 5. Dissolution of jarosite-K at acidic pH can occur through the following reaction (Eq. 6.19)



$$\text{Log } K_{eq} = 10^{-19.5}$$

Calculated equilibrium pH for the dissolution of jarosite-K indicates it could be contributing to the buffering of pH at the acidic buffer zone (pH 3.5-4). The equilibrium pH is within the range of the measured pH (Fig 6.22) but it is clear that as the pH drops to below 3.5 dissolution of jarosite-K alone cannot account for the pH.

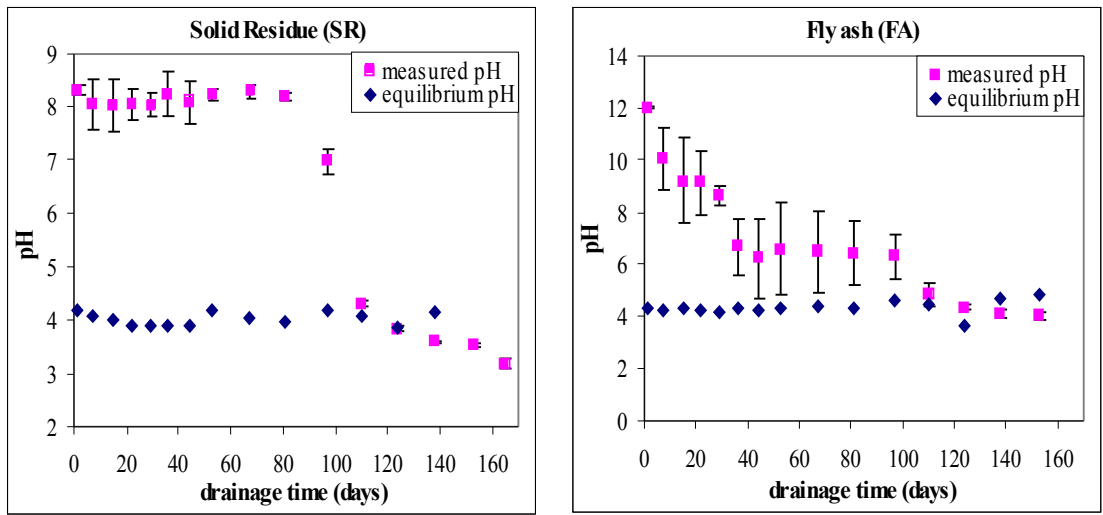


Figure 6.25: Equilibrium pH for the dissolution of jarosite-K for the SR and FA solid cores compared to measured pH of leachate.

(error bars represent 1 SD above and below the mean, n=4)

At 165 days of drainage all the column leachates were showing a pH drop to below 3, this drop in pH corresponded with an increase in the major contaminants concentration in the leachate (Mn^{2+} , Fe, SO_4^{2-}). At 165 days of drainage the Mn^{2+} concentration was higher than in the initial feed for all the columns while for SO_4^{2-} , FA, SR and SR + 5 % FA columns showed high levels. Therefore it can be said that the pH as the drainage came to a close was mainly buffered by free H^+ and formation of hydrogensulphate (HSO_4^-).

5.2.2.1.2 Solid residues (SR) + 6 % Ordinary Portland Cement (OPC) column cores

The SR + 6 % OPC cores exhibited two buffer regions at pH 10.5-11.5 and pH 4 –5.5. On contact with water OPC undergoes hydration releasing $\text{Ca}(\text{OH})_2$ which is highly soluble and causes the high pH of the initial leachates. The rapid drop in pH thereafter probably indicates completion of the hydration reactions and transformation of the released $\text{Ca}(\text{OH})_2$ to ettringite and gypsum (Cocke and Mollah, 1993). Calculation of saturation indices indicates that ettringite was precipitating in the initial leachates upto 15 days when $\text{pH} > 11.0$ (Fig 6.24 and Table E12). SEM-EDX also identified ettringite crystals in the solid cores (Fig 6.23).

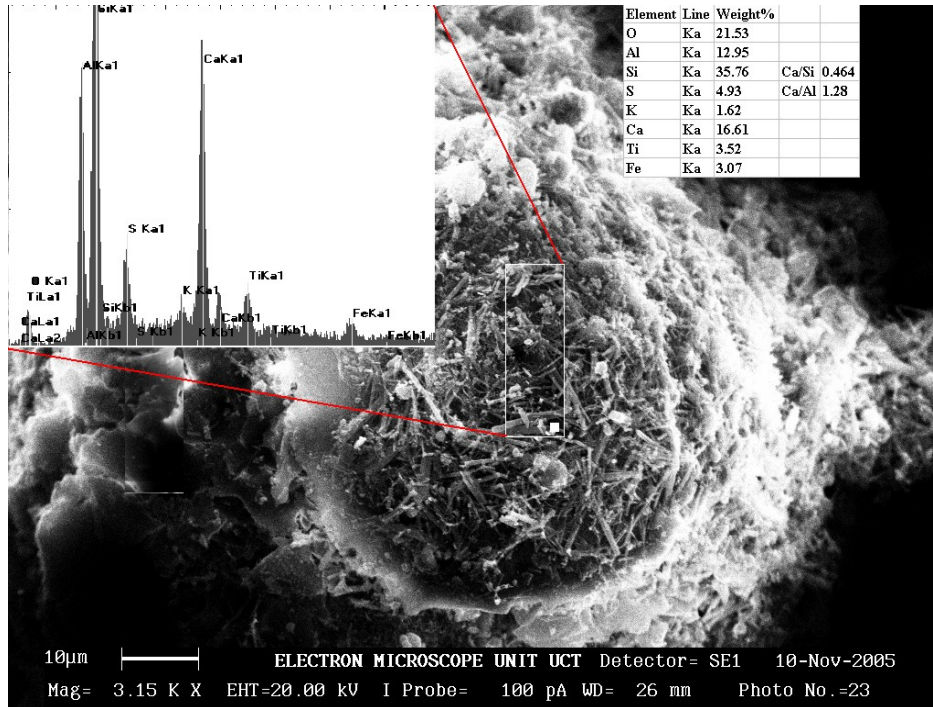


Figure 6.26: SEM micrograph showing ettringite crystals embedded in CSH gel matrix, the EDX pattern is superimposed showing the Ca/Al ratio which approximates that of ettringite. (Strong Si signal is observed, a contribution from underlying CSH gel)

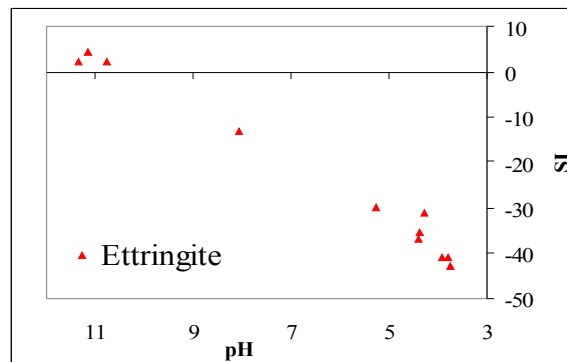


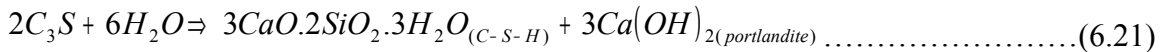
Figure 6.27: Saturation indices for ettringite with pH change as the drainage progressed for the SR + 6 % OPC solid cores.

Ettringite could be formed through two pathways during cement hydration and depending on the chemistry of the water being used. Cocke and Mollah. (1993) summarizes the hydration reactions of cement and points out that the first stage of cement hydration involves the formation of ettringite from calcium aluminates in presence of gypsum (Eq 6.20).



NB-cement nomenclature, A=Al₂O₃

The second stage involves the formation of CSH gel and generation of portlandite (eqn 7.21). SEM and SEM-EDX analysis did show extensive formation of CSH gel (Fig 6.25).



NB-cement nomenclature, C=CaO, S=SiO₂, C-S-H=calcium silicate hydrate gel.

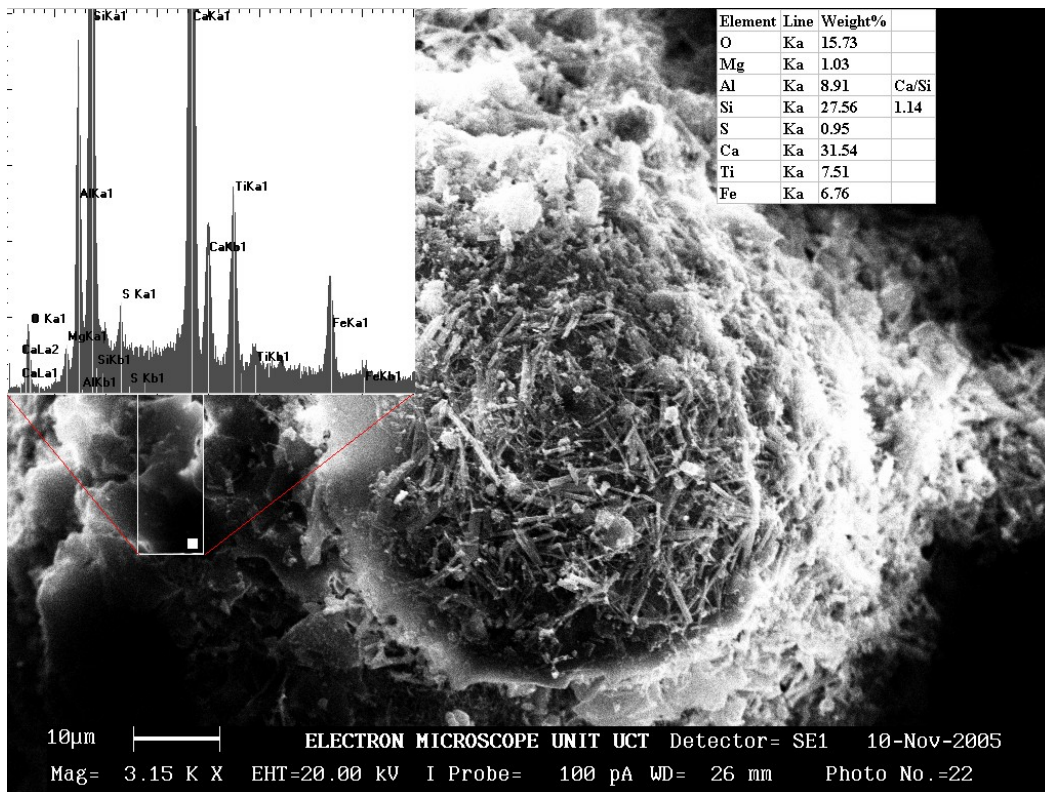
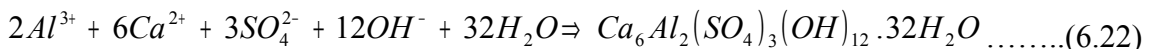


Figure 6.28: SEM micrograph showing the C-S-H gel that embedded the ettringite crystals, the EDS pattern superimposed showing Ca/Si ratio which approximates that of C-S-H gel (Taylor, 1997).

In the presence of high sulphate waters ettringite can form directly during the cement hydration reactions (Eq 6.22). The simulated AMD had high sulphate concentrations (14,407 mg/L) and ettringite precipitation was highly probable.



The SR + 6 % OPC maintained pH of the leachates above 10.5 for 22 days when 1.4 L of SAMD had been added. A sharp drop in pH was thereafter observed. The lack of the buffering at pH 6.5-9 in these SR + 6 % OPC solid core was attributed to the possible aggregation and physical encapsulation of the SR by the C-S-H gel formed (Figs 6.26 and 6.27). The interaction between the SR and SAMD was thereafter likely to be diffusion controlled.

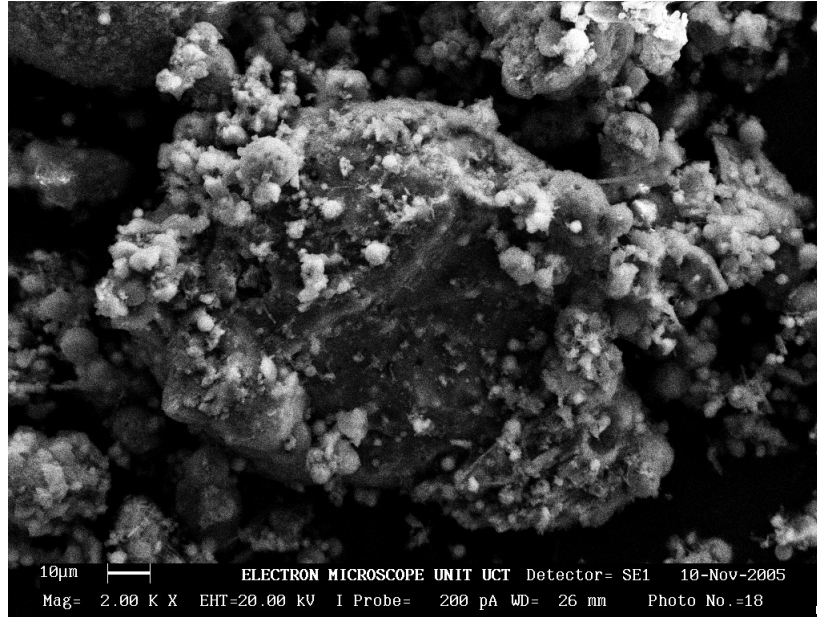


Figure 6.29: SEM micrograph showing extensive aggregation of the solid residue particles in the SR + 6 % OPC column cores.

Figure 6.30: SEM micrograph showing encapsulation of the solid residue particles in the SR + 6 % OPC column cores by a Si-rich gel.

The gel could not be conclusively identified by SEM-EDX.

PHREEQC simulation indicated that as the pH dropped to below 5, the leachates were at equilibrium or slightly over-saturated with respect to jurbanite. Calculation of equilibrium pH for the formation of jurbanite over the drainage period (29-165 days) shows that jurbanite could have been contributing to the buffering of pH at the range 4-4.5 as the drainage progressed (Fig 6.28). At some point the pH differed by 0.5 indicating that formation of jurbanite could not alone account for the pH observed.

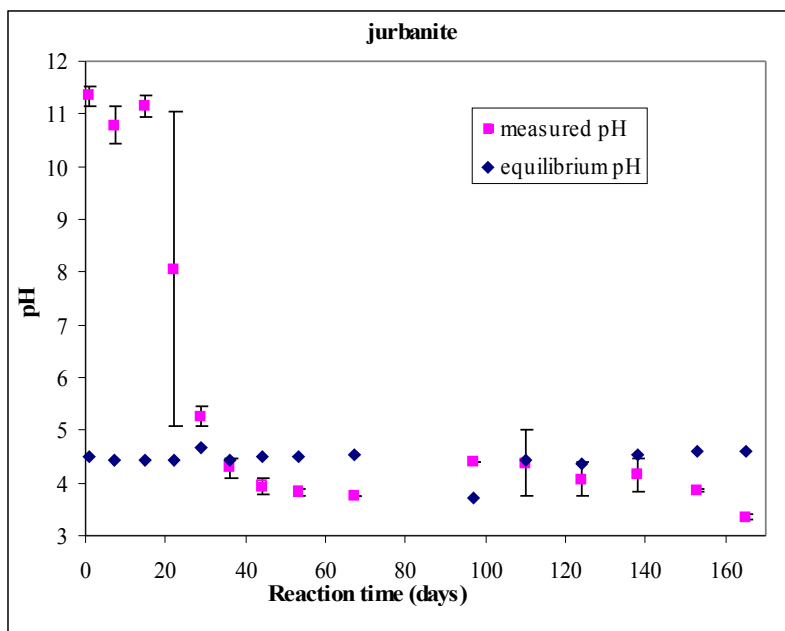


Figure 6.31: Equilibrium pH for the precipitation of jurbanite in SR + 6 % OPC solid cores compared to measured pH of leachate

(error bars represent 1 SD above and below the mean, n=4).

5.2.2.1.3 Conclusions

The FA cores, the solid residue (SR) + FA and solid residue (SR) + 6 % OPC cores were observed to undergo a stepwise acidification process with several acidity attenuation mechanisms involved as the drainage progressed. Initial leachate pH varied as follows: FA>SR +6 % OPC>SR+40 %>SR+25 %>SR≈SR+5 %. Dissolution of CaO in fly ash and SR blended with fly ash impacted high pH in the initial leachates while hydrations reactions in OPC blend SR contributed to high initial pH. Dissolution of SiO_{2(a)} and mullite in the SR contributed to sustained buffering at pH 7-9.5 for SR and fly ash blended SR. Encapsulation of solid residue particles by the calcium silicate hydrate gels (CSH) in OPC blended SR reduced interaction of particles with SAMD hence the buffering at pH 7-9.5 was not observed. At pH 6.5-7 PHREEQC simulation revealed that equilibrium of alunite with amorphous Al (OH)₃ was contributing to the buffering of pH in this range. PHREEQC modelling showed that equilibrium with jurbanite could have contributed to the buffering of pH in the range 4-4.5 in the OPC blend solid residue cores while for SR and FA solid cores equilibrium with K-jarosite could have contributed to the buffering of pH at the 3.5-4 however equilibrium with these minerals alone could not account for the pH observed.

5.2.2.2 Contaminants Attenuation by Fly Ash (FA), Solid Residues (SR), Solid Residues (SR) + 25 % FA and Solid Residues (SR) + 6 % Ordinary Portland Cement (OPC) column blends

The results of the efficiency of contaminants attenuation in SAMD with reaction time for the FA, SR, SR + 25 % FA and SR + 6 % OPC column blends cores are presented. From

the pH profiles discussion it was observed that the significant difference between the various SR + FA blends was that the duration that the leachate pH was sustained at \approx pH 8.0 and was extended to 110 days for the solid residue (SR) + 5 % FA and solid residue (SR) + 25 % FA as compared to the solid residue (SR) column cores. The FA and SR + 40 % FA column cores exhibited similar kinetics. The main mechanism in the fly ash blends is raising the pH and sustaining the buffering capacity at circum-neutral pH for efficiency clean-up of the SAMD, and this was observed to depend on the % FA in the blend. Addition of OPC to the SR was observed to introduce significant changes to the leachate chemistry as compared to the FA blends. On this basis the detailed discussion of the contaminants attenuation mechanisms will be confined to FA, SR, SR + 25 % FA and SR + 6 % OPC solid cores.

5.2.2.2.1 Attenuation in Fly ash column cores

The Figures 6.29- 6.30 below show Fe, Al, Mn, SO_4^{2-} attenuation trends with cumulative volume of SAMD drained through, Ca trends are also included due to its influence on SO_4^{2-} attenuation.

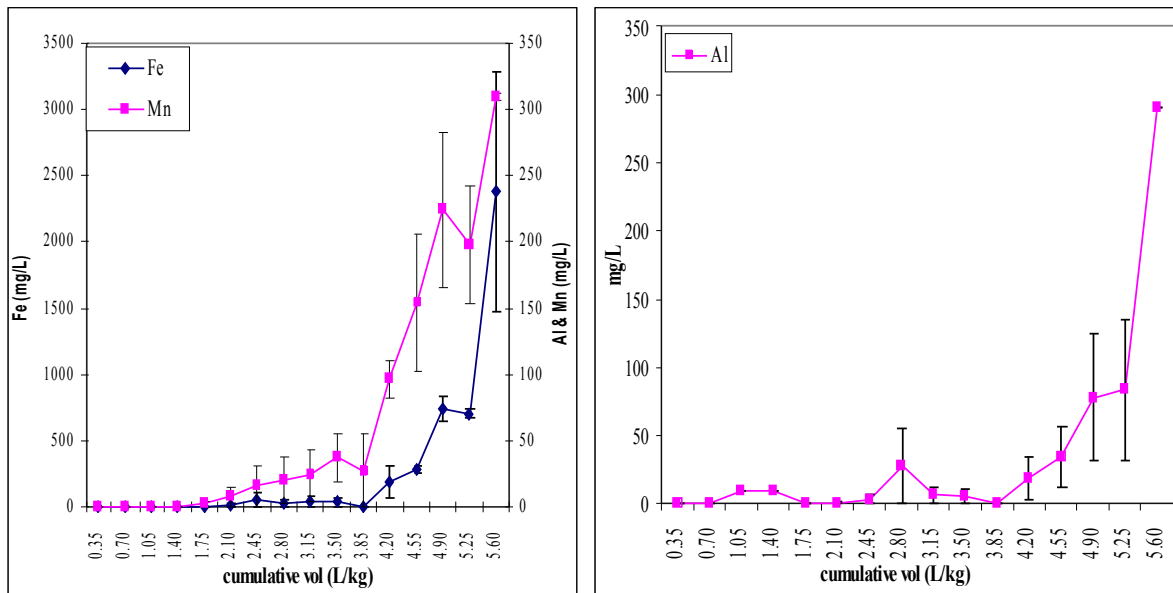


Figure 6.32: Fe, Mn and Al concentration in leachates versus cumulative volume (L/kg) of SAMD for FA solid cores.

(error bars represent 1 SD above and below the mean, n=4)

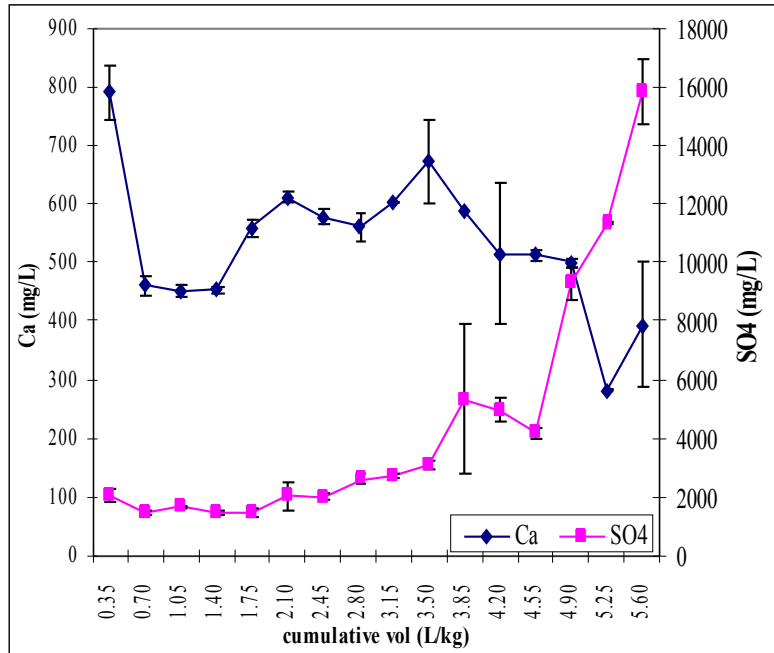


Figure 6.33: Ca and SO₄²⁻ concentration in leachates versus cumulative volume (L/kg) of SAMD for FA solid cores.

(error bars represent 1 SD above and below the mean, n=4)

a. Sulphate and calcium

The simulated AMD contained 14407 mg/L SO₄²⁻ in addition to possible release of SO₄²⁻ from the fly ash. At the onset of the drainage experiments, the pH of the leachate was highly alkaline due to dissolution of CaO in the fly ash (Figure 6.30). The removal of SO₄²⁻ from the AMD was quite efficient with SO₄²⁻ in the leachate dropping to ≈ 2000 mg/L compared to the initial feed, a reduction of 86% (Figure 6.30). Dissolution of soluble Ca salts and subsequent precipitation of gypsum accounts for the low levels of SO₄²⁻ in the leachates. The parallel trends displayed by the concentrations of Ca and SO₄²⁻ in the leachate up to 81 days when 3.5 L of SAMD had drained through probably indicates that gypsum could be controlling their concentration in solution. A gradual increase in SO₄²⁻ concentration in the leachates up to 97 days when 3.85 L of SAMD had drained through was observed as the pH dropped. As the SO₄²⁻ concentration increases, Ca starts to decrease indicating that the Ca concentration has dropped below the level at which gypsum super saturation is attained and gypsum is no longer exerting any control on SO₄²⁻ concentration. The highest concentration of SO₄²⁻ observed at 97 days is still far less than the concentration of the initial feed which indicates SO₄²⁻ attenuation mechanisms are still operational even as the pH enters the acidic buffer region.

b. Total iron, manganese and aluminium

The initial simulated AMD contained 200 mg/L Mn²⁺ and 5000 mg/L total iron (Fe²⁺/Fe³⁺). The alkaline conditions generated due to the dissolution of CaO in the fly ash created optimum conditions for the precipitation of Mn and Fe (Figure 6.29).

Concentration of Fe and Mn observed in the leachates for over 29 days when 1.75 L of SAMD had drained through were low, 0.002-2.24 mg/L Mn and 1.92-2.09 mg/L Fe. At 36 days of drainage the ability of fly ash to remove Mn^{2+} weakened and a gradual increase in concentration was observed with subsequent drainages. However a sharp increase in concentration in the leachate was observed at 110 days corresponding to a pH drop to below 6.0. However the highest Mn^{2+} concentration observed in the leachates was half the initial feed concentration indicating that Mn retention mechanisms were still active. At 36 days of drainage when 2.1 L of SAMD had drained through a gradual increase in concentration of Fe was observed. This was attributed to the un-precipitated Fe^{2+} in the initial feed as Fe^{3+} is precipitated out of solution at this pH 6-8. Analysis of leachates recovered at 36 days confirmed Fe^{2+} which increased in concentration with subsequent drainages. A sharp increase in Fe concentration is then observed at 110 days corresponding to pH drop to below 5.0. This again is attributed to un-precipitated Fe^{2+} in the initial feed. The mechanism of Fe removal is explained in section 6.2.2.6. |

The initial simulated AMD contained 1000 mg/L Al^{3+} . Al concentration in the leachates shows a distinct trend (Figure 6.31). Initially when the pH values are highly alkaline (Fig 6.6), the concentration in the leachate is low (0.021-0.189) mg/L for the first 7 days (Fig 6.29). This is followed by an increase in concentration as the pH drops to the range of 8-11.0. This is again followed by a drop in concentration at 29 and 36 days respectively (0.092 - 0.953 mg/L). A sharp increase in concentration is again observed at 53 days corresponding to a pH drop to below 6.0 The pH GRAPHS ARE PROVIDED INITIALLY AS SEPARATE FIGURES. This increase was attributed to the probable partial re-solubilization of earlier formed precipitates or possible channelling in one of the duplicate columns leading to low pH (4.82) and subsequent dissolution of earlier formed precipitates.

5.2.2.2.2 Solid residue (SR) column cores

The figures 6.31- 6.32 below shows Fe, Al, Mn, SO_4^{2-} attenuation trends with time, Ca trends are also included due to its influence in SO_4^{2-} attenuation.

a. Sulphate and calcium

The initial decrease in Ca concentration observed with FA columns is lacking in SR columns. That decrease was attributed to dissolution of CaO from the FA and reaction with sulphate from the SAMD in the FA columns. The decrease of only 1.29% in CaO content in the SR compared to fly ash reflects the free alkalinity content (as CaO) of the FA that was utilized in the active neutralization of AMD and shows the significant residual alkalinity in the form of CaO (7.14%) remaining in the SR after the primary neutralization step. This residual alkalinity can be slowly released over time in SR used as passive treatment systems. In the case of the SR columns, free alkalinity from FA was utilized during neutralization with AMD prior to recovery of the SR. Thus the increase in Ca that is observed (Figure 6.32) is an indication of the slow release of the residual CaO trapped in the glassy phase of the SR.

The SR initially exhibited a slightly higher efficiency of SO_4^{2-} removal than the fly ash solid cores, with concentrations of SO_4^{2-} below 2000 mg/L achieved up to 44 days when

2.45 L of SAMD had drained through (Fig 6.32). Thereafter an increase in concentration to 6500 mg/L after 53 days was observed when 2.58 L of SAMD had drained through the column. The increase of sulphate levels in the leachate correlated well with the observed Ca depletion. When more Ca was again released a reduction in SO_4^{2-} was again observed. This phenomena has been observed in the fly ash solid cores for elements like Al, Mn and Fe (Fig 6.29 and 6.30) and may be attributed to probable dissolution of precipitates previously formed at higher pH, once any buffering mechanism or the components responsible for the precipitation of gypsum such as CaO, are depleted.

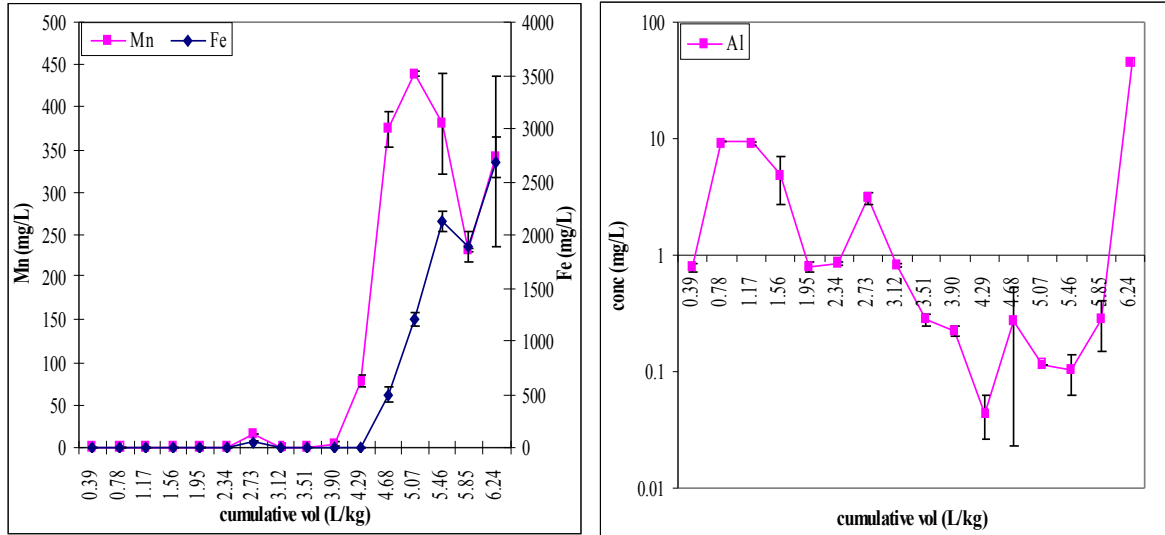


Figure 6.34: Fe, Mn and Al concentration in leachates versus cumulative volume (L/kg) of SAMD for SR solid cores.

(error bars represent 1 SD above and below the mean, n=4)

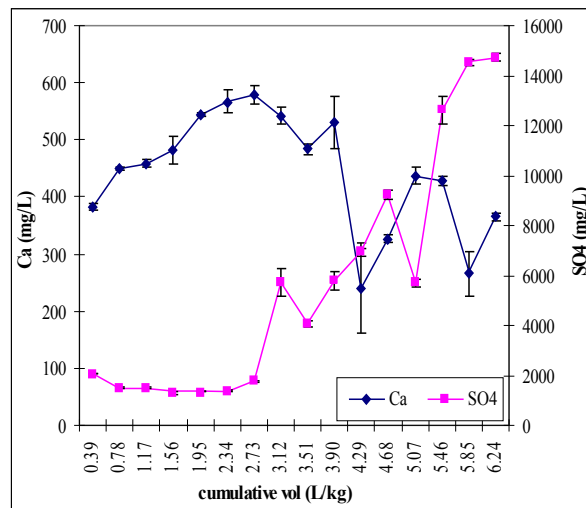


Figure 6.35: Ca and SO_4^{2-} concentration in leachates versus cumulative volume (L/kg) of SAMD for SR solid cores.

(error bars represent 1 SD above and below the mean, n=4)

The SO_4^{2-} concentrations thereafter were observed to increase sharply as the pH further decreased (Fig 6.32) and reached a maximum of 9500 mg/L at the acidic buffer region. This increase indicates that the SO_4^{2-} attenuation components of SR such as CaO are exhausted at between 53 and 67 days on addition of 3.51 L of SAMD. At the end of the drainage experiments the SO_4^{2-} concentration in the leachates was somewhat greater (~15000 mg/L) than in the initial SAMD feed (14407 mg/L). This result indicates that some re-solubilization of precipitates previously formed during the original neutralization step occurred under the strongly acidic conditions. These results indicates that SR may be used for a certain period of time for passive treatment of acid mine drainage or as barrier, but would need to be protected from constant active acidic flows once the attenuation components such as CaO are exhausted, if placed as back fill material. The total load of the sulphate removed and the total load fed was calculated and presented in Table 6.6.

b. Total iron, manganese and aluminium

The SR exhibited high efficiency in removal of Mn and Fe from SAMD. The concentrations for Fe remained below 1.8 mg/L and Mn below 0.24 mg/L up to the 10th drainage (Fig 6.31) on addition of 3.90 L/Kg of SAMD. From day 1 to 81 days the pH of the leachates was greater than 7.0 (Fig 6.8) and precipitation of these elements as insoluble hydroxides accounts for the low concentrations observed. An insignificant and short lived increase in concentration for both elements is observed at 44 days when 2.45 L of SAMD had been added, the increase does not correspond to any pH drop. This transitory increase may be attributed to re-equilibration of soluble species or partial re-dissolution of previously formed precipitates. A sharp increase in concentration for Mn at 97 and 110 days and Fe at 110 days coincided to a drop in pH to below 7.0.

Al concentrations remained below 9mg/L up to 110 days (Fig 6.31) when 4.2 L of SAMD had been added (Table 6.4) Considering the initial Al concentration in the simulated AMD of 1000 mg/L the SR show a high efficiency of Al attenuation. The trend for Al is similar to that of the FA solid cores, showing a small increase within 15 to 22 days up to 10mg/L and again at 44 days (Table 6.4) These increases do not correspond to any pH drop which may point to re-equilibration or dissolution of previously formed precipitates. Unlike the case of FA solid cores where the concentration increases as the pH drops below 5.0, for the SR the concentration remains below 0.27 mg/L. The concentration of Al reaches a maximum of 45 mg/L only under highly acidic conditions (Fig 6.6 and 6.8). This indicates that a great deal of Al is permanently adsorbed onto the surface and that the SR has a high capacity to retain Al.

5.2.2.2.3 Solid residues (SR) + 25 % FA

The Figures 6.33- 6.34 below show Fe, Al, Mn, and SO_4^{2-} attenuation trends over time for the blended mixture of solid residues (SR) + 25 % FA. Ca trends are also included due to its influence in SO_4^{2-} attenuation.

a. Sulphate and calcium

The first few days of drainage of SAMD through the solid residues (SR) + 25 % FA column showed a decrease in the leachate's SO_4^{2-} concentration from an initial SAMD value of 14407mg/L to 2472 mg/L and a further reduction to 909 mg/L at 7 days (Fig

6.34) when 0.7 L of SAMD had been added. The concentration remained below 1596 mg/L up to 44 days when 3.15 L of SAMD had been added (Table 6.4). A peak in concentration is observed at 53 days (5647 mg/L), followed by a subsequent drop to 2321 mg/L at 67 days (Fig 6.34 and Table 6.4). This peak in concentration has been observed in SR (Fig 6.32) and SR + 5 % FA columns (Table E3) and is attributed to re-solubilization of previously formed precipitates. This peak in concentration corresponds to the change of drainage intervals from 7 to 14 days (Table 6.4). The longer 14 day drainage interval imposed dry conditions which led to the precipitation of soluble sulphates after evaporation which re-dissolved on resumption of drainage. At 110 days a sharp increase in SO_4^{2-} concentration to nearly the original SAMD level was observed which coincided to a drop in pH to below 7.0.

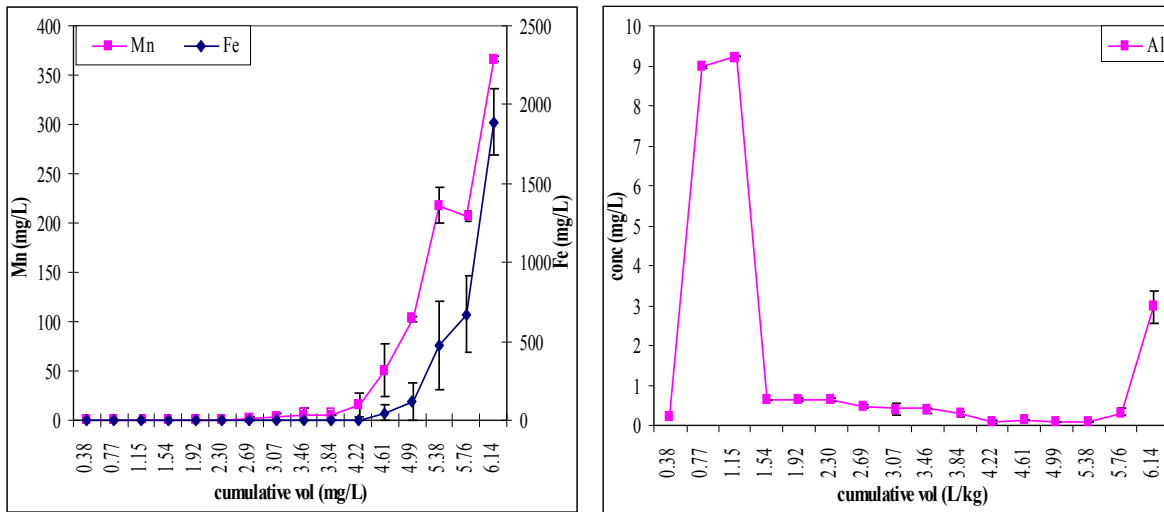


Figure 6.36: Fe, Mn and Al concentration in leachates versus cumulative volume (L/kg) of SAMD for SR + 25 % FA solid cores.

(error bars represent 1 SD above and below the mean, n=4)

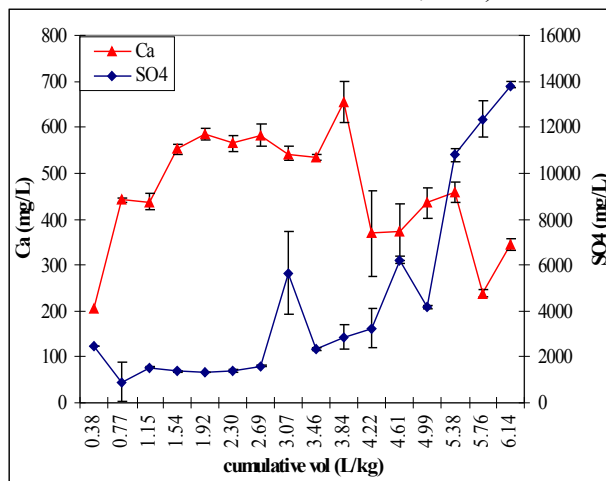


Figure 6.37: Ca and SO_4^{2-} concentration in leachates versus cumulative volume (L/kg) of SAMD for SR + 25 % FA solid cores.

(error bars represent 1 SD above and below the mean, n=4)

Domenech *et al* (2002) observed similar phenomena in their column experiments. These authors observed an accumulation of water soluble sulphates at the top of the column which they attributed to precipitation of soluble sulphates through evaporation.

A similar trend for Ca is observed for SR + 25 % FA solid cores as for SR, and SR + 5 % FA solid cores. The initial decrease at 7 days of drainage observed in FA columns was not observed for SR + 25 % FA columns. In the case of FA columns only, the initial concentration of Ca in the leachate was ~800mg/L which decreased over time. An increasing trend of the leachates from SR or FA blended with the SR columns, from below 400mg/L to approximately 700mg/L over time points to dissolution of the residual CaO in the glassy matrix. In SR or FA blended with the SR the initial Ca concentration in the leachate was thus considerably lower than in the case of the FA column only, showing again that the free alkalinity available in FA had been spent during the primary neutralization reaction and was not immediately available for reaction with the sulphate. A peak in Ca concentration which is observed at 81 days when 4.5 L of SAMD had been added, a phenomenon observed in all other solid cores. The cumulative Ca released varied in the following order: SR+ 25 % FA > SR + 5 % FA > SR + 6 % OPC which strongly indicates that Ca released in the leachate was directly linked to the % FA in the blend. A phenomenon observed for the Ca profile during the drainage experiment is that after the initial rapid depletion of Ca in the case of FA cores, Ca concentrations attain almost a steady state between 22-81 days of drainage (Table 6.4), whereas in the case of SR and SR blends Ca was released steadily into the leachate. This disparity points to two different reaction mechanisms relating to Ca uptake from solution or release from solid phases which must relate to differences in the sources of Ca in the FA blended SR, and shows that Ca in solution (via gypsum formation) was not solely responsible for the considerable reduction of sulphate concentration observed in the leachates from the SR and SR blended columns.

b. Total iron, manganese and aluminium

The concentration of Mn in the leachates decreased immediately from an initial concentration of 200mg/L in the SAMD applied as feed, and remained below 15.7 mg/L and Fe below 2.74 mg/L up to at 97 days (Fig 6.33). The pH of the leachates was maintained above 8.0 during this time. Precipitation of metal hydroxides at alkaline pH could account for the low concentration observed. At 110 days (Table 6.4) a steady increase in concentration is observed corresponding to the breakthrough of the pH front with a subsequent decrease in pH to below 7.0. At 124 days Mn attained a concentration of 200mg/L equivalent to the feed (SAMD) which increased to above 300mg/L with subsequent drainages. This was a strong indication that dissolution of previous formed precipitates, formed during the primary neutralization stage, was active under the acidic regime. Dissolution of the fly ash matrix could also be contributing to the high concentration of Mn because of the Mn content in the FA source (Table 6.5). By 165 days (Fig 6.33 and Table 6.4) the Fe concentration was still at ~2000mg/L and well below the initial SAMD feed concentration of 4726mg/L total Fe.

The concentration of Al exhibits a similar, substantial removal from 1000mg/L to less than 10mg/L over the duration of the experiment as was observed in other column cores (FA, SR, SR + 5 % FA) (Fig 6.33 and Table 6.4). The small peak (please note the scale)

at 7-15 days, corresponds to the phenomena observed in other columns. After 15 days of drainage the concentration remained below 0.64mg/L up to 153 days on addition of 3.6 L of SAMD when a small increase is observed. A highly efficient removal of Al is exhibited throughout the 165 days of leaching considering that the initial feed concentration was 1000 mg/L. This indicates that Al was being strongly adsorbed on the surfaces of the residue solids since the pH had entered the acidic zone and hydrolysis with precipitation of Al hydroxides would be minimal such low pH levels.

5.2.2.2.4 Solid residues (SR) + 6 % Ordinary Portland Cement (OPC)

The Figures 6.35- 6.36 below show Fe, Al, Mn, SO₄²⁻ attenuation trends with time, Ca trends are also included due to its influence in SO₄²⁻ attenuation.

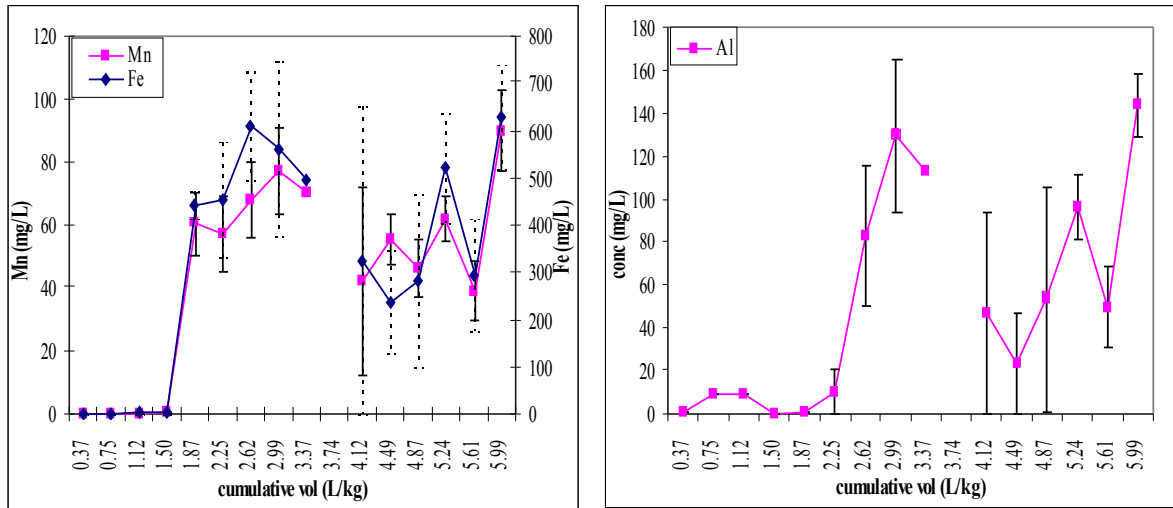


Figure 6.38: Fe, Mn and Al concentration in leachates versus cumulative volume (L/kg) of SAMD for SR + 6 % OPC solid cores.

(error bars represent 1 SD above and below the mean, n=4)

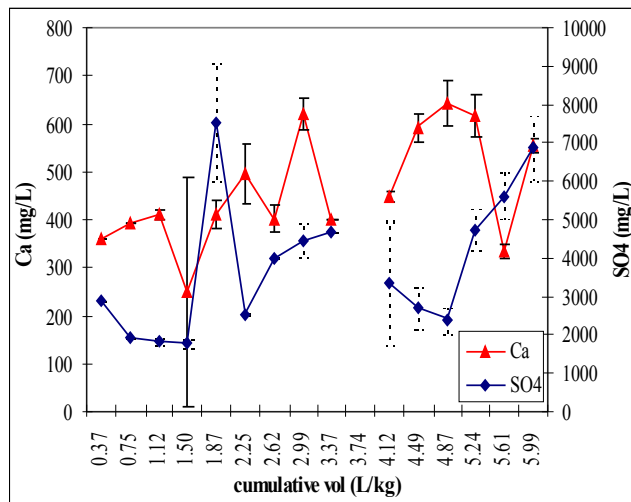


Figure 6.39: Ca and SO₄²⁻ concentration in leachates versus cumulative volume (L/kg) of SAMD for SR + 6 % OPC solid cores.

(error bars represent 1 SD above and below the mean, n=4)

a. Sulphate and calcium

For SR + 6 % OPC solid cores, the SO_4^{2-} concentration in the leachates immediately decreased from the SAMD feed concentration of 14407mg/L to 2875.8mg/L at day 1 and there after maintained a steady concentration for 7 - 22 days (1767-1906 mg/L) (Fig 6.36 and Table 6.4). The high pH generated at day 1 to 22 days may induce several processes that lead to the removal of SO_4^{2-} from the SAMD. Hydration of OPC releases Ca^{2+} and OH^- , Ca^{2+} and SO_4^{2-} thus can precipitate out as gypsum and ettringite in the presence of Al, while Fe, Al and Mn would precipitate out as metal hydroxides with corresponding adsorption of SO_4^{2-} . At 29 days of drainage an increase in concentration to 8000 mg/L of SO_4^{2-} was observed when 1.87 L of SAMD had been added (Table 6.4). This coincided with a pH decrease to below 5.5. The high SO_4^{2-} concentration found in the leachate probably resulted from the re-solubilization of previously formed gypsum and ettringite precipitates. This was followed by a decrease in concentration at 36 days of drainage indicating a re-equilibration. The concentration of SO_4^{2-} at 110 days was still below 3000 mg/L even at low pH, which is a low concentration compared to the other columns. This is a strong indication that SR + 6 % OPC solid cores have a high capacity to adsorb or incorporate SO_4^{2-} even at highly acidic conditions.

b. Total iron, manganese and aluminium

For SR + 6 % OPC solid cores the concentration of Mn in leachates remained below 0.35 mg/L up to 22 days while Fe levels maintained values below 2.07 mg /L (Fig 6.35). The pH of the leachates was maintained above 10.5 up to 22 days. The low concentration of these elements observed was attributed to precipitation of metal hydroxides at the high pH and possible incorporation in the resulting CSH gel. A sudden increase in concentration up to 60 mg/L for Mn and ~400mg/L for Fe was observed in leachates at 29 days on addition of 1.87 L/kg of SAMD (Table 6.4) when the pH decreased to below 6. Peaks in concentration for both elements are then observed at 44 and 53 days and again at 138 days, a phenomenon observed with other elements Zn, Ni and Cu. These peaks in concentration are attributed to dissolution of previously formed precipitates as the pH decreased to below 6 and 4 respectively. At 165 days both elements showed an increase in concentration in the leachates that corresponded to the pH decreasing to below 4 (Fig 6.35). The final concentrations at the close of the leaching experiment were 89.9 mg/L and 628.5 mg/L for Mn and Fe respectively, well below the initial feed concentrations. Therefore the SR + 6 % OPC solid cores showed higher efficiency of Mn and Fe removal compared to all other SR blends even at high acidic conditions. The concentration of both elements remained well below that of the initial feed. This indicates that addition of OPC could have induced other mechanisms for attenuation of these metals that are not prevalent in the other blends, such as encapsulation in the calcium silicate hydrate (CSH) gel.

The concentration profile for Al in the leachates from SR + 6 % OPC solid cores is similar to that observed in leachates from SR + 25 % FA and SR + 40 % FA (data not shown) solid cores. An initial decrease in concentration is observed at 7 - 15 days (9.01 - 9.33 mg/L) (Fig 6.35). This corresponds to the high pH buffer region where formation of $\text{Al}(\text{OH})_4^-$ will dominate (Drever, 1997). From 36 days the concentration increases somewhat in the leachate to a peak at 53 days of drainage (129.4 mg/L). This is a

phenomena observed in other solid cores. These peaks are attributed to the dissolution of previously formed precipitates. However this did not correspond to any pH drop as seen in the other cases as well. An increase in Al concentration to 150mg/L is again observed at 165 days as the pH drops to below 4 which are still well below the feed concentration of 1000mg/L. The concentrations at the close of the leaching experiments are higher than for other solid cores, which indicates that the Al attenuation capacity of this OPC blend is less than other FA blended SR (Figs 6.29, 6.31, 6.33, 6.35).

5.2.2.3 Decontamination efficiency of each column solid core

In order to estimate the efficiency of the column solid cores for passive decontamination of the percolating SAMD, total amounts of elements drained through the solid cores and thereafter recovered in leachates were calculated. The total amount of elements/ions in mmol drained through each column were calculated based on the total SAMD volume drained through for each column solid core and the recovery was calculated based on the leachate collected for the study period. The calculated % contaminant removed by each column is presented in Table 6.6.

Table 6.10: Total amount in mmol of ions drained through each column and calculated % contaminant removed by each column solid core

The removal achieved is graphically depicted in Fig 6.37 and shows that overall the SR and various blended wastes removed a significant amount of the total amount of contaminants fed through the various columns. A total input of 207.56 mmol of Al, 501.34 mmol of Fe, 41.51 mmol of Mn and 806.79 mmol of SO_4^{2-} was added to each column over the time of the study.

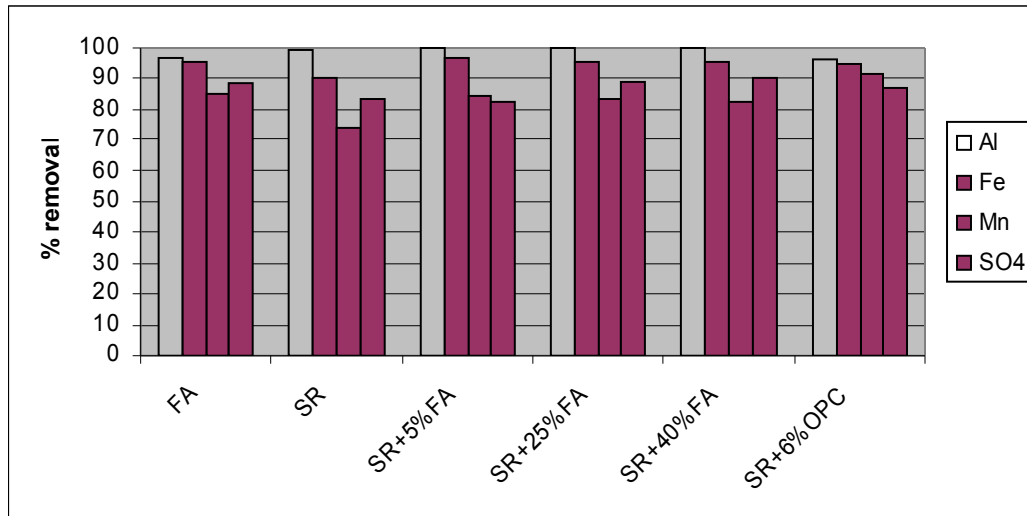


Figure 6.40: % removal of contaminants from the total SAMD feed solution applied.

The removal of contaminant elements from the feed solution by the various materials packed into columns can be seen in Table 6.6 and Figure 6.37 where the total amount (mmol) of each constituent drained through the columns and the total amount (mmol) of each constituent in the leachates for each column may be seen. The FA, SR + 25 % FA, SR + 40 % FA and SR + 6 % OPC have a somewhat higher capacity than SR and SR + 5 % FA column solid core to remove SO₄²⁻. Apart from the SR + 6 % OPC solid core the SO₄²⁻ removal seems to be favoured by increasing the % of FA in the blend and in general fairly good removal of between 82 and 90% of the total SO₄²⁻ feed is observed for the various materials tested. Dissolution of CaO from the added fly ash and formation of Ca(OH)₂ from OPC hydration in presence of SO₄²⁻ results in precipitation of gypsum.

The FA, SR + 5 % FA, SR + 25 % FA, SR + 40 % FA and SR + 6 % OPC exhibit superior capacity to attenuate Fe and Mn²⁺ than the SR solid cores which removed only 90% of Fe and 73% of Mn. In general high removal was observed for Fe (above 90%) and slightly less so for Mn (above 82%). This is a result of the free alkalinity from the unreacted fly ash or lime added in the various blends that raised the pH of the SAMD solution resulting in the precipitation of more of those elements from solution.

The SR and SR + FA solid cores however show a higher capacity than other columns in removal of Al (above 99%). The SR solid cores were observed to have a high capacity to remove Al even at low pH. The precipitated compounds are stable in all the columns and do not re-enter the leachate solution. The concentration of these elements only starts to increase in the leachate once the alkalinity in each column has been exhausted and the pH drops to below 4. Based on the calculated decontamination efficiency the dissolution observed in the early stages of the drainage experiments does not seem to be significant in contributing to release of previously immobilized contaminants.

5.2.2.4 Contaminants attenuation mechanisms and solubility controls

The contaminants profiles in the leachates as discussed in sub-sections 6.2.3.4.1-6.2.3.4.4 suggest several mechanisms that could be involved in attenuation of the

contaminants as the percolating SAMD feed interacts with the solid residue particles, fly ash particles and solid residue + OPC particles. The high efficiency of the FA and SR + FA blends to remove Fe, Mn and SO_4^{2-} suggests that the high alkalinity generated leads to precipitation of the heavy metals and that dissolution of CaO in the fly ash and components in the aluminosilicate matrix could be playing a role in the long-term attenuation of sulphate. The high efficiency of the SR cores to remove Al could be attributed to the slow release of alkalinity and buffering of pH at 6.5-9 for a large duration of the study. This pH range is within the hydrolysis pH of Al ($pK= 4.9$) and precipitation of various Al hydroxides is greatly favoured. The attenuation efficiency of the various blends for removal of various contaminants seems to be tied to the solid cores being able to release sufficient alkalinity. It is observed that the contaminants concentration in the leachates starts to increase as the pH drops to below 4 signalling the depletion of the alkalinity in the solid cores. However the SR + 6 % OPC cores exhibit high attenuation efficiency even as the pH drops to below 4. The above observations indicate that as the SAMD percolates through the solid cores the contaminants are subsequently attenuated by precipitation, co-precipitation and adsorption reactions. The following sub sections discuss the probable mechanisms responsible for the attenuation of the contaminants and the probable secondary solid-phase controls on the concentration of each contaminant in the leachates. Mechanisms responsible for the attenuation of the contaminants and the probable secondary solid-phase controls on the concentration of each contaminant in the leachates are discussed with reference to the various contaminant species.

5.2.2.4.1 Sulphate and calcium

The FA, and blends of SR + FA in column solid cores exhibited high efficiency of SO_4^{2-} attenuation for the first 81 days of the drainage experiments (Fig 6.30, 6.32, 6.34 and Table 6.4). The efficiency of SO_4^{2-} removal was greatly dependent on the % FA in the blended SR. The SR + 40 % FA column core maintained lower levels of SO_4^{2-} than the FA core for a longer duration of the study (Fig 6.30) indicating that SO_4^{2-} removal was through a combination of several mechanisms. The removal of SO_4^{2-} through gypsum precipitation seems to occur through two steps:

- a) Initial rapid dissolution of CaO from the fly ash and precipitation thereafter as gypsum in presence of the SO_4^{2-} rich SAMD for the FA and SR + FA column cores. This is observed in the initial rapid drop of SO_4^{2-} in these solid core leachates.
- b) An almost constant level of SO_4^{2-} is maintained thereafter which is parallel to the level of Ca in the leachates. This is most noticeable in the SR leachates. Dudas (1981) observed that after the initial rapid release of Ca from fly ash, slow dissolution of the fly ash matrix with concomitant nearly constant levels of Ca is observed. The Ca levels observed for the SR and SR + FA cores after the initial dissolution can be attributed to the dissolution of the fly ash matrix and could partly account for the continuous attenuation of SO_4^{2-} .

Calculation of saturation indices (SI) indicates that initially the leachates were slightly undersaturated with respect to gypsum for the FA, SR and SR + FA solid cores attaining equilibrium at between 36-110 days of drainage (Table 6.4 and Table E7, E8, E9, E10 and E11). This attainment of equilibrium corresponds to the peak in Ca concentration for

the mentioned column solid cores (Fig 6.30, 6.32, 6.34). This is most noticeable for SR cores where the leachates become highly oversaturated at between 53-97 days of drainage. This confirms that after the initial rapid dissolution of CaO, dissolution of CaO locked in the aluminosilicate matrix was occurring gradually as the drainage progressed and this is most evident in the SR solid cores. As the Ca concentration drops with increase in acidity the leachates become slightly undersaturated again and this is paralleled by an increase in SO_4^{2-} concentration in the leachates. Plots of $\text{Log } a_{\text{SO}_4^{2-}}$ versus $\text{Log } a_{\text{Ca}^{2+}}$ strongly points (a represents activity of the species as determined using PHREEQC) to control of Ca and SO_4^{2-} by precipitation of gypsum (Fig 6.37 and 6.38).

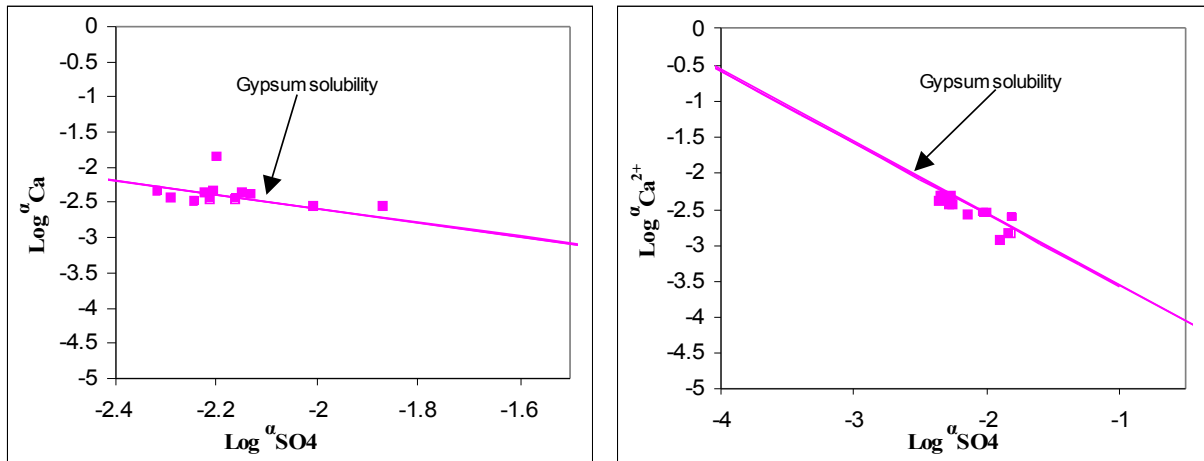


Figure 6.41: Plots of log SO_4^{2-} activity versus log Ca activity showing control of SO_4^{2-} and Ca by gypsum solubility in the leachates for FA and SR solid cores.

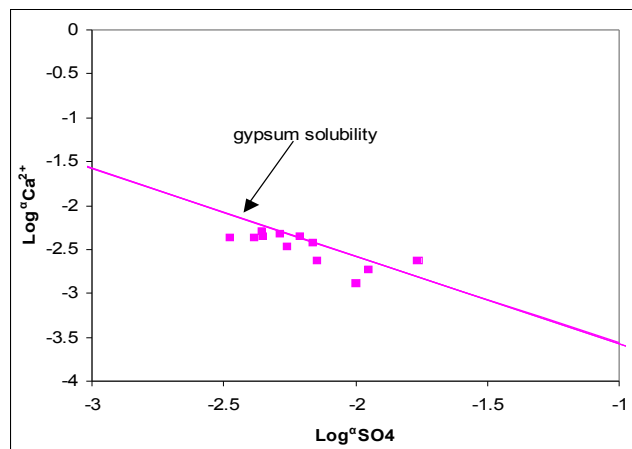


Figure 6.42: Plots of log SO_4^{2-} activity versus log Ca activity showing control of SO_4^{2-} and Ca by gypsum solubility in the leachates for SR + 25 % FA column solid cores.

Further evidence of the gypsum precipitation came from the XRD, SEM and SEM-EDX analysis of the leached solid cores. SEM and SEM-EDX analysis revealed extensive formation of gypsum crystals in the entire length of the solid core from top to bottom (Figs 6.39 and 6.40). High frequency of gypsum crystals was however observed in the top section of each column which showed the highest degree of interaction with SAMD. The presence of gypsum crystals on all the sections of the leached solid residue cores

indicates that under the strongly acidic conditions, gypsum was not significantly re-dissolved if any. XRD identified gypsum in all sections of the leached solid cores (Fig E1-E4).

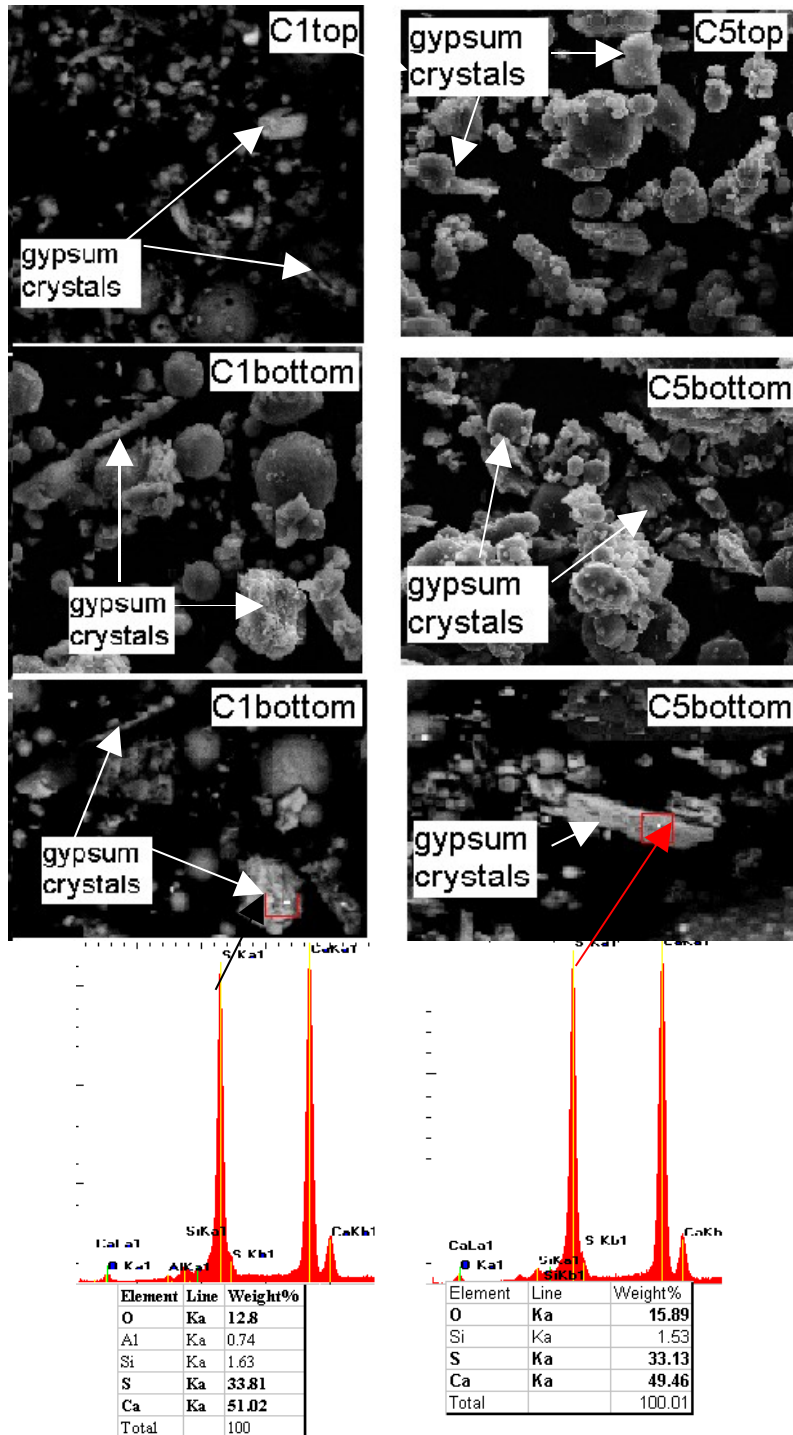


Figure 6.43: SEM micrographs of leached SR from column 1 (FA) and column 5 (SR + 25 % FA) showing gypsum crystals.

(C1, C5bottom-Backscattered signal, C5top-secondary electron signal, with accompanying EDX pattern of the spots analyzed (enclosed in a box)).

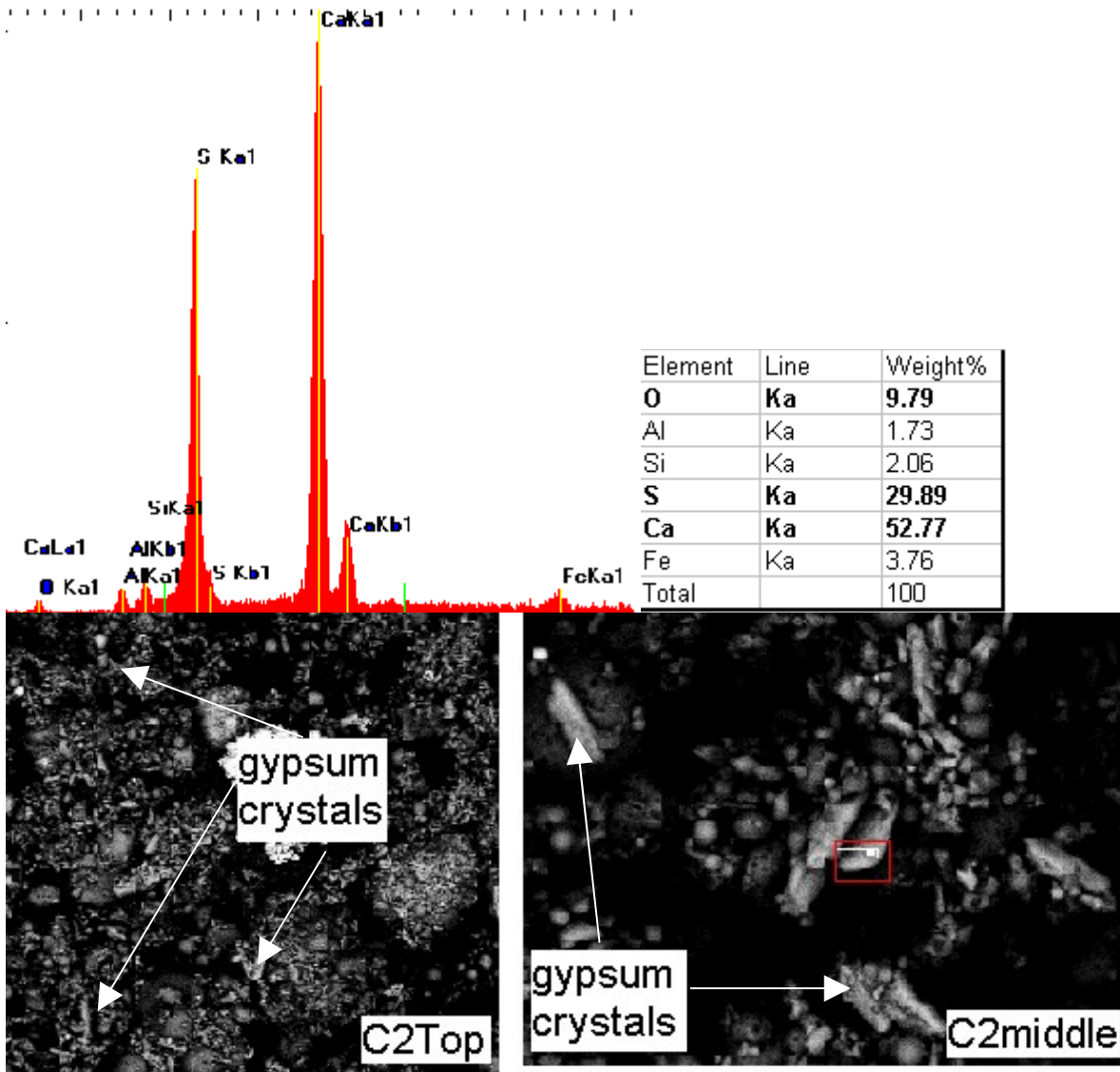


Figure 6.44: SEM micrographs of leached SR from column 2(SR) showing gypsum crystals.

(C2Top –Backscattered signal, magnification=500. C2middle-backscattered electron signal, magnification=3000, with accompanying EDX pattern of the spots analyzed (enclosed in a box)).

An observation of the SO_4^{2-} trends for the FA and SR + FA solid cores (Fig 6.30, 6.32, 6.34) indicates that the attenuation of SO_4^{2-} is greatest when Fe and Al are low in the leachates. Attenuation of SO_4^{2-} by Fe and Al mineral phases could be through structural incorporation in phases such as jarosite, jurbanite, alunite and adsorption by amorphous ferric hydroxides. This becomes more evident as the pH drops to below 4 when precipitation of ferrous and ferric ions decreases and a corresponding increase in SO_4^{2-} is observed. PHREEQC simulation predicted these minerals to be precipitating within the pH range 4.5-11 (Tables E7-E12). Regression of log Fe activity versus log SO_4^{2-} activity within the pH range 4.5-11 for the FA and SR + FA column cores leachates indicated a strong relationship (Fig 6.41 and Table 6.7). Although the strong regression observed is not a confirmation of any chemical interaction between SO_4^{2-} and Fe-mineral phases being formed, it's a strong indication that a form of interaction could be taking place.

This interaction could be structural incorporation of SO_4^{2-} or adsorption on the precipitate surfaces. Seth and Ghazi (1997) points out that Fe precipitates formed in acid mine drainage environments consist of between 600-800 mmol/kg SO_4^{2-} . Seth and Elliot (2000) go on to confirm that 30-45 % of this SO_4^{2-} is ammonium oxalate soluble meaning it's associated with the amorphous iron oxy hydroxides. Despite the high levels of Fe and Al precipitating out within this pH range no Fe or Al mineral phase was detectable by XRD.

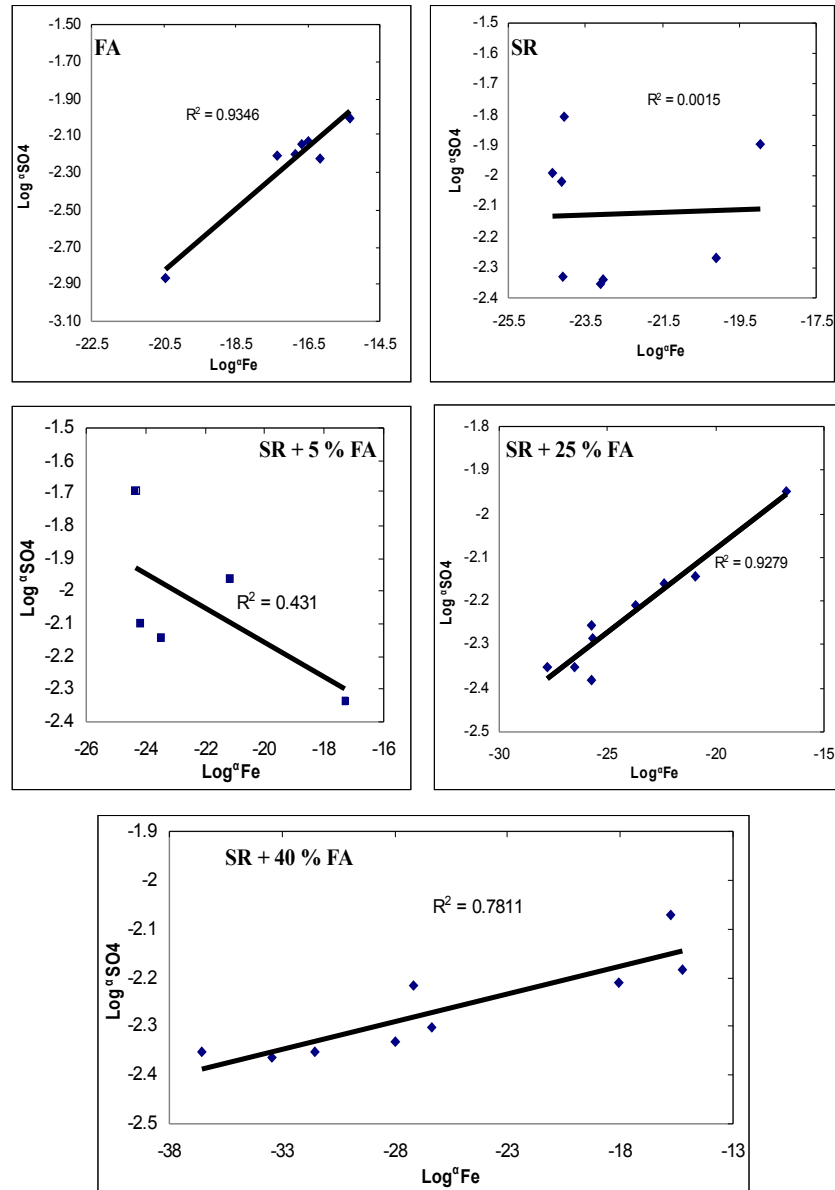


Figure 6.45: Regression analysis of log Fe activity versus log SO_4^{2-} activity for the FA, SR and SR + FA solid cores leachates.

(R^2 reported at 95 % confidence limits).

Table 6.11: Drainage time (days) and pH range over which the regression was calculated.

Column core	drainage time(days)	pH range	R ²
FA	36-124	7-8	0.9346
SR	22-97	8-8.5	0.002
SR +5% FA	44-110	7.5-6.5	0.431
SR +25% FA	15-124	8-8.5	0.9279
SR +40% FA	22-124	4.5-11	0.7811

In the SR + 6 % OPC column cores two mechanisms for the attenuation of SO_4^{2-} were identified as the column core acidified.

- a) Ettringite formation at the high pH generated by OPC hydration in presence of Al and SO_4^{2-} from SAMD.

Extensive formation of ettringite was observed in all sections of the column solid core, which means it did not undergo dissolution as the pH dropped to below 4. Ettringite is known to undergo incongruent dissolution to gypsum and Al-hydroxide at $\text{pH} \leq 10.7$ (Myeni *et al.*, 1998). Observation of ettringite in the leached solid cores is contrary to Myeni *et al.* (1998) findings since the pH dropped to below 4 during the course of the drainage experiments. Analysis of the ettringite crystal by SEM and SEM-EDX revealed that they were coated by C-S-H gel which resisted dissolution under the acidic regime and kept the crystals intact (Fig 6.25).

- b) Gypsum formation as the leaching of CaO in the aluminosilicate matrix occurred gradually as the drainage progressed. Apart from the sharp increase in SO_4^{2-} content in the leachates at 29 days of drainage, the Ca and SO_4^{2-} trends appear to be parallel which probably indicates control by the same mineral phases over the range 29-124 days when the pH was maintained at 4-4.5. SEM and SEM-EDX, XRD identified the presence of gypsum in all the sections of the leached solid cores (Fig 6.42 and Figs E1-E4). PHREEQC simulation predicted control of Ca and SO_4^{2-} by gypsum solubility except at $\text{pH} > 10.5$ (Fig 6.43) when ettringite was at equilibrium in the leachates (Fig 6.24).

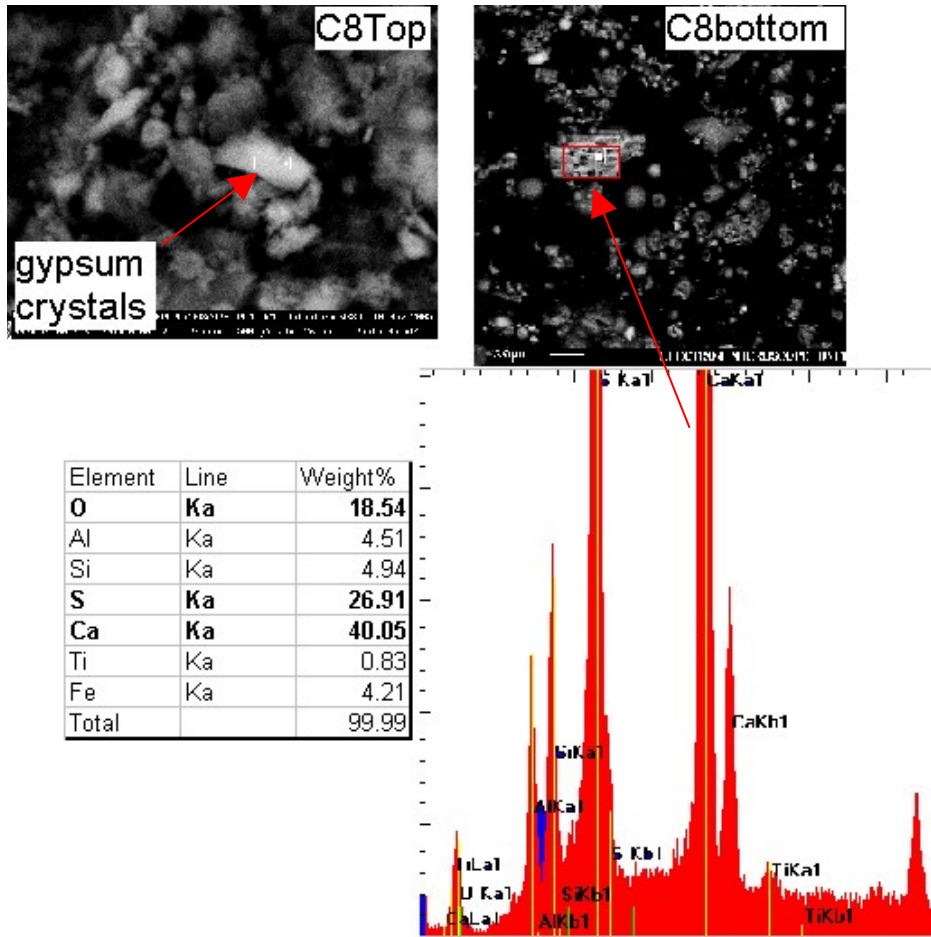


Figure 6.46: SEM micrographs of leached SR from column 8(SR + 6 % OPC) showing gypsum crystals.

(C8Top–Backscattered signal, magnification=14000. C8bottom-backscattered electron signal, magnification=1000, with accompanying EDS pattern of the spots analyzed (enclosed in a box)).

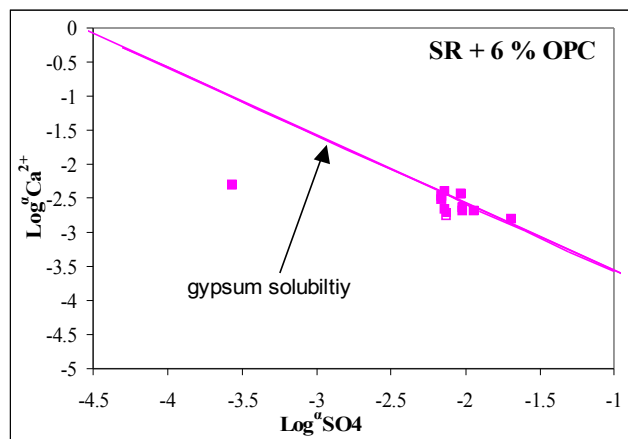


Figure 6.47: Plots of $\log \text{SO}_4^{2-}$ activity versus $\log \text{Ca}$ activity showing control of SO_4^{2-} and Ca by gypsum solubility in the leachates for SR + 6 % OPC column solid cores.

5.2.2.4.2 Sulphate, Aluminium and Iron

Alkaline materials such as fly ash are highly reactive when exposed to natural waters and are known to modify soil element dissolution patterns and to control surface and sub-surface water quality in their vicinity (Mattigod *et al.*, 1990). Reaction of these materials with acidic mine drainage produces varying pH(6-12) depending on FA: AMD ratios and the chemistry of the AMD (W.M. Gitari *et al.*, 2006). In addition the fly ash releases dissolved Ca, Al, Mg, K, Si and SO_4^{2-} which interact with species in AMD to form gypsum, amorphous Fe hydroxides, Al-hydroxides and jarosite-K type mineral phases.

It is reported that at near neutral pH Al-hydroxide phases such as gibbsite ($\gamma\text{-Al(OH)}_3$), boehmite ($\gamma\text{-AlOOH}$), and diaspore ($\alpha\text{-AlOOH}$) are precipitated (Fillipek *et al.*, 1987; Doye and Duchesne, 2003) and control Al concentration in solution.

Several authors have observed that in a $\text{Al}_2(\text{SO}_4)_3\text{-H}_2\text{O}$ system basic Al-sulphates, such as basaluminite ($\text{Al}_4(\text{OH})_{10}(\text{SO}_4) \cdot 5\text{H}_2\text{O}$), aluminite ($\text{Al}_2(\text{OH})_4(\text{SO}_4) \cdot 7\text{H}_2\text{O}$), jurbanite ($\text{Al}(\text{OH})\text{SO}_4 \cdot 5\text{H}_2\text{O}$) and alunogen ($\text{Al}_2(\text{SO}_4)_3 \cdot 17\text{H}_2\text{O}$) form at acidic pHs (<7) (Adams and Rawajfih, 1977; Khanna *et al.*, 1987, Nordstrom and Alpers, 1999). Myeni *et al.*, (1998) confirmed that at below neutral pH Al-hydroxy sulphate phases can precipitate rapidly in natural systems and thus potentially influence major and trace elements dynamics in these environments.

Due to the high concentration of Ca from fly ash, Al and SO_4^{2-} from SAMD, the system created in the drainage experiments for the FA, SR, SR + FA and SR + OPC resembled more closely a $\text{Ca(OH)}_2\text{-Al}_2(\text{SO}_4)_3\text{-H}_2\text{O}$ system that is open to Fe^{3+} , Fe^{2+} , K^+ , Mg^{2+} , Mn^{2+} , SiO_2 and CO_3^{2-} since the drainage was done in the open hence the system was in contact with CO_2 from the atmosphere. Myeni *et al.*, (1998) observed that addition of Fe^{3+} , Mg^{2+} , K^+ and Si(OH)_4^0 to the system formed Fe oxy-hydroxides, minerals belonging to alunite-jarosite family, clays and a zeolite leonhardtite.

Langmuir and Whittemore (1971) have suggested that Fe(OH)_3 and poorly crystalline goethite are the first ferric phases to precipitate when AMD is neutralized, but transforms to more stable phases, crystalline goethite and lepidocrocite. At $\text{pH} > 5$ ferrihydrite is formed from rapid oxidation and hydrolysis of Fe^{2+} (Schwertmann and Tylor, 1989).

Interaction of SAMD with FA, SR, SR + FA and SR + OPC solid cores generated pH in the leachates ranging from highly alkaline (> 10.7), near neutral (8-9.5) and acidic (3-6.5) as the drainage progressed. This section will discuss the precipitation of Fe-hydroxides, Al-hydroxides, Al-hydroxysulphates and jarosite-K type of minerals in the column solid cores as the acidification progressed to pH below 4 and justify their role in the control of the major contaminants and eventual clean-up of the percolating SAMD. Discussion will mainly center on the FA, SR, SR + 25 % FA and SR + 6 % OPC with an occasional mention of the other solid cores. Obtaining a positive proof that a solution is in equilibrium with a mineral phase involves two steps, first a saturation-state calculation based on a complete analysis of the water should indicate that the mineral occurs under equilibrium conditions and secondly examination of the reaction mixture should reveal evidence of crystal formation. Analysis of the leached SR by XRD did not reveal any crystalline Al or Fe mineral phases. This could be due to the amorphous nature of the

phases precipitating out or due to the diluting effect of the fly ash matrix. Therefore the SEM and SEM-EDX has been used extensively to analyze the leached solid residue cores to help draw a conclusion on the likely mineral phases that precipitated. As stated earlier in Chapter three the SEM-EDX analysis can only provide semi-quantitative data hence the identification of the mineral phases should be taken with caution. However several authors have successively utilized SEM-EDX technique to identify and confirm the presence of mineral phases in different matrices (Catalan *et al.*, 2002; Myeni *et al.*, 1998; Warren and Dudas, 1985)

5.2.2.4.3 Fe (oxy) hydroxides and Al (oxy) hydroxides

PHREEQC simulation predicted several Fe (oxy) hydroxides and Fe-hydroxysulphate to be precipitating on interaction of the SAMD with the FA, SR, SR + FA and SR + OPC. Calculation of SI indices indicated the leachates to be supersaturated with respect to Fe(OH)_{3(a)}, ferrihydrite, goethite and hematite (Figs 6.45, 6.46 and Table E7-E12). Precipitation of these phases during the drainage experiments explains the low concentrations observed in the leachates for 110 days (Figs 6.29, 6.31, 6.33, 6.35 and Table 6.4). An observation of Figures 6.45 and 6.46 shows that goethite, hematite and magnetite were predicted to be the most stable phases for all the column solid core leachates. The leachates were at over-saturation at pH > 3.4. Goethite and hematite have similar solubility (K_{sp} hematite $\cong 10^{-43}$ - 10^{-42} , K_{sp} goethite $\cong 10^{-44}$ - 10^{-43}) and stability, but slow kinetic rates, hampered nucleation of the stable phases by contaminating metal ions and anions, this leads to the formation of poorly crystalline metastable phases such as ferrihydrite and microcrystalline goethite at surficial temperatures (Bigham, 1994; Schwertmann and Taylor, 1989). At pH>6 the leachates appear to be over-saturated or at equilibrium with ferrihydrite, Bigham. (1994) observed that ferrihydrite is likely to form in slightly acidic to alkaline solutions with high levels of dissolved Fe. At pH > 4.29 the leachates appear to become saturated with Fe(OH)_{3(a)}.

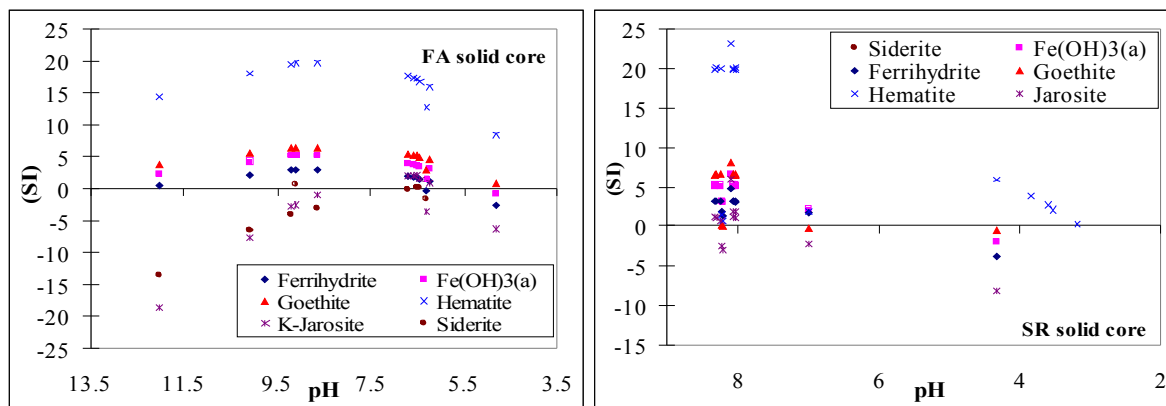


Figure 6.48: Plots of saturation indices for precipitating Fe-bearing mineral phases during the leaching study period for FA and SR solid core leachates.

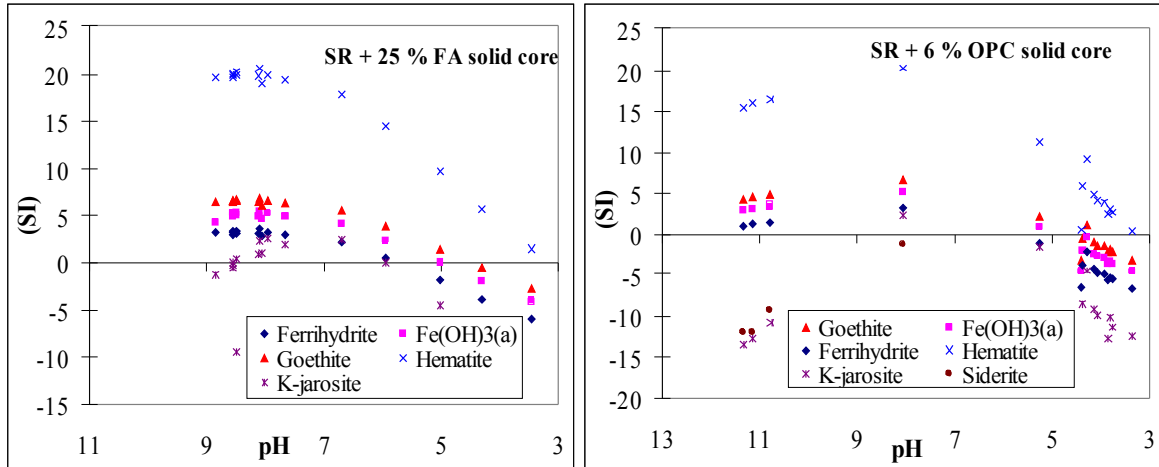
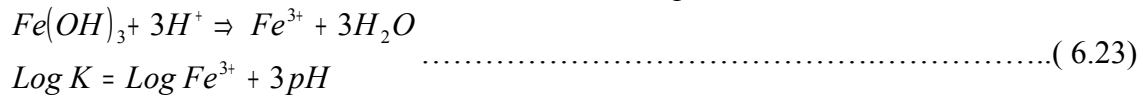


Figure 6.49: Plots of saturation indices for precipitating Fe-bearing mineral phases during the leaching study period for SR + 25 % FA and SR + 6 % OPC solid core leachates.

The leachates were observed to be saturated with respect to K-jarosite and (H, K, Na) Fe₃(OH)₃(SO₄)₂ over a pH range 6.43-6.68 for the FA solid core, 6.99-8.33 for the SR core and 5.94-8.52 for the SR + 25 % FA core but under-saturated over the entire pH range for the SR + 6 % OPC core (Figs 6.45 and 6.46). Azzie, (2002) observed over-saturation in a set of mine waters with respect to K-jarosite over the pH range 2.5-8 from some South African coal mines.

At this point it can be tentatively concluded that although PHREEQC predicts crystalline Fe-(oxy) hydroxides to precipitate, the precipitates are amorphous, XRD and SEM-EDX could not detect any crystalline phases in the leached SR. The high SO₄ content and presence of interfering ions in the SAMD could have hampered the precipitation of these mineral phases. These observations strongly suggest that some kind of amorphous Fe-oxy (hydroxide) phase is being formed. A regression of log activities of Fe³⁺ versus pH over the entire pH range indicates two slopes at pH>5.5 and the second at pH<5.5 (Fig 6.47). If precipitation of a pure ferric hydroxide was controlling the chemistry of the leachates (Eq 6.23) a plot of log Fe³⁺ activity versus pH should have a slope of -3. The observed 1st slope (-2.04 to -2.89) is roughly consistent with precipitation of a ferric hydroxide phase. The leachate chemistry is controlled by reactions involving Fe³⁺ at pH>5.5 while at pH <5.5 the chemistry of the leachate could not be interpreted in-terms of Fe³⁺ alone.



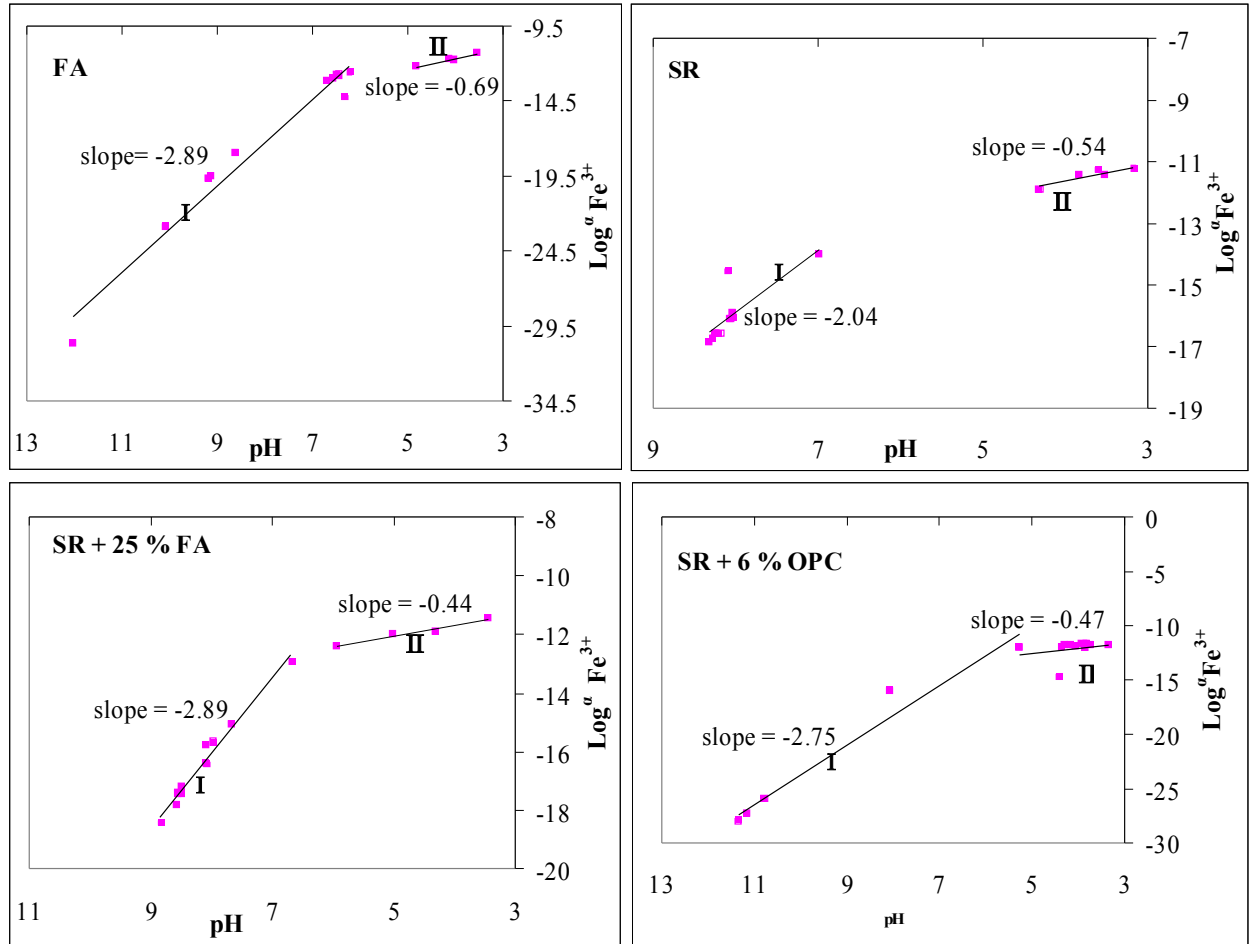


Figure 6.50: Logarithmic activity plot of the dissolved Fe^{3+} versus pH in the leachates for FA, SR, SR + 25 % FA and SR + 6 % OPC solid cores.

For a given condition, acid mine water may precipitate not the most over-saturated solid phase but other metastable phases due to kinetic reasons. If an equilibrium state is reached among all the dissolved species in aqueous phase and the precipitating solid phases, equilibrium modelling may be successively utilized to interpret and predict the chemical compositional changes of water solutions due to precipitation. The calculated activities of the dissolved species are plotted on a solubility diagram to deduce the precipitating mineral phases, since the alignment of the plotted activities may have different slopes according to the stoichiometry of the precipitating solid phase (Nordstrom, 1982; Sullivan *et al.*, 1988).

The Figures 6.48- 6.51 shows the solubility diagrams for selected phases in the Fe_2O_3 - SO_3 - H_2O system at 298 K and the calculated activities of Fe^{3+} in the leachates for the FA, SR, SR + 25 % FA and SR + 6 % OPC solid cores.

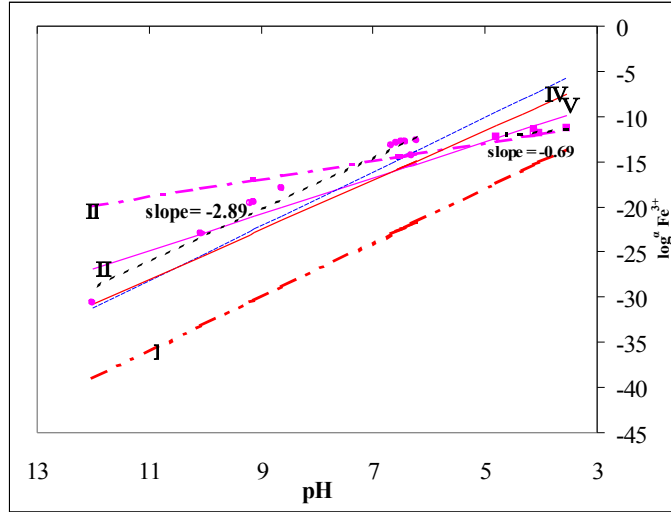


Figure 6.51: Plot of $\log \text{Fe}^{3+}$ activity against pH for the FA solid core leachates with solubility lines

(plot of $\log \text{Fe}^{3+}$ activity against pH for the FA solid core leachates with solubility lines for, I- $\text{Fe}(\text{OH})_3(\text{a})$ ($\log a_{\text{Fe}^{3+}} = -3-3\text{pH}$), II-K-jarosite ($\log a_{\text{Fe}^{3+}} = -2.8-2\text{pH}$), III- FeOHSO_4 ($\log a_{\text{Fe}^{3+}} = -7.94-\text{pH}$), IV-Ferrihydrite ($\log a_{\text{Fe}^{3+}} = 4.89-3\text{pH}$), V-Schwertmannite ($\log a_{\text{Fe}^{3+}} = 2.52-2.75\text{pH}$) added. Solubility lines calculated using an average $\log a_{\text{K}^+} = -2.15$ and $\log a_{\text{SO}_4} = -2.12$ (calculated values from measured data) and $\log K_s$ values for $\text{Fe}(\text{OH})_3(\text{a})$, K-jarosite, FeOHSO_4 , Ferrihydrite, Schwertmannite are -3 , -14.8 , -10.06 , 4.891 and 18.0 respectively (Jae Young yu, 1996; Bigham et al., 1996).)

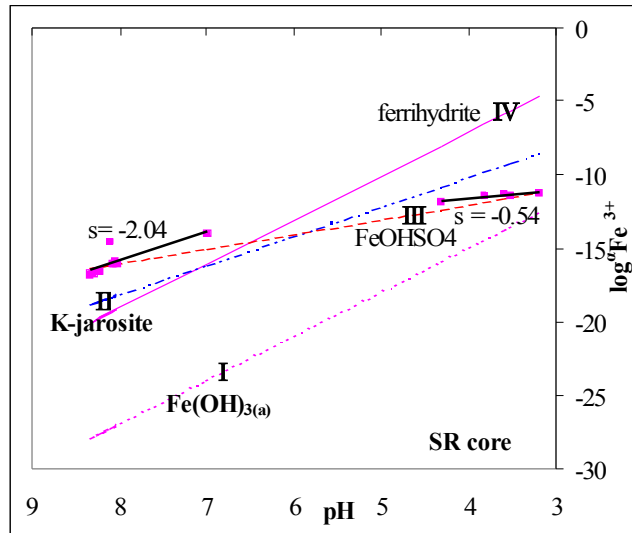


Figure 6.52: Plot of $\log \text{Fe}^{3+}$ activity against pH for the SR solid core leachates with solubility lines.

(Plot of $\log \text{Fe}^{3+}$ activity against pH for the SR solid core leachates with solubility lines for, I- $\text{Fe}(\text{OH})_3(\text{a})$ ($\log a_{\text{Fe}^{3+}} = -3-3\text{pH}$), II-K-jarosite ($\log a_{\text{Fe}^{3+}} = -2.16-2\text{pH}$), III- FeOHSO_4 ($\log a_{\text{Fe}^{3+}} = -8.03-\text{pH}$), IV-Ferrihydrite ($\log a_{\text{Fe}^{3+}} = 4.89-3\text{pH}$), added. Solubility lines calculated using an average $\log a_{\text{K}^+} = -3.25$ and $\log a_{\text{SO}_4} = -2.03$ (calculated values from measured data) and $\log K_s$ values for $\text{Fe}(\text{OH})_3(\text{a})$, K-jarosite, FeOHSO_4 , Ferrihydrite, are -3 , -14.8 , -10.06 and 4.891 respectively (Jae Young yu, 1996; Bigham et al., 1996a and 1996b)).

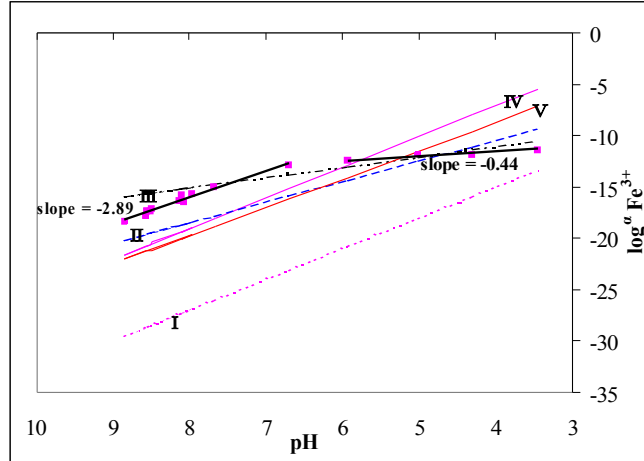


Figure 6.53: Plot of log Fe³⁺ activity against pH for the SR + 25 % FA solid core leachates with solubility lines

(plot of log Fe³⁺ activity against pH for the SR + 25 % FA solid core leachates with solubility lines for, I-Fe(OH)₃(a) ($\log^a \text{Fe}^{3+} = -3-3\text{pH}$), II-K-jarosite ($\log^a \text{Fe}^{3+} = -2.46-2\text{pH}$), III-FeOHSO₄ ($\log^a \text{Fe}^{3+} = -7.07-\text{pH}$), IV-Ferrihydrite ($\log^a \text{Fe}^{3+} = 4.89-3\text{pH}$), V-Schwertmannite ($\log^a \text{Fe}^{3+} = 2.51-2.75\text{pH}$) added. Solubility lines calculated using an average $\log^a \text{K}^+ = -3.23$ and $\log^a \text{SO}_4 = -2.09$ (calculated values from measured data) and log K_s values for Fe(OH)₃(a), K-jarosite, FeOHSO₄, Ferrihydrite, Schwertmannite are -3, -14.8, -10.06, 4.891 and 18.0 respectively (Jae Young yu, 1996; Bigham *et al.*, 1996a and 1996b)).

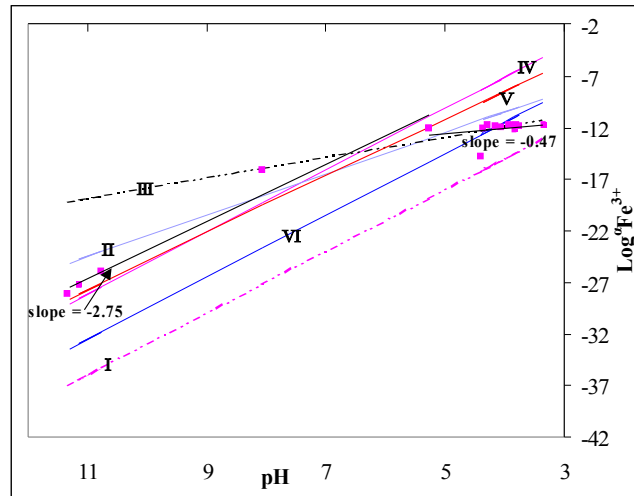


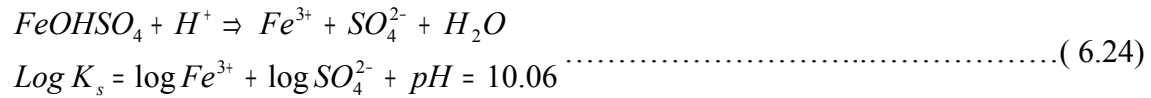
Figure 6.54: Plot of log Fe³⁺ activity against pH for the SR + 6 % OPC solid core leachates with solubility lines

(Plot of log Fe³⁺ activity against pH for the SR + 6 % OPC solid core leachates with solubility lines for, I-Fe(OH)₃(a) ($\log^a \text{Fe}^{3+} = -3-3\text{pH}$), II-K-jarosite ($\log^a \text{Fe}^{3+} = -2.55-2\text{pH}$), III-FeOHSO₄ ($\log^a \text{Fe}^{3+} = -7.83-\text{pH}$), IV-Ferrihydrite ($\log^a \text{Fe}^{3+} = 4.89-3\text{pH}$), V-Schwertmannite ($\log^a \text{Fe}^{3+} = 2.52-2.75\text{pH}$), α -goethite ($\log^a \text{Fe}^{3+} = 0.5-3\text{pH}$) added. Solubility lines calculated using an average $\log^a \text{K}^+ = -2.90$ and $\log^a \text{SO}_4 = -2.12$ (calculated values from measured data) and log K_s values for Fe(OH)₃(a), K-jarosite, FeOHSO₄, Ferrihydrite, Schwertmannite, α -goethite are -3, -14.8, -10.06, 4.891, 18.0 and 0.5 respectively (Jae Young yu, 1996; Bigham *et al.*, 1996a and 1996b)).

The activity diagrams reveal that the leachate water chemistry is mainly controlled by ferrihydrite at pH>5.5 for all the solid cores, precipitation of K-jarosite and schwertmannite may also control the leachate chemistry at pH 4-5.5 but it is not obvious (Figs 6.48- 6.51). Bigham *et al* (1996) in a study involving ochreous precipitates and

associated acidic mine drainage waters observed that above pH 5.5, mineralogy of the precipitates was influenced by ferrihydrite and those at intermediate pH values by schwertmannite. At pH <5.5 FeOH₂SO₄ seems to control the chemistry of the leachates.

If the chemistry of the leachates at pH < 4.5 was being controlled by the precipitation and dissolution of FeOH₂SO₄ (Eq 6.24) then a plot of calculated logarithmic activity of Fe³⁺ versus pH at constant SO₄ activity should have a slope of -1.



The observed regression slope at pH <5.5 ranged between (-0.44 to -0.69) (Fig 6.47) which is fairly close to -1 and suggests control of the leachate chemistry by FeOH₂SO₄. Sullivan *et al.* (1988) performed an oxidizing equilibrium study with oil shales containing pyrite and suggested that Fe³⁺ activities were controlled by FeOH₂SO₄ solubility at a relatively low pH

The Fe³⁺ activities are several orders of magnitude higher than those predicted from control by ferrihydrite. Apparent super-saturation with ferric hydroxides or ferrihydrite occurs at high pH values above about 4. The super-saturation may be explained by substitution or adsorption of sulphate for hydroxide ions or on ferrihydrite and the formation of a more soluble schwertmannite-like phase. Apparent super-saturation with respect to ferric hydroxide might also be explained by the formation of colloidal iron particles that passed through the 0.45µm nucleopore membranes. This apparent super-saturation behavior of ferrihydrite and other ferric hydroxide is commonly seen for both surface waters and ground waters (Nordstrom and Alpers, 1999). Regression analysis of the calculated log Fe³⁺ activity of the leachates yielded slopes ranging from (-2.04 to -2.89) which is inconsistent with the precipitation of a pure ferric hydroxide phase or ferrihydrite. Kimball *et al.* (1994) found a regressed slope of -2.23 from iron data on the acid mine waters during a neutralization experiment. The observed slope (-2.04 to -2.89) could be interpreted to represent a ferric hydroxide in which SO₄²⁻ has partially substituted hydroxide, i.e, Fe(OH)_{2.04-2.89}(SO₄)_{0.11-0.96}. Infra-red analysis of the leached SR identified structural sulphate which confirms incorporation of sulphate in the Fe-bearing mineral phases. Bigham (1994) noted that ferrihydrite is associated with mine drainage in the pH range of about 5 – 8. The slope of -2.04 to -2.89 is observed in the pH range 6.5-8.5 in this study. This suggests that the apparent stoichiometry is more likely to represent a sulphate-substituted ferrihydrite, schwertmannite or other hydrous ferric oxide with a molar Fe: OH of 1: (2.04-2.89). It is also possible that mixtures of different iron minerals phases are precipitating from these leachates over this pH range and the slope is not clearly resolvable into a particular reaction.

PHREEQC simulation predicted several Al (oxy) hydroxides and Al-hydroxysulphate mineral phases to be precipitating on interaction of the SAMD with the FA, SR, SR + FA and SR + OPC as the drainage progressed. Calculation of SI for Al-bearing mineral phases indicated super-saturation with respect to amorphous Al(OH)₃, basaluminite, gibbsite, jurbanite, alunite, boehmite, diaspore and ettringite at different stages of the drainage process (Figs 6.52- 6.55 and Tables E7-E12). The saturation state of the Al-bearing mineral phases appear to follow different patterns in each of the column probably due to the different pH regimes and chemical processes generated by the FA, SR, SR +

25 % FA and SR + 6 % OPC solid cores. The saturation of the Al-hydroxides ($\text{Al(OH)}_{3(a)}$), boehmite, gibbsite and diaspore seem to occur within the same pH range (4-11.3). At pH 4 (close to 1st $\text{pK}_1(\text{Al}^{3+}) = 4.91$) some form of hydrolyzed aluminum will precipitate (Fillipek *et al.*, 1987). However for SR (pH6.99) and SR + 25 % FA (pH 5) solid cores the pH at which initial saturation is predicted is higher than for FA (pH 4) and SR + 6 % OPC (pH 4). A possible reason could be that at high FA concentration and in presence of OPC large amounts of sulphate is removed even at lower pH hence formation of the (oxy)-hydroxides is more favourable.

At pH 4, FA and SR + 6 % OPC solid core leachates, sulphate concentration were in the range (2500-5000 mg /L) while SR + 25 % FA and SR leachates were in the range (6500-9000 mg /L). At pH>7 the sulphate concentration was below 2500 mg/L for SR and SR + 25 % FA core leachates which corresponds to the saturation range of boehmite, gibbsite and diaspore. The saturation of alunite, jurbanite and basaluminite on the contrary appear to be saturated at higher pH (5-8.09) for SR and SR + 25 % FA solid cores leachates, while for FA and SR + 6 % OPC solid cores, saturation is observed at pH (3.36-6.68). Ettringite saturation was only observed in FA and SR + 6 % OPC solid cores at pH > 11.15. Ettringite is only stable at pH>10 otherwise it undergoes incongruent dissolution to gypsum and Al-hydroxides (Myeni *et al.*, 1998).

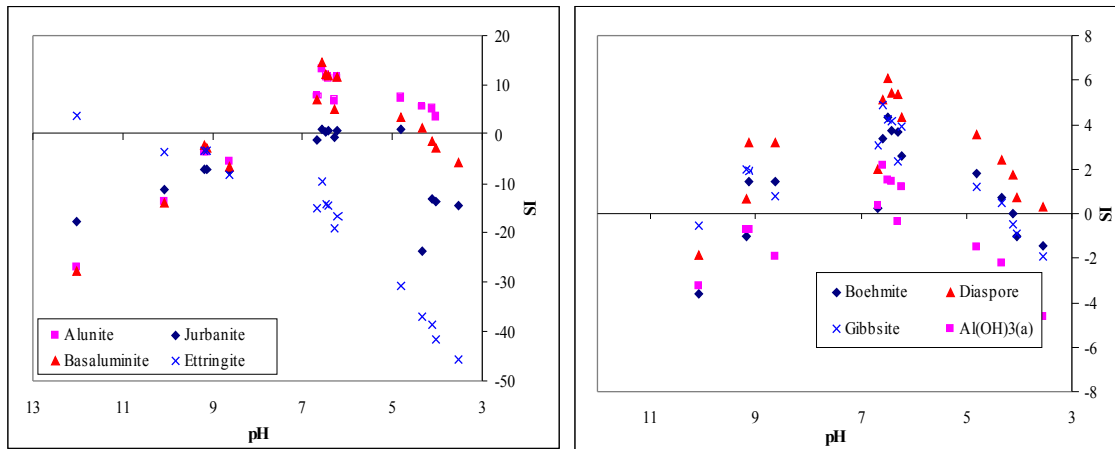


Figure 6.55: Plots of saturation indices for precipitating Al-(oxy) hydroxide and Al-hydroxysulphates mineral phases during the leaching study period for FA solid core leachates.

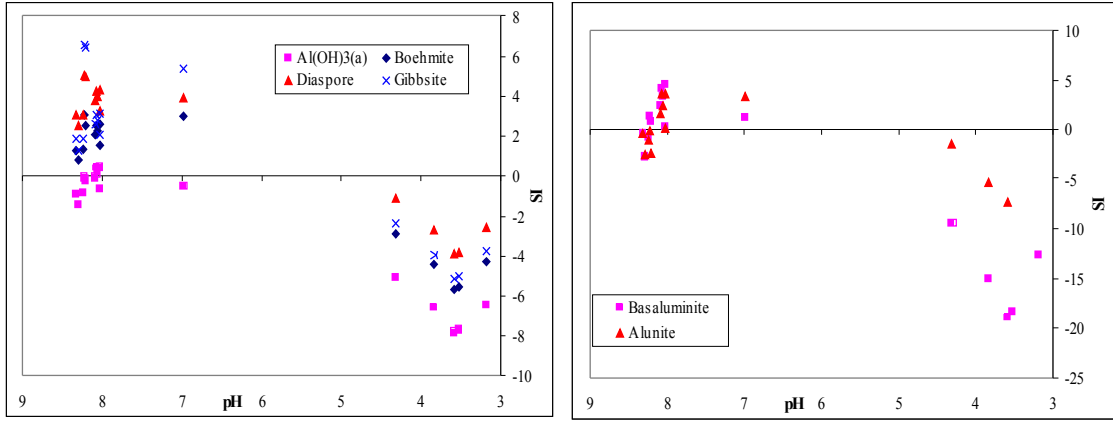


Figure 6.56: Plots of saturation indices for precipitating Al-(oxy) hydroxide and Al-hydroxysulphates mineral phases during the leaching study period for SR solid core leachates.

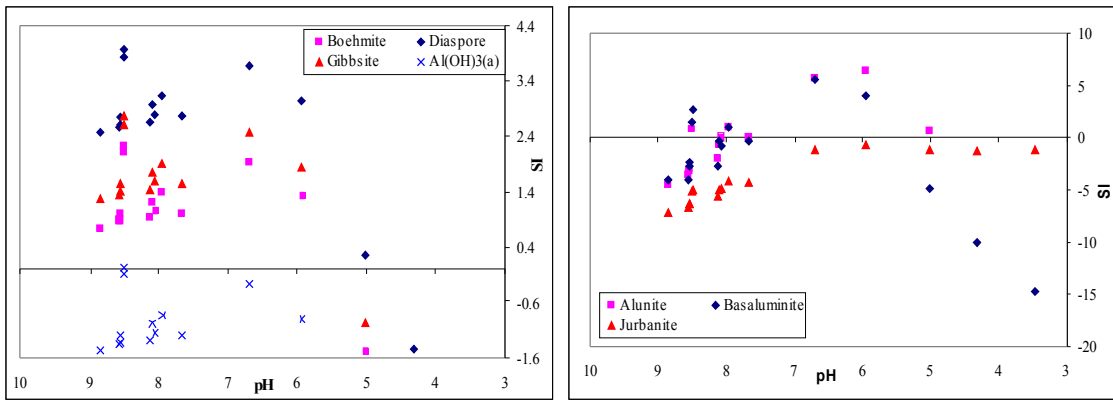


Figure 6.57: Plots of saturation indices for precipitating Al-(oxy) hydroxide and Al-hydroxysulphates mineral phases during the leaching study period for SR + 25 % FA solid core leachates.

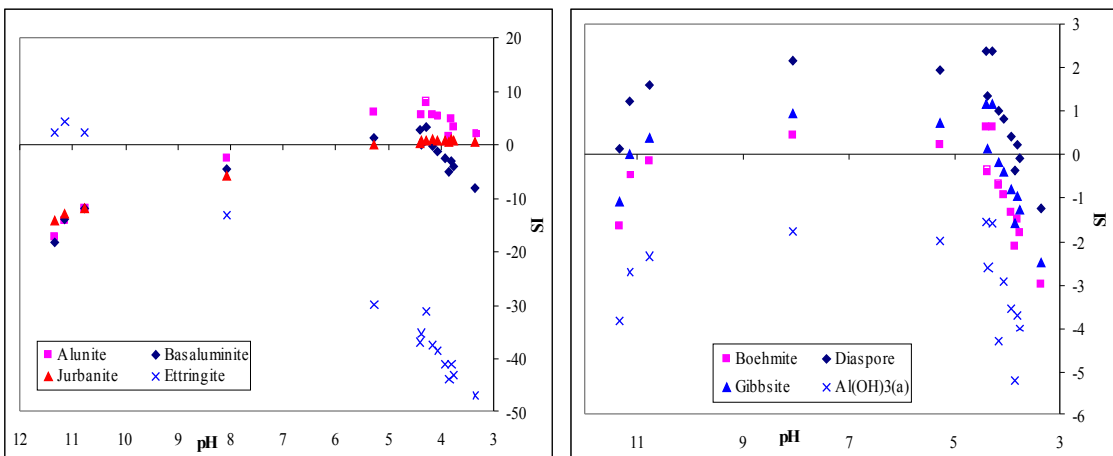


Figure 6.58: Plots of saturation indices for precipitating Al-(oxy) hydroxide and Al-hydroxysulphates mineral phases during the leaching study period for SR + 6 % OPC solid core leachates.

Similar to Fe^{3+} calculated Al^{3+} activities are plotted on a solubility diagrams to deduce the precipitating mineral phases, since the alignment of the plotted activities may have different slopes according to the stoichiometry of the precipitating solid phase. Figure

6.56 shows the solubility diagrams for selected phases in the $\text{Al}_2\text{O}_3\text{-H}_2\text{O}$ system at 298 K and the calculated activities of Al^{3+} in the leachates for the FA, SR, SR + 25 % FA and SR + 6 % OPC solid cores. The corresponding activities due to the precipitation of the pure aluminium hydroxide phases are also shown.

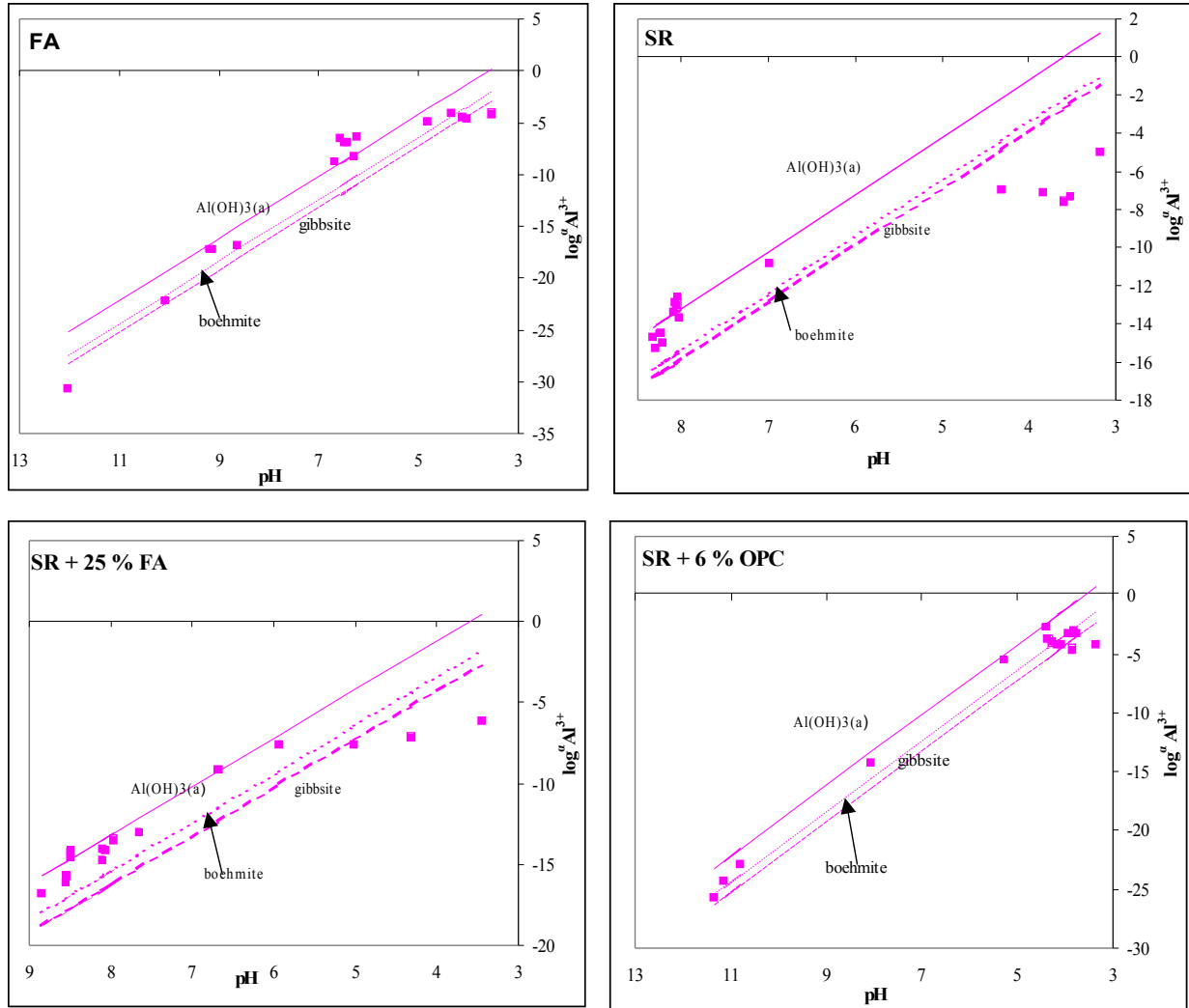


Figure 6.59: Plot of $\log \text{Al}^{3+}$ activity against pH for the FA, SR, SR + 25 % FA and SR + 6 % OPC solid core leachates with solubility lines.

(plot of $\log \text{Al}^{3+}$ activity against pH for the FA, SR, SR + 25 % FA and SR + 6 % OPC solid core leachates with solubility lines for $\text{Al}(\text{OH})_3(\text{a})$ ($\log^a \text{Al}^{3+} = 10.8 - 3\text{pH}$), gibbsite ($\log^a \text{Al}^{3+} = 7.74 - 3\text{pH}$), boehmite ($\log^a \text{Al}^{3+} = 8.58 - 3\text{pH}$), Solubility lines calculated using $\log K_s$ values for $\text{Al}(\text{OH})_3(\text{a})$, gibbsite, boehmite are 10.8, 7.74, and 8.58 respectively (Jae Young yu, 1996)).

Figure 6.56 suggests that the chemistry of the leachates is controlled by the precipitation of amorphous $\text{Al}(\text{OH})_3$ at between pH 5.5-9.5 for SR and SR + 25 % FA solid cores. In addition at pH 3.5-11 boehmite and gibbsite seems to be playing a role in the chemistry of the leachates for FA and SR + 6 % OPC solid cores. It can be tentatively concluded that amorphous $\text{Al}(\text{OH})_3$ is controlling Al^{3+} activity in the leachates for SR and SR + 25

% FA solid cores while boehmite or gibbsite are controlling Al^{3+} activity in the leachates for FA and SR + 6 % OPC solid cores. It has been discussed in this section that pH and SO_4^{2-} content in the leachates have a direct influence on whether Al-hydroxide or Al-hydroxysulphates will be kinetically favored to precipitate. A low SO_4^{2-} concentration (<2500 mg/L) seems to favor precipitation of Al-hydroxides and $SO_4^{2-} > 5000$ mg/L favors precipitation of Al-hydroxysulphates. To further elucidate the Al-hydroxysulphates precipitating under the pH and SO_4^{2-} regimes generated by the different solid cores. Ion activity diagrams relative to stability lines for Al-hydroxysulphates minerals; jurbanite ($Al(OH)SO_4 \cdot 5H_2O$), alunite ($KAl_3(SO_4)_2(OH)_6$) and basaluminite ($Al_4(OH)_{10}SO_4 \cdot 17H_2O$), gibbsite and $Al(OH)_{3(a)}$ were generated following the method of Wolt *et al.*(1992).

The solubility relations of basic Al-hydroxysulphates in solution can be expressed as $[2pH + pSO_4]$ and $[pAl + pOH + pSO_4]$ (Wolt *et al.*, 1992) using appropriate pK_{sp} for jurbanite (17.8), alunite (85.6) and basaluminite (117.7) as given by Nordstrom, 1982; Allison *et al.*, 1991 and the negative logarithm of the ion activity product of water, $pK_w=14$. The following relations derived by Wolt *et al.* (1992) were used in this study:

$$\text{Jurbanite: } p(Al)(OH)(SO_4) = [pAl + pOH + pSO_4] = 17.8 \dots\dots\dots(6.25)$$

$$\text{Basaluminite: } [pAl + pOH + pSO_4] = 8.4 + 3/4[2pH + pSO_4] \dots\dots\dots(6.26)$$

$$\text{Alunite: } [pAl + pOH + pSO_4] = (19.13 - 1/3[pK + pOH]) + 1/3[2pH + pSO_4] \dots\dots\dots(6.27)$$

Since gibbsite and $Al(OH)_{3(a)}$ were proved to be controlling Al^{3+} in the solid cores the following relations were also derived using $pK_{sp}=33.9$ and $pK_{sp}=31.2$ (Nordstrom *et al.*, 1990) for gibbsite and $Al(OH)_{3(a)}$ respectively.

$$\text{Gibbsite: } [pAl + pOH + pSO_4] = 5.9 + [2pH + pSO_4] \dots\dots\dots(6.28)$$

$$\text{Al(OH)}_{3(a)}: [pAl + pOH + pSO_4] = 3.2 + [2pH + pSO_4] \dots\dots\dots(6.29)$$

Figure 6.57 shows the stability lines of Al-hydroxysulphates minerals, gibbsite and $Al(OH)_{3(a)}$ imposed on the leachate ion activities plotted with $[pAl + pOH + pSO_4]$ as function of $[2pH + pSO_4]$. The data for the leachate solutions fall along the line fixed by amorphous $Al(OH)_{3(a)}$ from which Al^{3+} activity was calculated for SR and SR + 25 % FA solid cores and along the line fixed by gibbsite from which Al^{3+} activity was calculated for FA and SR + 6 % OPC solid cores (Fig 6.56). The leachate chemistry seems to be clearly unrelated to alunite solubility for all the solid cores. For the FA and SR + 6 % OPC solid core leachates the ion activities fall within the region circumscribed by the basaluminite, jurbanite and gibbsite solubility (Fig 6.57). For the FA solid cores basaluminite and gibbsite seem to be the stable solid-phases controlling Al^{3+} and SO_4^{2-} activities when $[2pH + pSO_4] \geq 19.56$ and at $[2pH + pSO_4] \leq 15.56$ basaluminite, jurbanite and gibbsite control the ion activities. In the SR + 6 % OPC solid cores a similar solid-phase trend is observed, at $[2pH + pSO_4] \geq 18.25$ basaluminite and gibbsite control the ion activities and at $[2pH + pSO_4] \leq 12.37$ basaluminite, jurbanite and gibbsite seem to control the ion activities. In the SR solid cores at $[2pH + pSO_4] \geq 15.87$ basaluminite and $Al(OH)_{3(a)}$ control the ion activities while at $[2pH + pSO_4] \leq 10.46$ jurbanite exerts control. For the SR + 25 % FA solid core at $[2pH + pSO_4] \geq 15.33$ basaluminite and $Al(OH)_{3(a)}$ control the ion activities while at $[2pH + pSO_4] \leq 14.06$ jurbanite exerts

control. There is ample evidence of solubility control of Al^{3+} activity by jurbanite under acidic and high SO_4^{2-} conditions (Wolt *et al.*, 1992; Von and Stehouwer, 2003; Agbenin, 2003).

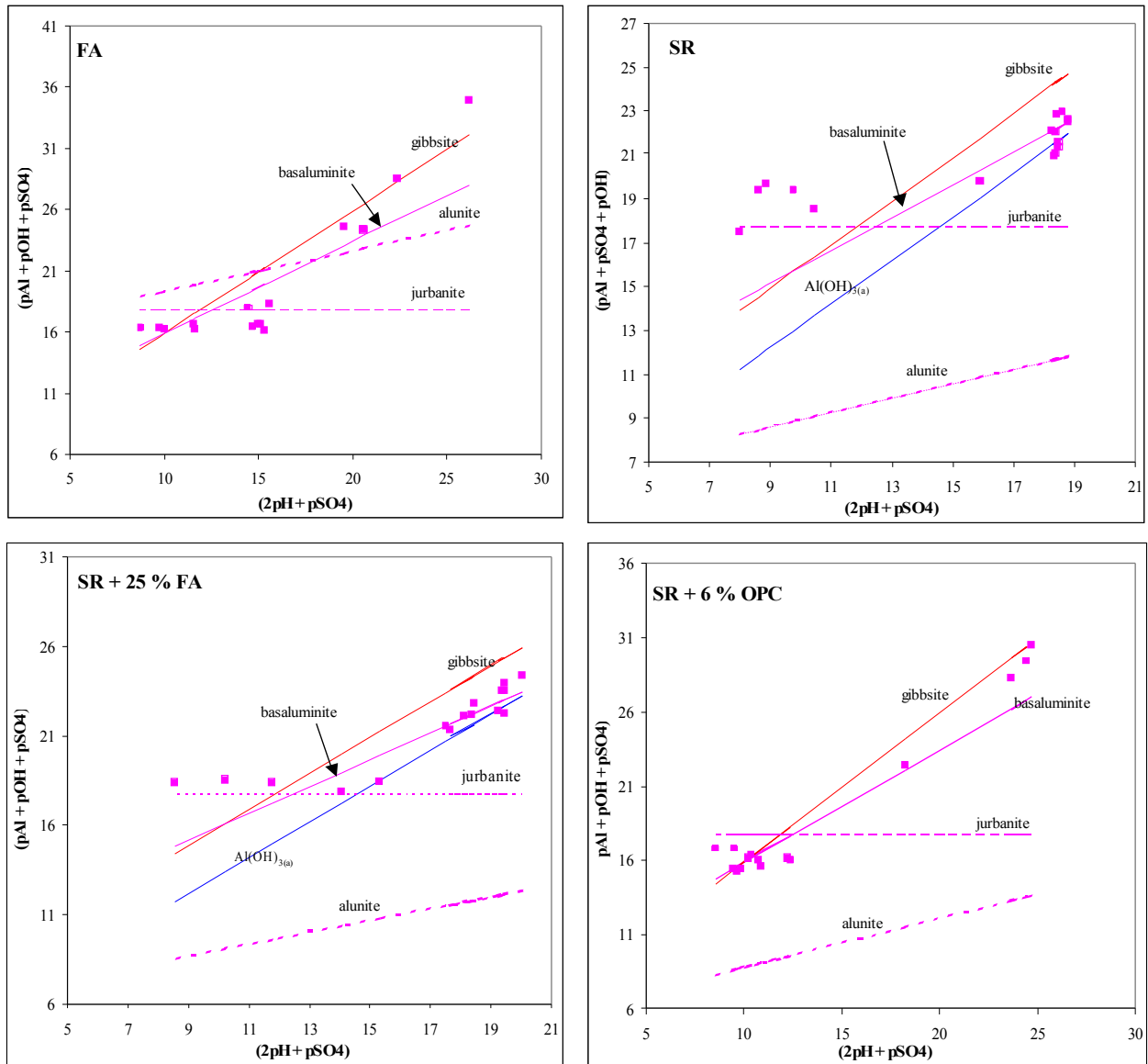


Figure 6.60: Leachate ion activities relative to stability lines for Al-hydroxysulphate minerals

(leachate ion activities relative to stability lines for Al-hydroxysulphate minerals, gibbsite and amorphous $\text{Al}(\text{OH})_{3(a)}$. Stability line of alunite was fixed using average value of pK and $p\text{OH}$ calculated using PHREEQC (FA: $p\text{OH}=7.21$, $pK^+=2.15$; SR: $p\text{OH}=7.31$, $pK^+=3.25$; SR + 25 % FA: $p\text{OH}=6.70$, $pK^+=3.25$; SR + 6 % OPC: $p\text{OH}=8.23$; $pK^+=2.90$) (average values derived from the data generated using PHREEQC)).

5.2.2.4.4 Manganese

PHREEQC simulation indicates that the leachates were saturated or over-saturated with respect to pyrolusite, nsutite and manganite at pH > 10.08 and rhodochrosite at pH 5.94-10.08 (Fig 6.58). Under mildly oxidizing and high pH conditions Mn^{2+} can be oxidized to Mn^{4+} / Mn^{3+} with formation of insoluble MnO_2 (pyrolusite), $MnOOH$ (manganite) and nsutite (MnO_2). The oxidation/reduction potential at pH >11.0 in this study ranged (-32.1-268 mv). Manganese autooxidizes at pH values of 8.5 or > and according to Eh-pH diagrams developed by Faulkner and Richardson, (1989) Mn^{2+} will be oxidized to MnO_2 at pH > 11 and Eh (mv) \geq 250. At circumneutral to alkaline pH values carbonate minerals that form in an open system could remove Mn^{2+} . Rhodochrosite was near saturation or at saturation at pH 6.99-10.08 in this study.

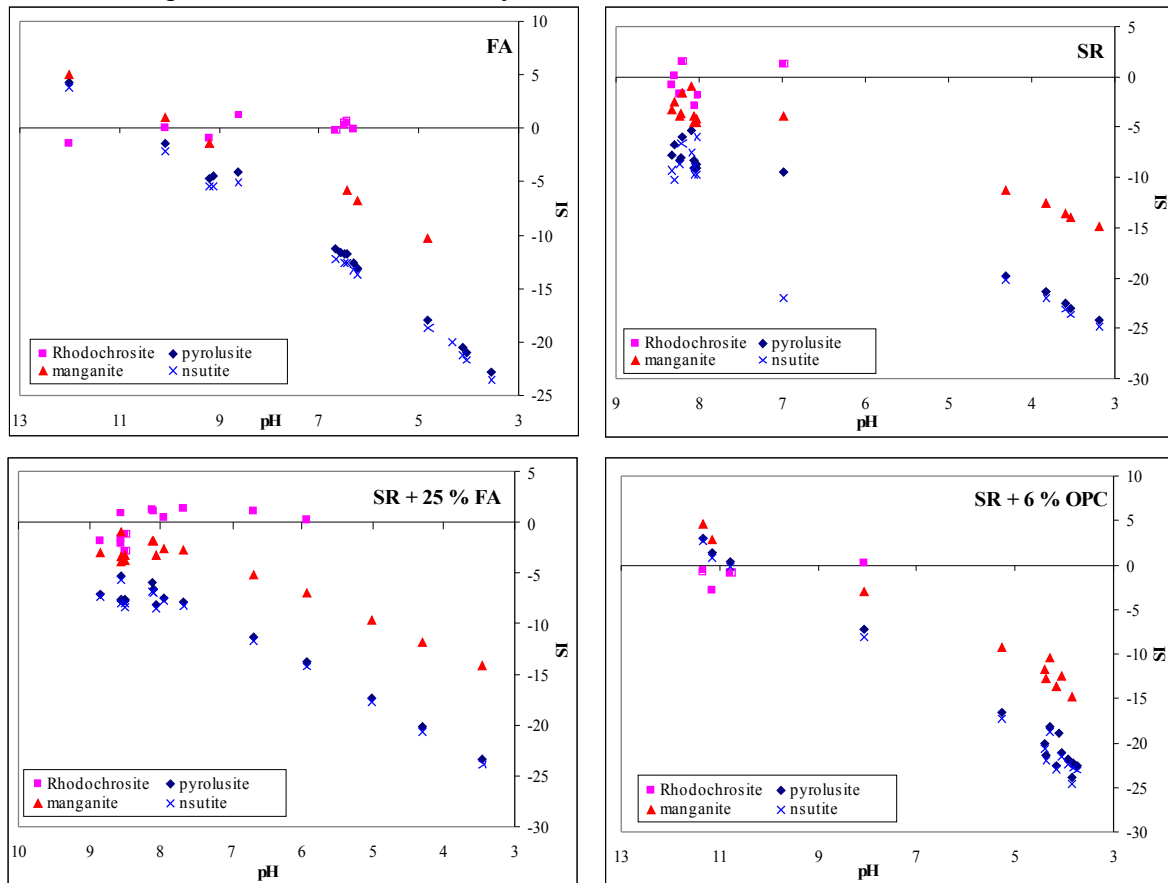
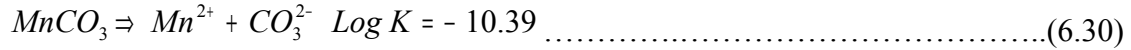


Figure 6.61: Saturation indices versus pH for selected Mn-bearing mineral phases for FA, SR, SR + 25 % FA and SR + 6 % OPC solid residue cores.

Komnitsas *et al.* (2004) treated simulated acidic leachates with limestone and red mud in a column leaching study and observed precipitation of rhodochrosite when pH was at alkaline values. Zachara *et al.* (1991) also supports the probability of rhodochrosite precipitation at alkaline pH values. To confirm the extent to which the precipitation of rhodochrosite was contributing to the attenuation of Mn^{2+} , solubility diagrams were constructed using activity of Mn^{2+} calculated using PHREEQC (Fig 6.59) (Eqns 6.30-

6.32). The CO_3^{2-} activities fall along the line described by rhodochrosite at pH 5.94 – 8.62 confirming the control of leachate chemistry by this mineral phase.



where

$$K = [\text{Mn}^{2+}][\text{CO}_3^{2-}] \quad \dots\dots\dots(6.31)$$

Taking logarithms to base 10 on both sides

$$\text{Log } \text{Mn}^{2+} = -10.39 - \text{Log } \text{CO}_3^{2-} \quad \dots\dots\dots(6.32)$$

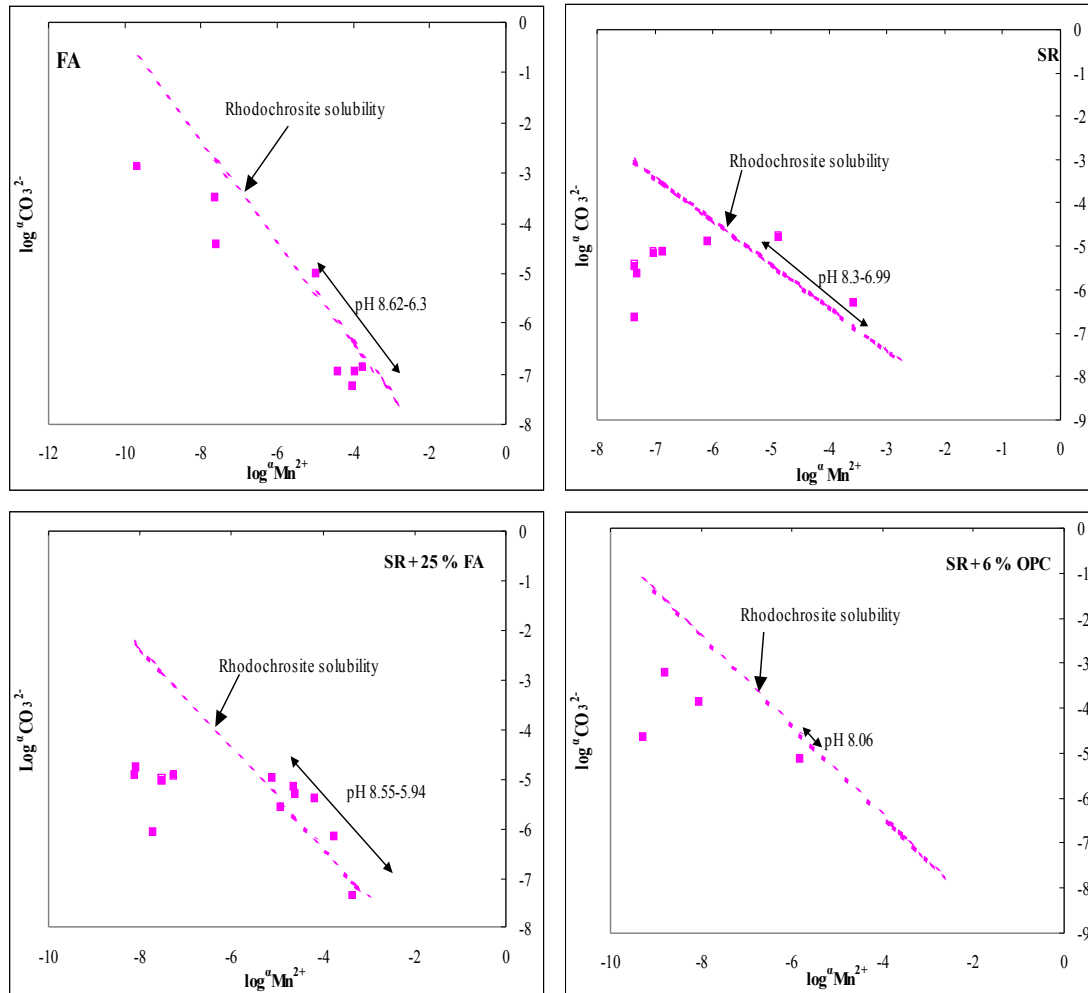


Figure 6.62: Leachate Mn^{2+} activities versus CO_3^{2-} activities for FA, SR, SR + 25 % FA and SR + 6 % OPC showing the pH ranges at which rhodochrosite controls Mn^{2+} activity.

Log $K = -10.39$ (WATEQ4 database) (Ball and Nordstrom, 1991).

Plotting of solubility lines of pyrolusite ($\beta\text{-MnO}_2$, $\log K = 41.38$) and manganite ($\gamma\text{-MnOOH}$, $\log K = 25.34$) over the pH range of the leachates revealed that both pyrolusite and manganite were controlling the chemistry of the leachate at $\text{pH} > 9$ for FA and SR + 6 % OPC solid cores. For SR and SR + 25 % FA the ion activities data cluster along the line defined by the manganite at $\text{pH} > 7.5$ (Fig 6.60). Hem and Lind (1993) titrated Mn-rich ground

waters with 0.1 molar NaOH solution with and without CO₂ present, these experiments yielded hausmannite which aged to manganite.

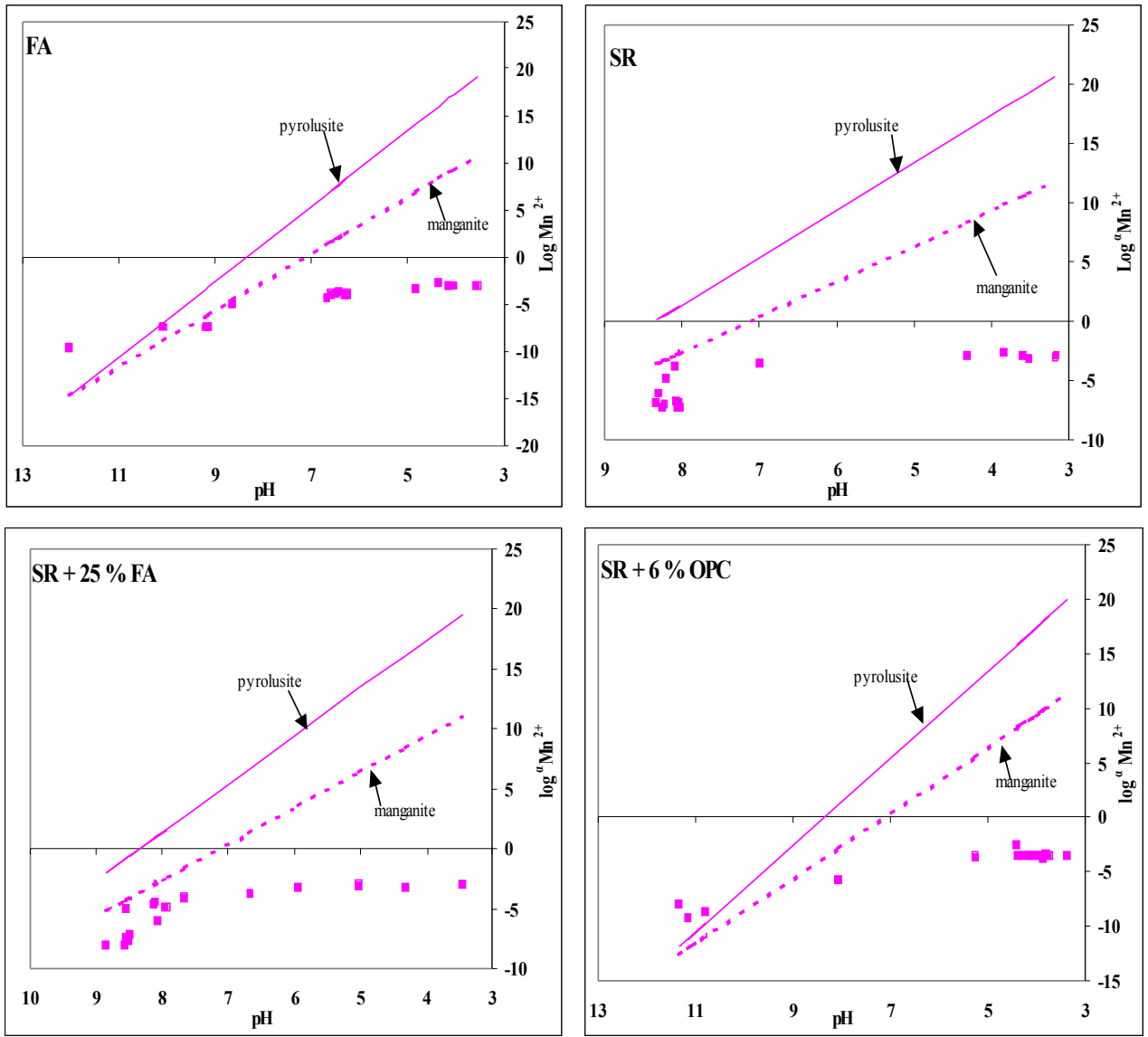


Figure 6.63: Logarithm of the activity of Mn²⁺ ion plotted against pH with equilibrium solubility lines.

(Logarithm of the activity of Mn²⁺ ion plotted against pH with equilibrium solubility lines for pyrolusite and manganite for FA, SR, SR + 25 % FA and SR + 6 % OPC solid cores. The default p_e = 4.0 in PHREEQC was assumed in calculating the Mn²⁺ activity in equilibrium with pyrolusite and manganite).

5.2.2.5 X-ray diffraction (XRD), Fourier Transform infra-red (FTIR), Scanning electron microscopy(SEM) and Scanning Electron microscopy-Energy dispersive X-ray spectroscopy (SEM-EDX) analysis of the leached column solid cores

In view of the findings of the modelling experiments suggesting that Fe-bearing hydroxide phases, Fe-hydroxysulphate mineral phases, Al-bearing hydroxide minerals, Al

–hydroxysulphates, Ca-SO₄ mineral phases and Mn-bearing mineral phases were likely to control the leachate chemistry as the drainage progressed. An attempt was made to correlate this information with direct physical evidence of these mineral phases in the leached SR. This section will present a discussion with a view to drawing a conclusion on the presence or absence of these predicted mineral phases.

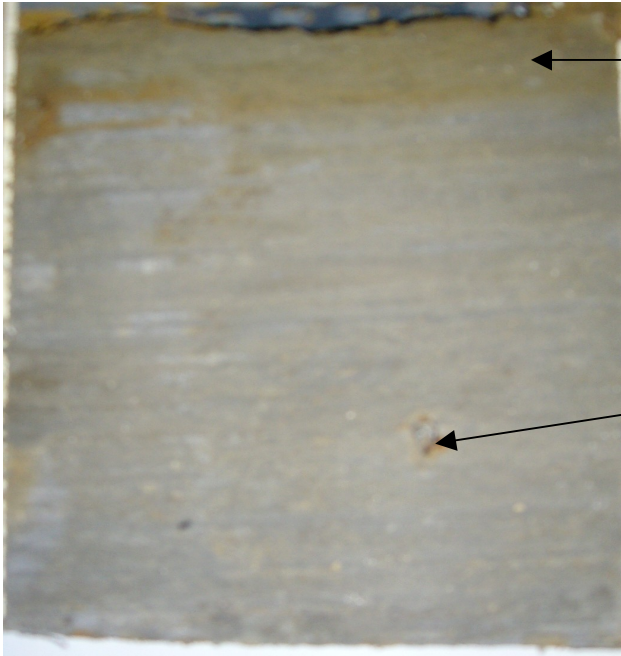
5.2.2.5.1 Visualization of the sectioned leached solid cores

Figure 6.61 and 6.62 below shows the surfaces of the sectioned column solid cores for FA and SR cores. After sectioning of the columns the extent of interaction of the synthetic acid mine drainage (SAMD) with FA and the SR (SR) was evident. Yellowish/brownish coloration was observed in all the leached solid cores. The highest intensity of the coloration was observed at the top layer of each of the leached solid cores. The least coloration was observed in the FA cores. The intensity of the yellowish/brownish coloration decreased down the length of the leached solid core. The highest intensity of the coloration was observed in the SR core.

Hard greyish cemented layers were observed in SR + 25 %, SR + 40 % FA and SR + 6 % OPC at length varying from 8.5 –13.5 cm down the length of the solid core. The appearance of these grayish layers suggested local formation of hardpan layers as a result of precipitates formed cementing the leached solid residue particles. The hardpan layer results from the migration of formed precipitates as the pH front moves down the column solid cores. The yellowish/brownish coloration is characteristic of ochreous precipitates that occur in acid mine drainage impacted environments (Jeong and Soo, 2003).

5.2.2.5.2 X-ray diffraction (XRD) analysis of the leached solid cores

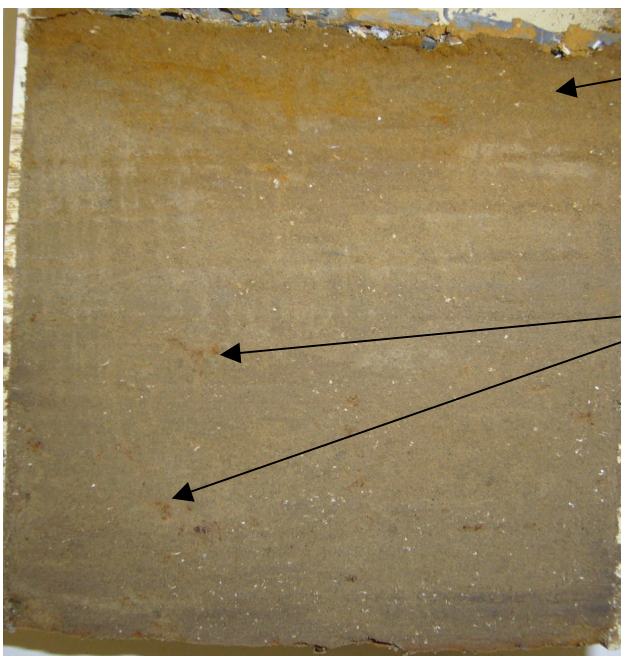
Although the visualization of the sectioned solid cores revealed extensive formation of ochreous precipitates in all sections of the solid cores, XRD did not reveal presence of any crystalline Al or Fe-bearing mineral phases (Figs 6.61-6.62). This would indicate that the precipitates were too amorphous to be detected by XRD or they were below detection limits. XRD revealed the presence of gypsum (CaSO₄. 2H₂O) and calcium sulphate hydrate (CaSO₄.0.6H₂O) as the only new crystalline mineral phases.



Yellowish/brownish colored top

Dark brown/yellow spot

Column 1 (FA)

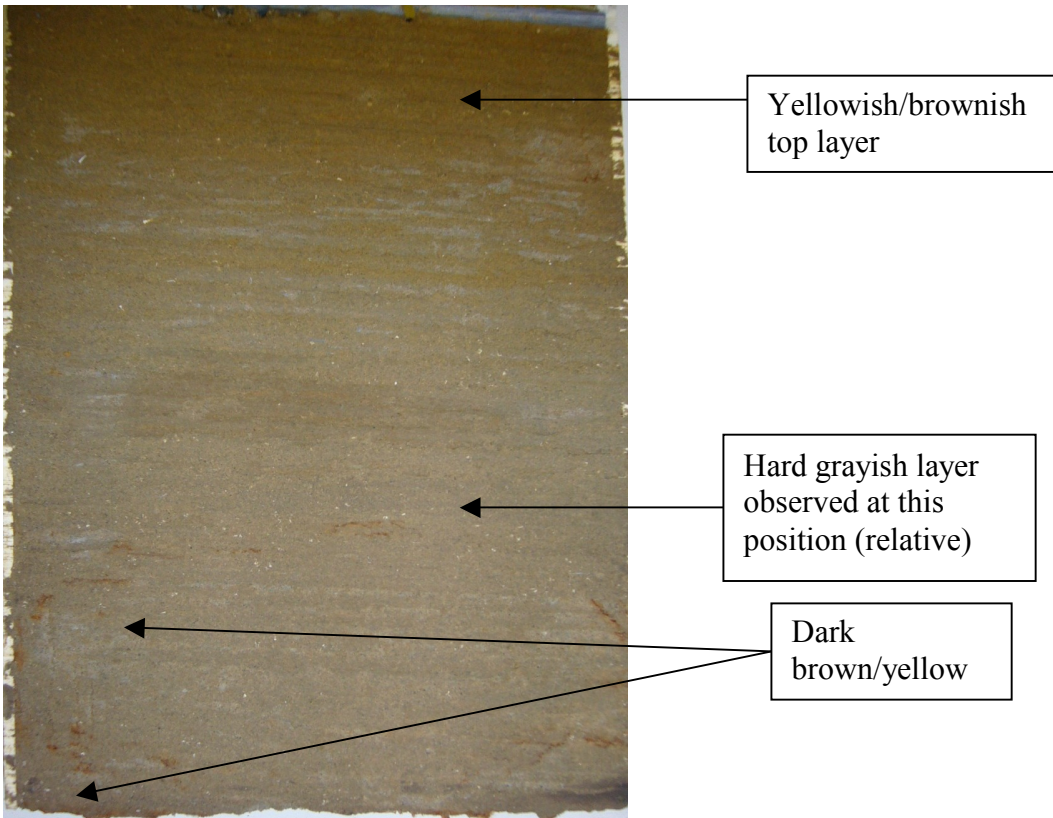


Yellowish/brownish top layer

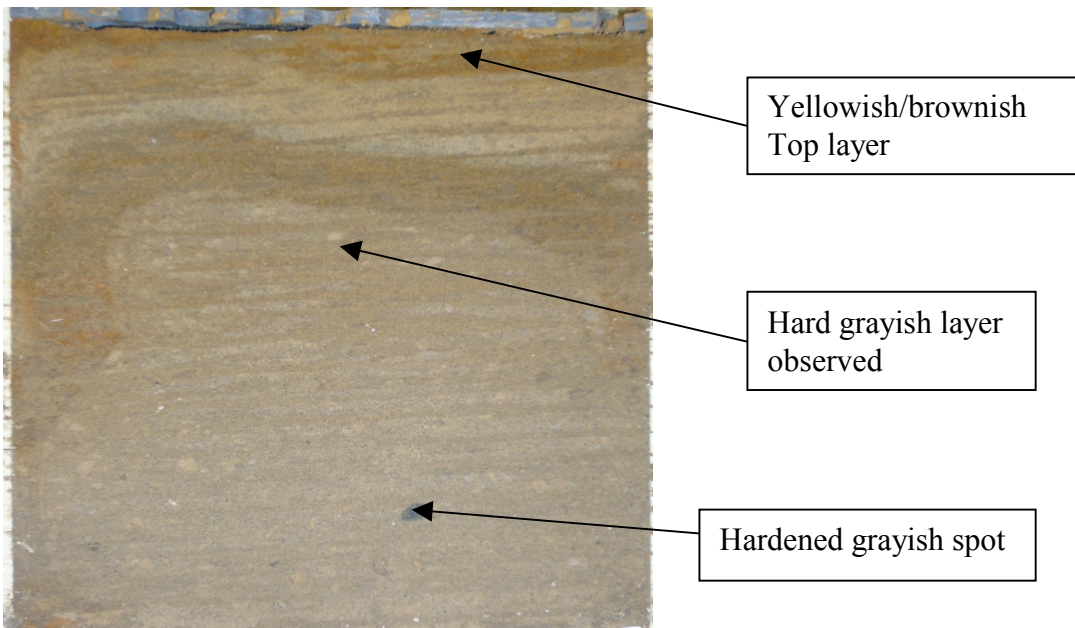
Dark brown/yellow spots

Column 2 (SR)

Figure 6.64: Digital photos of the sectioned FA and SR leached solid cores



Column 5(SR + 25 % FA)



Column 8 (SR + 6 % OPC)

Figure 6.65: Digital photos of the SR + 25 % FA and SR + 6 % OPC leached solid cores

5.2.2.5.3 Fourier Transform infra-red analysis (FTIR) of the leached solid residue cores

The main absorption bands observed in the leached solid residue core sections, leached Solid Residue+25% FA and leached Solid Residue+6%OPC core sections are presented in Table 6.8 and Figs 6.63- 6.66.

Table 6.12: Characteristic absorption bands observed for FA, SR, SR + 25 % FA and SR + 6 % OPC leached solid residue cores.

Absorption band/peak(cm^{-1})	Leached solid cores			
	FA	SR	SR + 25 % FA	SR + 6 % OPC
3200-3600	✓	✓	✓	✓
2800-2915 with peaks at 2912,2844 and 2812	✓	✓		✓
2290, 2350	✓	✓	✓	✓
1600-1606	✓	✓	✓	✓
1360,1382-1390			✓	✓
1070-1134 with peaks at 1122-1134 and a shoulder at 986-996	✓	✓	✓	✓
656-658	✓	✓	✓	✓
596-600	✓	✓	✓	✓
436-454	✓	✓	✓	✓

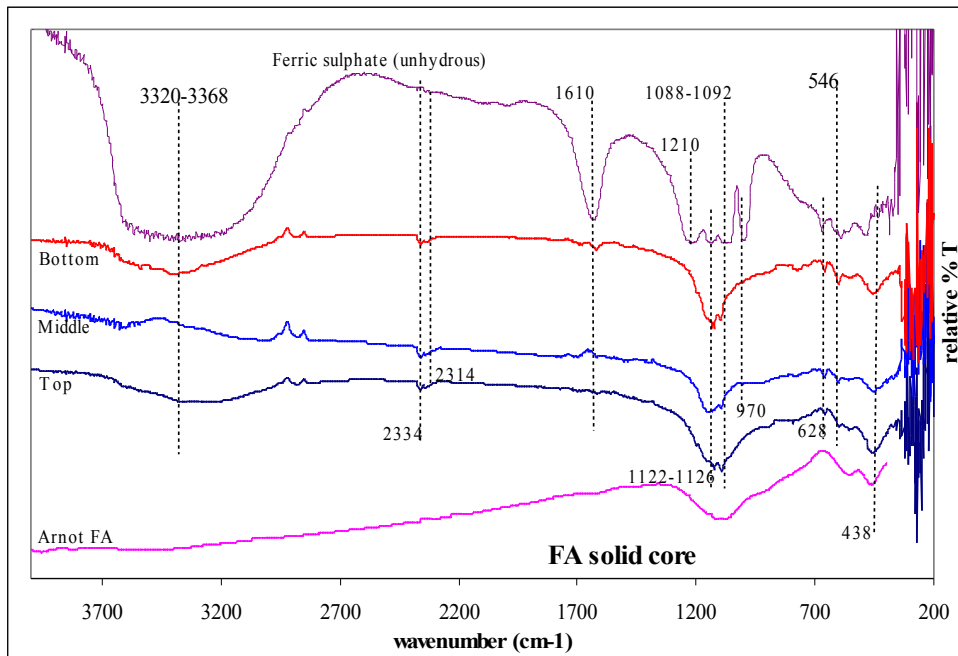


Figure 6.66: Infra-red spectra for the top, middle and bottom slices of the fly ash (FA) leached SR cores with the spectra of a pure unhydrous ferric sulphate imposed for comparison.

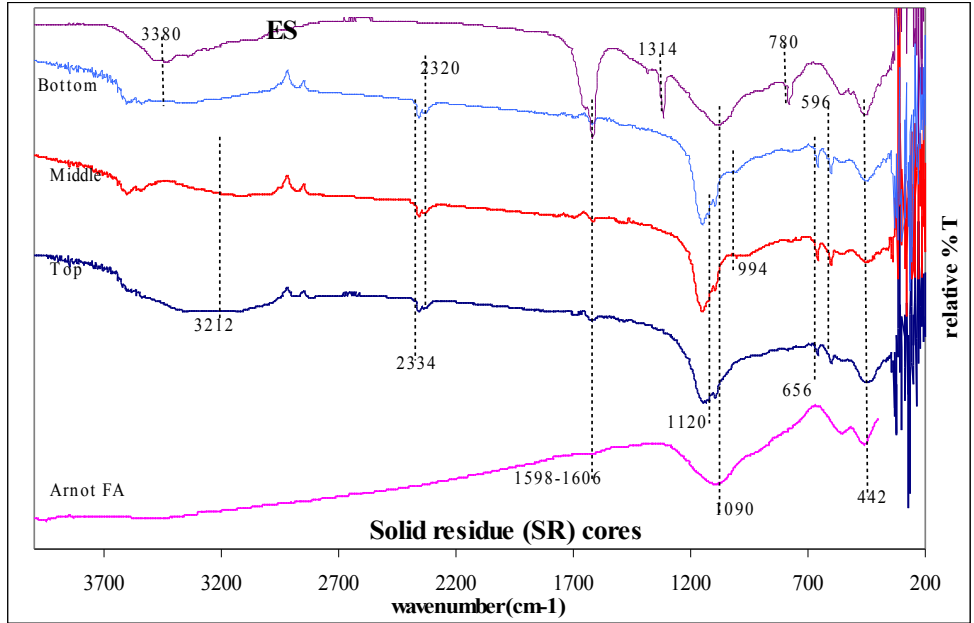


Figure 6.67: Infra-red spectra for the top, middle and bottom slices of the leached SR (SR) cores with the spectra of ammonium oxalate extracted (ES) top slice imposed for comparison.

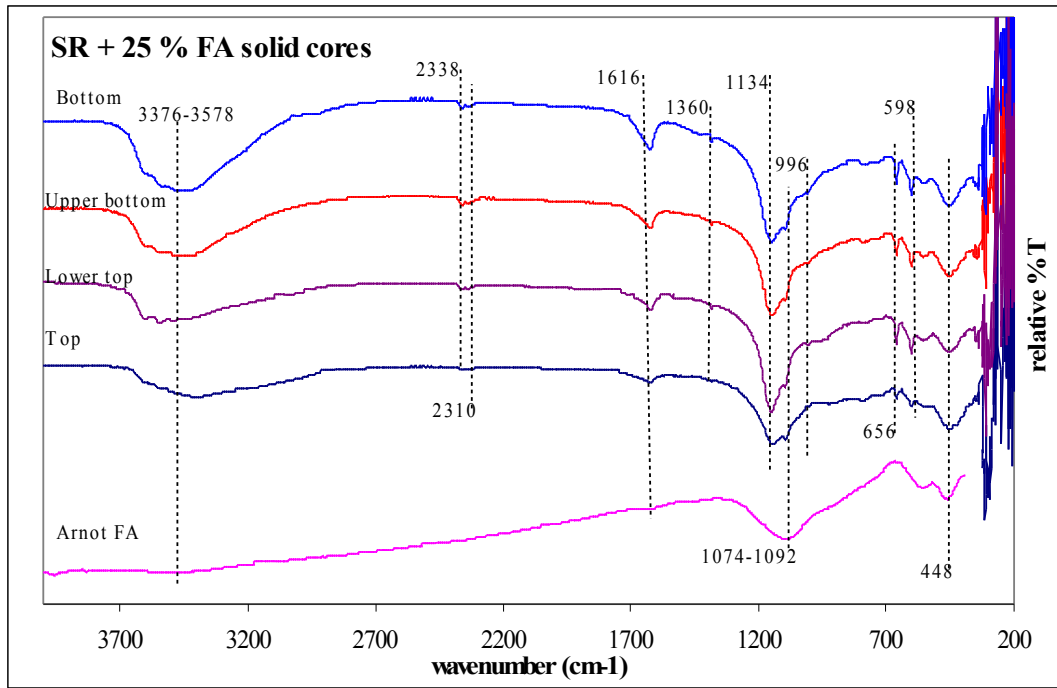


Figure 6.68: Infra-red spectra for the top, lower top, upper bottom and bottom slices of the leached solid residue (SR) + 25 % FA cores.

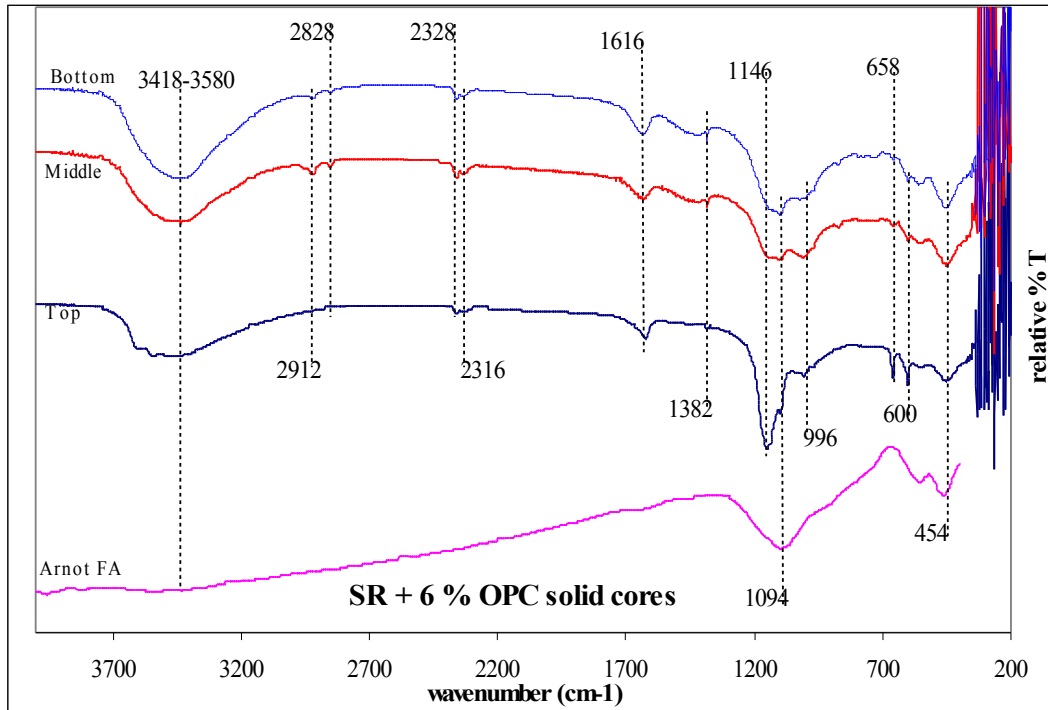


Figure 6.69: Infra-red spectra for the top, middle and bottom slices of the leached solid residue (SR) + 6 % OPC cores.

The unreacted fly ash displayed absorption bands within the region of 1594-1600, 900-1120 and 440-554 cm^{-1} . A weak broad band was observed within the region of 3300-3500 cm^{-1} . The bands within the 3300-3500 cm^{-1} region correspond to stretching vibrations for structural OH groups while bands within 1594-1600 cm^{-1} correspond to OH stretching vibrations for strongly adsorbed water (Fig 6.63). The band from 900-1120 cm^{-1} with a maximum at 1074 cm^{-1} is common for aluminosilicates and is usually well developed in spectra for glass materials (Farmer, 1974). XRD of Arnot fly ash revealed presence of quartz and mullite (Fig E1-E4). Farmer (1974) further observes that the aluminosilicate bands from 900 – 1200 cm^{-1} with a maximum at 1025 cm^{-1} will partially mask the characteristic absorption bands for SO_4^{2-} containing compounds. All the leached solid residue cores displayed the bands at 3200-3600 cm^{-1} and 1600-1606 cm^{-1} due to stretching vibrations for structural and strongly adsorbed water OH groups respectively (Figs 6.63-6.66).

All the leached solid residue cores displayed strong absorption bands within the region 1070-1134 with peaks at 1122-1134 and a shoulder at 986-996 cm^{-1} . Bigham *et al.* (1990) compared IR spectra of a few natural and synthetic specimens of Fe hydroxides and sulfates and found that any specimen containing SO_4^{2-} either chemically bonded or adsorbed, shows absorption bands between 1100-1200 cm^{-1} . This band is attributed to the stretching vibrations of SO_4^{2-} (ν_3). The SAMD interacting with the FA and the FA blend solid residue during the drainage experiment contained $\text{SO}_4^{2-} > 14000 \text{ mg/L}$ and PHREEQC simulation predicted precipitation of iron (oxy)-hydroxides and iron hydroxysulphates.

Unlike in the unreacted fly ash the absorption band at 1100-1200 cm^{-1} in all the leached solid residue cores shows splitting into two bands with a peak at 1120-1138 cm^{-1} , a second peak at 1092 cm^{-1} and a shoulder at 994-996 cm^{-1} for the FA and 6 % OPC blend solid residue cores. Several authors (Lazaroff *et al.*, 1985; Bigham *et al.*, 1990; Lazaroff *et al.*, 1982) point out that if the symmetry of SO_4^{2-} decreases with coordination, a splitting of the ν_3 fundamental occurs. For unidentate complex (C_{3v} symmetry) two bands appear.

Appearance of the ν_1 (970 cm^{-1}) mode may also indicates low site symmetry for SO_4^{2-} . Thus the bands at 1120-1138 cm^{-1} , at 1092 cm^{-1} and shoulder at 994-996 cm^{-1} most probably arise from the formation of a bidentate complex between SO_4^{2-} and Fe in leached solid residue precipitates. Such complexes form as a result of replacement of OH groups with SO_4^{2-} at the mineral surface through ligand exchange or within the structure during precipitation. However it would be difficult to distinguish by IR whether this SO_4^{2-} is adsorbed or structural since these two bonds could be similar in energy and geometry (Bigham *et al.*, 1990).

The leached solid residue cores exhibited sharp absorption peaks at 656 cm^{-1} and 600 cm^{-1} which were attributed to structural OH deformation and $\nu_4(\text{SO}_4^{2-})$ respectively (Nakamoto, 1997). Lazaroff *et al.* (1982) points out that the shoulder at 640-650 cm^{-1} could indicate presence of jarosites. K-jarosite was predicted to be precipitating by PHREEQC in the FA, SR, SR + 25 % FA and SR + 6 % OPC solid cores. The top section of the FA, SR, SR + 25 % FA leached solid cores exhibited broad absorption bands of the type usually associated with amorphous solids. Comparison with IR spectra of anhydrous ferric sulphate suggests that the solid precipitates are composed of ferric-oxide sulphates (Fig 6.63). Lazaroff *et al.* (1982) observed similar IR spectra for amorphous ferric sulphate precipitates produced by bacteria oxidation. That the absorption maxima observed at 1122-1134 cm^{-1} and a shoulder at 986-996 cm^{-1} is due to IR activity of SO_4^{2-} is confirmed by the disappearance of the absorption bands on treating the leached SR with ammonium oxalate for four hours in the dark (Fig 6.64) (Schwertmann *et al.*, 1982). The presence of strong absorption bands at 778 cm^{-1} corresponding to OH deformation of goethite appear to suggest increased intensity of goethite after ammonium oxalate extraction (Shokarev *et al.*, 1972). The peaks observed at 436-454 cm^{-1} are most likely Fe-O stretching vibrations (Kulumani and Jasobanta, 1996). Gypsum is revealed by the $2\nu_3(\text{SO}_4^{2-})$ overtone near 2130-2220 cm^{-1} (Sutter *et al.*, 2005).

Conclusions

The FTIR results revealed the incorporation of SO_4^{2-} in the resulting Fe and Al mineral phases either through adsorption or structural incorporation. Splitting of the ν_3 fundamental mode arises from the formation of a bidentate complex with the metal ions, however the results could not reveal whether the SO_4^{2-} is structural or adsorbed.

5.2.2.5.4 Scanning electron microscopy (SEM) and Scanning Electron microscopy-Energy dispersive X-ray spectroscopy (SEM-EDX) analysis of the leached column solid cores

Excessive aggregation of the solid residue particles in the leached solid cores was observed confirming the extent of formation of mineral phases other than gypsum and ettringite. As observed and discussed in chapter five of this work, the precipitated mineral phases tend to fill voids between the particles or deposit on the surface of the leached particles. Moreover PHREEQC simulation strongly predicted precipitation of Al, Fe-(oxy) hydroxides, Al-hydroxysulphates, Fe-hydroxysulphates and it is predicted that some Ca-Al-hydroxysulphates could also have been precipitating in course of the drainage experiment. None of these phases were detected by XRD probably due to poor crystallinity or low concentration due to dilution by the residue matrix. In this section an attempt is made to semi-quantitatively identify these mineral phases in the leached solid residue (SR) and solid residue (SR) + 6 % OPC solid cores. Due to the limitations of the SEM-EDS as per the analysis volume ($1\mu\text{m}^3$) there is bound to be a contribution from the underlying matrix and the results should be taken with caution. The results can only provide a general trend of enrichment of elements in the identified precipitates or crystals and hence only a general conclusion can be drawn. The un-reacted Arnot fly ash was also analyzed by SEM-EDS to provide the baseline for comparison with the solid residue samples. For all the SEM-EDS analysis the K_{α} line was utilized in calculations of the % elemental concentration of the areas and spots analyzed.

Figure 6.67 below shows the SEM-EDS analysis areas that were done for the leached solid residue cores and Table 6.9 shows the EDS elemental composition results. Where applicable the results are discussed and conclusions drawn in relation to the EDS analysis of the Arnot fly ash, three areas on the Arnot fly ash were analyzed to give an average background concentration. Precipitates or crystals aggregating on the solid residue particles were selected for analysis.

The area SR-06 concentration differs from the fly ash in that P and S are detectable and Ca increases which would suggest a Ca, S rich precipitate is being formed, probably CaSO_4 or gypsum. The precipitates appear to project in three dimensions which means they are crystalline. The decrease in Fe, Si, O, and Ti probably represents the dilution effect due to increase in Ca and S, but Al is observed to increase. This area of analysis would probably represent a deposition of a Ca, S rich crystalline phase on a fly ash residue that resisted dissolution and this could probably explain the strong Al-Si-O-Fe signal. Spot SR-07 appears to be amorphous precipitates cementing the residue particles together. An enrichment of Fe, Al, S is observed. This is supported by the increase in the Al/Si ratio (0.76) as compared to the fly ash (0.38) and also the decrease in O/Al ratio as compared to fly ash ($1.2 \rightarrow 0.66$) (Table 6.9). The increase in Fe, Al, and S would probably suggest some kind of Fe, Al-hydroxysulphates. A corresponding increase in Cu would probably be due to adsorption in the precipitating phases.

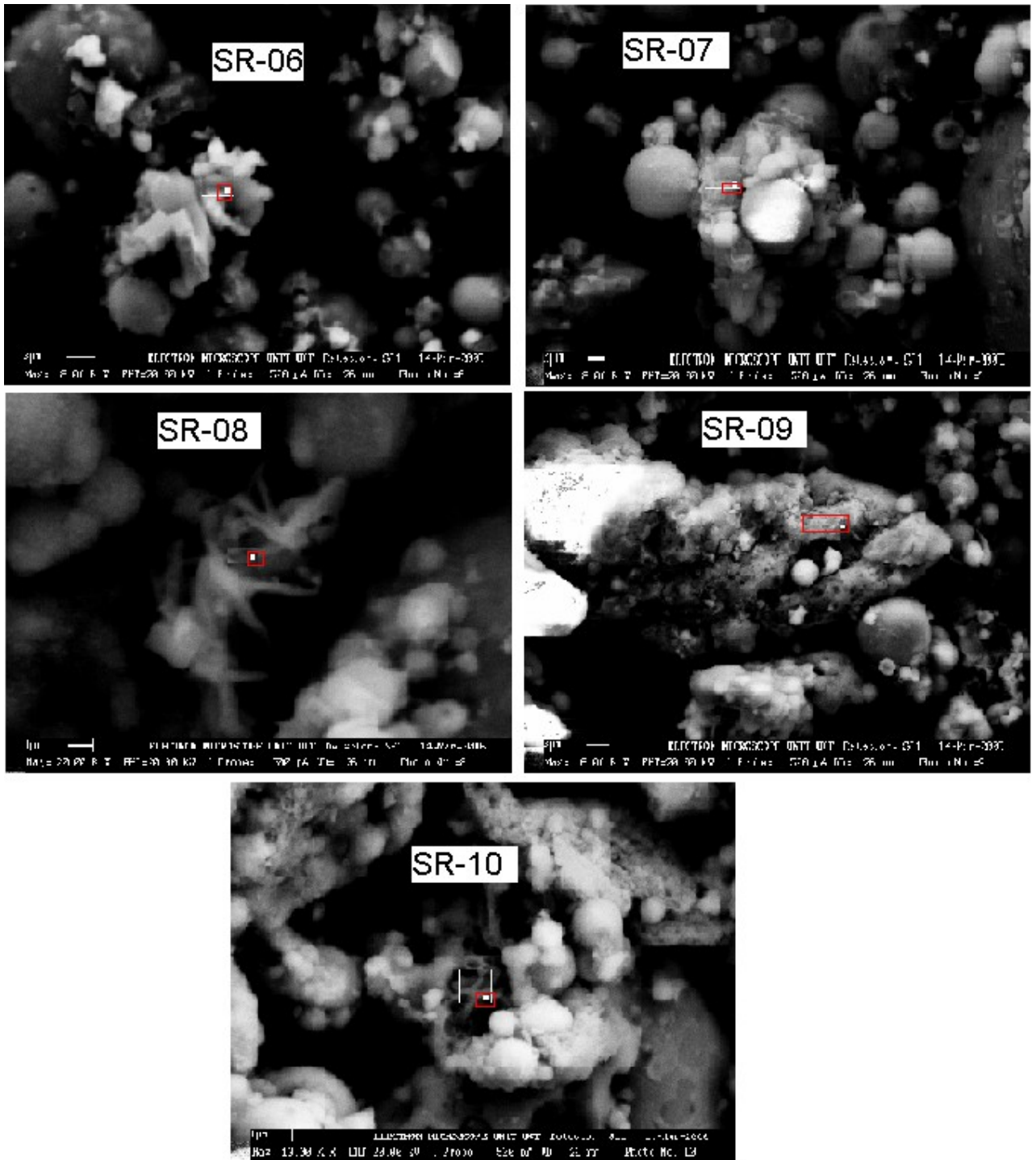


Figure 6.70: SEM backscattered micrographs showing spots where EDX analysis was done for the solid residue (SR) cores.

Table 6.13: EDS elemental analysis results (weight %) for the solid residue cores

The area SR-08 represents a crystalline material that has structures projecting outwards and some circular formations resulting in hollow openings in-between. The concentration trends indicate enrichment in Fe, S and Al (note the Al/Si ratio increases to 1.6 as compared to FA (0.38) (Table 6.9) suggesting a similarity to the precipitates observed at area SR-07. This indicates that SR-07 and SR-08 may be crystalline phases, it is only that the detailed crystalline nature of the SR-07 could not be revealed at the lower magnification (SR-07, magnification=8000: SR-08, magnification = 20000). Area SR-09 represents an O, Al-rich amorphous phase aggregating together to form a dense mass. There is relative increase in O as compared to fly ash which strongly suggests an Al-(hydro) oxide phase. PHREEQC modelling predicted precipitation of amorphous $\text{Al}(\text{OH})_{3(a)}$. SR-10 is a crystalline material resembling the morphology of crystals observed in area SR-08. It is enriched in Al, O, S and Ca.

In conclusion, crystalline phases enriched in Al, Fe, S and O were observed to have precipitated in the solid cores (SR). Although they cannot be conclusively assigned to a particular mineral phase from the semi-quantitative EDS elemental analysis due to limitations stated earlier, their elemental contents suggests Al, Fe-hydroxysulphates or Al, Fe-(hydro) oxides. The enrichment in Ca, Al, S and O would also suggest formation of monosulphate type of minerals ($3\text{CaO} \cdot \text{Al}_2\text{O}_3 \cdot \text{CaSO}_4 \cdot 12 \text{H}_2\text{O}$) similar to hydrating cement in SO_4^{2-} rich waters (Cocke and Mollah, 1993). Gypsum was also observed to be forming and depositing on the solid residue particles that resisted dissolution.

Figure 6.68 below shows the various areas analyzed for SR + 6 % OPC leached solid cores and Table 6.10 shows the corresponding EDS analysis results.

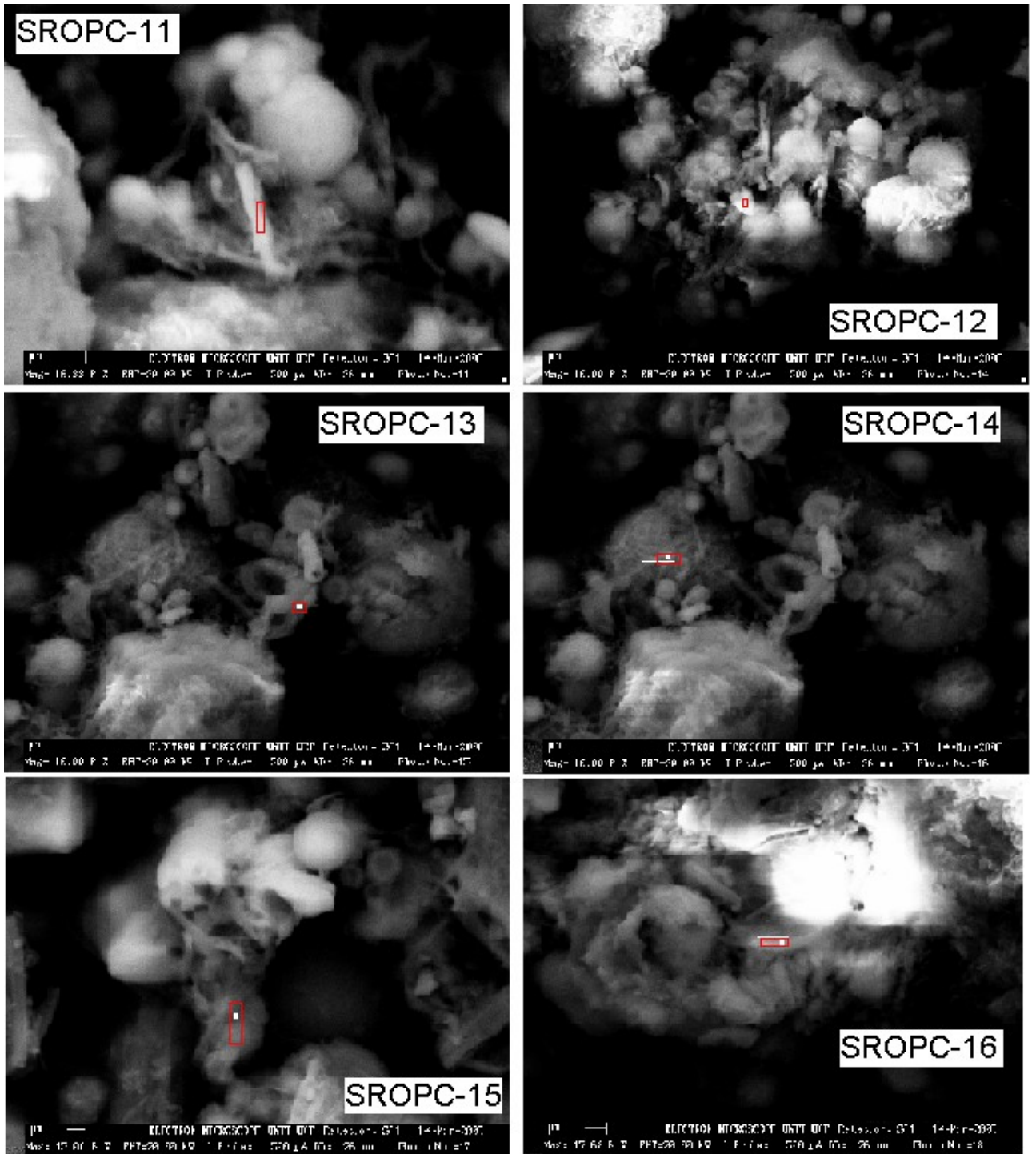


Figure 6.71: SEM backscattered micrographs showing spots where EDX analysis was done for the SR + 6 % OPC solid cores.

Table 6.14: EDX elemental analysis results (weight %) for the SR + 6 % OPC solid cores.

Arnot FA	SROPC-11		SROPC-12		SROPC-13		SROPC-14		SROPC-15		SROPC-16		
Element	Weight %	Element	Weight%	Element	Weight%								
O	14.52	O	19.69	O	17.71	O	15.15	O	20.23	O	12.65	O	16.63
Mg	1.64	Mg	4.28	Mg	1.94	Mg	2.94	Mg	1.33	Mg	0.38	Mg	4.55
Al	12.11	Al	8.45	Al	9.71	Al	9.15	Al	28.33	Al	4.97	Al	10.04
Si	32.01	Si	17.48	Si	24.4	Si	18.79	Si	39.19	Si	4.96	Si	19.51
P		P	3	P	1.16	S	4.86	S	0.68	S	3.59	S	10.78
S		S	3.41	S	8.89	Ca	18.5	Ca	6.3	Ca	70.93	Ca	14.68
Ca	2.57	Ca	33.31	Ca	26.13	Ti	2.06	Fe	3.94	Fe	2.51	Mn	1.82
Ti	2.53	Ti	0.99	Ti	1.43	Mn	1.82					Fe	21.98
Mn		Mn	1.92	Fe	8.62	Fe	26.73						
Fe	36.66	Fe	6.53										
Cu	0.7	Cu	0.94										
Total %	102.74	Total %	100	Total %	99.99	Total %	100	Total %	100	Total %	99.99	Total %	99.99

Area SROPC-11 represents a tube-like structure. The structure is observed to be enriched in Ca, Si, and O, the Ca/Si ratio = 1.9 (Table 6.10) that would strongly suggest this to be calcium silicate hydrate gel. Cocke and Mollah. (1993) observes that CSH gels have Ca/Si ratio ranging from 1.5-1.7. Kindness *et al.* (1994) observed this crumbled foil morphology that is consistent with CSH on reacting tricalcium silicate with Cr (iii) salts. The presence of Mg, Fe, Ti, Cu and Mn, S, Al suggests incorporation or precipitation of metal-(hydro) oxides in the cement matrix. Area SROPC-12 represents a mass of what appears to be amorphous precipitates and crystals adhering to these precipitates. The precipitates appear to be enriched in Ca, S, O and Si. The Ca/Si ratio of 1:1 would suggest a CSH gel but the presence of S and Ca/Al ratio of 3 would suggest calcium aluminate hydrate gel or Ca, Al-hydroxysulphate could also be present. These precipitates can best be described as a mixture of CSH, calcium aluminate hydrate gels or Ca, Al-hydroxysulphate. SROPC-13 is a crystalline phase with a structure similar to spot SR-10, SR-08 observed in the SR. The elemental composition closely resembles that of SROPC-12 except the decrease in Ca and enrichment of Fe. The Ca/Si ratio of 0.98 suggests this is not CSH gel. The increase in O/Al ratio (1.7) would suggest formation of Fe-(hydro) oxide within the CSH gels. The formation of the Fe-(hydro) oxide is supported by the fact that S is observed to decrease compared to SROPC-12.

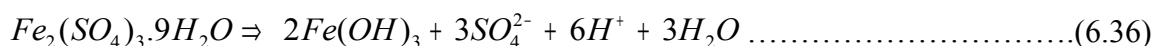
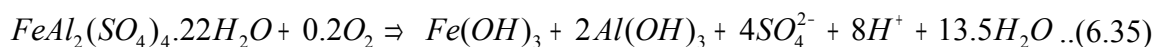
The area SROPC-14 appears to be a mass of solid which is enriched in O, Si and Al suggesting a strongly etched solid residue particle or a mass of solid residue particles encapsulated with CSH gel as suggested by the high Ca content. The lower Ca/Si ratio (0.16) would suggest contribution of the Si signal from the encapsulated or underlying aluminosilicate residual matrix.

Area SROPC-15 represents an aggregating mass of precipitates that do not appear to be crystalline. They are enriched in Ca, Al and O, the Ca/Si ratio of 14.3 (Table 6.10) suggests this not to be a CSH gel and neither a calcium aluminate hydrate gel. The high calcium content (70.9 %) in combination with S (3.59) would suggest a gypsum or calcium sulphate phase. This is supported by the enrichment of O as indicated by the increase in the O/Al ratio (2.54) compared to FA (1.2). Area SROPC-16 structure closely resembles material observed at area SROPC-11, judging by the Ca/Si=0.75, Al/Si=0.51

The pH profile of solids down the column SR exhibit similar patterns for all the columns. The fly ash (FA) cores showed a higher pH upto a depth of 5 cm than SR, SR + 5 % FA, SR+ 25 % FA and SR + 40 % FA solid cores. This is attributed to the residue alkalinity present in the fly ash (FA) core. The residues at the top of the solid cores had a pH ranging from 3.0-4.0, at the middle 5.0-6.0 to the bottom section at pH 6.0 -7.40. The solid cores show a clear transition from being acidic at the top, the SAMD contact point, to circum-neutral at the bottom. The transition is gradual for FA, SR + 25 % FA and SR+ 40 % FA solid cores and sharp for SR and SR + 5 % FA solid cores. The profile of SR + 6 % OPC solid core deviates from the pattern observed, from pH 4.31 at a depth of 1 cm, the pH changed to 7.66 at a depth of 2 cm and is maintained at pH > 8.0 upto the bottom of the solid core. The pH of solid residue cores for column SR + 6 % OPC were constantly higher than for SR, SR + 5 % FA, SR+ 25 % FA and SR + 40 % FA solid cores. The high pH of the SR + 6 % OPC solid residue cores could have been due to cementation reactions of ordinary Portland cement (OPC), where the generated calcium silicate hydrate gels (CSH) encapsulated the solid residue particles reducing the surface area of contact with the leachant. This was confirmed by SEM and SEM-EDX analysis. The leachates from this column had initially high pH (Fig 6.69) which represented the onset of OPC hydration reactions followed by the release of the CSH products and portlandite. The pH thereafter dropped to below 4.0. This confirms the prediction that after formation of the CSH gel the interaction of the solid residue particles with SAMD was significantly reduced and the slow dissolution of the aluminosilicate matrix and mullite inhibited. The hydration reactions of OPC generate portlandite following reactions (6.33) and (6.34) (Taylor, 1998) and will contribute to the initially high pH of the leachates.



The low pH exhibited by all the solid cores at the top of the column could be due to several reasons, this represents the SAMD leachant which is neutralized before moving down the column hence this represents the region of maximum depletion of alkalinity. Being in contact with the atmosphere, oxidation of Fe²⁺ is bound to be maximum, precipitation of the oxidized Fe²⁺ and subsequent hydrolysis of Fe³⁺ in the leachant generates more acidity that consumes some of the alkalinity generated by the solid cores. Hydrus sulphate minerals are likely to have formed under these conditions. All the solid cores showed increased intensity of the yellowish coloration associated with iron hydroxides and (oxy) hydroxysulphates in the top section. At high Fe concentrations in solution, secondary sulphate phases can precipitate on the surface of the solid residue particles especially under evaporating conditions. These columns were left to dry for 7-14 days between drainages and such precipitates could have formed at the surface of the solid residue cores due to evaporation. The hydrous sulphate minerals can be a source of acidity (Alpers *et al.*, 1994). This is could have been released by dissolution on resumption of drainage, example Halotrichite and Coquimbite (reactions 6.35 and 6.36 respectively).



It can be concluded at this point that addition of fly ash to the SR slows down the acidification of the column solid cores. Blending with OPC reduces the interaction of the SR with the leachant due to encapsulation of the residue particles by the generated CSH gel. This slowed down the acidification of the solid residue core and dissolution of the aluminosilicate matrix and mullite with subsequent reduction in Ca released. This probably would explain the low SO_4^{2-} attenuation efficiency of SR + 6 % OPC solid core as compared to FA, SR + 25 % FA and SR + 40 % FA cores.

5.2.4 Sequential chemical extraction (SSE) of the leached solid residue (SR) cores

In the section of contaminant attenuation profiles it has been shown that the main mechanisms responsible for retention of the contaminants is precipitation, adsorption, oxidation and hydrolysis as the pH is buffered at alkaline (10-12) and circumneutral pH (6-9.5). Precipitates identified include gypsum, ettringite and those predicted to be precipitating by PHREEQC include $\text{Al}(\text{OH})_3(\text{amorphous})$, $\text{Fe}(\text{OH})_3(\text{amorphous})$, FeOHSO_4 , jurbanite, manganite and rhodochrosite.

A widely used technique for understanding elemental distributions in the solid phase in soil and sediments involves the use of selective sequential extractions (SSE) (Chao, 1984; Tessier *et al.*, 1985). SSE procedures have also been used on mine waste contaminated areas (Kuo *et al.*, 1983; Ramos *et al.*, 1994; Ma and Rao.,1997). The use of SSEs is based on the premise that chemical reagents can remove elements from specific fractions of the solid phase by destroying the binding agents between metals and the matrix (Tessier *et al.*, 1979). However the amount of any one given element extracted from a particular phase is dependent on the reagent concentration and type, extraction sequence and solid/solution ratio hence the term operationally defined values (Miller *et al.*, 1986).

The sequential extraction of the solid residue cores was done to assess the mass of trace metals associated with each of the dominant secondary mineral phases and also qualitatively correlate the contaminant retention capacity of the FA, SR + FA and SR + OPC blends. A second objective of the sequential extraction was to confirm the mechanisms proposed for the attenuation of the contaminants. Three fractions were considered: water soluble fraction, amorphous fraction and reducible fraction. The amorphous fraction was considered to be significant based on the fact that despite the high % attenuation efficiency of the contaminants, no crystalline Al or Fe bearing mineral phases were detected by XRD. Consequently selective sequential extractions were done on FA, SR, SR + 25 % FA and SR + 6 % OPC on top, middle and bottom solid core slices. However due to the similarity of the extraction profiles of the SR and SR + 25 % FA cores the discussion of the results is confined to FA, SR and SR + 6 % OPC solid cores. The tables 6.12- 6.15 show sequential extraction results for FA, SR, SR + 25 % FA and SR + 6 % OPC leached solid cores. Detection limits (mg kg^{-1}) for each fraction are presented together with the results in Table 6.12.

5.2.4.1 Water soluble fraction

The water soluble fraction contains metals derived from re-dissolution of water soluble phases such as gypsum ($\text{CaSO}_4 \cdot 2\text{H}_2\text{O}$) or calcium sulphate hydrate ($\text{CaSO}_4 \cdot 0.6 \text{H}_2\text{O}$),

both were identified by XRD in the leached solid cores (Fig E1-E4). These can also result from the re-dissolution of tertiary phases which could have accumulated during the drying and evaporation of core surface during the drainage experiments (an interval of 7-14 days was imposed between respective drainages). It can also include metals desorbed from Mn, Al or Fe (oxy) hydroxide surfaces.

5.2.4.1.1 Fly Ash (FA) leached solid core

Fe concentration showed an increase from 10.7 mg kg⁻¹ at the top to 4446 mg kg⁻¹ at the bottom, this indicates the retention profile of Fe as acidification of the FA core occurs. The least acidified part of the core (bottom) retains most of the Fe in the pore water (Table 6.12).

This further indicates that the Fe in this fraction is probably derived from dissolution of previously precipitated phases which moved with the pH front as the core acidified. Ca exhibited high concentration at the top decreasing at the bottom section. This indicates that the retention profile of Ca was probably dictated by precipitation of soluble phases such as gypsum which decreased as the SO₄²⁻ was attenuated with migration of the SAMD down the solid core. SEM-EDX revealed gypsum crystals to be highly concentrated at the top section of the solid cores (Fig 6.70).

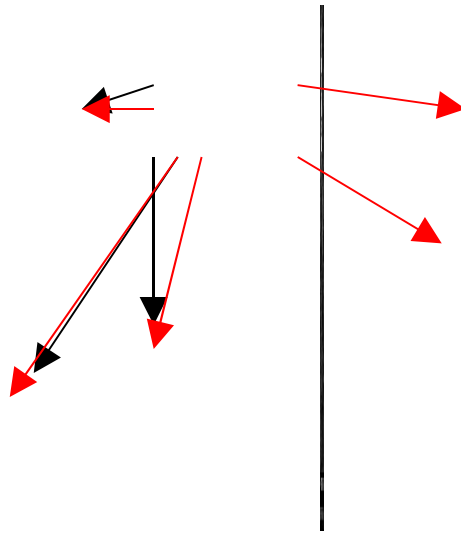


Figure 6.73: SEM micrograph showing numerous gypsum crystals in the top section of the leached solid residue (SR) cores.

Al, Mn, Ni, Zn, Cu, B, Sr and Mg show a similar retention profile with high concentration at the top and bottom section. However for Al, Ni, Zn, Cu, B and Sr the bottom section registered higher concentration, this corresponds to the high pH of the pore water at this section (Fig 6.69). This probably indicates the high concentration were

Table 6.16: Sequential extraction results for the FA solid core (results presented as mean±SD for n=3 extractions, DL-detection limits)

Fly Ash solid core		water soluble fraction (mg kg ⁻¹ dry solids)									
	Al	Fe	Mn	Si	Ca	Ni	Zn	Cu	B	Sr	Mg
Top	229.3±9.4	10.7±8.4	116.0±4.0	BDL	3466.2±70.6	7.6±0.8	2.9±0.7	BDL	0.35±0	44.3±0.7	1082.3±41.9
Middle	170.4±24.2	2758.0±89.9	2.01±0.6	BDL	2698.3±493.4	BDL	BDL	BDL	BDL	4.5±0.4	21.2±11
Bottom	1790.7±73.1	4446.4±364.6	17.2±0.51	486.6±15.3	1138.3±68.9	31.5±1.5	40.7±17.1	2.1±0.9	70.3±0	75.7±3.1	253.7±10.3
DL	0.018	0.577	0.005	0.706	3.34	0.009	0.007	0.001	0.084	0.0005	1.56
		Amorphous fraction (mg kg ⁻¹ dry solids)									
	Al	Fe	Mn	Si	Ca	Ni	Zn	Cu	B	Sr	Mg
Top	1960.5±178.6	BDL	1786.1±21.9	BDL	84598.7±11208	BDL	48.5±7.5	BDL	BDL	1056±70.7	20570.8±1299
Middle	15484.5±669.4	18056.1±3772.4	58.1±15.7	5669.8±0	BDL	225.8±0	131.3±9.3	105.2±72.2	1410±0	68.1±3.6	1172.9±75.5
Bottom	49718.3±2533	94258.7±6998	487±45.4	12468.7±749	102398.1±12115	641.4±64.6	231.2±13.5	102.8±6.7	73.1±0	3191.1±155.9	6381.9±241.2
DL	0.332	10.86	0.088	13.3	62.83	0.164	0.128	0.018	1.58	0.010	29.42
		Reducible fraction (mg kg ⁻¹ dry solids)									
	Al	Fe	Mn	Si	Ca	Ni	Zn	Cu	B	Sr	Mg
Top	3.7±2.8	BDL	292.9±2	BDL	11899.4±2698	BDL	18.7±0	BDL	4.3±0	201.8±4.5	3876.2±21.2
Middle	2149.5±8.6	922.3±214	76.8±8.4	251.8±124	BDL	24.5±18.9	16.5±15.3	16.2±0	26.3±0	8.9±0.02	630.4±48.7
Bottom	7486.7±305.3	13136±344	200.6±14.5	1868.8±18.9	15786.5±178	90.4±4.1	28.9±3.7	7.3±2.4	BDL	536.7±2.1	983.2±42.5
DL	0.05	1.62	0.013	1.98	9.39	0.024	0.019	0.003	0.236	0.002	4.90

Table 6.17: Sequential extraction results for the solid residue (SR) leached solid core (results presented as mean±SD for n=3 extractions)

Solid residue core		water soluble fraction (mg kg ⁻¹ dry weight)									
	Al	Fe	Mn	Si	Ca	Ni	Zn	Cu	B	Sr	Mg
Top	744.7±13.7	BDL	158.4±3.3	BDL	3835.6±136	4.2±0	7.3±1.1	BDL	BDL	71.5±1.8	850.7±23
Middle	BDL	5184.8±297	0.71±0.7	85.6±0	852.3±0	5.7±0.4	91.5±30	BDL	49±14.6	9.5±0.5	5.9±0.2
Bottom	2385.9±130	4536.6±275	20.3±1	866.9±85.5	2487.1±180	32.6±1.2	6.3±6.3	3.2±0	BDL	173.9±5.7	350.3±20.7
		Amorphous fraction fraction (mg kg ⁻¹ dry weight)									
	Al	Fe	Mn	Si	Ca	Ni	Zn	Cu	B	Sr	Mg
Top	6969.7±21.2	BDL	1803.9±86	BDL	54358.3±2317	BDL	404.1±266	BDL	BDL	1170.7±20	14094.2±588
Middle	25056.7±635	13289±3729	7.8±7.3	5064.1±1111	BDL	BDL	2358.5±0	BDL	BDL	189.4±134	1360.2±101
Bottom	53632.4±1811	53682.5±2302	339.7±0.97	18056.9±58	97514.9±3816	342.3±18.8	181.3±81	35.5±3.5	BDL	4772.8±126	6604.7±176
		Reducible fraction fraction (mg kg ⁻¹ dry weight)									
	Al	Fe	Mn	Si	Ca	Ni	Zn	Cu	B	Sr	Mg
Top	1.9±0	BDL	212.5±19.7	BDL	9993.4±988	BDL	71.9±63	BDL	BDL	250.1±18.5	3578.8±222
Middle	1195.1±51	2760.9±376	189.8±7.9	804.9±104	BDL	12.7±0	372.5±0	BDL	BDL	27.6±7.9	1316±56
Bottom	10433.4±1777	8460.8±59.5	371.9±12	3255.3±38.8	18507±2037	49.1±1.6	15.3±3	3.6±0	BDL	884.4±1.2	1315.6±1

Table 6.18: Sequential extraction results for the SR + 25 % FA leached solid core (results presented as mean±SD for n=3 extractions)

SR + 25 % FA solid core				Water soluble fraction (mg kg ⁻¹ dry weight)							
	Al	Fe	Mn	Si	Ca	Ni	Zn	Cu	B	Sr	Mg
Top	759.4±1	BDL	147.2±3.8	13.7±5.4	3880.8±380	BDL	12.9±6	DBL	BDL	72±0.5	752.1±7.4
Middle	279.4±47	3934.4±390	1.8±1	BDL	1510.5±1120	16.5±3	BDL	31.2±12.2	BDL	6.8±0.1	21.6±1.4
Bottom	2674.6±48	4599.5±65	22.6±0.1	616.9±28	3373.3±2148	9.1±0.4	BDL	6.6±0.6	BDL	206.4±13	394.7±4.5
				Amorphous fraction (mg kg ⁻¹ dry weight)							
	Al	Fe	Mn	Si	Ca	Ni	Zn	Cu	B	Sr	Mg
Top	7564.8±262	38.4±0	1614±123	642.7±207	66183.1±323	BDL	127.8±60.7	BDL	BDL	1135.6±32.4	11427±1070
Middle	27389±287	19341.5±681	29.9±3	5226.7±1122	46022.2±7122	219.5±17.8	BDL	319±16.4	BDL	69.3±2	1426.6±27.8
Bottom	43568.5±9322	47850.9±17577	332.3±98.3	11582.3±1448	135313.5±47718	142.5±9.2	16.2±0	102.5±3.9	BDL	4120.9±1248	5560.2±1389
				Reducible fraction (mg kg ⁻¹ dry weight)							
	Al	Fe	Mn	Si	Ca	Ni	Zn	Cu	B	Sr	Mg
Top	21.2±14.3	BDL	143.8±15.2	BDL	13786±609	5.6±5.6	56.6±36.3	3±0	BDL	264.3±17.8	4080.7±353
Middle	2467.7±142	2715.5±67.8	321.5±6.9	4208.1±2745	41130.3±30499	58.9±7.2	BDL	35±12.7	377±0	15.6±1.5	1936.5±56.7
Bottom	8412.9±288	9977.1±822	436.5±6.3	2446.3±133	23765.9±1175	23.1±0.3	19.7±0	16.8±1	BDL	939.3±35.1	1249.5±59

Table 6.19: Sequential extraction results for the SR + 6 % OPC leached solid core (results presented as mean±SD for n=3 extractions).

SR + 6 % OPC leached solid core		Water soluble fraction (mg kg ⁻¹ dry weight)									
	Al	Fe	Mn	Si	Ca	Ni	Zn	Cu	B	Sr	Mg
Top	316.6±2.1	31.9±18.5	66.8±6.4	17.4±7.3	5067.2±629	3.6±0.84	0.93±0.3	3.5±1.6	7.3±0	72.8±0.3	455±38.5
Middle	918.6±97.9	3441.9±274	2.1±0	84.6±71.2	63561.3±22827	5.1±0	BDL	19.1±0.06	17.6±0	5.6±0.16	46.2±4
Bottom	2662.6±65.5	5713.4±754	22.4±0.72	714.5±29.1	10500.4±152	6.6±0.5	BDL	7.1±0.5	BDL	271.4±3.5	371.3±7.6
		Amorphous fraction (mg kg ⁻¹ dry weight)									
	Al	Fe	Mn	Si	Ca	Ni	Zn	Cu	B	Sr	Mg
Top	141.6±71.5	434.2±0	912.5±19	BDL	94080.9±6561	66.9±15.2	4.5±4.5	20.9±8.1	163.8±0	1785.2±47	15522.2±598.4
Middle	23705.3±353	25404.8±432	1567.6±7.2	3783.9±1	1704152.7±66180	140.6±49.2	BDL	163.7±40.9	BDL	95.1±5.7	10917.3±183
Bottom	66678±1020	117019.6±3051	4741±506	21531±1207	315495.3±22965	177.2±15.5	71.6±10.7	131.5±46.4	BDL	7535.8±71.7	17065.5±2484
		Reducible fraction (mg kg ⁻¹ dry weight)									
	Al	Fe	Mn	Si	Ca	Ni	Zn	Cu	B	Sr	Mg
Top	33.3±12.9	42.3±42.3	2.4±0.5	BDL	15687.2±1139.6	11.5±0.3	BDL	6.67±2	0.073±0	245.3±2.5	740.8±24.5
Middle	2286.1±153	2089.5±610	114.3±16.7	578.8±0	240551.4±13117	27.3±1	BDL	63±34.4	BDL	7.2±0.5	1380.9±70
Bottom	7867.3±274	12448.8±805.8	319.5±6.6	2944.8±8.1	35617.6±6599	17.1±0.32	5±6.3	20.7±4.7	BDL	980.7±5	2120.4±374.4

derived from soluble mineral phases that precipitated at alkaline pH. The high concentration at the top and bottom section could also be indicative of re-dissolution of tertiary mineral phases formed as a result of evaporation and drying of the pore water at the top and bottom of the solid cores. The solid cores were in contact with the atmosphere at the top and bottom. Si, Ni, Zn, Cu and B were not detected in the middle section.

5.2.4.1.2 Solid residue (SR) leached solid core

Al, Mn, Ca, Sr and Mg show a similar profile with high concentration exhibited at the top and bottom section, with the middle section only exhibiting low or non detectable concentrations (Table 6.13). This profile is similar to that observed for FA solid cores. Fe, Zn and B exhibit a similar trend showing high concentration in the middle section. Si, Ni and Cu show a similar pattern increasing down from the surface to the bottom of the solid core. This trend mirrors the increasing pH of the pore water in the solid residue core (Fig 6.69). This probably indicates re-dissolution of previously formed precipitates under the circum-neutral pH regime.

5.2.4.1.3 Solid residue + 6 % Ordinary Portland Cement (SR + 6 % OPC) leached solid core

Al, Fe, Si, Ca and Ni show increasing trend from top to the bottom section of the SR + 6 % OPC solid core. This increasing trend mirrors the pH profile of the pore water (Table 6.15 and Fig 6.69) in the solid core and probably reflects the dissolution of mineral phases precipitated during the high pH initially generated on initial contact with SAMD. Mn, Sr and Mg exhibit high concentration in the top and bottom sections. For Mn this probably indicates dissolution of phases that formed as a result of oxidation at alkaline pH near surface where supply of O₂ was adequate. PHREEQC predicted manganite to be controlling Mn²⁺ activity at alkaline pH. Rhodochrosite that formed under alkaline pH (8-9) as predicted by PHREEQC would dissolve as the solid core acidifies.

5.2.4.2 Amorphous fraction

Mineralogical analysis of the leached solid residue cores by XRD did not reveal any crystalline Fe or Al-bearing mineral phases. FTIR analysis suggested adsorption or incorporation of SO₄²⁻ in Al or Fe bearing mineral phases. However visualization of the sectioned leached solid cores revealed extensive yellowish/brownish coloration, characteristic of ochreous precipitates (Jeong and Soo, 2003) (Fig 6.61- 6.62). SEM and SEM-EDX revealed amorphous precipitates, ettringite, gypsum and CSH gels in the leached solid residue cores. PHREEQC simulation predicted precipitation of amorphous Al(OH)_{3(amorphous)}, Fe(OH)_{3(amorphous)}, FeOHSO₄, jurbanite, ferrihydrite in the leachates of the solid residue cores. The ammonium oxalate extraction (AOD) in the dark was intended to remove the amorphous Fe, Al and Mn (oxy) hydroxides together with adsorbed or co-precipitated ions. The AOD does not specifically extract one particular phase but all non-crystalline Al, Fe and Mn all at once from the solid phase (Jackson *et al.*, 1986)

5.2.4.2.1 Fly Ash (FA) leached solid core

Al, Fe, Si, Ni, Zn, Cu, and Ca show an increase from the top to the bottom section (Table 6.12). It should be noted that the increase of Al (from 1960.5-49718.3 mg kg⁻¹), Fe (detection limit to 10.86-94258.7 mg kg⁻¹) and Si (13.3-12468 mg kg⁻¹) is significantly greater than for other elements. This suggests that the increase in AOD extracted Ni, Zn, and Cu corresponds to the amounts adsorbed on amorphous Al, Fe and Si precipitates down the solid core. Mn, Sr and Mg show a similar concentration profile with high concentration at the top and bottom section. The high concentration for Mn at the top section indicates that Mn was retained at the top section where high pH was generated initially and oxidation was likely occurring. PHREEQC simulation predicted formation of magnetite at alkaline pH. For Mg this could also represent dissolution of precipitates formed under the alkaline pH regime or increased adsorption of Mg. Sr probably represents increased retention as celestite (SrSO₄) which was predicted to be precipitating by PHREEQC and would consequently undergo dissolution under the acidic conditions employed. Ca concentration profile indicates a trend that is not dictated by adsorption on amorphous Al or Fe phases but by a phase like gypsum. The increased concentration in this fraction is probably due to increased dissolution of gypsum under the acidic regime employed. The fact that Ni, Cu, Zn and B were detected in the middle section of this fraction while they were at detection limits in the same section for the water soluble fraction strongly indicates their adsorption onto the Al and Fe amorphous precipitates.

5.2.4.2.2 Solid residue (SR) leached solid core

Al, Fe and Si show a steady increase from the top to bottom section of the SR solid core (Table 6.13). This points to an increase in amorphous precipitates down the solid core and relocation of precipitates formed earlier at the top of the solid core. The trend mirrors the pH profile of the pore water in the solid core with the pH increasing down the solid core (Fig 6.69). The non-detectability of Ni and Cu in the top and middle section and subsequent detection in the bottom section probably indicates translocation with the amorphous Al and Fe precipitates. Ca exhibits high concentration at the top and bottom section being undetected in the middle section. Mn, Sr and Mg were detected in all the sections with the top and bottom section exhibiting high concentrations.

5.2.4.2.3 Solid residue + 6 % Ordinary Portland Cement (SR + 6 % OPC) leached solid core

Al, Fe, Mn and Si exhibited an increasing trend from the top to the bottom section of the SR + 6 % OPC solid residue core (Table 6.15). This strongly indicates the importance of the amorphous precipitates in retaining the contaminants in the solid cores. A marked efficiency of the SR + 6 % OPC solid core than FA and SR in retention of the contaminants is observed. This is most noticeable with Fe, the amount retained in the bottom section is double (117019 mg kg⁻¹) compared to that retained by SR (53682 mg kg⁻¹). A similar phenomenon is observed with Mn, Mg, Cu, Sr and B. This probably indicates the role encapsulation of the precipitates and solid residue particles by the CSH gel had on the contaminants retention capacity of this solid core. SEM-EDX identified Fe, Mn rich Ca-Si-Al-O gels (Fig 6.71) in this solid core which suggests adsorption or incorporation of Mn in amorphous Fe rich precipitates or Al-Si-O rich gels.

Figure 6.74: Backscattered SEM micrograph showing Fe, Mn, S rich Ca-Al-Si-O gel with accompanying EDX analysis.

This could also represent encapsulation of Mn (oxy) hydroxides and Fe amorphous (oxy) hydroxides in Al-Si-O or Ca-Si-Al-O gels. Encapsulation was extensive in this solid core as identified by SEM (Fig 6.72).

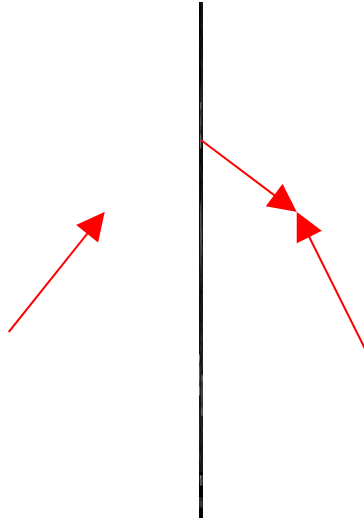


Figure 6.75: SEM micrograph showing Ca-Si-Al-O rich gel encapsulating precipitates and solid residue particles

(CSO-Ca-Si-O gel was identified earlier on by SEM-EDX).

The increased Ca retention as compared to other solid cores was due to precipitation of gypsum, ettringite and the high Ca content of OPC (Table 6.5). The increased retention could also be due to incorporation of Ca in precipitating Si-Al-O rich gels that were identified in the solid residue cores by SEM-EDX (Fig 6.71). This solid core also exhibited increased retention of B. Eary *et al.* (1990) points out that borate can be incorporated in precipitating aluminum hydroxides.

5.2.4.3 Reducible Fraction

Sequential extraction of this fraction was intended to quantitatively estimate the effect of the strongly acidic SAMD on the crystalline Fe, Mn (oxy) hydroxides and also estimate possible formation of crystalline Fe, Al and Mn (oxy) hydroxides in the fly ash residues.

5.2.4.3.1 Fly ash (FA) leached solid core

The Fe concentration in leached FA solid cores shows an increase (from detection limits 1.62 mg kg^{-1} to 13136 mg kg^{-1}), indicating increasing retention of crystalline Fe (oxy) hydroxides as the pH of the pore water increased (Fig 6.69). Al shows a smooth increase in concentration from top to bottom ($3.7\text{-}7486 \text{ mg kg}^{-1}$) which also indicates increased retention of Al (oxy) hydroxides as the pH of the pore water increases. Mn registered

high concentration in the top and bottom section, a phenomenon that was observed in the water soluble and amorphous fractions. This reinforces the fact that Mn could have been mainly retained as Mn (oxy) hydroxide. Increased retention at both the top and bottom section is consistent with increased oxidation due to ingress of O₂ gas since the column surface was open and thus in direct contact with the atmosphere. Ca, Cu, Zn and Ni do not show any definite trends in this fraction.

5.2.4.3.2 Solid residue (SR) leached solid core

Al, Fe and Si show an increasing trend from non-detectability for Fe and Si at the top section to highest concentration at the bottom section similar to the FA solid cores. This probably points to increased retention of Al, Fe as crystalline (oxy) hydroxides. It is also possible that the trend could be a reflection of the gradation of the fly ash residual matrix as the AMD percolates down the solid residue core. This study did not attempt to quantify the crystalline Al, Fe and Mn (oxy) hydroxides in the un-reacted fly ash. The concentration for the other elements observed probably represents fractions locked in the residual matrix or adsorbed in the Al and Fe (oxy) hydroxides that formed during the drainage. B was not detected indicating that it is only present as soluble salts on the surfaces of the fly ash spheres and not in the aluminosilicate matrix. Mg seems to be highly concentrated in the top section for all the extractions but shows highest concentration in the amorphous fraction.

In conclusion the importance of amorphous precipitates in the attenuation of contaminants was demonstrated in the high concentrations retained in the amorphous fraction in the sequential extractions. Gypsum precipitation was also observed to be a significant SO₄ retention pathway as also evidenced by the high concentrations of Ca observed in the water soluble fraction and also in the amorphous fraction. High retention of contaminants Fe, Mn, Al, Ca and Si was observed in the amorphous fraction in the SR + 6 % OPC solid core which renders credence to the fact that formation of amorphous calcium silicate hydrate, calcium ferrite hydrate and possibly calcium aluminate hydrate gels were contributing to the increased contaminants retention in this solid core. Glasser (1970) observes that cation immobilization by CSH gels and by (hydr) oxide precipitation is the most important in cement systems.

5.2.5 Conclusions

Column leaching has been used to simulate conditions of co-disposal of solid waste such as mine spoils and fly ash or sludge from different chemical processes. The aim was to model the situation in the field and thereafter use the information to predict the effect on the environment probably on disposal of sludge or co-disposing two solid waste streams. In this study SR were modified with fly ash at varying % and 6 % Ordinary Portland Cement, fly ash was also monitored as a control and their effect on the chemistry of the synthetic AMD was evaluated with drainage time.

This study considered a worst case scenario by using a highly polluted AMD simulating Navigation Dam toe seep (5000 ppm Fe, 14407 mg/L SO₄²⁻, 1000 mg /L Al, 250 mg/L

Mn²⁺ and 4253 mg/L CaCO₃ acidity). As a passive treatment barrier it can possibly be effectively used to treat large quantities of moderately polluted AMD.

Sequential extractions revealed that the amorphous fraction, deposited upon the column solids during the flow of SAMD, was the most important fraction in the retention of the major contaminants and was most enhanced in the OPC blend SR due to formation of amorphous CSH gels.

The leachate chemistry revealed interesting results. Acidification of all the solid cores was observed to occur in a stepwise fashion. Blending of the SR with fly ash had several effects on the leachate chemistry, the initial leachate pH was observed to be dependent on the % fly ash in the blend and secondly it influenced the duration of sustainability of buffering at pH 7-9.5. A significant feature of the solid residue and fly ash blended solid residue cores was the sustained buffering at pH 7-9.5. Another significant feature of the solid residue core drainage results is the potential of the SR to buffer pH at 7-9.5 and contribute to contaminants attenuation for extended periods of time. This was quite significant, since the SR resulted from the primary treatment of AMD with fly ash where the free alkalinity due to surface CaO had been fully utilized. This important finding confirmed the importance of these SR for the purpose of mine backfilling since these materials will continue to passively buffer pH and clean-up percolating AMD. Another important finding is that blending with 6 % OPC occluded the release of this alkalinity from the SR but this was compensated by the inducement of other attenuation mechanisms even at pH below 5. However by the end of the drainage experiments at 165 days, contaminants concentration in the leachates in the SR + 40 % FA solid residue cores were observed to be increasing. Since this particular core contaminants concentrations release kinetics were observed to follow that of the fly ash solid core closely, it could be argued that at 165 days the buffering capacity due to CaO was exhausted and this solid core was now entering the phase where the dissolution of SiO_{2(amorphous)} and mullite were buffering the pH at 7-9.5.

Therefore it is recommended for longer drainage experiments probably for one year or longer to be carried out to ascertain the final break-up of the alkalinity of these solid cores and also confirm to what extent the re-dissolution of the previously formed precipitates will occur.

Another recommendation would be to assess whether the SR can be used as passive treatment barriers, this would require probably the drainage of the SR with SAMD under a dynamic flow regime to quantify the amount of coal mines waste water that can be treated over a given period of time.

5.3 STRENGTH TESTING OF SOLID RESIDUES

The investigation focussed upon the characteristics necessary for application of neutralisation SR as backfill materials, with or without additional binders. The materials were tested for their strength development for 410 days and the results are presented in this section.

5.3.1 Materials and methods

5.3.1.1 FA and AMD

Fresh fly ash was obtained from Arnot power station. Samples were taken at the first bag filter and were labelled “Arnot C1 FA”. Acid mine drainage was sampled at the toe seep of Navigation plant, in Landau colliery. An elemental analysis of that wastewater was performed at Eskom facilities (Table 6.16).

Table 6.20: Composition of Navigation toe seep AMD used to prepare SR.

Component	Concentration (mg/L)
Al	404
As	< 0.01
B	51.11
Ba	1.12
Be	< 0.005
Ca	448
Cd	< 0.005
Co	2.17
Cr	3.44
Cu	10.56
Fe	6024
Hg	< 0.01
K	3.17
Mg	346
Mn	65.85
Na	55.7
Ni	< 0.005
Pb	13.49
Se	< 0.02
SO ₄	22560
Sr	36.64
Zn	< 0.004

5.3.1.2 Preparation of SR from the neutralisation of AMD with FA

Different types of SR were prepared by reacting Arnot FA and Navigation AMD at different FA: AMD ratios. The neutralisation of AMD by FA was performed at pilot scale, in a 250 L tank located at Eskom facilities (Figure 6.73). The FA: AMD mixture was agitated vigorously in order to facilitate the neutralisation process (Petrik *et al.*, 2004). Agitation was maintained for an extended period of time (several hours) with the objective of reaching a circumneutral pH. The pH of the reacting mixture was thus monitored during each neutralisation experiment.



Figure 6.76: Pilot-scale reactor used for the neutralisation of AMD with FA and preparation of SR.

The details of the preparation of three types of SR from the neutralisation of Navigation AMD by Arnot FA at different FA: AMD ratios are indicated in Tables 6.17, 6.18 and 6.19. At the end of the neutralisation reactions, the mixtures were transferred into buckets and were left for a few hours for settling and separation of phases. The supernatants were then separated from the (wet) SR. The remaining SR and supernatants were both kept in tightly locked plastic containers.

Table 6.21: Experimental details of the preparation of SR from Arnot C1 FA and Navigation AMD at a FA:AMD ratio of 1:3.

FA:AMD ratio	1:3					
FA	Arnot C1					
Mass of FA (kg)	41.66					
AMD	Navigation toeseep					
Volume of AMD (L)	125					
Agitation speed (rpm)	1000					
Time (min)	0	30	60	90	120	150
pH	2.70	5.45	5.51	5.41	5.37	5.32
Time (min)	180	210	270	390	420	1350
pH	5.30	5.28	5.29	5.56	5.88	8.83
Total time of neutralisation (min)	1381					

Table 6.22: Experimental details of the preparation of SR from Arnot C1 FA and Navigation AMD at a FA:AMD ratio of 1:4.

FA:AMD ratio	1:4	
FA	Arnot C1	
Mass of FA (kg)	50	
AMD	Navigation toeseep	
Volume of AMD (L)	200	
Agitation speed (rpm)	1500	
Time (min)	0	320
pH	2.79	7.74
Total time of neutralisation (min)	320	

Table 6.23: Experimental details of the preparation of SR from Arnot C1 FA and Navigation AMD at a FA:AMD ratio of 1:6.

FA:AMD ratio	1:6							
FA	Arnot C1							
Mass of FA (kg)	20.83							
AMD	Navigation toeseep							
Volume of AMD (L)	125							
Agitation speed (rpm)	1000							
Time (min)	0	30	60	90	120	180	210	1113
pH	2.84	4.65	5.48	5.52	5.43	5.29	5.26	4.90
Total time of neutralisation (min)	1129							

5.3.1.3 Determination of moisture content

The moisture content was measured for the calculation of the amount of binder (Castle cement) to be added when preparing the blended materials used in stability and flowability testing.

The moisture content of wet solid residues, Arnot C1 fly ash and Castle cement was determined to obtain the dry weight of solid in each material. A mass of 100 g of material was dried at 105 °C for over 12 hours. The moisture content analyses were duplicated for solid residues.

5.3.1.4 Determination of specific gravity

The specific gravity of dry solid residues, Arnot C1 fly ash and Castle cement was determined. A mass of 50 g of material was dried at 105 °C for over 12 hours. The dried solids were transferred into a flask whose mass was previously measured. The mass of the flask containing dry solids was measured. The flask was then filled with water until saturation. The mass of the flask containing solids and water was measured. Finally, the flask was emptied out and filled again with water. The mass of the flask containing only water was measured. Specific gravity analyses were duplicated.

5.3.1.5 Flow test using marsh cone

To estimate the amount of water that would be needed to make the slurry suitable for pumping underground, the solid residues and Arnot C1 fly ash were submitted to marsh cone tests.

The three samples of solid residues were tested for flowability without binder. Samples made by reacting a) Arnot C1 FA and Navigation AMD at 1:4 ratio and b) Arnot C1 FA and Navigation AMD at 1:6 ratio were also tested with the addition of 3% binder (Castle cement) in the slurry. One marsh cone test was performed on Arnot C1 fly ash, without binder. The masses used to prepare slurries were 2000 g for solid residues and 1500 g for fly ash. The mass of fly ash was reduced to 1500 g to have similar amounts of dry solids in all the slurries, according to the results of moisture content

Slurries were made by adding tap water to the solids. After each addition of water, 1 L of slurry was placed in the marsh cone and the time for this volume to run out was measured. Several amounts of water were added successively until the run out time dropped to less than 10 seconds. The resulting value was taken as the required water content for make-up of pumpable slurry.

5.3.1.6 Materials supplied to CSIR for strength testing

Four solid samples were sent for particle size, permeability and strength testing at CSIR:

- Arnot C1 fly ash
- SR from the reaction between Arnot C1 FA and Navigation AMD at a FA:AMD ratio of 1:3
- SR from the reaction between Arnot C1 FA and Navigation AMD at a FA:AMD ratio of 1:4
- SR from the reaction between Arnot C1 FA and Navigation AMD at a FA:AMD ratio of 1:6.

The solid samples were sent in plastic bags. To store them more safely, it was decided to transfer the contents into sealed buckets. There was a definite indication of preferential settling in the bags containing solid samples. To minimise this, small amounts were transferred into each bucket in turn, so that each one had similar material.

In addition, two 20 L containers of process water were supplied. These waters proceeded from the following reactions:

- neutralisation of Navigation AMD with Arnot C1 FA at a FA:AMD ratio of 1:3
- neutralisation of Navigation AMD with Arnot C1 FA at a FA:AMD ratio of 1:6.

5.3.1.7 Preparation of the cylinders and curing for strength tests

The unconfined compressive strength and elastic modulus of the three samples of SR supplied to CSIR were tested. In order to prepare samples for the tests, slurries were prepared by mixing the SR with process water resulting from the neutralisation of AMD with FA. The amount of water added to each sample corresponded to the amount required to obtain a pumpable slurry, as defined by the marsh cone tests (Petrik *et al.*, 2005). Once

prepared, each slurry was split and poured into different cylindrical tubes for strength testing to be performed in duplicate after various periods of curing. The tubes were placed under plastic bags, a bottle of water being placed next to them to maintain the required level of humidity for the curing process. Additional samples were prepared for curing and strength testing, by blending the slurries of SR with 3 % binder (Castle cement). The provisional schedule of curing and strength testing, with the different blends and periods of curing, is given in Table 6.20. The period of curing extended over 14 to 410 days. Samples blended with 3 % cement were tested after 14 days for the 1:3 and 1:6 ratios and up to 410 days for 1:4 ratio.

Table 6.24: Schedule of curing for strength testing of SR.

SR	Arnot C1 FA : Navigation AMD 1:3 ratio		Arnot C1 FA : Navigation AMD 1:4 ratio		Arnot C1 FA : Navigation AMD 1:6 ratio	
	Binder none	3 % cement	none	3 % cement	none	3 % cement
Time of curing (days) before strength test		14		14		14
	90		90	90	90	
	180		180	180	180	
	410		410	410	410	

5.3.2 Results

5.3.2.1 Moisture content

The moisture content was quite similar for the three different solid residues, ranging from 29 to 34 % (Table 6.21). There was no linear correlation between the solid to liquid (FA to AMD) ratio of the neutralisation reaction and the residual water content in the slurry. Fly ash by itself and cement contained, as expected, very little water. Fly ash was sampled fresh from the power station filter bags, where it is dry. It was then kept in a sealed container.

Table 6.25: Moisture content of solid residues, Arnot C1 FA and Castle cement

Material	Arnot FA Navigation AMD 1:3 ratio	Arnot FA Navigation AMD 1:4 ratio	Arnot FA Navigation AMD 1:6 ratio	Arnot C1 FA	Castle cement
	Replicate 1 (%)	29.74	34.46		
Replicate 2 (%)	29.26	32.26	31.92	-	-
Mean (%)	29.50	33.36	31.63	0.09	0.15

5.3.2.2 Specific gravity

The gravity of solid residues was similar for the three different samples, ranging from 2.23 to 2.28 (Table 6.22). There was no linear correlation between the FA to AMD ratio of the neutralisation reaction and the density of the residual solid. Arnot fly ash by itself and cement also had specific gravities in the same range, 2.23 and 2.78 respectively.

Table 6.26: Specific gravity of solid residues, Arnot C1 FA and Castle cement

Material	Arnot FA Navigation AMD 1:3 ratio	Arnot FA Navigation AMD 1:4 ratio	Arnot FA Navigation AMD 1:6 ratio	Arnot C1 FA	Castle cement
Replicate 1	2.283	2.240	2.283	2.226	2.795
Replicate 2	2.285	2.230	2.282	2.234	2.770
Mean	2.284	2.235	2.282	2.230	2.783

5.3.2.3

5.3.2.4 Flow test using marsh cone

None of the three solid residues could flow through the marsh cone without addition of water (Tables 6.23, 6.24 and 6.25). The amount of water needed in the slurry to it to flow through the cone in less than 10 s ranged from 680 to 893 mL for solid residues prepared at FA:AMD ratios of 1:3 and 1:4, respectively. This corresponded to slurry density of 1.61 and 1.49. As a comparison, the test held on Arnot C1 FA showed that a slurry density of 1.63 was enough for the mixture to flow (Table 6.26). Values obtained for FA and for solid residues containing the largest amount of FA (namely ratio 1:3) were quite similar. These tests demonstrated that if the solid residues are to be applied underground, a slurry having a density of around 1.5-1.6 will have to be prepared by adding water to the backfill material or, more practically, the slurry remaining after neutralization should only be dewatered up to a point falling within this range.

Table 6.27: Marsh cone tests results for solid residues obtained from the reaction between Arnot C1 FA and Navigation AMD at a FA:AMD ratio of 1:3

Mass of water (g)	Total mass of water (g)	Run out time (s)	Relative Density of slurry	Mass fraction of solids	Flow rate of solids (g/s)	Water/solid ratio
590	590	--	1.656	0.705	--	0.418
80	670	10.10	1.616	0.678	108.494	0.475
10	680	9.10	1.611	0.675	119.495	0.482

Table 6.28: Marsh cone tests results for solid residues obtained from the reaction between Arnot C1 FA and Navigation AMD at a FA:AMD ratio of 1:4

Mass of water (g)	Total mass of water (g)	Run out time (s)	Relative Density of slurry	Mass fraction of solids	Flow rate of solids (g/s)	Water/solid ratio
667	667	--	1.583	0.666	--	0.501
100	768	--	1.540	0.635	--	0.576
51	818	24	1.521	0.620	39.261	0.614
50	868	11.02	1.503	0.606	82.610	0.651
10	878	10.50	1.500	0.603	86.125	0.659
15	893	9.62	1.495	0.599	93.061	0.670

Table 6.29: Marsh cone tests results for solid residues obtained from the reaction between Arnot C1 FA and Navigation AMD at a FA:AMD ratio of 1:6

Mass of water (g)	Total mass of water (g)	Run out time (s)	Relative Density of slurry	Mass fraction of solids	Flow rate of solids (g/s)	Water/solid ratio
633	633	--	1.624	0.684	--	0.463
50	683	28.56	1.599	0.667	37.353	0.499
31	714	16.81	1.585	0.657	61.958	0.522
15	729	13.18	1.579	0.652	78.125	0.533
21	749	11.18	1.570	0.646	90.696	0.548
20	770	10.10	1.561	0.640	98.909	0.563
11	780	9.75	1.557	0.637	101.661	0.571

Table 6.30: Marsh cone tests results for Arnot C1 FA

Mass of water (g)	Total mass of water (g)	Run out time (s)	Relative Density of slurry	Mass fraction of solids	Flow rate of solids (g/s)	Water/solid ratio
1.3	1.3	--	2.228	0.999	--	0.001
100	101	--	2.069	0.937	--	0.068
200	301	--	1.849	0.833	--	0.201
200	502	--	1.704	0.749	--	0.335
70	572	17.18	1.665	0.724	70.144	0.381
10	582	15.46	1.659	0.720	77.321	0.388
20	602	12.70	1.649	0.713	92.640	0.402
20	622	11.19	1.639	0.707	103.562	0.415
20	642	9.80	1.629	0.700	116.458	0.428

5.3.2.5 Stability of SR without binder

After 14 days of curing, no material was strong enough to be weighed and tested (Table 6.27). The SR was completely saturated after having been hermetically sealed. After 28 days of curing, the SR made from the reaction between FA and AMD at a ratio of 1:6 showed a 0.005 MPa elastic unconfined compressive strength. They were the only samples that showed any cementing effect at that date, and this effect was very small. After 90 days of curing, all three SR developed a significant strength. The elastic unconfined compressive strength increased with an increasing amount of ash used for the AMD neutralisation reaction. Compressive strengths increased to 0.049 MPa, 0.036 MPa and 0.031 MPa for the 1:3, 1:4 and 1:6 ratios respectively. After 180 days a significant increase in strength was again noticed for all the ratios. After 410 days the increase in strength was more prominent. Materials prepared using ratio 1:3 reached an unconfined compressive strength of 0.201 and this is quite distinct. Ratios 1:4 and 1:6 also reached 0.099 and 0.85 respectively. This is encouraging in the objective to use such a material for backfilling. It should be noted that despite having kept the samples in a closed humid environment, some drying took place that may have affected the curing of the material.

The elastic modulus could not be measured, after 14 and 28 days of curing because of the instability of the material at those times (Table 6.28).

Table 6.31: Elastic unconfined compressive strength of SR without binder

Time of curing (days)	Sample	Arnot FA Navigation AMD 1:3 ratio	Arnot FA Navigation AMD 1:4 ratio	Arnot FA Navigation AMD 1:6 ratio
14	-	Too soft to be tested	Too soft to be tested	Too soft to be tested
28	Replicate 1 (MPa)	Too soft to be tested	Too soft to be tested	0.005
90	Replicate 1 (MPa)	0.047	0.042	0.032
	Replicate 2 (MPa)	0.051	0.030	0.029
	Mean (MPa)	0.049	0.036	0.031
180	Replicate 1 (MPa)	0.157	0.054	0.064
	Replicate 2 (MPa)	0.157	0.068	0.068
	Mean (MPa)	0.157	0.061	0.066
410	Replicate 1 (MPa)	0.203	0.100	0.081
	Replicate 2 (MPa)	0.199	0.098	0.088
	Mean (MPa)	0.201	0.099	0.0845

Table 6.32: Elastic modulus of SR without binder

Time of curing (days)	Sample	Arnot FA Navigation AMD 1:3 ratio	Arnot FA Navigation AMD 1:4 ratio	Arnot FA Navigation AMD 1:6 ratio
14	-	Too soft to be tested	Too soft to be tested	Too soft to be tested
28	-	Too soft to be tested	Too soft to be tested	Too soft to be tested
90	Replicate 1 (MPa)	13.1	19.6	22.2
	Replicate 2 (MPa)	11.8	10.3	14.7
	Mean (MPa)	12.5	15.0	18.5
180	Replicate 1 (MPa)	56.7	19.7	25.8
	Replicate 2 (MPa)	70.9	23.6	52.5
	Mean (MPa)	63.8	21.7	39.2
410	Replicate 1 (MPa)	59.1	44.3	24.9
	Replicate 2 (MPa)	81.1	18.7	24.9
	Mean (MPa)	70.1	31.5	24.9

After 90 days, the elastic modulus analysis could be performed. There is some variability observed between replicate samples but the general trend indicated that SR recovered from Arnot FA and Navigation AMD neutralization at a 1:3 ratio developed a significant strength (Table 6.28) without binder and the other samples of SR compressive strength increased over time to acceptable levels, with the strength improvement typically doubling over the time interval tested.

The elastic modulus of SR increased from 12.5 MPa for the 1:3 ratio to 18.5 MPa for the 1:6 ratio (Table 6.28). After 180 days, the distinctive behaviour of ratio 1:3 vs. ratios 1:4 and 1:6 was again observed, with a much higher elastic modulus. The same distinction was maintained after 410 days also, elastic modulus of 1: 3 ratio reaching 70.1 MPa. The trends confirm that the elastic modulus generally increased for SR prepared with an increasing amount of ash in the AMD neutralisation reaction.

The fact that the strength and elastic modulus was greatest for the solid residue samples that had been prepared with the highest amount of ash (thus which had been exposed to the lowest volume of AMD per unit of fly ash) indicates that the strength development in the SR is a function of reactions taking place with unconsumed pozzolanic components in the ash. This also indicates that the species contributing to strength development are similar to the species contributing to the neutralization efficacy of the fly ash. Figure 6.74 is a graphical representation of the difference in uncompressed strength developed by the materials recovered from different FA to AMD ratios. It is quite apparent that material recovered from 1:3 ratio has developed significant strength when compared to its counterparts.

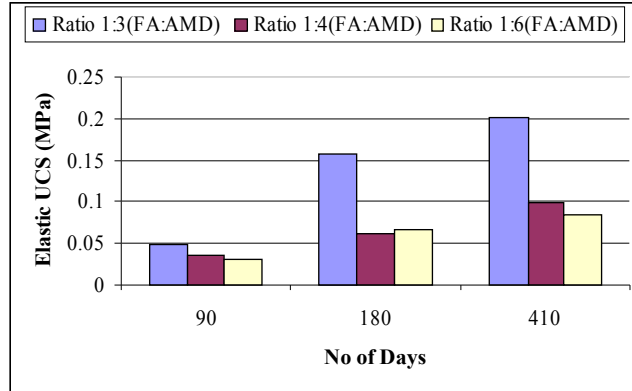


Figure 6.77: Graph showing difference in Elastic UCS of the materials derived from different FA:AMD reactions

5.3.2.6 Stability of SR with cement binder

Testing of samples that were prepared for curing and strength testing, by blending the slurries of SR with 3 % binder (Castle cement) are presented in this sub-section. Various samples were tested for the elastic unconfined compressive strength and the elastic modulus after 14, 28, 90, 180 and 410 days (Table 6.29).

Table 6.33: Elastic unconfined compressive strength of SR with 3 % cement binder.

Time of curing (days)	Sample	Arnot FA	Arnot FA	Arnot FA
		Navigation	Navigation	Navigation
		AMD	AMD	AMD
		1:3 ratio	1:4 ratio	1:6 ratio
14	Replicate 1 (MPa)	0.214	0.070	0.081
	Replicate 2 (MPa)	0.244	0.071	0.078
	Replicate 3 (MPa)	0.233	Not tested	0.084
	Mean (MPa)	0.230	0.071	0.081
28	Replicate 1 (MPa)		0.106	
	Replicate 2 (MPa)	Not tested	0.111	Not tested
	Mean (MPa)		0.109	
90	Replicate 1 (MPa)		0.240	
	Replicate 2 (MPa)	Not tested	0.214	Not tested
	Mean (MPa)		0.227	
180	Replicate 1 (MPa)		0.270	
	Replicate 2 (MPa)	Not Tested	0.287	Not Tested
	Mean (MPa)		0.279	
410	Replicate 1 (MPa)		0.297	
	Replicate 2 (MPa)	Not Tested	0.304	Not Tested
	Mean (MPa)		0.301	

After 14 days the elastic unconfined compressive strength of SR prepared by mixing FA and AMD at ratios of 1:6 and 1:4 with the additional 3% cement binder was lower than 0.1 MPa (Table 6.29), but significantly higher than the strength of SR without additional binder (Table 6.27). However, the material prepared from the reaction performed at a FA:AMD ratio of 1:3 and blended with cement developed a significant strength (0.23 MPa)

after only 14 days. In that case, the addition of cement did provide a significant stabilisation.

After 28 and 90 days of curing, only the material prepared from the reaction performed at a FA: AMD ratio of 1:4 and blended with cement was tested. After 28 days, the strength of this blend was slightly better than after 14 days, reaching 0.11 MPa. It increased again after 90 days and reached an acceptable value for filling purposes: 0.23 MPa. The rise in strength seemed to be stabilising after 180 days and was more than double of the SR without the additional binder. After 410 days it reached around 0.30 which is again significant when compared to its stability without adding binder.

After 14 days of curing, the elastic modulus of the residual solids blended with cement tended to increase with an increasing amount of ash in the mixture (Table 6.30). The elastic modulus increased from 36 MPa for the 1:6 ratio to 84 MPa for the 1:3 ratio. Similar to unconfined compressive strength, only the material prepared from the reaction performed at a FA:AMD ratio of 1:4 and blended with cement was tested after 14 days of curing. While the elastic modulus remained unchanged between 14 and 28 days (53 MPa), it then increased sharply to 92 MPa. The increase in stability continued between 90 and 180 days but a slight drop in the value observed at 410 days. Further tests have to be performed to confirm this behaviour.

Table 6.34: Elastic modulus of SR with 3 % cement binder

Time of curing (days)	Sample	Arnot FA Navigation AMD 1:3 ratio	Arnot FA Navigation AMD 1:4 ratio	Arnot FA Navigation AMD 1:6 ratio
14	Replicate 1 (MPa)	61.7	52.5	30.2
	Replicate 2 (MPa)	81.0	54.5	54.5
	Replicate 3 (MPa)	109.1	Not tested	24.0
	Mean (MPa)	83.9	53.5	36.2
28	Replicate 1 (MPa)		61.7	
	Replicate 2 (MPa)	Not tested	45.0	Not tested
	Mean (MPa)		53.4	
90	Replicate 1 (MPa)		88.6	
	Replicate 2 (MPa)	Not tested	94.5	Not tested
	Mean (MPa)		91.6	
180	Replicate 1 (MPa)		166.8	Not tested
	Replicate 2 (MPa)		149.3	
	Mean (MPa)	Not tested	158.1	
410	Replicate 1 (MPa)		170.2	
	Replicate 2 (MPa)	Not Tested	128.9	Not Tested
	Mean (MPa)		149.6	

As a whole, the results of elastic unconfined compressive strength and modulus testing tend to favour the utilisation of SR for backfilling, as they show that the materials have the ability to develop strength over the long term. When blended with 3 % cement, the stability of the residual solids is highly increased, making them even more suitable for backfilling.

5.4 Hydraulic transport of SR precipitated from AMD treatment

This particular section of the report refers to the rheological behaviour of the SR. Two aspects of the rheological behaviour were investigated. The first one concentrated on the rheological behaviour of the SR obtained from the reactions that used different ratios of FA and AMD. The second investigation looked at the influence of FA- Particle Size Distribution (PSD) on the rheological behaviour.

5.4.1 Rheological behaviour of SR obtained from different FA and AMD reactions

5.4.1.1 Introduction

Pipelines are used to transport products and waste materials over distances ranging from a few kilometres to several hundred kilometres. Inter-process transfer at processing plants is invariably achieved by hydraulic means. Suspension properties are varied, typically spanning a range of particle densities and particle sizes from 100 μm to the submicron colloidal sizes, while concentrations may range from a few percent to close to the maximum packing fraction. Plant efficiencies require much higher concentrations to be processed than the one that can be delivered by conventional pipelines. Furthermore, from a disposal viewpoint it is no longer acceptable, either environmentally or economically, to transport waste materials at low concentrations to large tailing catchments. Thickened discharge and high concentration co-disposal systems are now actively sought. More accurate prediction of the conveying characteristics is therefore essential for design and economic analysis of suspension pipelines. A move to higher concentrations of wider size distribution material has several major impacts on the flow behaviour of these suspensions:

- The increase in concentration of fine particles invariably converts the conveying fluid to a non-Newtonian suspension.
- The presence or increase of coarse particles makes viscometric data alone insufficient for pipeline design.

The hybrid systems of non-Newtonian carrier fluid and coarse burden are complex. Existing design methods do not adequately predict the suspensions behaviour for many important operational conditions. Therefore, it is proposed that the necessary research required resolving these issues for the application at hand be conducted at the Flow Process Research Centre, of Cape Peninsula University of Technology (CPUT), where extensive research on industrial suspensions can be conducted in unique viscometers, rheometers and pipeline test facilities.

A collaboration between with the Flow Process Research Centre (FPRC) at CPUT was initiated to carry out research on the hydraulic transport of residual solids precipitated from AMD treatment with FA. Laboratory scale rheometer studies were carried out on the solids obtained from the reaction between Tutuka FA and Navigation AMD in 1:3, 1:4 and 1:6 ratios (FA:AMD).

5.4.1.2 Literature

5.4.1.2.1 Rheological Modelling

One of the more general models (Slatter & Chhabra, 2003) which has been used consistently in the literature to describe the time independent viscous characteristics of mineral slurries is the Yield Pseudoplastic or Herschel-Bulkley model, where

$\tau = \tau_y + K \dot{\gamma}^n \quad \text{and} \quad \eta = \frac{\tau_y}{\dot{\gamma}} + K \dot{\gamma}^{n-1} .$	(Eq 6.37)
---	-----------

This model is also able to describe Power-law pseudoplastic behaviour (by setting $\tau_y = 0$) and Bingham plastic behaviour (by setting $n = 1$). The general forms of these models are shown in Figure 6.75 to Figure 6.77. The Newtonian model would appear as a horizontal line in Figure 6.77. Referring to Figure 6.77, it can be seen that all three models illustrate shear thinning behaviour, as viscosity decreases with an increase in shear rate.

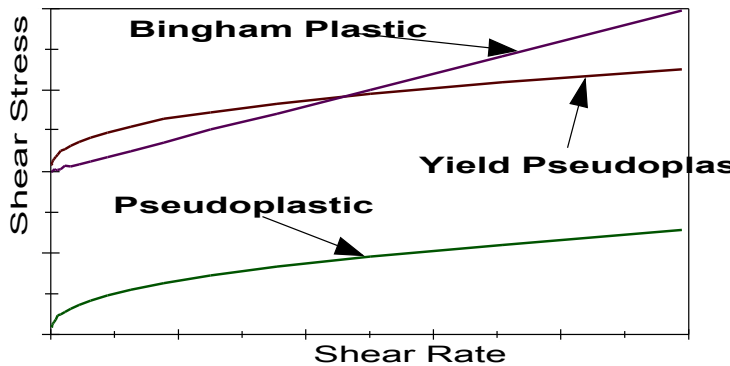


Figure 6.78: General form of the flow curve (or rheogram) - linear axes.

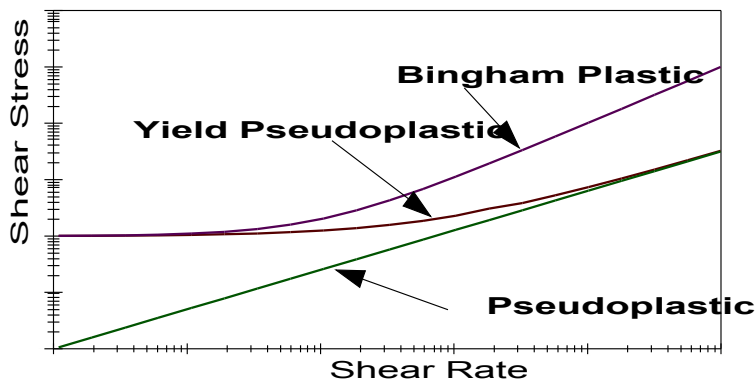


Figure 6.79: General form of the flow curve (or rheogram) - logarithmic axes.

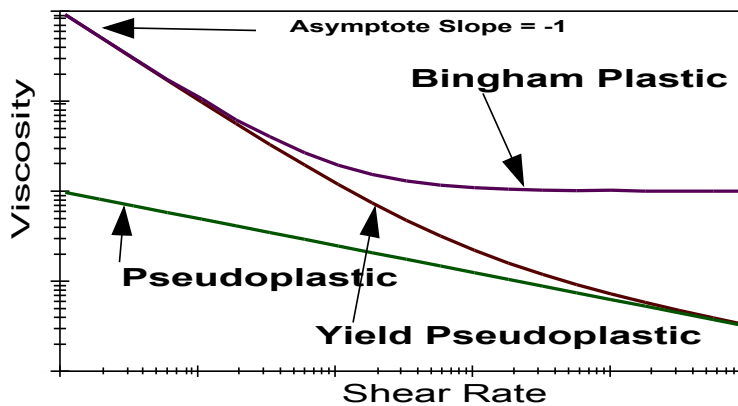


Figure 6.80: General form of the viscosity diagram for the rheological models on logarithmic axes.

5.4.1.2.2 Correlation of rheological parameters with concentration

Solids concentration is perhaps the most important parameter affecting slurry rheology and in this section it is shown how slurry rheology can be correlated with concentration. It is important that *a priori* methods are used in order to relate rheology to concentration for the most meaningful and comparable results to be obtained.

Besides solids concentration, a related factor influencing the rheology of the slurry is maximum packing density which in turn is influenced by the particle size distribution. Very little work has been done in attempting to relate these and other particle properties to the rheology (Dabak & Yucel, 1987). Unfortunately there is no correlation proposed for the flow behaviour index (n). Despite this, the rheological constants can be correlated against concentration using simplified versions of the correlations proposed by Landel *et al.* (1963) for the fluid consistency index (K) and Dabak & Yucel (1987) for the yield stress (τ_y).

$K = \mu_w \left(1 - \frac{C_v}{C_{vmax}} \right)^{-m},$	(Eq 6.38)
$\tau_y = a \frac{C_v^3}{C_{vmax} - C_v}.$	(Eq 6.39)

The constants C_{vmax} , a and m characterise a particular slurry and are evaluated empirically from rheological characterisations at several different concentrations over the range of interest. The flow behaviour index n can be correlated using polynomial regression.

$n = c_1 C_v^2 + c_2 C_v + c_3.$	(Eq 6.40)
----------------------------------	-----------

5.4.1.2.3 Pipe Flow Models

Laminar pipe flow for Herschel-Bulkley fluids can be predicted from the following equation (Govier & Aziz, 1972):

$\frac{32Q}{\pi D^3} = \frac{8V}{D} = \frac{4n}{K^n \tau_0^3} (\tau_0 - \tau_y)^{\frac{1+n}{n}} \left[\frac{(\tau_0 - \tau_y)^2}{1+3n} + \frac{2\tau_y(\tau_0 - \tau_y)}{1+2n} + \frac{\tau_y^2}{1+n} \right]$	(Eq 6.41)
---	-----------

where $\tau_0 = \frac{D\Delta p}{4L}$ and $V = \frac{Q}{A}$.

Turbulent flow can be predicted using a roughness Reynolds number, Re_r as follows (Slatter, 1999):

$\frac{V}{V_*} = 2.5 \ln \left(\frac{0.5D}{d_{rep}} \right) + 2.5 \ln(Re_r) + 1.75$	(Eq 6.42)
--	-----------

where d_{rep} = representative particle size determined by the greater of the d_{85} particle size or the pipeline hydraulic roughness
 V_* = shear velocity.

The shear velocity is found from the following equation:

$V_* = V \sqrt{\frac{f}{2}} = \sqrt{\frac{\tau_0}{\rho}}$	(Eq 6.43)
---	-----------

If $Re_r \leq 3.32$ then the friction factor for smooth wall turbulent flow is calculated from:

$\frac{V}{V_*} = 2.5 \ln \left(\frac{0.5D}{d_{rep}} \right) + 2.5 \ln(Re_r) + 1.75$	(Eq 6.44)
--	-----------

If $Re_r > 3.32$ then the equation for full rough wall turbulent flow is:

$\frac{V}{V_*} = 2.5 \ln \left(\frac{0.5D}{d_{rep}} \right) + 4.75$	(Eq 6.45)
--	-----------

which reduces to $\frac{1}{\sqrt{f}} = 4.07 \log \left[\frac{3.34D}{d_{rep}} \right]$. (Eq 6.46)

5.4.1.3 Objectives

The objectives of this investigation are:

- Prepare residual fly ash suspensions at various concentrations
- Perform standard tube tests
- Perform rheological investigation using a portable rheometer
- Comment on and discuss the significance of non-Newtonian behaviour
- Analyse the flow data using appropriate pipe flow models
- Make recommendations for design based on optimum concentration and pipe diameters

The project deliverables are:

- Design equations to predict laminar and turbulent behaviour for the optimum concentration of the residual fly ash suspension given the rheology and a pipe diameter
- Calculation of the specific power consumption

5.4.1.4 Measuring apparatus and procedure

The experiments related to rheological studies of FA-AMD sludge were carried out at Eskom CR&D in Rosherville. The equipment (BBTV) was transported from CPUT to Eskom CR&D. Large volumes of sludge were prepared using the pilot scale mixing rig available at Eskom. Residual solids were obtained from the reaction between Tutuka FA and Navigation AMD in 1:3, 1:4 and 1:6 ratios (FA:AMD). Unfortunately, due to unforeseen problems at Eskom and since the equipment was damaged during transport, the full scale experiments had to be postponed. However, laboratory scale rheometer studies were carried out.

A Paar-Physica MC1 rheometer was used to conduct rheological investigation of the residual fly ash over a range of shear rates using the controlled rate mode of operation with a vane-in-cup geometry. For high solids concentrations it is recommended that a vane be used to eliminate slip. The shear rate range of the rheometer is $1 \cdot 10^3 \text{ s}^{-1}$. During the tests, turbulence was induced at shear rates higher than 500 s^{-1} . The rheological parameters were therefore obtained over a shear rate range from 1 to 500 s^{-1} .

The test matrix used is given in Table 6.31. For each ratio of FA to AMD prepared, the slurry was allowed to settle overnight before supernatant was removed. Three concentrations were prepared for tests in the rheometer. The reason for this is because it is not known if chemical reaction and time of reaction would change the properties of the residual slurry. From a practical point of view, since the same type of ash is used, the rheology of the resulting sludge should be the same for any given value of relative density.

The relative density (RD) of the sludge was measured and used as a control parameter. The samples were well mixed and observed after mixing. The sample with $\text{RD} < 1.4$ tended to settle during tests and the resulting torque measured by the rheometer was too low. For higher RD's the settling process was slower, but there was always a thin layer of

supernatant (1 - 3 mm). Heavy particles settled within less than a minute while it took about two hours for the fine ones to settle, leaving a clear supernatant of at least 1 mm. Because of this phenomenon, the sample was not poured into the cup of the rheometer, but a spatula was used instead to obtain a homogenous sample for measurement.

Table 6.35: Test matrix for residual solids suspensions

FA:AMD ratio	RD prepared	Cv (%)
1:3	1.43	33.1
	1.53	40.8
	1.58	44.6
1:4	1.43	33.1
	1.52	40.0
	1.57	43.8
	1.62	47.7
1:6	1.45	34.6
	1.52	40.0

5.4.1.5 Results

5.4.1.5.1 Rheological Investigation

In order to determine the rheological parameters, a flow curve is needed, measuring the shear stress over a range of shear rates. In this case, the range of shear rates was from 1 to 1000 s⁻¹. For any suspension, there may be time dependant behaviours. This is important when constructing the flow curve, because if there are significant changes with time, the flow curve should be constructed using viscosities measured at a time where it is constant. This phenomenon was investigated by measuring the change of viscosity with time as given in Figure 6.78. The following observations were made about the slurries. The slurry viscosity was stable with time for the first 100 seconds, after which it started to drop as the solid particles began to settle out. At higher shear rates, i.e. shear rates >250 s⁻¹, the particles were kept in suspension and there was no significant decrease in the viscosity. A similar behaviour was observed for the other concentrations of the residual slurry. Based on this information, the time taken to test each point on the viscosity and flow curves was chosen as 5 seconds.

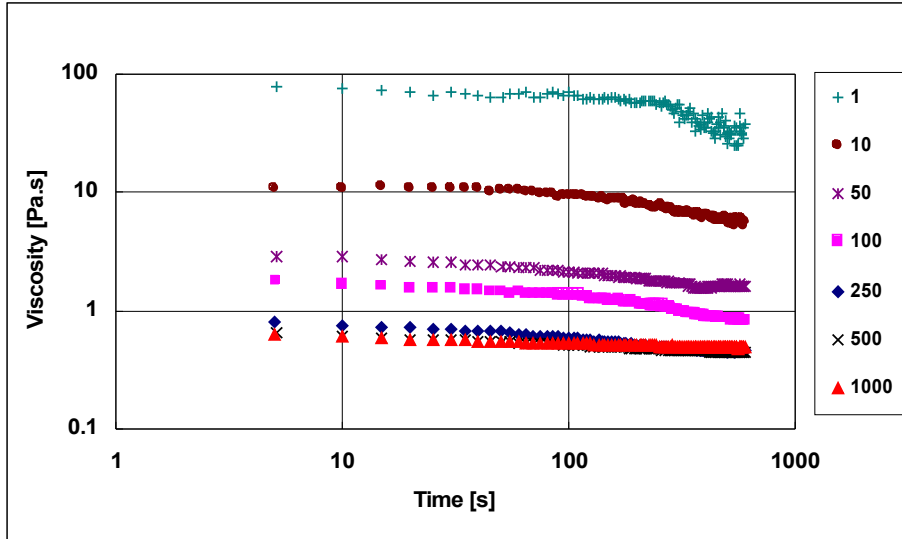


Figure 6.81: Viscosity versus time for the 1:6 residual solids slurry at RD 1.45 for various shear rates.

All samples displayed shear-thinning behaviour as shown in figures 6.79 to 6.81, which means that the viscosity decreased with increasing shear rate. In this case, it changed by approximately two orders of magnitude.

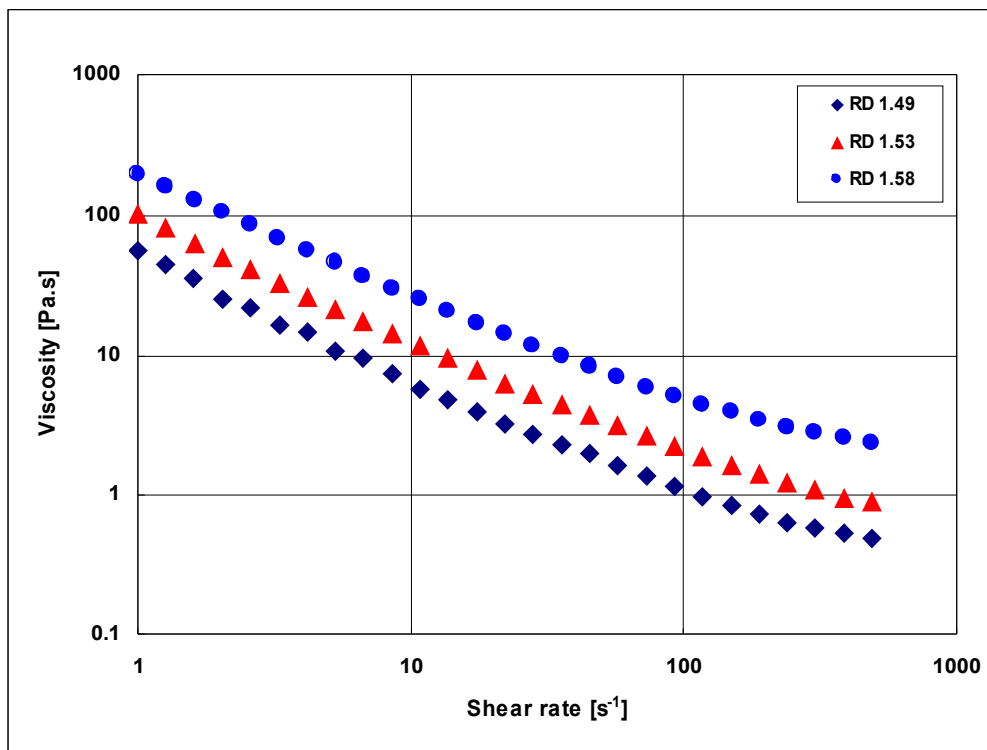


Figure 6.82: Viscosity curves for various concentrations of the 1:3 residual solids slurry.

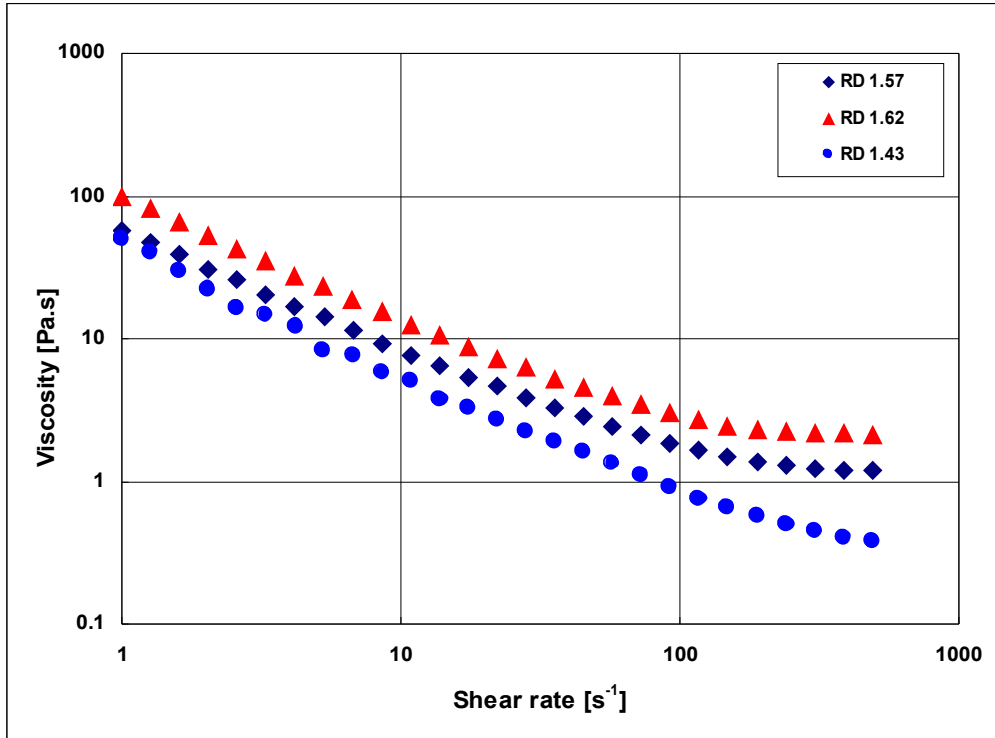


Figure 6.83: Viscosity curves for various concentrations of the 1:4 residual solids slurry.

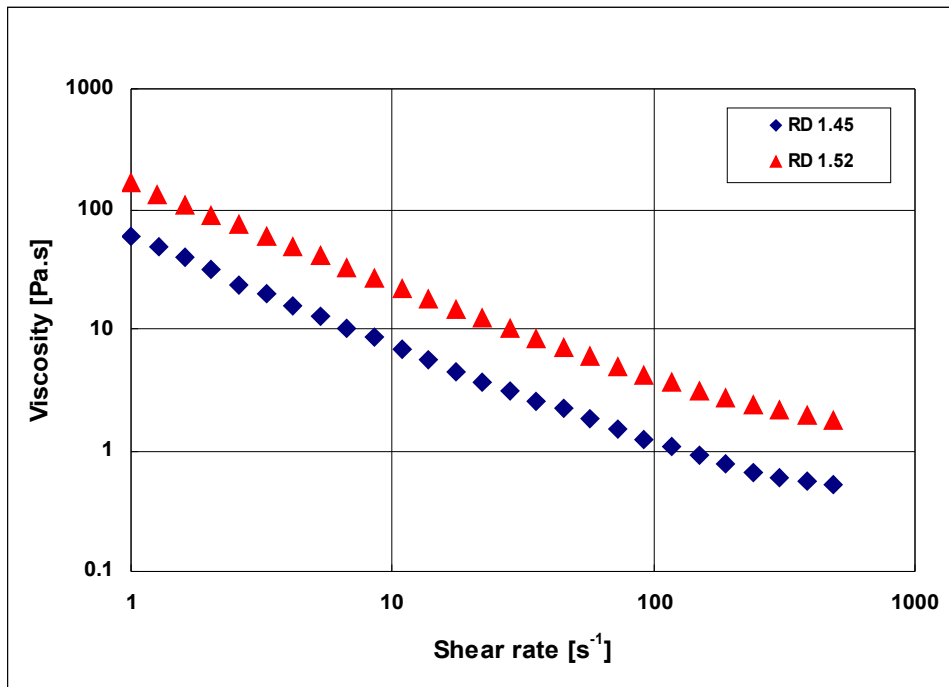


Figure 6.84: Viscosity curves for various concentrations of the 1:6 residual solids slurry.

From the flow curve it was observed that all samples had a yield stress and the data was well approximated by the Herschel-Bulkley model (HB) over a shear rate range 1 – 500 s⁻¹, as shown in figures 6.82 to 6.84.

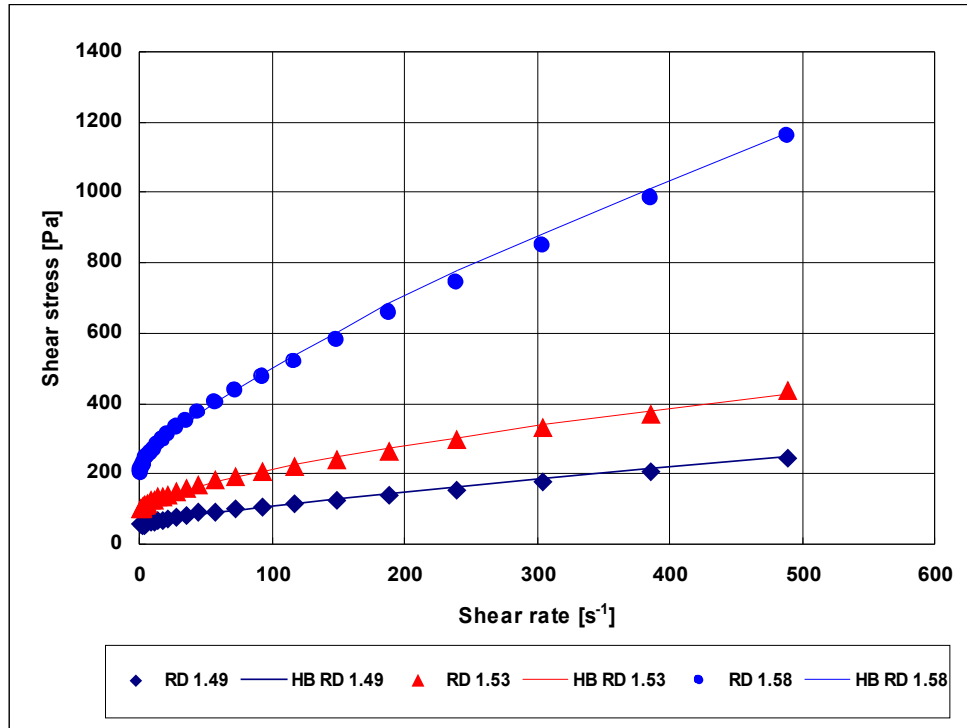


Figure 6.85: Flow curves for various concentrations of the 1:3 residual solids slurry.

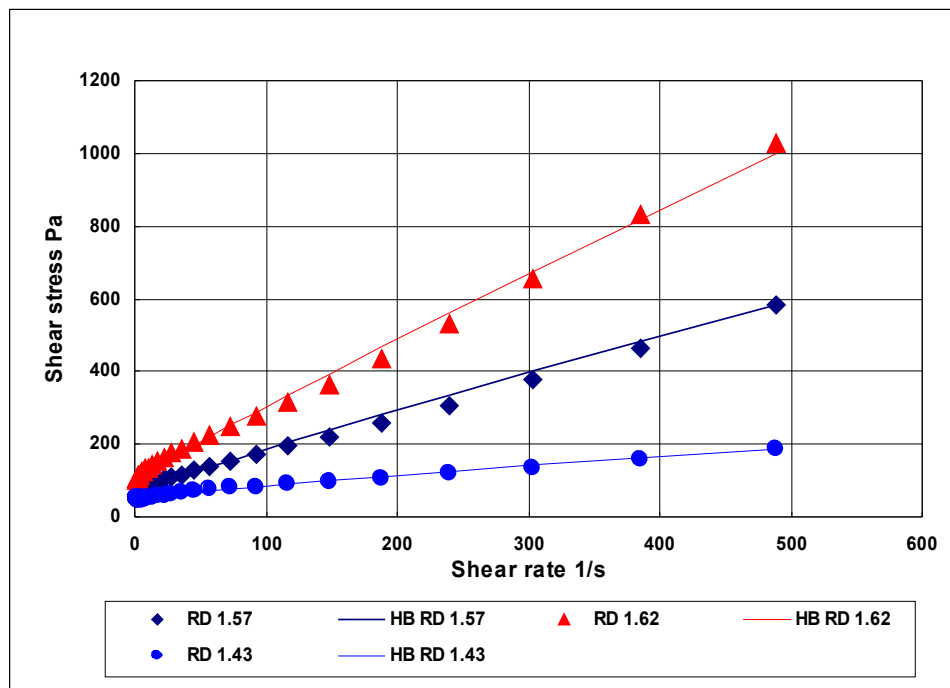


Figure 6.86: Flow curves for various concentrations of the 1:4 residual solids slurry.

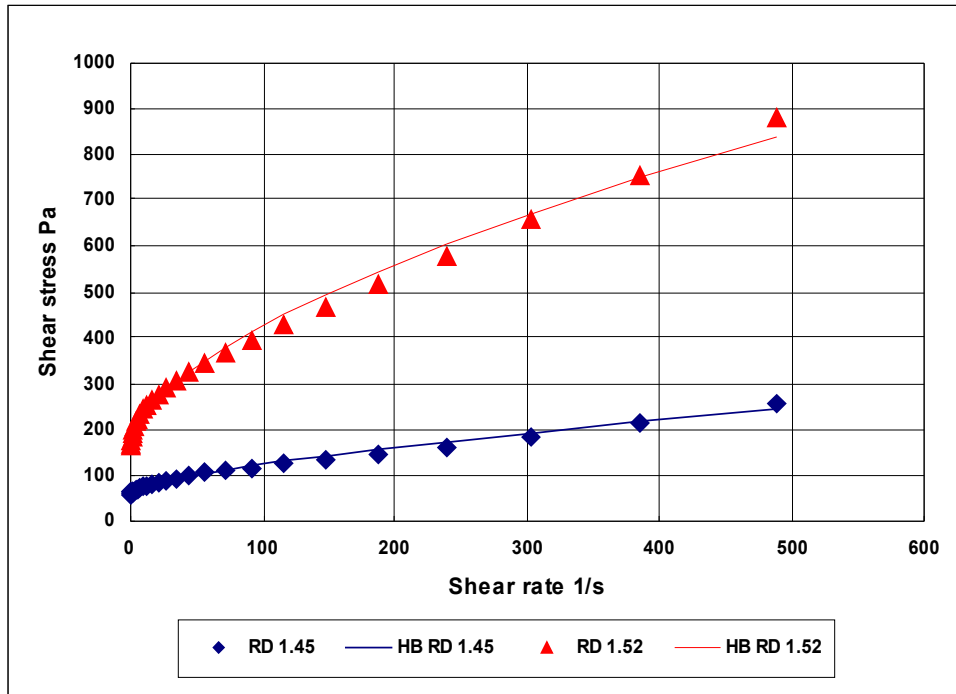


Figure 6.87: Flow curves for various concentrations of the 1:6 residual solids slurry.

It needs to be pointed out that for the residual solids slurry 1:4, the shear thinning behaviour was less significant than for the other two slurries and the values of the behaviour index, n , approached unity. The rheological parameters obtained from the flow curves are given in Table 6.32.

Table 6.36: Rheological parameters

FA:AMD	RD	Ty (Pa)	K (Pa.s ⁿ)	n
1.3	1.49	54.22	1.42	0.79
	1.53	95.84	5.67	0.66
	1.58	201.57	10.10	0.74
1.4	1.43	45.21	1.16	0.77
	1.57	62.10	1.92	0.90
	1.62	105.96	2.43	0.95
1.6	1.45	60.02	2.53	0.69
	1.52	161.07	16.80	0.60

A comparison of the yield stress values of the residual slurries at various relative densities, revealed that each slurry from a specific FA: AMD ratio resulted in its own trend for T_y versus RD plot, as given in Figure 6.85. This could be due to two reasons:

(1) differences in particle size distribution due to the sampling method which involved taking more concentrated slurry from the bottom of the container or (2) incomplete chemical reaction due to insufficient base material present to neutralise all the acid.

The yield stress plays an important role in determining the pumping head in pipe line design.

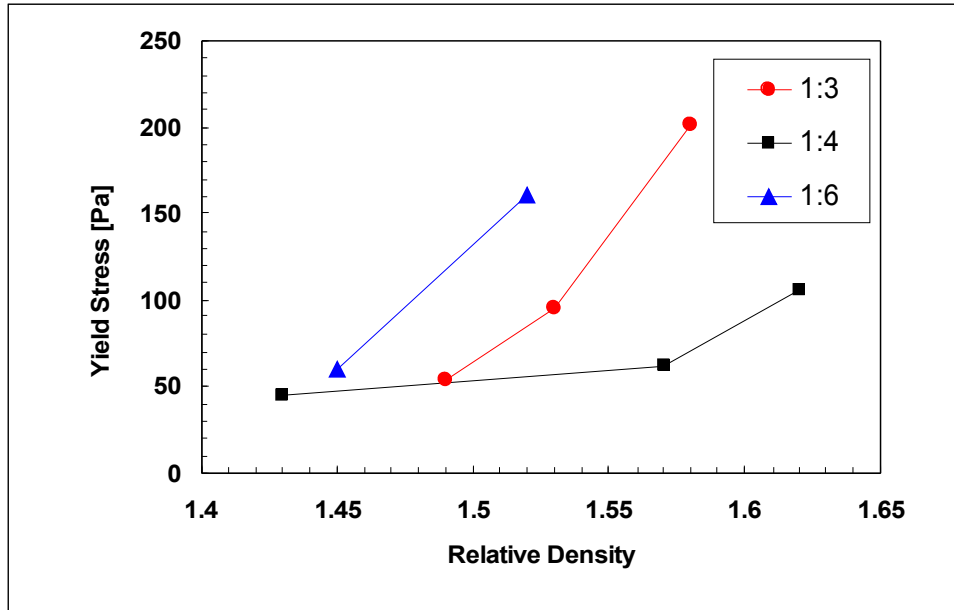


Figure 6.88: Yield stress versus relative density for all residual slurries, each at various concentrations.

5.4.1.5.2 Application of rheology to pumping conditions

The above rheological results can be used to develop system pumping head curves for the slurry. If fixed mass transfer rate and pipe diameter are chosen, then a number of these curves over a range of concentrations can be used to predict the optimum slurry concentration for the minimum specific power consumption. For the purposes of this report, a mass transfer rate of 2000 kg/day and a pipe diameter of 150 mm have been chosen. These have been illustrated for the 1:3 slurry. The first step is to correlate the rheological parameters against concentration. The results of the correlation for the 1:3 slurry are given in Table 6.33 and Figure 6.86.

Table 6.37: Results of the rheological parameter correlation for the 1:3 slurry.

n poly	
c ₁	0.3856
c ₂	-0.8393
c ₃	1
m	12.0402
a	679.17
C _{max}	0.8

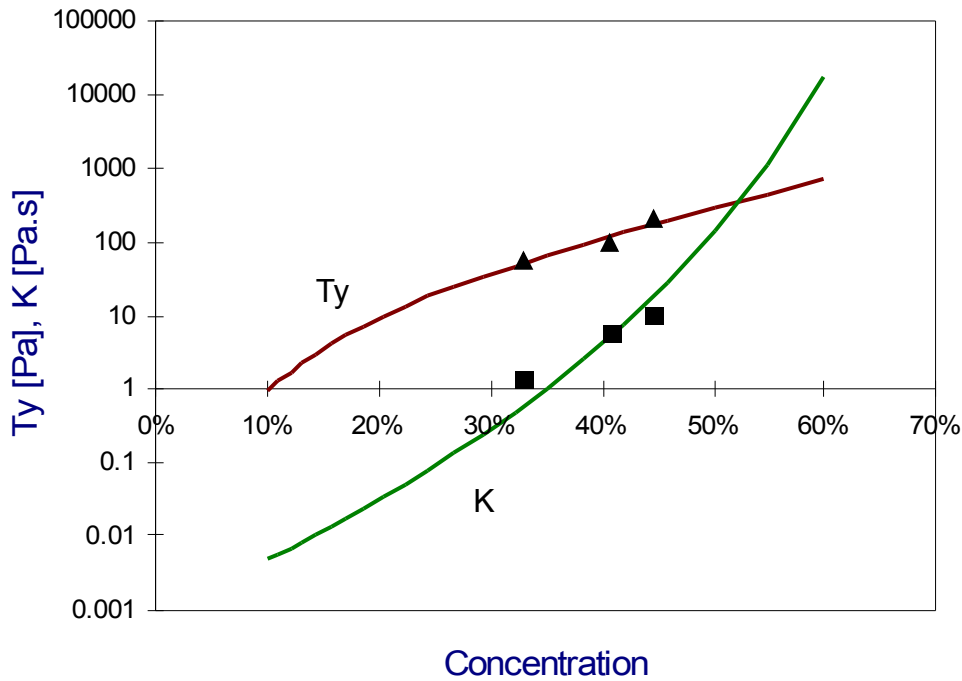


Figure 6.89: Results of the rheological parameter correlation for the 1:3 slurry.

For illustration purposes, three concentrations were chosen to show the pumping curves. These are presented in detail in Table 6.34.

Table 6.38: Details for the three pumping curve examples A, B and C.

	C _v	SPC	S _m	T _v Pa	K Pa.s ⁿ	n	V m/s
A	21.4%	0.131	1.278	11.3	0.0422	0.838	2.67
B	23.2%	0.110	1.302	15.0	0.0623	0.826	2.45
C	27.2%	0.165	1.354	25.9	0.1489	0.800	2.09

The pumping curves for the three pumping curve examples A, B and C are presented in Figure 6.87 to 6.89. Figure 6.89 clearly shows that the optimum slurry pumping concentration occurs for slurry B at a C_v value of 23.2%, for chosen fixed values of mass transfer rate and pipe diameter.

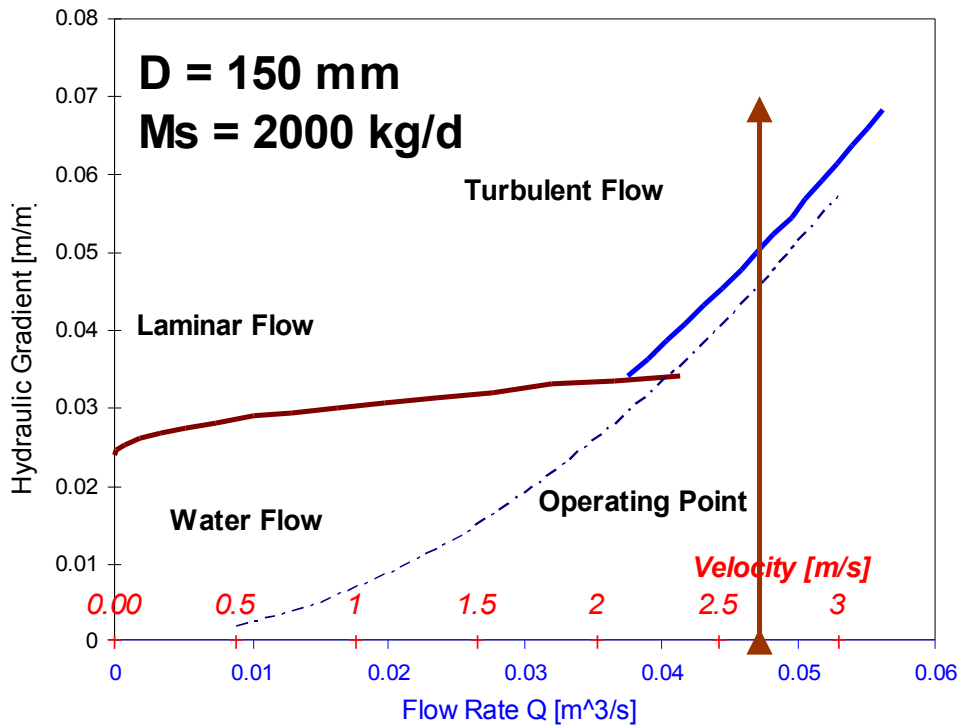


Figure 6.90: Pumping system curve for slurry A.

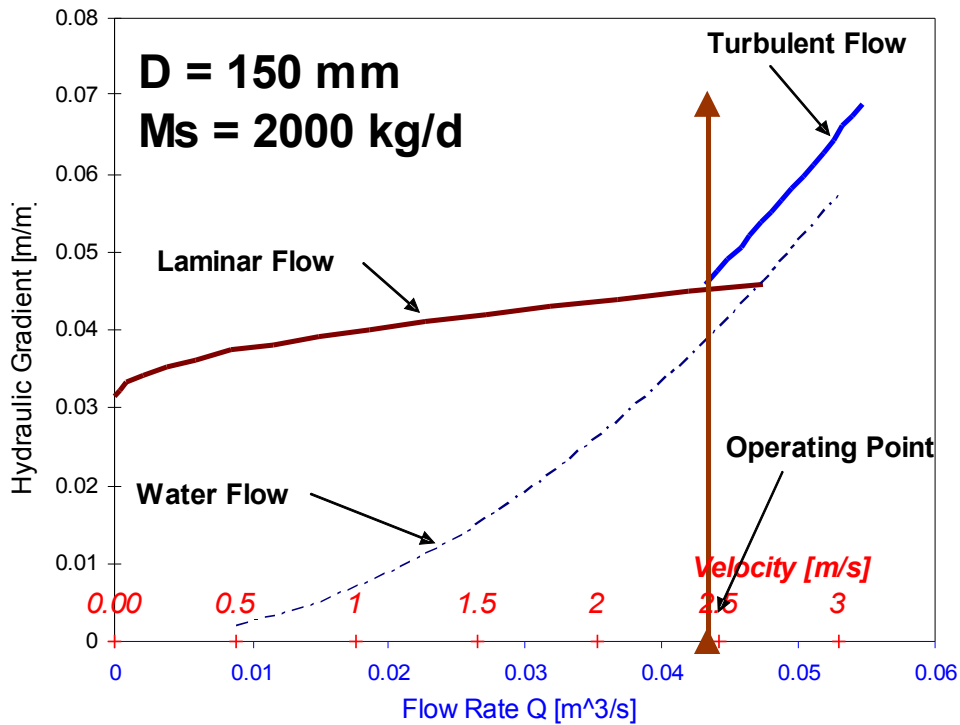


Figure 6.91: Pumping system curve for slurry B.

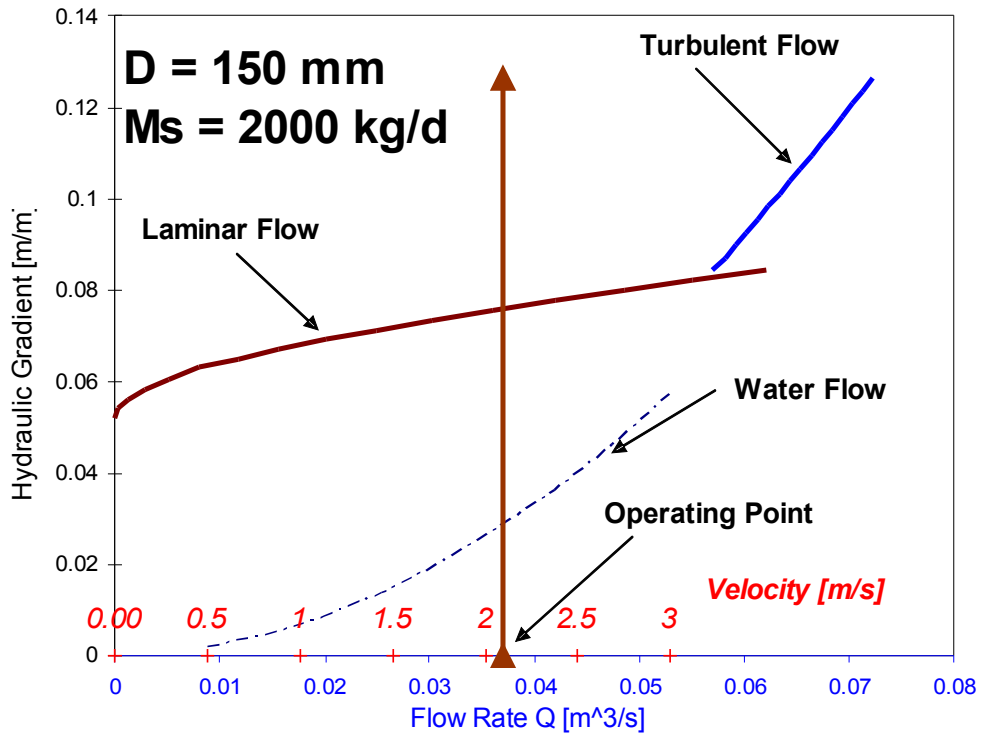


Figure 6.92: Pumping system curve for slurry C.

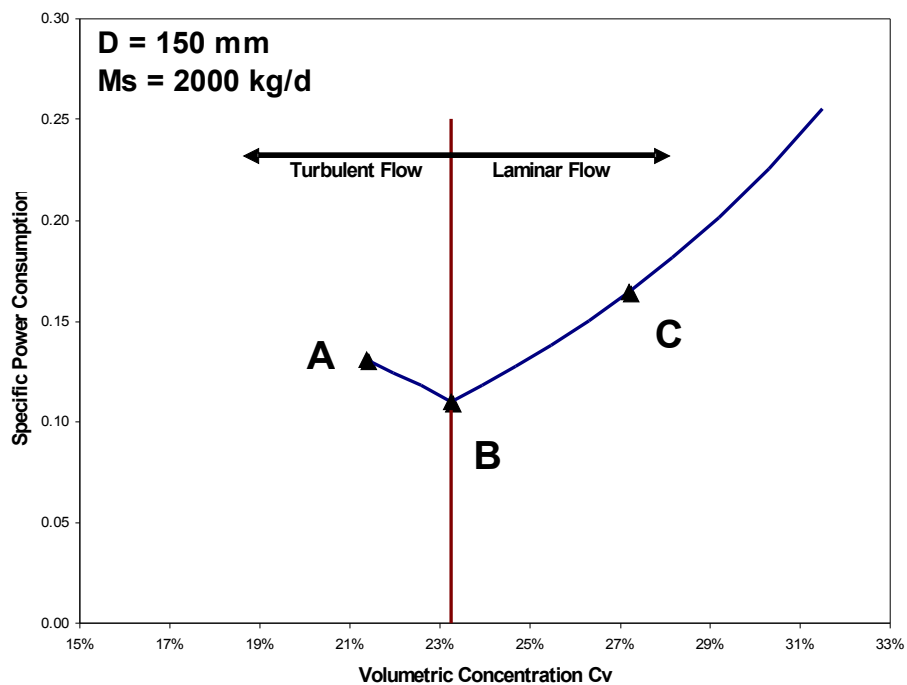


Figure 6.93: Specific power consumption vs. concentration for the 1:3 slurry.

5.4.1.6 Discussion and recommendations

An extensive series of tests need to be conducted to verify the behaviour of the slurries at different FA: AMD ratios. Non-Newtonian behaviour is evident from $RD = 1.4$. A critical RD after which the yield stress increase exponentially could possibly be between 1.52 or 1.57. These values correspond to C_v of 43% and 47.3% ($S_s = 2.2$) respectively and a moisture content of approximate 30%. However, the rheometer data need to be verified by actual pipe and pump tests. Furthermore, the rheology quoted in this work is closely related to the exact particle size and particle shape of the fly ash. All this needs to be accounted for to obtain a reliable and predictable rheological behaviour of the slurry and ensure that optimum pumping conditions are determined.

Due to a range of unforeseen circumstances during the trials at Eskom, pipe tests could not be completed and these should be conducted as soon as possible. The pump curves can easily be determined for any specific slurry when the application is better defined.

5.4.2 Influence of FA-Particle Size Distribution (PSD) on the rheological behaviour of SR

5.4.2.1 Introduction

The properties of the fly ash (FA) change from one power station to the other and also with time depending on the conditions in the furnace and the quality of the coal feedstock. This change in properties of FA can influence the rheological properties of the precipitated SR. The Environmental & Nano Sciences Group (ENS) approached the Flow Process Research Centre of CPUT to investigate the influence of particle size of FA on the rheological properties. The influence of PSD on the reaction kinetics of AMD neutralization with FA is provided as Appendix F.

5.4.2.2 Literature

This section will sketch the flow behaviour of suspensions in terms of the properties and behaviour of the particles and their interaction with the suspending medium, which is usually water. For pipeline design, only the measured rheological properties such as the viscosity and the yield stress are used, regardless of the detailed nature of the particles in the suspension and the fluid in which these particles are suspended. It is however important to try and understand the variables that affect suspension behaviour in order that the rheology of suspensions can be manipulated or controlled in processing applications. The rheology of a suspension depends both on its physical and chemical nature. This work explores the physical basis for the fly ash rheology.

The physical parameters that will affect the viscosity of suspensions are particle concentration, particle size, particle size distribution and particle shape. These factors will be discussed briefly in this section.

5.4.2.2.1 Particle concentration

If particles are added to a fluid the viscosity will increase. This viscosity increase is due to the additional energy required when streamlines are distorted in the presence of particles. The streamlines curve around the particles instead of remaining parallel as they would in a uniform shear field. In dilute suspensions of non-interacting particles this is the only effect responsible for the viscosity increase. If, however, the particle concentration is increased, the distortion of streamlines around one particle influences the degree of streamline distortion around a neighbouring particle (Heywood, 2000). There exist a mutual influence on the hydrodynamic forces generated in the fluid separating the particles and the particles therefore become interacting. These hydrodynamic forces will dominate at higher shear rates. (Iyer & Stanmore, 2000).

In addition to the hydrodynamic effects, there will also be mechanical effects as a result of the particle concentration. Mechanical effects may be quantified in terms of collision frequency, resulting in momentum transfer. The frequency will depend on the rate at which the suspension is being sheared, the particle concentration and particle size.

For sub-micron size particles, Brownian motion will enhance the rate of momentum transfer substantially (Iyer & Stanmore, 2000). Collisions are induced either through the shear field or by Brownian motion. Further mechanical interaction between particles may manifest itself in frictional forces generated during particle- particle contact as a result of the liquid layer being squeezed out giving direct solid-solid contact and a consequent higher energy dissipation rate through friction (Heywood, 2000).

Two or three particles may group together at this point (known as flocs) trapping some liquid between them. These flocs will enclose a volume of water that becomes trapped, and so the total floc volume is significantly larger than the total particle volume. Under these conditions, the particle size and volume are irrelevant as the floc is now the basic unit (Heywood, 2000).

Suspension behaviour can be subdivided into 3 categories based on the solids concentration: Dilute, Medium and High concentrations. Several workers have derived expressions for determining the viscosity for these types of suspensions and a brief review will be given in the next section.

5.4.2.2.2 Dilute Suspensions

Early studies of suspensions dealt with dispersed, dilute suspensions of non-interacting spherical particles. The work of Einstein (1906) is the usual starting point and he related the relative viscosity as a linear function of the volume fraction (volumetric concentration, (ϕ)) of the particles. The relative viscosity is the ratio of the suspension viscosity to the viscosity of the suspending liquid.

$$\eta_r = \frac{1 + \frac{\phi}{2}}{(1 - \phi)^2} \cong 1 + 2.5\phi \quad (\text{Eq 6.47})$$

where $\phi < 0.2$.

5.4.2.2.3 Medium suspension

For medium suspensions where $0.3 < \phi < 0.6$ the Krieger-Dougherty equation is mostly used (Bournonville & Nzihou, 2002).

$$\eta_r = \left(\frac{1}{1 - \frac{\phi}{\phi_m}} \right)^{2.5\phi^m} \quad (\text{Eq 6.48})$$

5.4.2.2.4 High concentrations

These previous equations however fail to predict the infinite viscosity when ϕ approaches the maximum volume fraction, ϕ_m , of particles in suspension that will still flow. Frankel and Acrivos (1967) derived an expression for viscosity as $\phi \rightarrow \phi_m$ (Heywood et al., 2000).

$$\eta_r = \frac{9}{8} \frac{\left[\left(\frac{v}{v_m} \right)^{\frac{1}{3}} \right]}{\left[1 - \left(\frac{v}{v_m} \right)^{\frac{1}{3}} \right]} \quad (\text{Eq 6.49})$$

All of these expressions do not specifically allow for non-Newtonian effects, but could be used at a specific shear rate. These equations are valid for spherical particles, whereas for non-Newtonian suspensions, the particles are usually non-spherical, irregular or flat plate-like. There are also electric attractive or repulsive forces present that complicate the prediction of the viscosity. All of these expressions, and there are many more than those listed here, fail in that they relate viscosity to solids concentration without containing any parameters which take into account the effects of particle size, shape and size distribution. This leads to serious errors in the prediction of the viscosity especially at high solids concentrations (Heywood et al., 2001). However, recent work of Bournonville and Nzihou (2002) attempted to address this issue and proposed a model for viscosity that takes into account both shear rate and solid volume fraction and is given in Eq.4. They investigated the effect of concentration, yield stress and hydrodynamic interactions on the rheology of municipal solid waste incinerator fly ashes.

$$\mu_r = \left[1 + \frac{D}{\dot{\gamma}^E} \frac{\left(\frac{\phi}{\phi_{\max}} \right)}{\left(1 - \frac{\phi}{\phi_{\max}} \right)} \right]^G \quad (\text{Eq 6.50})$$

The parameter G is found in the Krieger-Dougherty equation with a value 2.5, the parameter E (0.5) is the exponent as found in the Casson model and D a value associated with the yield stress.

A summary of the effect of particle size distribution of recent studies are given below:

An increase in fines will increase the yield stress (Iyer & Stanmore, 1999). Studies on coal-water slurries revealed that an increase in the fines fraction will result in low volume fractions obtained with high viscosities (Boylu, Dincer & Atesok, 2004). Higher volume fractions can be obtained with increased particle size distribution. They also found that non-spherical particles will result in lower volume fractions because the particles can not fill the voids effectively.

The volume fraction is important in the correlations of slurry rheology as can be seen from the equation above. The determination of the maximum volumetric packing fraction is important for viscosity predictions and need to be determined experimentally. The volumetric packing fraction ϕ is calculated from the mass fraction of solid and the densities of the solid particles and the slurry.

For fly ash it was found that a large percentage of calcium and sodium ions are retained in the diffuse double layer. The thickness of the diffuse double layer influences the closeness of packing for fine particles and the limiting value of ϕ_m . The rheological behaviour of a slurry changes significantly when the concentration approaches the maximum packing fraction (Iyer & Stanmore, 2000).

The maximum packing fraction is considered as a closely packed volume relating to particle properties such as shape and particle size distribution. For suspensions with $\phi_m > 0.53$, ordering must take place for mobilization and these arguments were supported by light scattering studies on hard colloidal spheres. It was also found that the finest fraction of particle size distribution will control the non-Newtonian behaviour of the slurry. This fines fraction has been identified as $\sim 10 \mu\text{m}$ for cement slurries and also fly ash (Iyer & Stanmore, 2000).

Luckham and Ukeje (1999) investigated the effect of particle size distribution on the viscous contribution to the rheology of the suspension. The relative viscosity was plotted against the volume fraction. The maximum packing fraction can be done by plotting square root of the viscosity against effective volume fraction. It is important to take the absorbed layer into account when calculating the volume fraction and to determine the maximum packing fraction. They found that the yield stress, storage modulus and viscosity decreases with increasing poly dispersity.

With the appropriate particle size distribution the suspension viscosity can be kept constant while the volume fraction is increased due to the small particles that can fit into spaces created by the large particles (Ohlero & Ferreira, 2004).

Although almost all studies found that the addition of coarser particles will reduce the viscosity, Heywood et al. (1993) found that the fly ash suspension with higher d_{50} gave higher pressure drop (viscosities), but ascribed it to the difference in pH that would affect the degree of flocculation of the fines.

During flocculation, aggregates called flocs are formed. Aggregates have irregular shape and contain a void fraction, and can therefore be described by a fractal dimension, D_f . The mass fraction dimension is a measure of the compactness of an object, where $D_f = 3$ for a solid sphere (Franks et al., 2004). The yield stress gives an indication of the interparticle bond strength of the suspension (Franks et al., 2004). The fractal dimension is related to the yield stress as given in Eq. 6.51 where G is a constant associated with the interparticle spacing and the zeta potential between the particle surfaces and together with m can be obtained from a plot of τ_y versus ϕ . The parameter m is related to the fractal dimension by Eq. 6.52.

$$\tau_y = G\phi^m \quad (\text{Eq 6.51})$$

$$m = \frac{(d + X)}{d - D_f} \quad (\text{Eq 6.52})$$

X and d are the Euclidian dimensions of the clusters, with values of 1 and 3 respectively (Tseng & Lin, 2003).

It is difficult to quantitatively describe particulate material with a wide particle size distribution. One can use the d_{10} , d_{50} or d_{90} values from a typical particle size distribution test. Another method often used in the field of soils mechanics is the Rosin-Rammler equation as given in Eq. 6.53 where x is the sieve size, k is the fineness modulus and m is the distribution modulus (He et al., 2006). These investigators (*ibid*) found that the yield stress increases exponentially with increasing distribution modulus (m) and decreased with increasing characteristic sizes (d_{50} and k)

$$P(x) = 1 - \exp\left[-\left(\frac{x}{k}\right)^m\right] \quad (\text{Eq 6.53})$$

It is clear from the literature that it is difficult to predict the viscous behaviour of suspensions such as fly ash. It was shown that the particle size distribution can affect the rheology, with the finer particles being the main contributor to increased viscosities and yield stresses. The evaluation of the maximum packing volume fraction is critical for the prediction of viscosity and fractal dimension can help in understanding the colloidal structure of the flocs.

5.4.2.3 Objectives

The objectives of this investigation were to

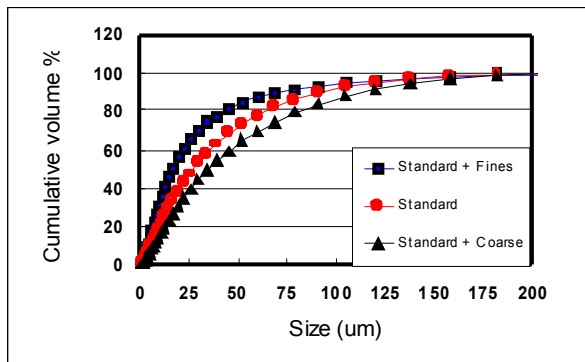
- Prepare fly ash samples with various particle size distributions
- To react the ash with AMD
- To perform a rheological characterisation of the residual fly ash suspension using a portable rheometer
- Comment and discuss the significance or the effect of particle size distribution on the rheological parameters.
- To evaluate the effect of changes in rheology due to slight alteration in particle size distribution on pumping head.

5.4.2.4 Sample Preparation

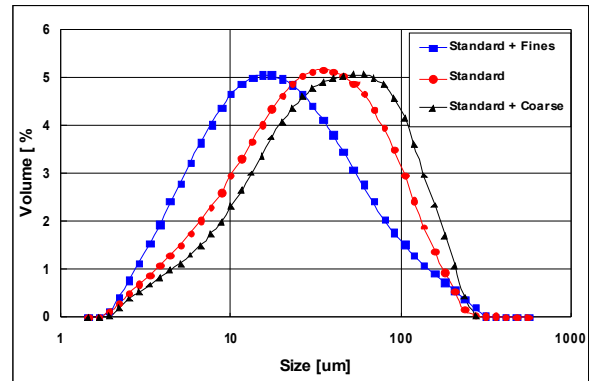
The fly ash was obtained from Arnot power station. The density of the fly ash was 2200 kg/m³. The particle size distribution of the ash was determined with a Malvern Particle Sizer and showed a mean particle size (d_{50}) of 30.75 μm . This standard sample of fly ash was altered to increase the volume of fines (>25 μm) and coarse (75-150 μm) fraction before the neutralization. The fractions were obtained using standard sieves. The (d_{50}) of the sample with maximum fine was 20 μm and the sample with the minimum amount of fines (or maximum amount of coarse) was 40 μm as shown in Table 6.35.

Table 6.39: Malvern Particle Sizer Results for standard and modified ash samples

Sample	Specific surface area (m ² /g)	d_{10} (μm)	d_{50} (μm)	d_{90} (μm)
Standard	0.344	7.49	30.75	102.32
Fines Enriched	0.469	4.56	19.42	81.82
Coarse Enriched	0.271	9.51	40.86	129.25



Cumulative particle size distribution of standard and modified ash



Volume % particle size distribution plot of standard and modified ash

Figure 6.94: Graphs showing cumulative PSD and Volume % of PSD in the standard and modified ash

The Rosin-Rammler parameters obtained from the Malvern Particle Sizer are given in Table 6.36 .

Table 6.40: Rosin-Rammler parameters for standard and modified ash samples

Sample	m	k (μm)
Standard	1.55	47.75
Fines Enriched	1.49	38.74
Coarse Enriched	1.47	57.41

5.4.2.4.1 Measuring Apparatus and Procedure

The above FA (both the standard and enriched samples) was reacted with AMD at a ratio of 1:3. The pH was measured and the reaction was terminated when the pH reached 7. The reaction time, pH and conductivity for each of the suspensions are given in Table 6.37

Table 6.41: Reaction time and pH of suspensions

Sample	Reaction time (hrs)	pH	Conductivity (μs)
Standard	7.30	7.50	5.02
Fines Enriched	5.30	8.45	4.96
Coarse Enriched	11.30	7.39	5.26

The sample was then allowed to settle for 90 minutes, after which the supernatant water was carefully removed. The suspension was allowed to settle for another 90 minutes and more to obtain various concentrations of each suspension. The rheology after the initial 90 minutes is crucial because it is presumed that the initial pumping stage will occur after such settling time in the plant. This suspension will be pumped to the backfill plant where it will be allowed to settle further. This will be beneficial because the pumping cost will be lower and the process water can be pumped back to the plant over a short distance. However, this method of allowing the slurry to settle over time complicated the comparison of the rheological behaviour of the suspensions with various particle size distributions. There was no control over the concentration of suspension obtained after each settling time, so direct comparison at specific volume concentrations is rather difficult. Figure 6.92 is not an accurate graph of settling time (except for first 90 and 180 minutes), but rather gives an indication of the range of concentrations achieved for each suspension. For the standard sample, a higher concentration was achieved quickly and was diluted (with its own supernatant) to obtain a range of other concentrations which could possibly match the other suspension concentrations. For an accurate analysis of the effect of particle size distribution only, it is essential that both the concentration and chemistry remain constant.

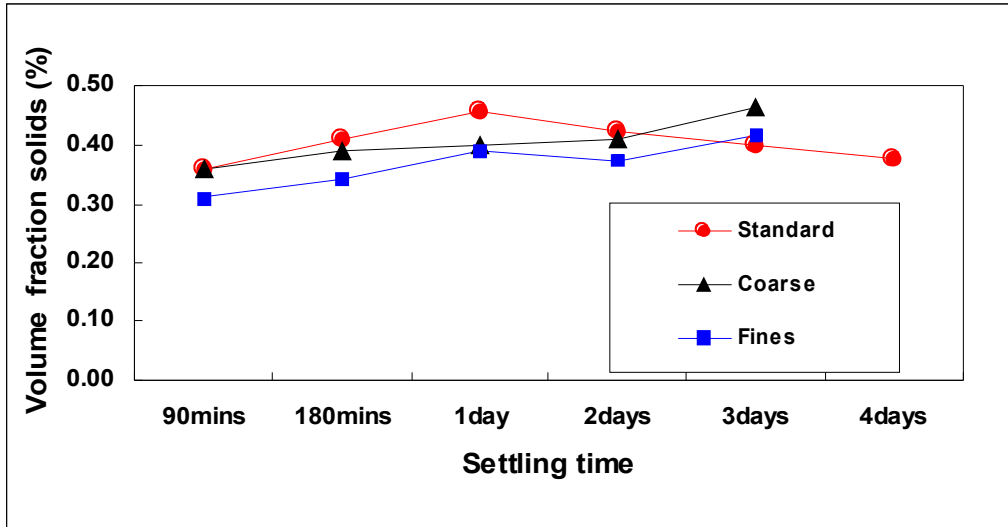


Figure 6.95: Volume fractions obtained for each suspension.

The volume concentration was obtained from the mass fraction, which was in turn obtained by drying the sample.

A Paar-Physica MC1 rheometer was used to conduct rheological investigation of the residual fly ash tests over a range of shear rates using the controlled rate mode of operation with a vane-in-cup geometry. For high solids concentrations it is recommended that a vane be used to eliminate slip. The shear rate range of the rheometer is $1 - 10^3 \text{ s}^{-1}$. During the tests, turbulence was induced at shear rates higher than 500 s^{-1} . The rheological parameters were therefore obtained over a shear rate range from $1 - 200 \text{ s}^{-1}$.

5.4.2.5 Results

5.4.2.5.1 Rheological Investigation

The fly ash tested behaved as quick settling slurries at volumetric concentrations below 30%. As the concentration is increased, inter-particle interactions become stronger, resulting in non-Newtonian behaviour. The fly ash suspensions displayed typical shear-thinning behaviour, i.e. the viscosity decreased with increasing shear rate. There are some time effects present when the fluid is tested first in the increasing shear rate and then the decreasing shear rate range. However, this structure is broken down after high shear rates and a constant curve can be obtained. This is shown in Figure 6.93. For comparative purposes, all tests were carried out starting from high shear to low shear to achieve an equilibrium curve.

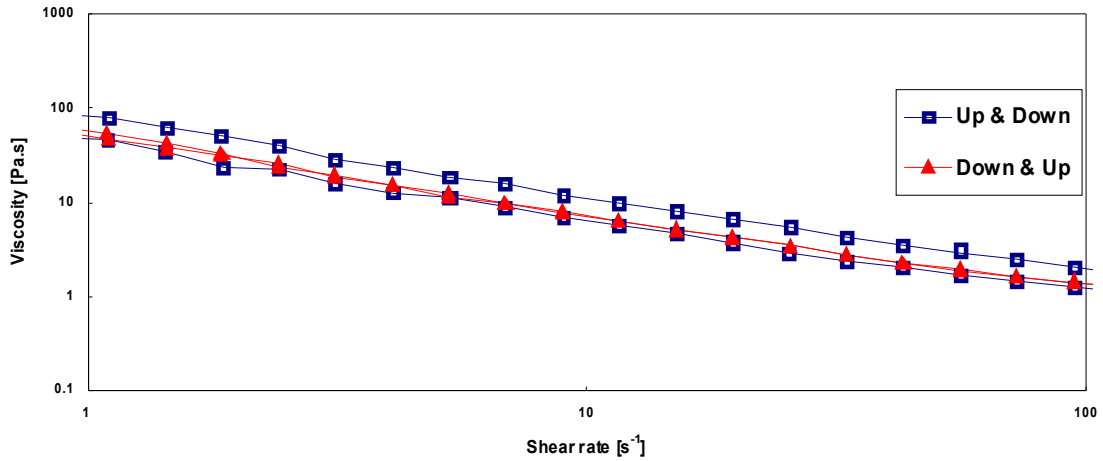


Figure 6.96: Time dependant behaviour of fly ash

5.4.2.5.2 Effect of concentration

Various concentrations were obtained by allowing the suspension to settle with time. The viscosity increased with increasing concentration as given in Figure 6.94. At least four concentrations were obtained for each suspension. Suspensions with volumetric fraction of less than 0.36 were too dilute to be tested in the rheometer. In the case of the coarse enriched suspension with a volume fraction of 0.36, results could not be obtained with the rheometer because the sample was too dilute.

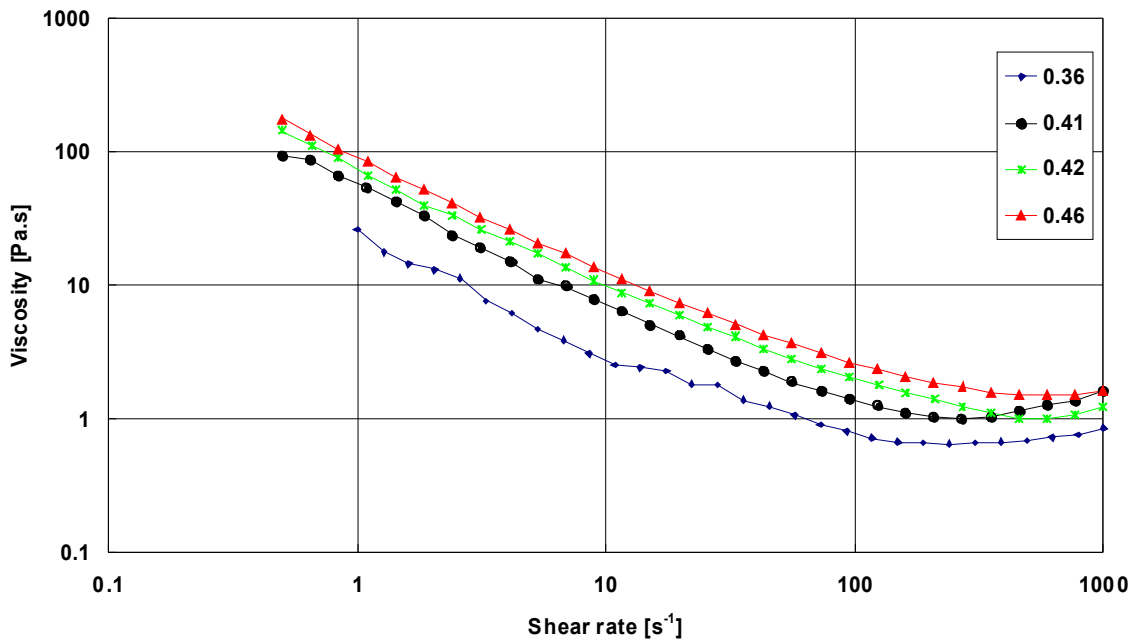


Figure 6.97: Effect of concentration on the viscosity for the standard suspension

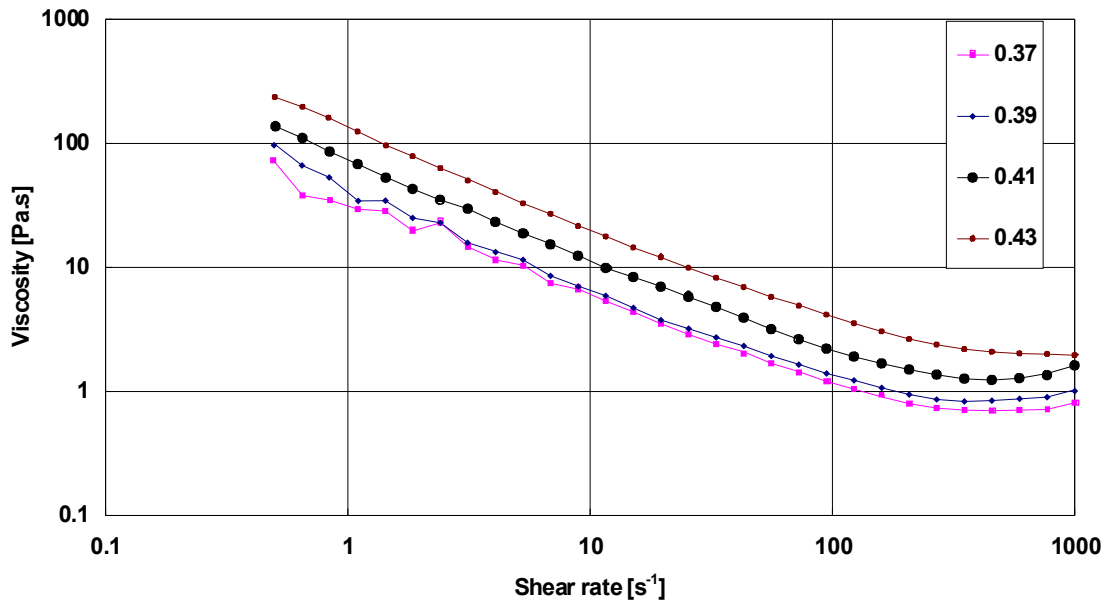


Figure 6.98: Effect of concentration on the viscosity for the fines enriched suspension

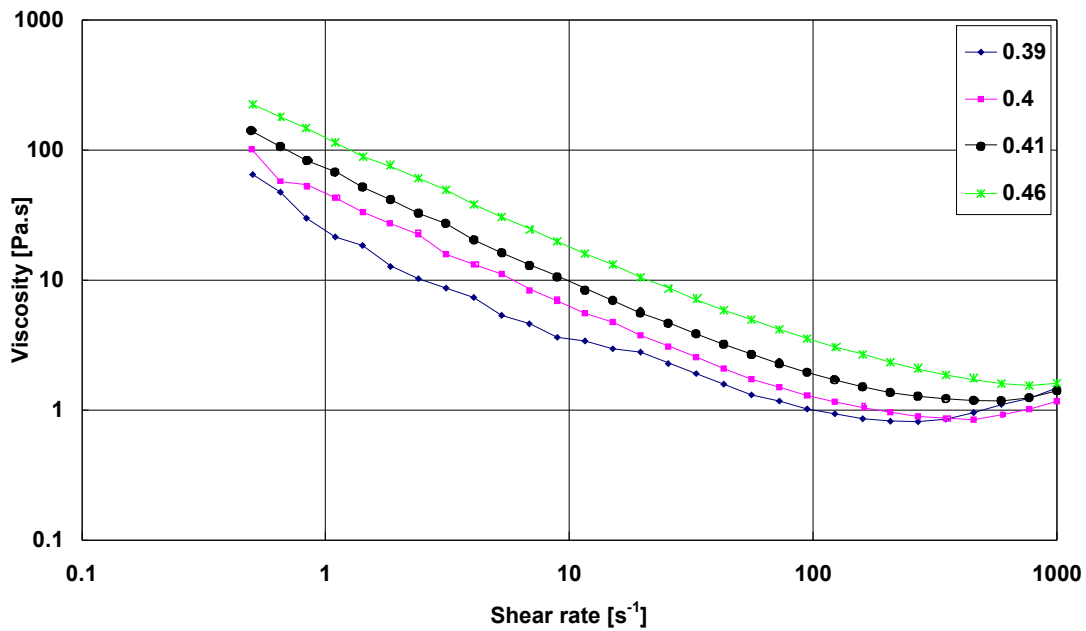


Figure 6.99: Effect of concentration on the viscosity for the coarse enriched suspension

To model the behaviour of the viscosity with both shear rate and concentration, the Bournonville and Nizhou (2000) model was applied and the constants were determined. One of the parameters required for this model is the maximum packing fraction. There are several approaches available for this as given in the literature review. The first approach used was to plot the yield stress as a function of volume fraction as shown in

Figure 6.97. The yield stresses were obtained from the flow curves by fitting the Herschel-Bulkley equation to the experimental data.

Figure 6.97 shows that the maximum volume fraction is below 0.5. It was indeed very difficult to obtain concentrations higher than 0.46 as it appears as if very little process water was available for immobilization.

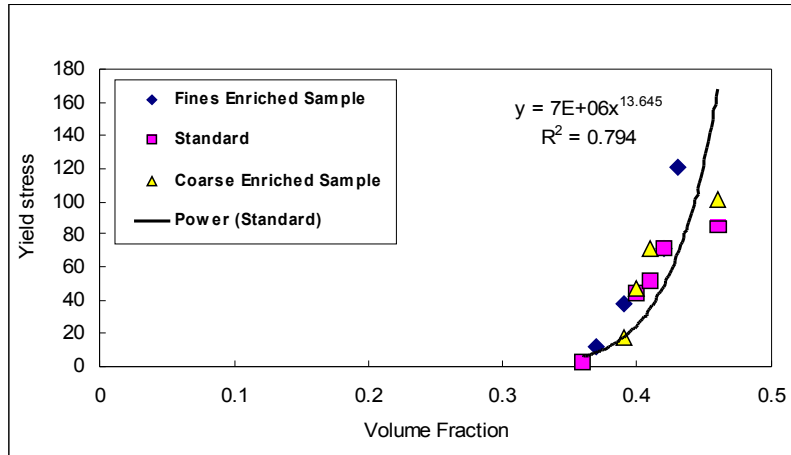


Figure 6.100: Yield stress dependence on concentration

The maximum packing fraction can also be obtained from a plot of $1-\mu^{1/2} = a\phi+b$ (Luckham and Ukeje, 1999). The viscosity was taken at a shear rate of 10 s^{-1} and 100 s^{-1} for each suspension.

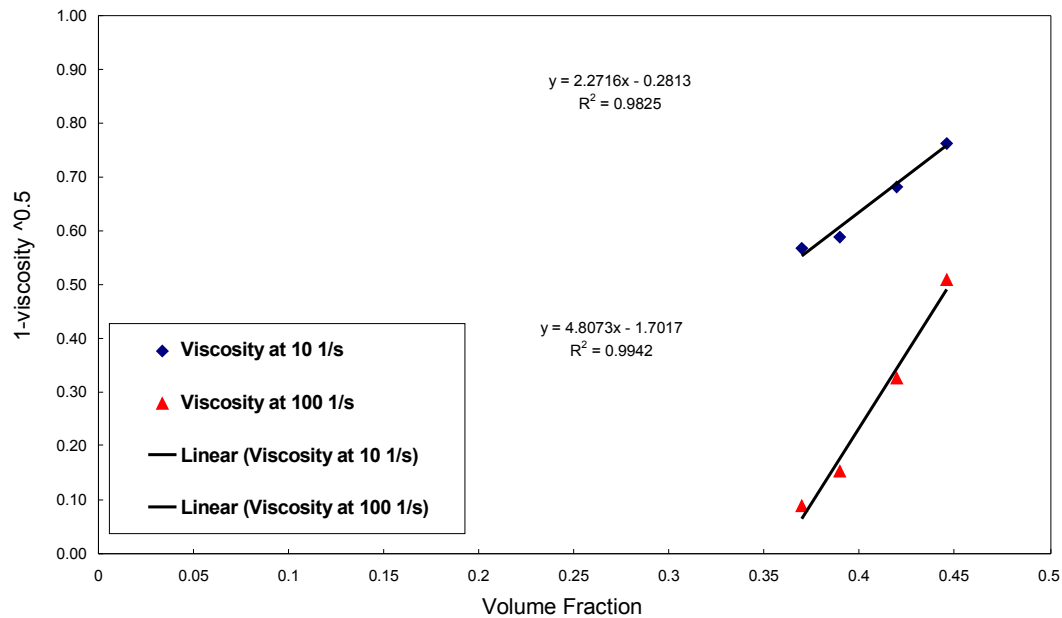


Figure 6.101: The $1-\mu_r^{1/2} - \phi$ relationship at shear rates of 10 and 100 s^{-1} for fines enriched sample

For the fines enriched suspension, a similar result for the maximum packing fraction of 0.51 was obtained when calculated at shear rates of 10 and 100 s⁻¹. For the standard sample, quite different results were obtained, i.e. a $\phi_m = 0.48$ at 10 s⁻¹ and $\phi_m = 0.57$ at 100 s⁻¹. For the coarse enriched suspension values of $\phi_m = 0.53$ and 0.54 were obtained at 10 and 100 s⁻¹. However, all these values obtained are lower than 0.63 that is usually obtained for spherical particles. But this is in agreement with Iyer & Stanmore (2000), who stated that suspensions with non-spherical particles will result in lower obtainable volume fractions. The non-sphericity of the particles is a result of the precipitation of heavy metals onto particles. According to Tseng and Lin (2003) an increase in fines will lead to increased colloidal activity which will result in lower volume fraction obtained and higher viscosities or yield stresses. In the case of their nano-particle suspensions a maximum volume fraction of 0.15 was achieved. The results shown in Table 6.38 are clearly showing a similar trend.

Table 6.38 shows the maximum volume fraction that was used when applying Eq. 4 to the experimental results.

Table 6.42: Values of D, E and G constants from Eq. 7.50

	ϕ_m	D	E	G
Standard	0.57	94.2	0.38	1.92
Fine	0.51	125.5	0.44	1.77
Coarse	0.54	106.2	0.44	1.82

A comparison of the experimental results and the model are shown in Figures 6.99 and 6.100.

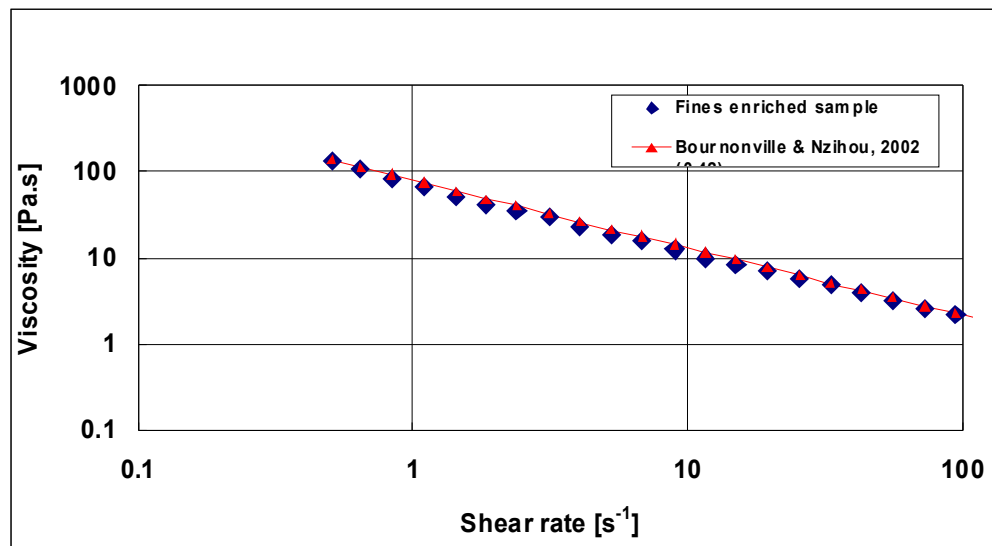


Figure 6.102: Comparison between model and experimental result for fines enriched sample

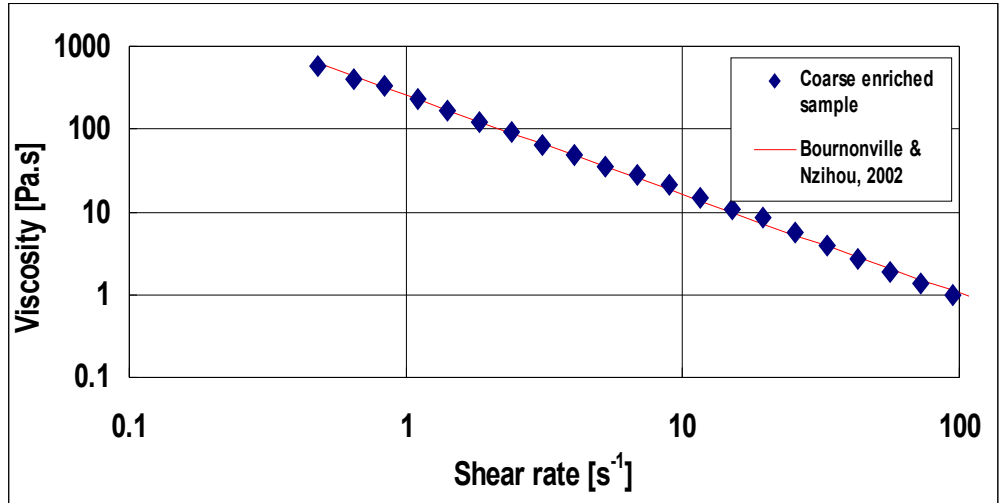


Figure 6.103: Comparison between model and experimental result for coarse enriched sample

5.4.2.5.3 Pumping Predictions

It is general knowledge that an increased particle size distribution range will result in lower viscosities and that an addition of fines will result in higher viscosities (Boylu et al., 2004). However, in these tests, it was not the case. The sample with a fines fraction of 40% resulted in higher shear stresses than that of the fines fraction of 48% (Fig 6.101). This result was also observed for a volume fraction of $\phi = 0.41$.

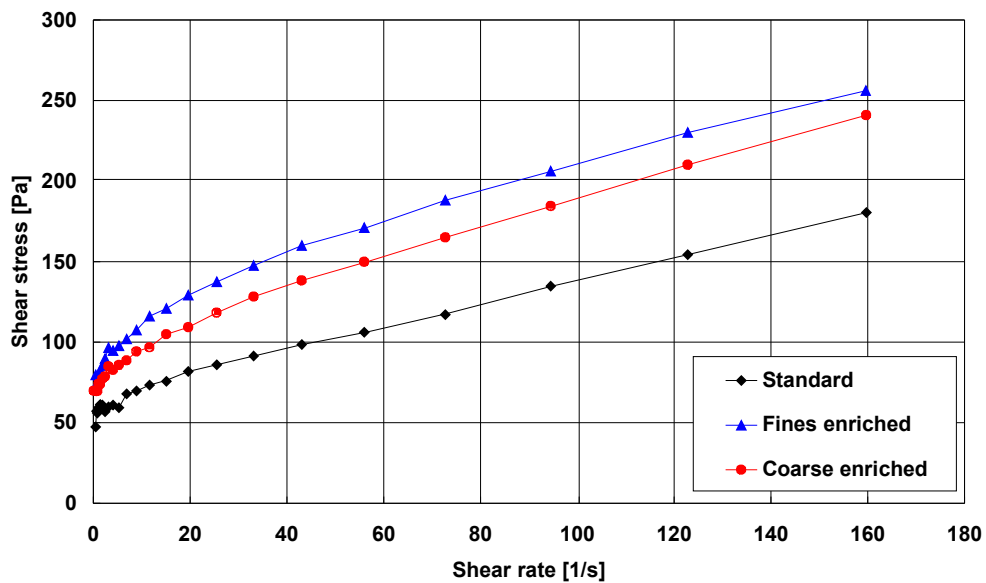


Figure 6.104: Effect of fines at a volume fraction $\phi = 0.41$

There is a significant effect of particle size distribution on the hydraulic gradient. The 28% increase in fines could result in increased shear stresses of 53%. Figure 6.102 shows the resulting increase in the hydraulic gradient in a 150 mm pipe line. Also demonstrated is that if the assumption of decrease viscosity with addition of coarse particles is adopted, it would be assumed that using the pumping conditions for the standard sample would be sufficient if not conservative, which is clearly not the case.

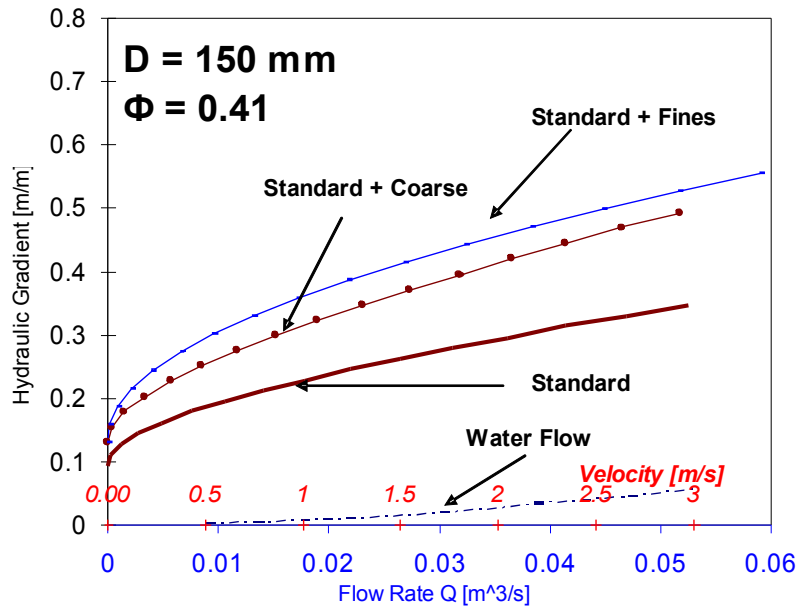


Figure 6.105: Hydraulic gradient for various particle sizes

5.4.2.5.4 Deposition Behaviour

Slump test were conducted using suspensions of higher concentrations. The photo's (Figure 6.103) show that the slump remains the same. It gives some angle of deposition, allowing run-off of very clear supernatant until the material dries. The yield stress is able to remain at least as long as it takes to dry. Most of the water drained off within one day. The fines enriched sample took slightly longer to dry and showed no cracks, unlike the other two samples.

5.4.2.6 Discussion

The rheology of fly ash is not a trivial matter to measure or to understand, as witnessed by the large amount of literature available on the topic. For the fly ash under investigation, non-Newtonian behaviour is evident from a volumetric concentration of 0.35. The critical concentration after which the yield stress increase exponentially corresponds to a C_v of 43%. In contradiction to most other work done, the suspension with the maximum fraction of coarse did not decrease the viscosity as expected, but increased it.

It appears from the results that there is a cross over point at $\phi = 0.41$, where the coarse enriched suspension changes from being less viscous to more viscous than the standard sample. Heywood et al. (1993) reported a similar case

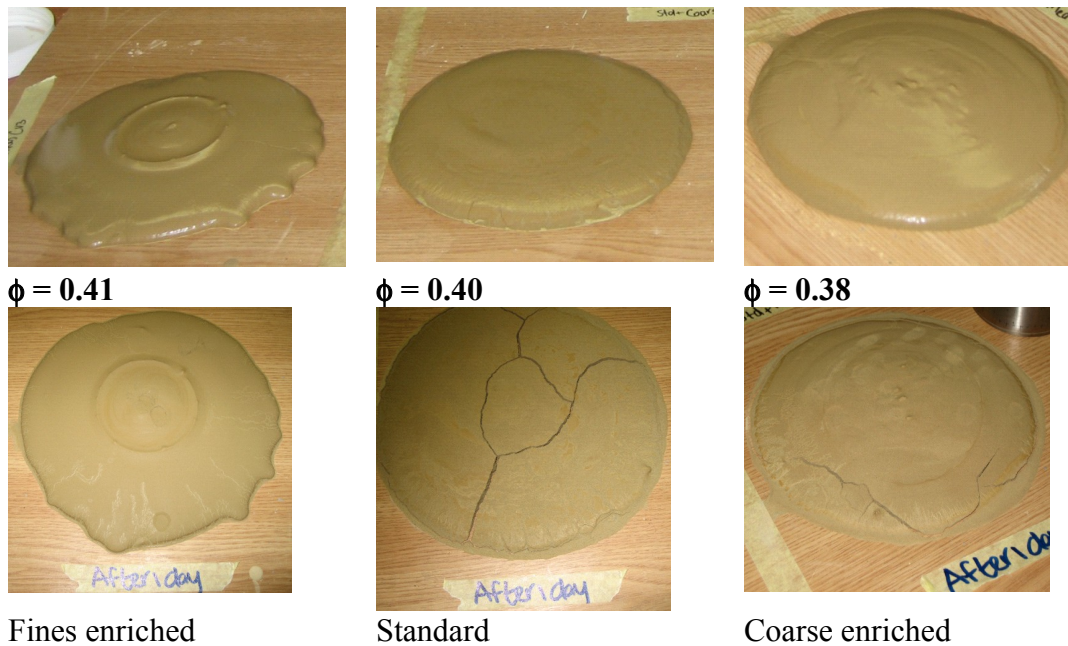


Figure 6.106: Slump tests for various suspensions fresh and after 1 day

but contributed it to the difference in pH. In this case, the pH was 7.54 and 7.87 for the standard and coarse enriched suspension. It was observed from a test where a suspension was made from coarse fraction (75 – 150 μm) only, that thixotropic behaviour increased. There was no structural breakdown as was observed (Fig 6.101) in the previous samples after which an equilibrium curve was obtained. So it can be assumed that the coarser particles have an adverse effect on the viscosity and should be investigated further (Ohlero & Ferreira, 2004). According to Cyr et al. (2000), any suspension can show shear thickening behaviour if the volume fraction is high and the suspension is non-flocculated. The other parameters that mostly contribute to shear thickening behaviour are particle shape, size and distribution. If nothing else, this work has shown the importance of the effect of particle size distribution on the rheology of fly ash suspensions. Parameters were found for Eq 6.50 for these suspensions and it is able to predict the viscosity over a range of concentrations as well as shear rate. We were unable to correlate these to the particle size distribution parameters so far and this work will be continued.

5.4.2.7 Conclusions

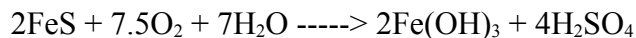
The effect of particle size distribution on the rheology of fly ash suspension has been demonstrated. It is recommended that the particle size distribution of the existing plants that intend to use the new treatment for AMD be measured over time to establish the envelope for which the pumping system should be designed. An in-depth study of the effect of chemistry on the rheology should also be conducted to ascertain the effect of pH and zeta potential on the rheology of the suspension as these are critical factors that influences the slurry rheology.

6 Ash walling studies to control surface AMD

6.1 Introduction

Acid mine drainage (AMD) is one of the most serious environmental problems facing the mining industry. It is formed by the oxidation of pyritic compounds in the surrounding strata of the mineral being mined. This oxidation is often catalysed by bacteria.

When water (rain or ground) comes into contact with this oxidation product a highly acidic effluent is formed. As this effluent flows through the surrounding environment it leaches heavy metals forming a more complex solution. The equation is simplified as follows:



Although it is known that bacteria catalyse this reaction, the exact mechanism is unknown. Twenty two different species of bacteria have been proven to associate with mine waters, *Thiobacillus ferroxidans* being the most common (O'Brien, 2000). *Thiobacillus* metabolises inorganic compounds including sulphates to obtain energy (White, 2000).

The concentration of heavy metals within the effluent is dependant on the surrounding strata. In some cases the high buffering capacity of the rock may cause the effluent to be circumneutral (O'Brien, 2000). Normally, however, the leachate has a low pH, dissolved solids of 4000-5000mg/L and sulphate concentrations in the thousands of mg/L (Gericke *et al.*, 2001).

At present approximately 44 ML of AMD are formed daily, with a projected figure of 131 ML per day by 2020. Although major efforts have been made to reduce and treat this effluent, approximately 700 000m³ of highly acidic water flows into the Loskop Dam annually (White *et al.*, 2001).

Several treatment technologies are available for the treatment and control of AMD. These range from lime neutralisation (Gericke, *et al.*, 2001) and electrochemical protection (Pulles *et al.*, 1996) for treatment to capping and neutralisation with alkaline materials for control and minimisation. AMD treatment is costly and requires constant management (Anon, 2000). In the case of lime draining the drains foul quickly with iron precipitates and the failed, heavy metal containing residues have to be disposed of and stored in hazardous waste sites in the long term.

Eskom burns approximately 100 Mt of coal annually and in so doing produces 22 Mt of inorganic, aluminosilicate fly ash (Willis, 1999). Approximately 1% of this is used in various commercial applications while the remainder is stored on ash dumps (Reynolds, 1999). Eskom power stations are mostly situated in the Mpumalanga coalfields and thus the fly ash and AMD are in close proximity.

Fly ash has been used to reduce AMD as a backfill and capping media internationally (pers. comm. Dr D Hassett). The high pH, small grain size, high availability, low water content, low permeability and pozzolanic activity of fly ash make it an effective means of combating AMD.

Fly Ash from Kendal, Matla and Duhva power stations were used for the Ash columns studies. Columns of different length were prepared using FA types mentioned and AMD from Middleburg, Landau and Navigation mines was percolated through these columns. These column studies performed to simulate conditions in which FA is in contact with AMD over long periods (280 days) to model the placement of ash in acidic environments for establishing suitable monitoring criteria and to understand the mineralogical characteristics and the chemical interactions taking place in ash in contact with AMD over the longer term. These columns showed quite a good neutralizing capacity over an extended period of time. The analysis of the leachants that were collected at the bottom of the columns after each drainage was presented in the previous final WRC report (Petrik et al., 2005). The XRD and XRF analysis of all the FA columns was also presented in our previous final WRC report (Petrik et al., 2005). This section of the report will only deal with the characterisation (FTIR, Raman and SEM-EDS) of Matla FA columns that were percolated using Landau AMD. This section will also refresh our memory on the XRD and XRF results that were presented in the previous report as mentioned above.

6.2 Materials and Methods

Fly ash from Matla power station and AMD from Landau colliery were collected. Matla ash was used to pack 100 mm diameter, perspex columns of different sizes: 1.5, 1.0, 0.5 and 0.25 m in length. Each column type was duplicated and given the annotation A or B. The mass of the column before and after filling was noted to ensure that duplicate columns contained the same amount of fly ash. Navigation AMD was percolated through these columns. The AMD was gravity fed through all 8 columns simultaneously (Figure 7.1). The neutralisation capacity of the columns has previously been reported.

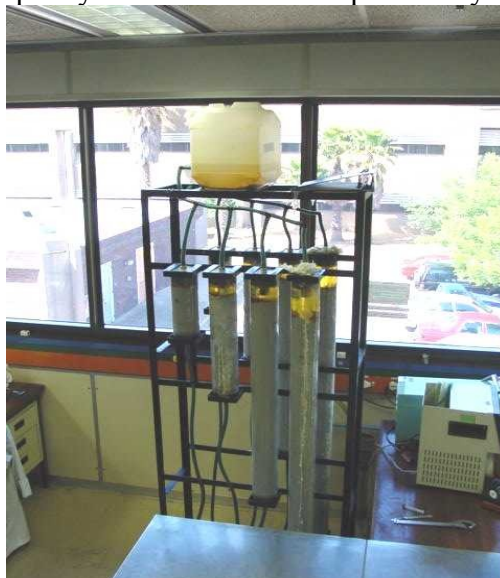


Figure 7.107: Gravity fed AMD through ash columns.

The columns were run until the alkaline permeate from the columns returned to pH 8.5, indicating a slow loss of neutralisation capacity over time. Once this end point was achieved, the flow was stopped and the ash removed from the perspex as a solid column. Leachate chemistry has previously been reported.

In order to have a better understanding of the chemistry of FA that would have been altered by the percolation of AMD, samples were collected at varying depths in the columns. The top, middle and bottom parts of the columns were sampled. A sample of the original Matla FA, not submitted to percolation of AMD, was also collected for analysis.

6.2.1 Fourier Transformed Infra Red Spectroscopy

The ash samples were analysed using Fourier Transform Infrared Spectroscopy (FTIR). Infrared (IR) spectroscopy is one of the widely used spectroscopic techniques in chemistry. It consists of the absorption measurement of different IR frequencies by a sample positioned in the path of an IR beam. By using this technique, the main objective is to determine the chemical functional groups in the sample analysed. Different functional groups absorb characteristic frequencies of IR radiation (Sherman Hsu, 1997). Before FTIR spectroscopy analysis, all the samples that were collected from the columns were crushed and ground to fine powder, then dried for about 12 h at 100 °C. For each FA sample, 0.0025 g of material was mixed with 0.4975 g of CsI. CsI was used as transparent support material to prepare the pellets used for the current analysis. The samples were analysed using a Perkin Elmer 1000 series FTIR instrument. The wave number range used for the analysis was 4000 to 350 cm^{-1} .

6.2.2 Raman Spectroscopy

The ash samples were analysed using Raman Spectroscopy. Raman spectroscopy is primarily a structural characterisation tool. When light is scattered from a molecule most photons are elastically scattered. The scattered photons have the same energy (frequency) and, therefore, wavelength as the incident photons. However, a small fraction of light (approximately 1 in 10^7 photons) is scattered at optical frequencies different from, and usually lower than, the frequency of the incident photons. The process leading to this inelastic scatter is termed the Raman effect (www.kosi.com).

Before the Raman spectroscopic analysis, all the samples that were collected from the columns were crushed and ground to fine powder, then dried for about 12 h at 100 °C. Raman spectra were acquired with the micro-Raman attachment (Olympus BX40 microscope) of a Jobin-Yvon T64000 Raman spectrometer operated in single spectrograph mode, with a holographic notch filter and a 600 grooves/mm grating. The excitation wavelength was the 514.5 nm line of a Coherent Innova Model 308 argon ion laser and the backscattered light was detected with a liquid-nitrogen cooled CCD detector. The diameter of the laser beam at the sample was approximately 1.5 μm , and the laser power measured at the sample was 1.5 mW. Laser plasma lines were removed from the incident light with a narrow band pass interference filter. The integration time was 2 minutes per spectrum. Measurements were done at ambient pressure and temperature. No

fixed volume of sample was analysed, as just a scoop (a small amount) was taken out with a small spatula and placed under the microscope. The analysis is thus essentially of a few grains on the surface of the sample.

6.2.3 Scanning Electron Microscopy (SEM) and Energy Dispersive X-Ray Spectroscopy (EDS)

SEM-EDS analysis was used to evaluate and confirm the mineralogical changes resulting from the interaction of the AMD with the FA columns. Powder samples for SEM and SEM-EDS were loaded on copper stubs coated with carbon graphite glue mixture and then carbon coated for 30 minutes. Both backscatter and secondary electron modes were used for image acquisition.

6.3 Results and Discussions

6.3.1 FTIR Analysis

According to Lee & van Deventer (2002), fly ash shows some particular characteristics when analysed with FTIR spectroscopy (Table 7.1). The strong bands at 1165 and 1080 cm^{-1} and the medium band at 798 cm^{-1} are attributable to α -quartz. The strong band at 561 cm^{-1} and the shoulders at 1138 and 620 cm^{-1} are indicative of mullite. An amorphous aluminosilicate phase is likely to cause vibration at around 1070-1080 cm^{-1} since similar vibrations can be observed for natural and glassy aluminosilicate materials. The broad band located at 500-650 cm^{-1} is also indicative of silicate and aluminosilicate glasses, which possess long range structural order in the form of rings of tetrahedron or octahedron. The very broad band between 950 and 1200 cm^{-1} at the T-O-Si (T = Al or Si) stretching vibration region is due to the multi phase nature of the fly ash.

Table 7.43: Assignments of infrared active bands that are detected for fly ash.

Wave number (cm ⁻¹)	Assignment	Bond
1080 (sh)	Asymmetric stretching	Si-O-Si and Al-O-Si
1074 (s)	Asymmetric stretching	Si-O-Si and Al-O-Si
1165 (sh)	Asymmetric stretching	Si-O-Si
1138 (sh)	Asymmetric stretching	Si-O-Si and Al-O-Si
950-1200 (s)	Asymmetric stretching	Si-O-Si and Al-O-Si
882 (s)	Si-O stretching, OH bending	Si-OH
798 (m)	Symmetric stretching	Si-O-Si
727 (sh)	Symmetric stretching	Si-O-Si and Al-O-Si
620 (sh)	Symmetric stretching	Si-O-Si and Al-O-Si
561 (s)	Symmetric stretching	Al-O-Si
466 (s)	Bending	Si-O-Si and O-Si-O

s = strong, m = medium, sh = shoulder

The IR peaks and their assignments for Matla fly ash and various layers of Matla fly ash columns are detailed in Appendix G. Figures 7.2 to 7.5 show the absorbance spectra for the bottom, middle and top layers of the 1.5, 1, 0.5 and 0.25 m columns. The absorbance is plotted along the primary y-axis and the wave number is plotted on the x-axis. In order to have a better understanding of the transformation of the chemistry of the original fly ash with the passage of AMD, the spectrum of the original Matla fly ash is added to each of the graphs.

The major peaks for Matla fly ash (Figure 7.2) correspond to asymmetric stretching of aluminosilicate (Si-O-Si and Al-O-Si) at 1096 cm⁻¹, symmetric stretching of mullite (Al-O-Si) at 560 cm⁻¹ and bending vibrations (Si-O-Si and O-Si-O) at 460 cm⁻¹ (Lee & van Deventer, 2002). Furthermore, the symmetric stretching (at 3436 cm⁻¹) and symmetric bending (at 2342 cm⁻¹) of OH groups were observed. Symmetric bending vibrations of H₂O were also observed at 1622 cm⁻¹.

The spectra of all three layers of the 1.5 m column (Figure 7.2) largely remained the same as the one of the original ash. Nevertheless, three significant changes were observed in the top layer spectrum:

1. The asymmetric stretching of Si-O-Si and Al-O-Si at 1096 cm⁻¹ shifted to higher wave numbers, by 56 cm⁻¹. The shifting of the Al/Si-O-Si band can be attributed to the structural reorganisation of aluminosilicate glassy phases and could possibly reflect structural environments of jennite (calcium silicate) (Yu *et al.*, 1999). The shifting of the Al/Si-O-Si peak thus illustrates the replacement of Al³⁺ or Si²⁺ ions by Ca²⁺ in the Al/Si-O-Si structure, due the percolation of AMD.
2. Two new peaks appeared at 660 cm⁻¹ and 600 cm⁻¹. They can be attributed to the depolymerisation of the original aluminosilicate phase, due to the passage of acidic AMD (Lee & van Deventer, 2002).
3. The vibrations of Al-O-Si and Si-O-Si at 560 cm⁻¹ and 460 cm⁻¹ became weaker.

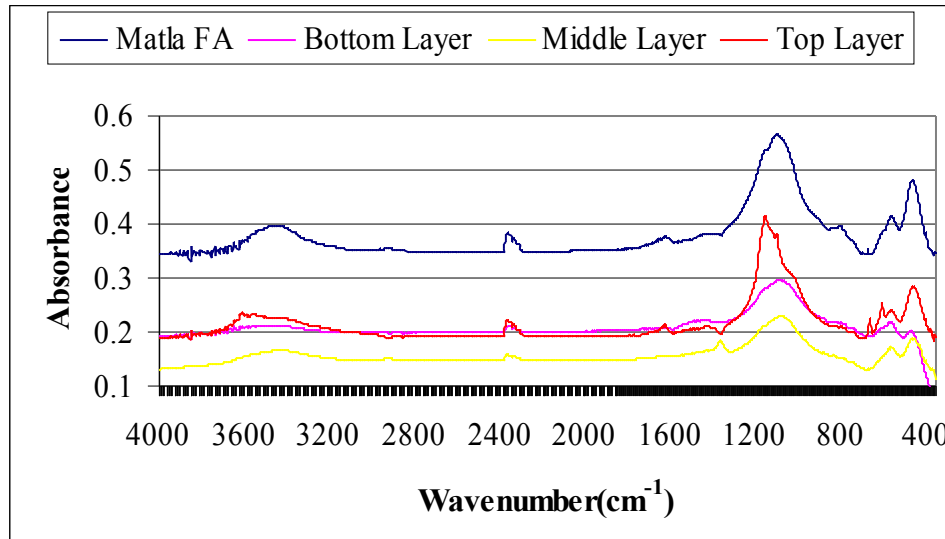


Figure 7.108: IR spectra of different layers of the 1.5 m Matla FA column.

The three differences described above between the original Matla FA and the top layer of the 1.5 m were also observed in the 1 m column (Figure 7.3). The 1.5 and 1 m columns seemed to behave similarly under AMD percolation.

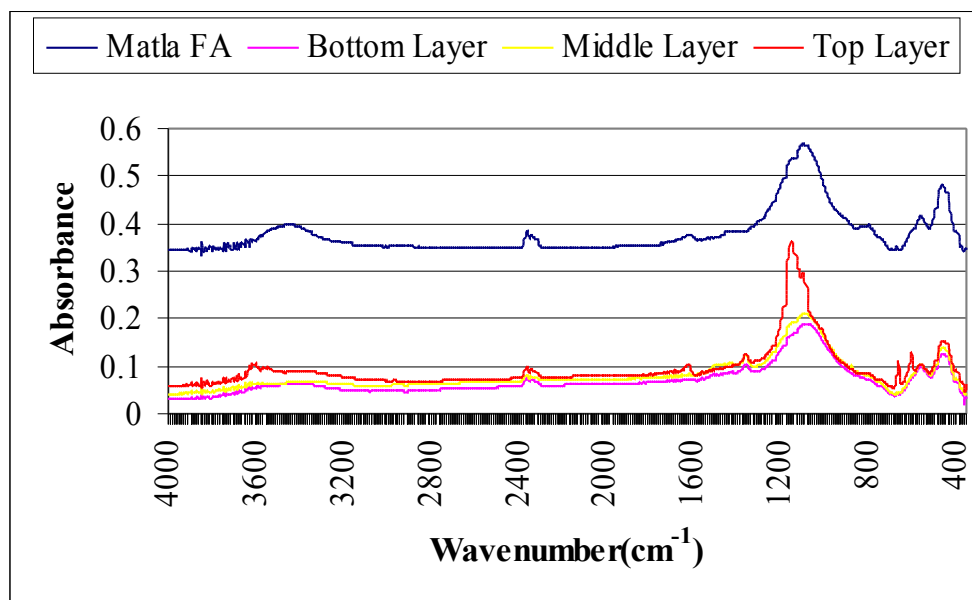


Figure 7.109: IR spectra of different layers of the 1 m Matla FA column.

The 0.5 m column also showed the three differences described previously between the original Matla FA and the top layer of the column (Figure 7.4). Unlike in the 1.5 and 1 m columns, for the 0.5 m column the shifting of the asymmetric stretching of Al/Si-O-Si band to higher wave numbers and the new peaks at 660 cm^{-1} and 600 cm^{-1} were observed in the top layer but also in the middle layer.

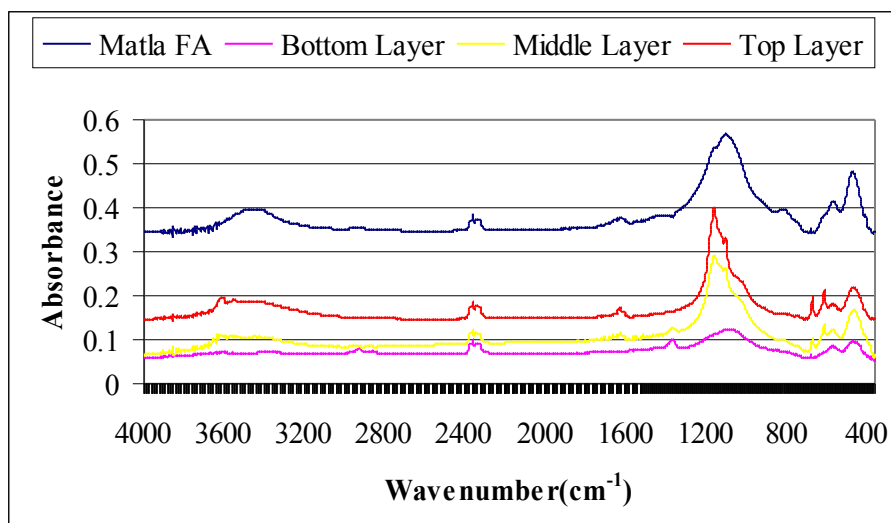


Figure 7.110: IR spectra of different layers of the 0.5 m Matla FA column.

The three differences that were observed for the 1.5, 1 and 0.5 m columns when compared to the original fly ash were observed again for the top layer of the 0.25 m column (Figure 7.5). The shifting of the Al/Si-O-Si band to higher wave numbers and the new peaks at 660 cm^{-1} and 600 cm^{-1} were observed for both the middle and bottom layers of the 0.25 m column.

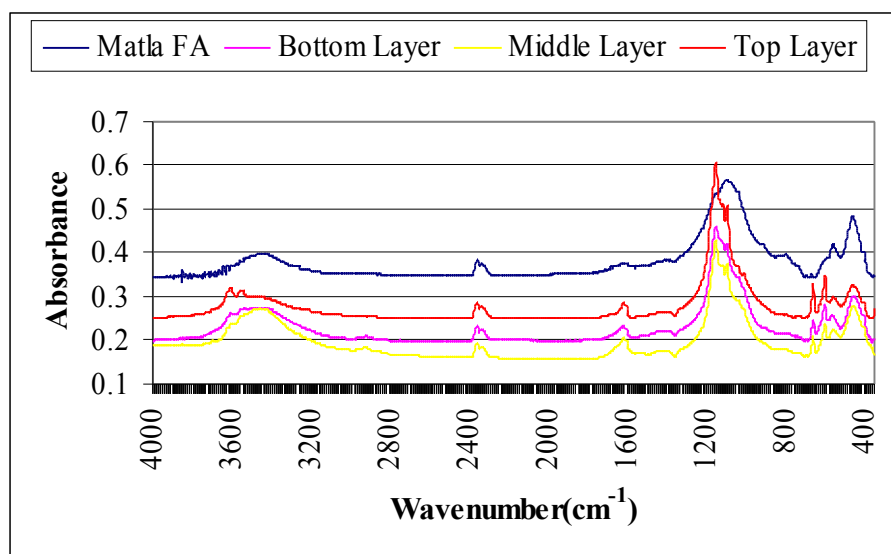


Figure 7.111: IR spectra of different layers of the 0.25 m Matla FA column.

6.3.1.1 Conclusions

The IR spectroscopy analysis showed that the percolation of AMD had an effect on the chemistry of fly ash. It was noticed that the shifting of the Al/Si-O-Si band to higher wave numbers and the appearance of new peaks at 660 cm^{-1} and 600 cm^{-1} depend on the

length of the column. In other words, when the length of the column was above 1 m, then chemical species from the percolated AMD would only be available and react in the top layer. When the length of the column was shortened (0.5 and 0.25 m); then these species were available to all the fly ash of the column, thereby allowing the reaction to take place in the entire column.

6.3.2 Raman Analysis

Figures 7.6 to 7.9 show the Raman spectra for the bottom, middle and top layers of the different columns. The intensity is plotted along the primary y-axis and the wave number or the Raman shift is plotted on the x-axis. In order to have a better understanding of the transformation of the chemistry of the original fly ash with the passage of AMD, the spectrum of the original Matla fly ash is added to each of the graphs.

The major peaks for Matla fly ash (Figure 7.6) correspond to Al-O and Si-O stretching which are in the frequency range of 800 to 1100 cm^{-1} and O-Si-O or O-Al-O deformation vibrations in the region below 500 cm^{-1} (Soma & Soma, 1985). The two broad peaks observed at 1351 and 1622 cm^{-1} are characteristic of carbon. The latter peak may appear when crystalline graphite is present and the former appears when the graphite structure becomes disordered (Soma & Soma, 1985). The peak at 461 cm^{-1} can be assigned to alpha quartz. The presence of a sharp peak at 1019 cm^{-1} can be assigned to symmetric stretching of CaSO_4 and the peak at 965 cm^{-1} can be assigned to K_2SO_4 (Scheetz & White, 1985).

The spectra of all three layers of the 1.5 m column (Figure 7.6) largely remain the same as the one of the original ash. Nevertheless, three significant changes are observed in the spectra:

1. A new peak appears at about 1089 cm^{-1} . This can possibly be attributed to precipitation of calcite (calcium carbonate) (Soma & Soma, 1985).
2. There is a shift in the graphite (1351 cm^{-1}) peak towards lower wave numbers. This is observed for all the layers in the column. The reason for this shift could possibly reflect the depolymerisation of the original graphitic structure by the passage of AMD.
3. The CaSO_4 peak that was observed in the raw FA and the top layer of the column was absent in the middle and bottom layers and a new peak was observed. This new peak at about 990 cm^{-1} can be assigned to the precipitation of Na_2SO_4 (Scheetz and White, 1985). When the AMD is passed through the column the pH of the solution changes and different elements precipitate out of solution at different pH values. This could be the reason why Na is precipitating as Na_2SO_4 in the middle and bottom layers but not in the top layer.

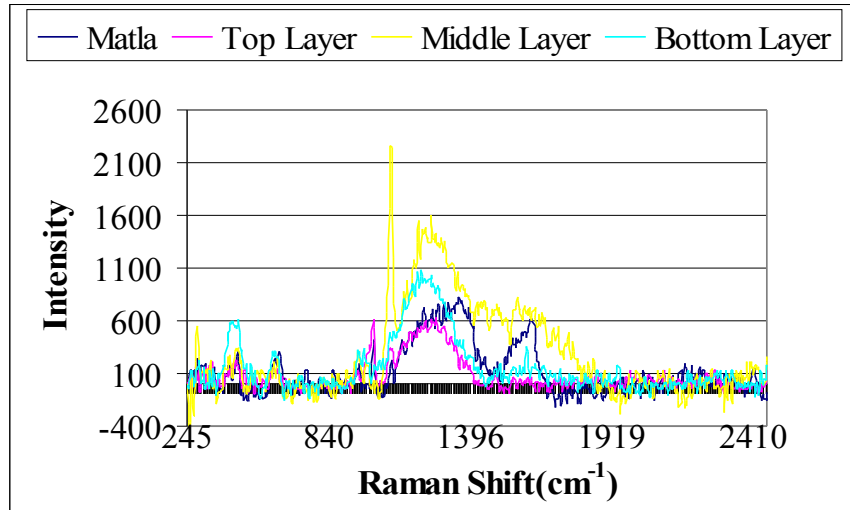


Figure 7.112: Raman spectra of different layers of the 1.5 m Matla FA column.

Figure 7.7 shows the Raman spectra for the 1 m column. The three differences described above between the original Matla FA and the three layers of the 1.5 m column are also observed in the 1 m column. The 1.5 and 1 m columns seem to behave similarly under AMD percolation.

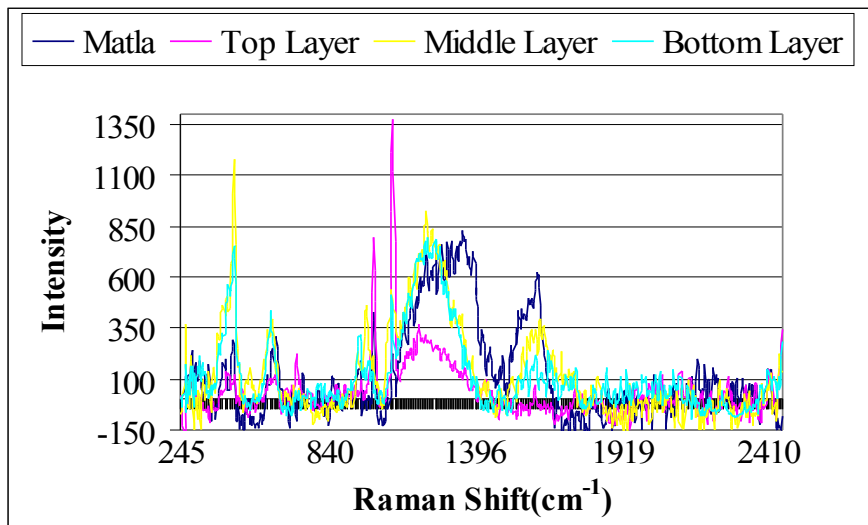


Figure 7.113: Raman spectra of different layers of the 1m Matla FA column.

Figure 7.8 shows the Raman spectra for the 0.5 m column. There is no major difference observed between the peaks of last two columns (1.5 and 1 m) and the peaks of this column.

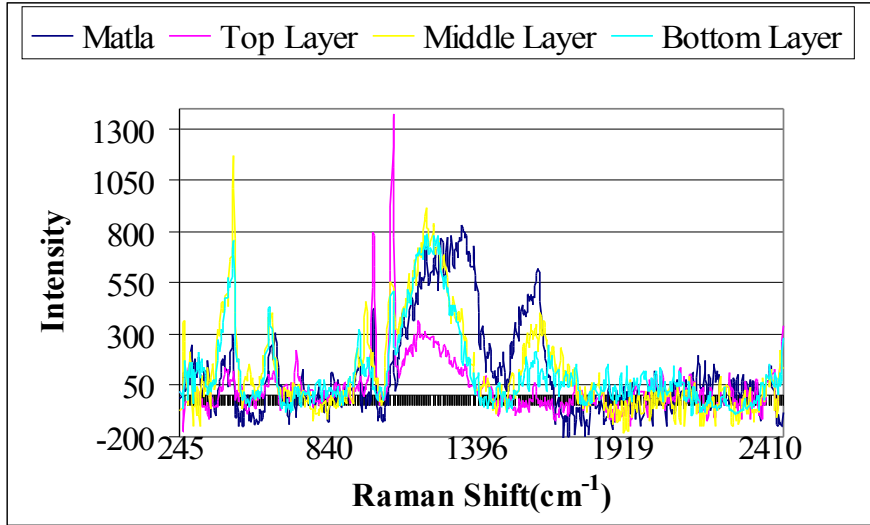


Figure 7.114: Raman spectra of different layers of the 0.5 m Matla FA column.

Figure 7.9 shows the Raman spectra for the 0.25 m column. The calcite peak at 1089 cm^{-1} and Na_2SO_4 peak at 990 cm^{-1} that was observed for the previous columns is not present or very weak in these column spectra. This could be attributed to the size of the column. When compared to other columns, the length of the 0.25 m column is very short (total length is approximately equal to the half the length of the top layer of the 1.5 m column) and the AMD that passes through the column would quickly percolate to the bottom parts of the column. This would not give the FA enough time to overcome the buffering capacity of AMD. On the other hand the longer residence time of the AMD in longer columns would also help in the precipitation of calcite and Na_2SO_4 .

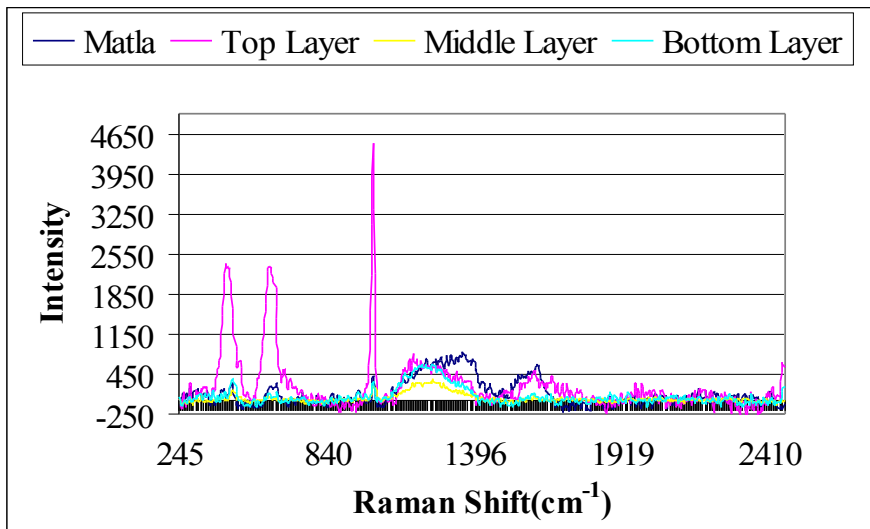


Figure 7.115: Raman spectra of different layers of the 0.25 m Matla FA column.

6.3.2.1 Conclusions

Raman analysis shows that percolation of AMD had an effect on the chemistry of the FA. Three distinct changes were observed upon the percolation of AMD through FA columns. The first one being the precipitation of calcite, the second one was depolymerisation of the graphitic structure and the third one was dissolution of CaSO_4 structure and precipitation of Na_2SO_4 in the middle and bottom layers. The precipitation of calcite and Na_2SO_4 was not observed in the 0.25 m column. It was thought that the longer residence time of the AMD through the longer columns would slow the flow of AMD and contribute to dissolution and phase changes of the quartz and alumino-silicate phase of the ash and would have also helped in the precipitation of calcite and Na_2SO_4 . The phase changes of aluminium silicate were also observed during the FTIR studies that were presented in the second interim report on this large scale study (Petrik *et al.*, 2005a). It was also observed during the FTIR studies that there was replacement of Al^{3+} or Si^{2+} ions by Ca^{2+} in the Al/Si-O-Si structure. It also reflects the precipitation of jennite (calcium silicate) upon the percolation of AMD through FA columns.

During the Raman analysis it was observed that all the columns, except the 0.25 m column, were similar in behaviour. The Raman analysis also complements the XRD results of the FA columns that were presented in a previous report to WRC (Petrik *et al.*, 2005), including non precipitation of calcite in the 0.25 m column. The only difference that was observed between XRD and Raman studies is that the precipitation of gypsum by XRD analysis was observed after the passage of AMD through Matla FA columns, whereas it was identified only in the unreacted/raw Matla FA using Raman analysis.

6.3.3 Characterisation of FA columns leached with AMD using scanning electron microscopy coupled with energy dispersive X-ray spectroscopy

Matla FA and all the three layers of the 0.5 m Matla FA column were characterised using Scanning Electron Microscopy (SEM) and Energy Dispersive X-Ray Spectroscopy (EDS) analysis. As per the FTIR results that were presented in the previous interim report, the top and middle layers of the 0.5 m column had similar chemistries, whereas the chemistry of the bottom layer was a bit different from the other two. It was also observed that the shorter the length of the column was, the greater the changes were observed with respect to chemistry. Hence it was thought that the 0.5 m column would be ideal for the SEM and EDS analysis and only this column was taken for analysis

Figure 7.10 shows pictures of the original/unaltered Matla fly ash. The pictures were taken with two different detectors: Quadrant Back Scattered Detector (QBSD) and Secondary electron Detector (SD). QBSD gives contrast based on atomic number of sample materials. SD is used to analyse the topography of the sample. As per the SD micrograph the topography of the Matla FA is characterized by round, semi spherical particles and irregular shaped particles of different sizes. The normal large ash cenospheres are visible as well as numerous smaller spherical particles. With the secondary detector images of the morphology of irregular particles are more clearly discerned. Using the QBSD, the difference in contrast between metallic and non-metallic particles of the Matla FA can be clearly seen, which proves to be useful in identifying the particles on which EDS studies can be performed.

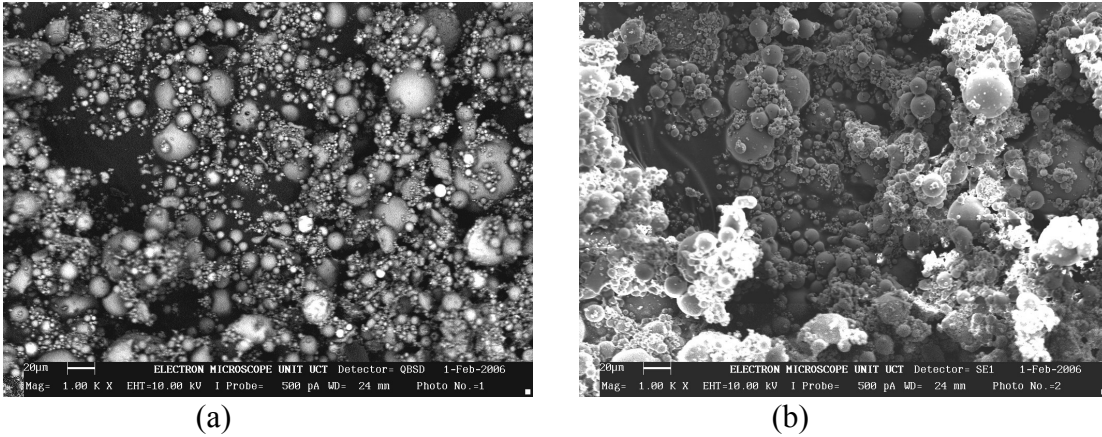


Figure 7.116: SEM micrographs of Matla fly ash taken using a back scattered detector (a) and a secondary detector (b).

EDS studies were carried out on particles of Matla ash (Figure 7.11) in order to identify their chemical composition. The particles were analysed in such a way to represent the character of the particles. As per the QBSD and EDS studies the small spherical and more dense particles were dominated by Fe with a weight percentage of 86.03 %, followed by Si, Al and Ca with weight percentages of 5.35, 5.18 and 2.51 % respectively and may represent fractions of the ball mills used to grind the coal because of the high Fe content. The other less regular particles were dominated by Si, (51.72 %), followed by Al and O with weight percentages of 28.68 and 19.60 % respectively. Since Matla FA is characterised by the abundance of such irregular particles the chemistry of FA is dominated by the presence of Si and Al species. Some particles compositions were dominated by Si and O, (93 %), which indicates the presence of the quartz phase.

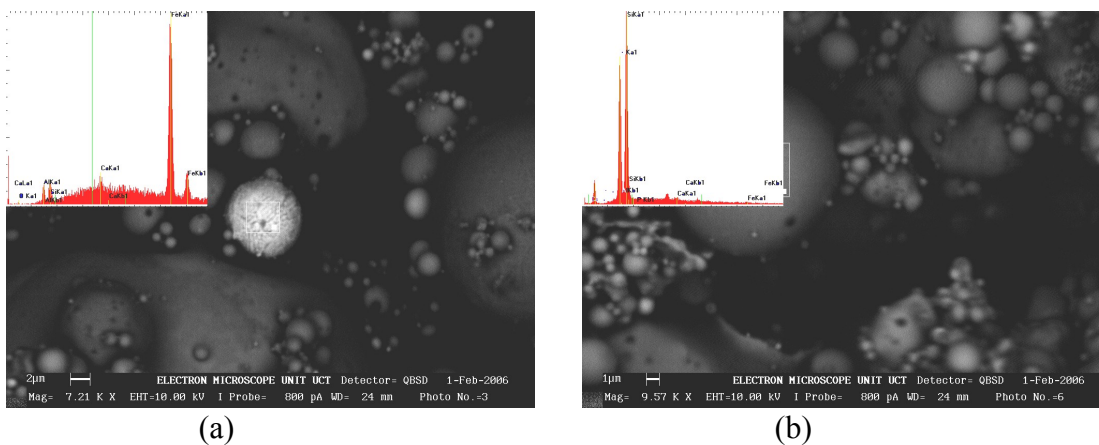


Figure 7.117: SEM micrographs and EDS spectra of small spherical (a) and larger irregular (b) particles of Matla fly ash.

Figure 7.12 shows the SEM micrographs taken on samples from the top layer of the 0.5 m ash column which was in contact with the raw AMD for the longest period of time. As per the SD micrograph it can be clearly observed that the FA particles have a rugged topography and are coated with precipitates. With the QBSD micrograph it was noticed

that the fly ash particles have been coated with precipitates rich in the metal species (based on the bright nature of the particles coated) that were initially present in AMD. During neutralisation of AMD with FA, some of the metal species present in the AMD were adsorbed or precipitated on to the surface of FA particles.

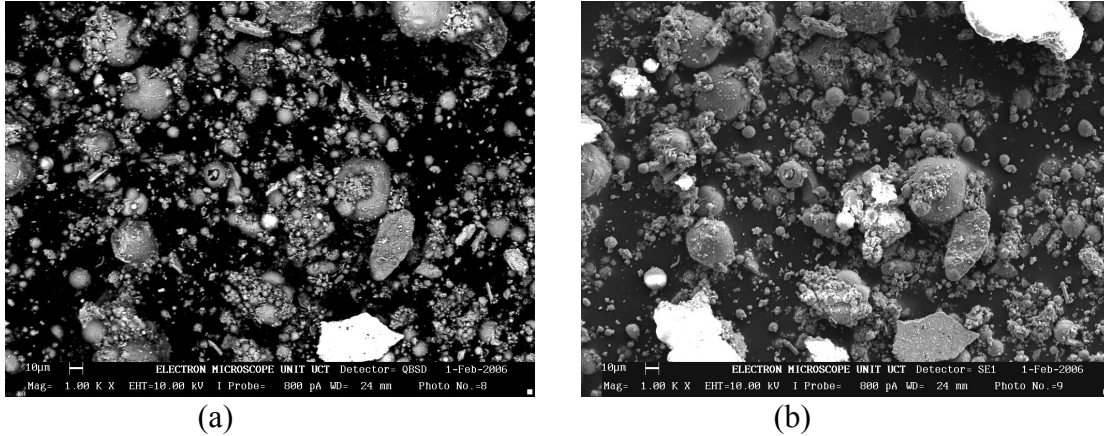


Figure 7.118: SEM micrographs of the top layer of the 0.5 m ash column taken using a back scattered detector (a) and a secondary detector (b).

Further evidence for the precipitation of metal species on ash particles is provided in Figure 7.13. As per the EDS studies of the material recovered from the top of the column, Cu, Al and Fe were enriched in this particle compared to the unreacted Matla FA. The weight percentage of different elements was as follows: O-36.33 %, Al-6.60 %, Si-32.86 %, Fe-8.32 % and Cu-15.88 %.

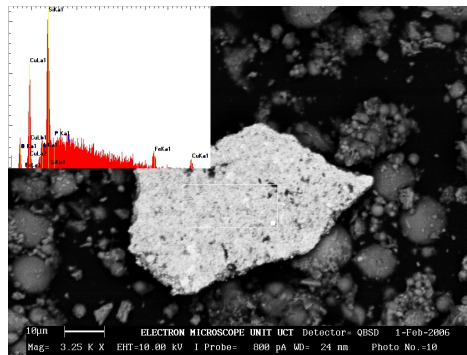


Figure 7.119: SEM micrograph and EDS spectrum of the material that was observed in the top layer of the 0.5 m ash column

Furthermore, from the EDS analysis of an agglomerated particle from the top of the column (Fig 7.14), it was observed that precipitation of metals as hydroxides and sulphides took place while AMD was passed through the ash column. The weight percentage of different elements was: O-29.87 %, Al-22.65 %, Si-31.15 %, S-4.62 %, Ca-4.63 %, Fe-6.22 % and Cu-0.87 %. The micrographs show that there was a high degree of amorphous material deposited between or upon the characteristic mullite spheres of FA,

which could relate to the minerals such as calcite or gypsum found in XRD analysis of these columns (Petrik *et al.*, 2005).

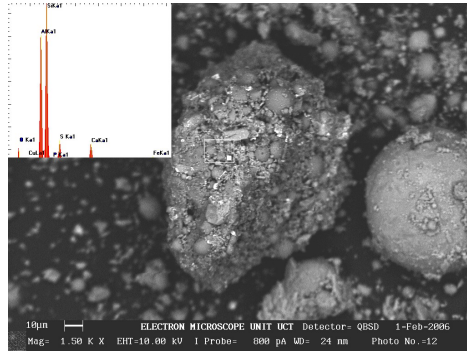


Figure 7.120: SEM micrograph and EDS spectrum of an agglomerated particle of the top layer of the 0.5 m ash column.

From SEM micrographs of the middle layer of the 0.5 m FA column (Figure 7.15), it was observed that the degree of the metal adsorption on the surface of the particles was minimised compared to the top of the column (traces of metal particles adsorbed only). This was observed from the micrographs obtained from both QBSD and SD.

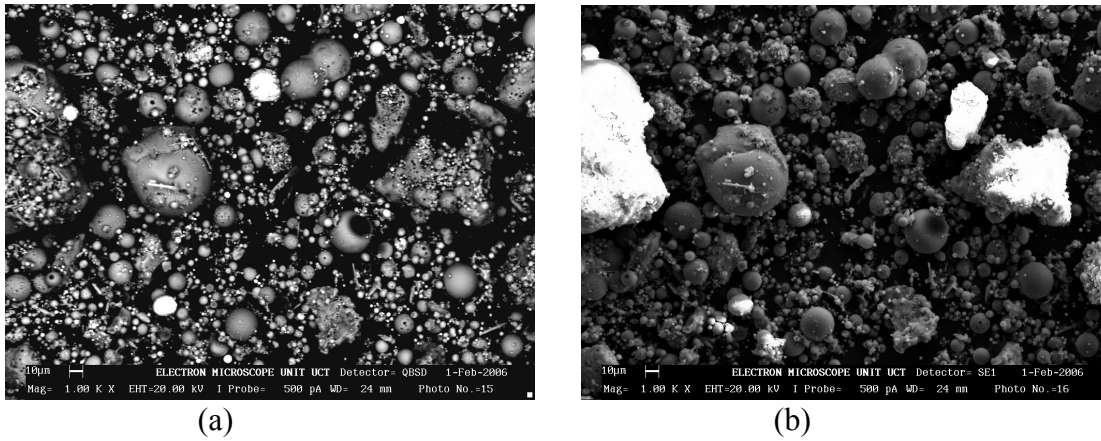


Figure 7.121: SEM micrographs of the middle layer of the 0.5 m ash column taken using a back scattered detector (a) and a secondary detector (b).

An EDS analysis of particles sampled from the middle layer of the column (Figure 7.16) indicated the precipitation of metals (Fe-70.75% and Al-3.20%) as discussed above.

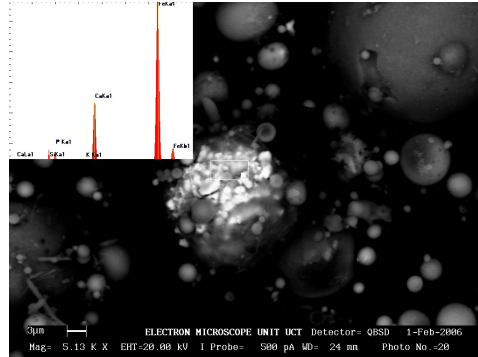


Figure 7.122: SEM micrograph and EDS spectrum of particles from the middle layer of the 0.5 m column.

Based upon the SEM micrograph of the bottom layer of the 0.5 m column (Figure 7.17), the metal adsorption on the surface of the FA particles was almost nil (as per both QBSD and SD micrographs), which indicates that after the percolation of AMD through the column of ash, interaction with FA reduced the metal load considerably. This was previously confirmed by elemental analysis of the permeate. The corresponding data were presented in the previous phase of this study. Even so, some particles of metallic nature were observed as per the EDS studies (Figure 7.18). Percentages of different elements as per the EDS studies were as follows: O-5.08%, Al-8.12%, Si-18.23%, P-2.65%, S-0.50%, K-0.71% and Fe-63.95%.

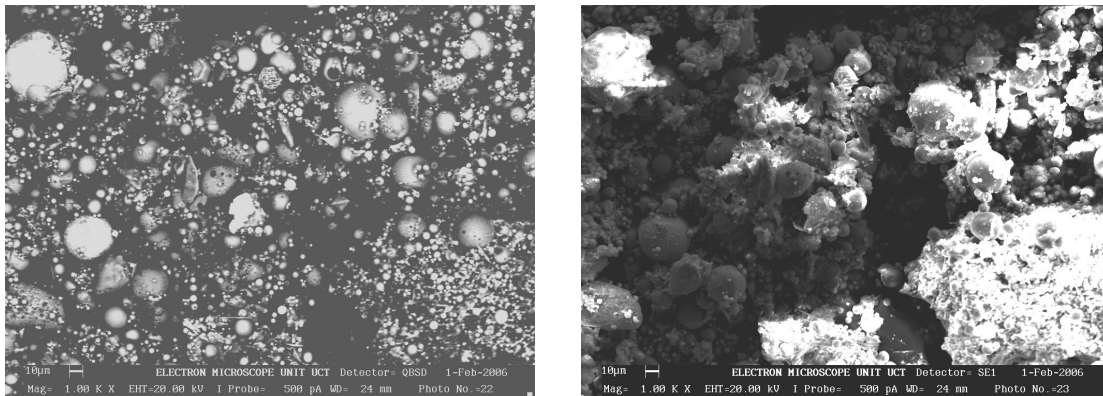


Figure 7.123: SEM micrographs of the bottom layer of the 0.5 m ash column taken using a back scattered detector (a) and a secondary detector (b).

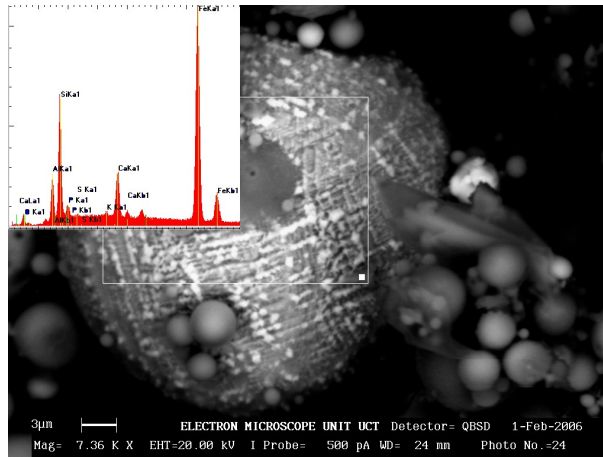


Figure 7.124: SEM micrograph and EDS spectrum of sample from the bottom layer of the 0.5 m ash column.

By comparing the EDS and SEM results of the three layers it is evident that the degree of metal precipitation and subsequent adsorption on the surface of FA particles was higher at the first contact point between FA and AMD, at the top layer, and became lower by the time the water had percolated through the column to reach the bottom layer. Apart from the degree of metal adsorption, no other significant morphological changes were observed among the three zones of the columns that were examined, indicating that if minerals from FA were solubilised during contact with AMD, it was to a less than microscopic degree. Precipitation or adsorption of trace elements is not expected to give rise to large agglomerated particles but to changes at the nanoscale or smaller. The sulphate content of the AMD has been entrained upon the ash as mineral phases CaSO_4 and NaSO_4 , as was also shown by XRD and Raman analysis. The Fe content was reduced through the formation of Fe_2O_3 , as shown per XRF analysis. According to XRF analysis (Petrik *et al.*, 2005) the Fe_2O_3 content was higher in the top layers of the columns, which findings correlated very well with the findings of SEM and EDS.

6.3.4 Conclusions from the fly ash column studies

- Raman analysis indicated that the precipitation of calcite took place when AMD was passed through the FA columns. This precipitation was not observed for the 0.25 m column. This was also confirmed by the XRD studies, which showed that the major mineral phases that were precipitated after the passage of AMD were gypsum and calcite (Petrik *et al.*, 2005b). Calcite was not observed by XRD either, in any of the layers of the 0.25 m column.
- Depolymerisation of the graphitic structure was observed upon the passage of AMD through the FA columns.
- As per the Raman analysis, it was observed that the precipitation of Na_2SO_4 took place in the middle and bottom layers of the all the columns except the 0.25 m column.
- With the SEM and EDS studies it was observed that the ash particles were coated with metal species, particularly Fe in the top layer of the columns. This was also observed by the XRF studies (Petrik *et al.*, 2005). As per the XRF studies it was noticed that high amounts of Si, Al and Ti were present in the middle and bottom

layers of the columns showing that the dissolution of these elements (especially in the top layers) play a role in the neutralization of AMD and blocking the columns. Higher concentrations of Fe were observed in the top layer indicating immediate precipitation of Fe as the AMD came in contact with ash. As per the XRF studies it was also observed that the sulphate is enriched in the top of the longer columns and increased levels are observed through out of the shorter columns, probably because of the high availability of AMD in a shorter column.

- As per the EDS studies, it was observed that the precipitation of metals took place as metal hydroxides and sulphides. This strengthens our argument that metals precipitate as hydroxides during the AMD - FA neutralisation reaction.
- As per the SEM analysis, it was observed that a high degree of amorphous material was deposited between or upon the characteristic mullite spheres of FA, which could relate to minerals such as calcite or gypsum. This complements the results obtained from XRD and Raman spectroscopy. As per the XRD results the sulphate removal can also be attributed to the precipitation of ettringite.
- Chemical changes such as precipitation of calcite, gypsum and sodium sulphate in the longer columns indicated that the slow passage of AMD through the column has given ample time for FA to react. Looking at FTIR and Raman results it can be concluded that dissolution of phase changes is quick (as it was observed in all the layers of 0.25 column-FTIR results), but precipitation of elements will favour the longer contact time (as the precipitation was not observed in the 0.25m column-raman results).

This study shows that fresh FA is suitable for the passive treatment of AMD. Thus, a significant potential exists to reduce AMD pollution arising in spoil heaps and underground, by application of ash walls to prevent AMD generation. The use of FA or solid residues for backfilling may play a role in mitigating the environmental concerns around current flows and future production of AMD.

7 General Conclusions

Large scale treatment of AMD with FA and backfilling with solid residues was delayed due to Anglo's decision to not fund a pilot scale plant at Navigation. However, there is a positive response from bhpbilliton and as per the current situation a pilot scale rig at Middleberg mine and a suitable place to run pilot scale studies on backfilling with solid residues is planned. The plant is expected to up and run by March' 2007. Quite a number of meetings were held with people from different backgrounds in order to make sure that the project gets a head start. A detailed project proposal that includes cost comparison between FA treatment and limestone treatment. It can be concluded from these studies that FA treatment is competitive in terms of comparison of cost beneficiation with limestone treatment. Apart from this there are several benefits that one can gain from the FA treatment as explained in the report.

Getting access to the historical ash placement studies was very difficult. UWC has managed to visit one of the ash placement sites "Ermelo" in June'06 but nothing interesting found there. There were no signs of ash filling as it was done long time back. No further attempts were made to access remaining sites as in September' 06 Coaltech informed UWC that the project has come to an end.

The solid residues obtained from the pilot scale rigs at Eskom and CSIR were tested for their chemical, physical and rheological suitability to backfill mines. The chemical durability was ascertained by column studies in which columns are filled with solid residues by itself, FA by itself, different combinations of solid residues and FA and solid residues +6% OPC. For logistical constraints simulated AMD was added to the columns and it was found that all the columns have high buffering capacity extended for long periods of time. Despite being taken part in the active treatment, solid residues were still left with some neutralization capacity that could treat the simulated AMD for quite long time. The strength testing was carried out on the solid residues obtained from different FA: AMD reactions. Experiments were carried out with and without adding binders to the solids. It was noticed that after 28 days the solids derived from the 1: 3(without binder) reaction have started gaining some strength and after 410 days they gained enough strength so that they can be used for backfilling. Solids derived from 1: 4 and 1: 6 ratios also gained considerable strength after 410 days. The solids that were tested with addition of binder have performed really well and gained considerable strength after 28 days only. After 410 days they gained a strength that is approximately three times in magnitude when compared to the solid residues that were tested without adding binder. The rheological studies indicated that solids exhibited a shear thinning behaviour that is increase in viscosity with increasing shear rate. The results have to be validated by means of pipe tests. Tests were also carried out to understand the influence of FA Particle Size Distribution (PSD) on its capacity to neutralize AMD and influence on the rheological properties of solid residues. The results indicated that FA-PSD has an influence on the reaction kinetics with AMD and rheological behaviour. The sample enriched with fine particles showed the greatest viscosity and also neutralization with this sample took less time when compared to the other samples.

Ash filled with columns of varying length was used for Ash walling studies. AMD was gravity fed through the columns and leachates were collected at the bottom. The drainage

of AMD continued until the permeates from all the columns reach a pH of approximately 8.5. ICP Analysis of permeates showed that the quite a good percentage of toxic element attenuation has taken place. Analysis of the FA columns indicated that Fe concentration in AMD was precipitated as soon as it came in contact with AMD. Increased concentration of Al, Si and Ti in the middle and bottom layers suggested that dissolution of these elements has played a role in the neutralization of AMD. Sulphate concentrations were reduced due to the precipitation gypsum and other mineral phases. Finally, it can be concluded that the passive barrier treatment by employing FA as an in situ barrier is successful and can be used in the real mining environment.

8 References

1. Adams, F., and Z. Rawajfih. 1997. Basaluminite and alunite: A possible cause of sulphate retention by acid soils. *Soil Sci. Soc. Am. J.* 41: 686-692.
2. Agbenin, O. John. 2003. Soil saturation extract composition and sulphate solubility in a tropical semiarid soil. *Soil Sci. Soc. Am. J.* 67: 1133-1139.
3. Allison, J.D., D.S. Brown, and K.J. Novo-Gradac. 1991. MINTEQA2, A geochemical assessment data base and test cases for environmental systems: Vers. 3.0 users manual. Report EPA/600/3-91/-21. Athens, GA: U.S.EPA.
4. Alpers, C.N., D.W. Blowes, D.K. Nordstrom and J.L. Jambor. 1994. Secondary minerals and acid mine-water chemistry. In *Environmental geochemistry of sulfide mine-wastes*, ed, by D.W. Blowes, and J.L. Jambor, Shortcourse Handbook, V.22, Mineralogical Association of Canada, pp 247-270.
5. Azzie, B. A-M. Coal mine waters in South Africa: Their geochemistry, quality and classification. PhD Thesis, 2002. University of Cape Town, SA.
6. Barret J.R., Coulthard M A. and Dight P.M. 1978. Determination of fill stability. *Mining with backfill - 12th Canadian Rock Mechanics Symposium*, Canadian Institute of Mining and Metallurgy, Quebec., 19, 85 – 91.
7. Benzaazoua, M; Tikou Belem, Bruno Bussiere. 2002. Chemical factors that influence the performance of mine sulphidic paste backfill. *Cement and Concrete Research* 32, 1133-1144.
8. Benzaazoua, M; Tikou Belem, Bruno Bussiere. 2002. Chemical factors that influence the performance of mine sulphidic paste backfill. *Cement and Concrete Research* 32, 1133-1144.

9. Bigham J.M. 1994. Chapter 4: Mineralogy of ochre deposits formed by sulfide oxidation. In: Jambor JL, Blowes DW (eds) Environmental geochemistry of sulfide Mine-wastes, short course handbook. Mineralogical Association of Canada (Vol 22), Waterloo, Ontario, pp 103-132.
10. Bigham J.M., Schwertmann U., Carlson L and Murad E. 1990. A poorly crystallized oxyhydroxysulfate of iron formed by bacterial oxidation of Fe(II) in acid mine waters. *Geochim. Cosmo. Acta* 54: 2743-2758.
11. Bigham, J.M. & Nordstrom, D.K. 2000. Iron and aluminum hydroxysulfates from acid sulfate waters. In: Sulfate Minerals: Crystallography, Geochemistry, and Environmental Significance (eds C.N. Alpers, J.L. Jambor & D.K. Nordstrom), pp. 351–403. Mineralogical Society of America, Washington, DC.
12. Bournonville B and Nzihou A. 2002. Rheology of non-Newtonian suspensions of fly ash: effect of concentration, yield stress and hydrodynamic interactions. *Powder Technology* 128. 148 – 158.
13. Boylu F, Dinçer H and Ateşok G. 2004. Effect of coal particle size distribution, volume fraction and rank on the rheology of coal-water slurries. *Fuel Processing Technology*. 85. 241 – 250.
14. Brownlow, A. H. 1979. *Geochemistry*. Englewood Cliffs, NJ: Prentice-Hall, Inc.
Chao, T.T. 1984. Use of partial dissolution techniques in geochemical exploration. *J.Geochem. Explor.* 20: 101-135.
15. Cocks, D.L., Mollah, M.Y.A. The Chemistry and leaching mechanisms of hazardous substances in cementitious solidification/stabilization systems. In: *Chemistry and microstructure of solidified waste forms*; Spence, R.D., Ed; Lewis publishers, Boca Raton, FL, 1993: pp 187-241.

16. Cocke, D.L., Mollah, M.Y.A. The Chemistry and leaching mechanisms of hazardous substances in cementitious solidification/stabilization systems. In: Chemistry and microstructure of solidified waste forms; Spence, R.D., Ed; Lewis publishers, Boca Raton, FL, 1993: pp 187-241.
17. Coussot P and Piau J M. 1994. On the behaviour of fine mud suspensions. *Rheologica Acta*. 33. 175 – 184.
18. Cyr M, Legrand C and Mouret M. 2000. Study of shear thickening effect of superplasticizers on the rheological behaviour of cement pastes containing or not mineral additives. *Cement and Concrete Research*. 30. 1477 – 1483.
19. Dabak T. and Yucel O. 1987. Modelling of the concentration and particle size distribution effects on the rheology of highly concentrated suspensions. *Powder Technology*, V, 52, 193-206.
20. Davies C.W. 1962. *Ion Association*. Butterworth Publications, Washington D.C.
De Kretser R G, Scales P J and Boger D V. 1998. Surface chemistry-rheology inter-relationships in clay suspensions. *Colloids and Surfaces A: Physicochemical and Engineering Aspects*. 137. 307 – 318.
21. Domenech C., C. Ayola and J. de Pablo. 2002. Sludge weathering and mobility of contaminants in soil affected by the Aznacollar tailing dam spill (SW Spain). *Chemical Geology* 190. 355-370.
22. Doye Isabelle and Josee Dusesne. 2003. Neutralization of acid mine drainage with alkaline industrial residues: Laboratory investigation using batch-leaching tests. *Applied Geochemistry* 18. 1197-1213.
23. Drever, J.I. 1997. *The geochemistry of natural waters: Surface and groundwater environments* 3rd Edition, Prentice-Hall Inc., New Jersey, 436 p.

24. Dudas, M. J. 1981. Long-term leachability of selected elements from fly ash. *Environ. Sci. Technol.* 15: 840-843.
25. Early L.E, Dhanpat Rai, S.V. Mattigod, and C.C. Ainsworth. 1990. Geochemical Factors Controlling the Mobilization of Inorganic Constituents from Fossil Fuel Combustion Residues: II. Review of the Minor Elements. *J. Environ. Qual.* 19: 202-214.
26. Eaton, A.D., Clesceri, L.S., Greenberg, A.E. and Franson, M.A.H. (eds.) 1995. Standard methods for the examination of water and wastewater, 19th Edition. American Public Health Association, American Water Works Association and Water Environment Federation, Washington DC, USA.
27. Eckert, D.J, 1988. Recommended pH and lime requirement tests. P 6-8. In W.C. Dahnke (ed), Recommended chemical soil test procedures for the North Central Region, North Dakota Agri. Expt. Sta. Bulletin No. 499 (Revised).
28. Faulkner, S.P and Richardson, C.J. 1989. Physical and chemical characteristics of freshwater wetland soils; In Hammer. D.A. (ed), constructed wetlands for wastewater treatment-municipal, industrial, and Agricultural: Lewis Publishers, Chelsea, Mich., pp 41-72.
29. Fillipek, H. L., Nordstrom, D.K. and Ficklin H. W. 1987. Interaction of acid mine drainage with waters and sediments of west squaw creek in the West Shasta Mining District, California. *Environ. Sci. Technol.*, Vol. 21, No. 4. pg 388-396.
30. Gitari M.W, LF Petrik, DL Key, C. Okujeni. 2004. Neutralisation of acid mine drainage with fly ash: A laboratory investigation of metal and SO₄ removal in the process waters. 37th National Convention of the South African Chemical Institute (SACI), July 2004.

31. Glasser, F.P. 1970. Chemistry of cement-solidified waste forms. In: chemistry and microstructure of solidified waste forms; Spence, R. D., Ed.; Lewis Publishers, Boca Raton, FL, 1993; pp1-40.
32. Govier G.W. and Aziz K. 1972. The flow of complex mixtures in pipes. Van Nostrand Reinhold, New York.
33. Hem, J.D. and Lind, C.J. 1993. Manganese minerals and associated fine particulates in the streambed of Pinal Creek, Arizona, USA: a mining-related acid drainage problem. *Applied Geochem*, 8: 67-80.
34. Heywood N I and Alderman N J. 2000. Suspension and Paste Rheology for the Process Industries. Hyprotech courses and workshops: 15 November 2000. Oxfordshire, UK. AEA Technology plc.
35. Heywood N I, Mehta K B and Poplar D. 1993. Assessment of flow properties of pulverized fuel ash slurries at high concentration. Proc of 12th International Conference on Slurry Handling and Pipeline Transport: Hydrotransport 12, 28-30 September 1993, Brugge, Belgium, edited by C.A. Shook. London: Mechanical Engineering Publications.
36. Ilgner H.J. Cost-effective utilisation of fine and coarse ash to maximise underground coal extraction and to protect the environment. Coaltech 2020 Report, Secunda, Coal Indaba Conference, 2002, 19 p.
37. Ilgner H.J. The benefits of ashfilling in South African coal mines. Coal - the future, 12th International Conference on Coal Research, ICCR, SAIMM, 2000.
38. Iyer R S and Stanmore B. 1999. The effect of water absorption and the role of fines on the yield stress of dense fly ash slurries. *Cement and Concrete Research* 29. 765 – 767.

39. Iyer R S and Stanmore B. 2000. The distortion of the diffuse double layer and its effects on flow properties of dense flyash slurries. *Colloids and Surfaces A: Physicochemical and Engineering Aspects*. 166. 133 – 144.
40. Jackson, M.L., C.H. Lim., and L.W. Zelazny. 1986. Oxides, hydroxides and aluminosilicates, p113-119. In A Klute (ed). *Methods of soil analysis. Part 1*. 2nd ed. Agron. Monogr. 9. ASA and SSSA, Madison, WI.
41. Jeong, J.K and Soo, J.K. 2003. Mineralogy of ferrihydrite and schwertmannite from the acid mine drainage in the Donghae Coal Mine Area. *J. Miner. Soc. Korea*. 16: 191-198.
42. Khanna, P.K., Prenzel, J., Meiwes, K.J., Ulrich, B., Matzner, E., 1987. Dynamics of sulfate retention by acid forest soils in an acidic deposition environment. *Soil. Sci. Soc. Am. J.* 51, 446-452.
43. Kimball, B.A., R.E. Broshears, K.E. Bencala, and D.M. McKnight. 1994. Coupling of hydrologic transport and chemical reactions in a stream affected by acid mine drainage. *Environ. Sci. Technol.* 28: 2065-2073.
44. Kindness A; A Macias and F.P. Glasser. 1994. Immobilization of chromium in cement matrices. *Waste Management*, Vol. 14. No. 1. pp, 3-11.
45. Komnitsas K., G. Bartzas and I. Paspaliaris. 2004. Efficiency of limestone and red mud barriers: Laboratory column studies. *Minerals Engineering*, Volume 17, Issue 2, February 2004, pg 183-194.
46. Kosi. A brief look at Raman scattering theory. Available online at: <http://www.kosi.com/raman/resources/tutorial/index.html>.
47. Kulumani Parida and Jasobanta Das. 1995. Studies on Ferric Oxide Hydroxides II. Structural properties of goethite samples (α -FeOOH) prepared by Homogeneous

precipitation from $\text{Fe}(\text{NO}_3)_3$ solution in the presence of sulfate ions. *Journal of colloid and interface science*. 178, 586-593.

48. Kuo, L., P.E. Heilman and A.S. Baker. 1983. Distribution and forms of copper, zinc, cadmium, iron and manganese in soils near a copper smelter. *Soil Sci*. 135: 101-109.

49. Landel R.F., Moser B.G. and Bauman A.J. 1963. Fourth International. Congress on Rheology, Part 2, p. 663, Interscience Publishers, New York, 1965.

50. Langmuir, D and Whitmore, D. O. 1971. Variations in the stability of precipitated ferric oxyhydroxides. In: Hem, J.D. (ed) *Non-equilibrium systems in natural water chemistry*. Advances in chemistry series, nr 106, pp 209-234.

51. Langmuir, Donald. 1997. *Aqueous Environmental Geochemistry*. Prentice-Hall, Inc.

52. Lazaroff N., Melanson L., Lewis E., Santoro N., and Pueschel C. 1985. Scanning electron microscopy and infrared spectroscopy of iron sediments formed by *Thiobacillus ferrooxidans*. *Geomicrobiol. J.* 4, 231-268.

53. Lazaroff N., Sigal W., and Wasserman A. 1982. Iron oxidation and precipitation of ferric hydroxysulfates by resting *Thiobacillus ferrooxidans* cells. *Appl. Environ. Microbiol.* 43, 924-938.

54. Lee, W.K.W. and van Deventer, J.S.J. 2002. Structural reorganization of class F class ash in alkaline silicate solutions. *Colloids and Surfaces A: Physicochemical Engineering Aspects*, 211, 49-66.

55. Lindsay, W.L. 1979. *Chemical equilibria in soils*. John Wiley and Sons, New York.

56. M.W. Gitari, L.F. Petrik, O. Etchebers, D.L Key, E. Iwuoha and C. Okujeni. 2006. Treatment of acid mine drainage with fly ash: Removal of major contaminants and trace elements. *Journal of Environmental Science and Health-Part A.*, A41 (8) (In press).

57. M.W. Gitari; L.F. Petrik; O. Etchebers; V.R. Kumar Vadapalli; D.L. Key, and E. Iwuoha. Utilization of fly ash for remediation of coal mines waste water: Reaction on AMD and possible backfilling with residual solids. A paper presented at The South African Institute of mining and Metallurgy. Colloquim: Sustainable development in the life of coal mining in South Africa, 13th July 2005, Carnival city, Boksburg.
58. Ma, L.Q., and G.N. Rao. 1997. Chemical fractionation of cadmium, copper, nickel and zinc contaminated soils. *J. Environ.Qual.* 26: 259-264.
59. Mattigod, S.V., Dhanpat Rai, Eary, L.E. and Ainsworth, C.C. 1990: Geochemical factors controlling the mobilisation of inorganic constituents from fossil fuel combustion residues: 1. Review of the major elements. *Journal of environmental quality*, 19,188-201.
60. Miller, W.P., D.C. Martens and L.W. Zelazny. 1986. Effect of sequence on extraction of trace metals from soils. *Soil Sci. Soc. Am, J.* 50: 598-601.
61. Myeni, B.C.S., Triana, J.S., and Logan, T. T. 1998. Ettringite solubility and geochemistry of the $\text{Ca}(\text{OH})_2\text{-Al}_2(\text{SO}_4)_3\text{-H}_2\text{O}$ system at 1 atm pressure and 298 K. *Chemical Geology*,148, 1-19.
62. Nakamoto, K.. Infrared and Raman spectra of inorganic and coordination compounds, Part A: Theory and application in inorganic chemistry. 1997. 5th edition, John Wiley and Sons Inc., New York.
63. Nordstrom, D.K and Alpers, C.N. 1999. Geochemistry of acid mine waters. In: The environmental geochemistry of mineral deposits part A: processes, techniques and health issues, Plumlee, G.S and Logsdon M.J. (Eds), *Reviews in Economic Geology Vol 6A*,133-160, SEG Inc, Michigan.
64. Nordstrom, D.K., L.N. Plumber, D. Langmuir, E. Busenberg, and H. M. May. 1990. Revised chemical equilibrium data for major water-mineral reactions and their limitations.

In chemical modeling of aqueous systems II, ed D.C. Melchior and R.L. Basset. Am. Chem. Soc. Ser. 416, pp. 398-413. Washington, DC: Am. Chem. Soc.

Nordstrom, S.K. 1982. The effect of sulfate on aluminum concentrations in natural waters: Some stability relations in the system $\text{Al}_2\text{O}_3\text{-SO}_3\text{-H}_2\text{O}$ at 298°K. *Cosmochim Acta* 46: 681-692

65. Olhero S M and Ferreira J M. 2004. Influence of particle size distribution on rheology and particle packing of silica-based suspensions. *Powder Technology* 139. 69 – 75.

66. Parkhurst, D.L. 1995. User's guide to PHREEQC-A computer program for speciation, Reaction-Path, Advective-Transport, and Inverse Geochemical calculations. U.S. Geological Survey water-Resources Investigations Report 95-4227.

67. Petrik L., White R., Klink M., Somerset V., Burgers C., Fey M.V. 2004. Utilization of fly ash for acid mine drainage remediation. Water Research Commission final report K5/1242.

68. Petrik L., Burgers C., Gitari W., Surender, D., Reynolds K., Ellendt A., Etchebers O., Vadapalli R., Key D., Iwuoha E. 2005. Stability and neutralization capacity of potential mine backfill material formed by neutralisation of fly ash and acid mine drainage. Water Research Commission final report K5/1458.

69. Ramos, L., L.M. Hernandez and M.J. Gonzalez. 1994. Sequential fractionation of copper, lead, cadmium and zinc in soils from or near Dona National Park. *J. Environ. Qual.* 23: 50-57.

70. Ribet, I., C.J. Ptacek., D.W. Blowes and J.L. Jambor. 1995. The potential for metal release by reductive dissolution of weathered mine tailings. *Journal of contaminant hydrology* 17, 239-273.

71. Rimstidt, J.D., and H.L. Barnes. 1980. The kinetics of silica water reactions. *Geochim. Cosmochim. Acta.* 44: 1683-99.
72. Roy, W. R., and Griffin, A. Robert. 1984. Illinois Basin Coal Fly Ashes. 2. Equilibria Relationships and Qualitative Modeling of Ash-Water reactions. *Environ. Sci. Technol.*, Vol. 18, No, 10.
73. Scheetz B.E. and White W.B. 1985. Characterization of crystalline phases in fly ash by microfocus Raman spectroscopy. *Proceedings of the Materials Research Society Symposium, Boston, USA, 43, 53-60.*
74. Schwertmann, U., Schulze, D.G., Murad, E., 1982. Identification of ferrihydrite in soils by dissolution kinetics, differential X-ray diffraction, and Mossbauer Spectroscopy. *Soil Sci. Soc. Am. J.* 46, 869-875.
75. Schwertmann, U and Taylor, R.M. 1989. Iron oxides. In: Dixon JB, Weed SB (eds) *Minerals in soil environments*, 2nd edn. Society of America (SSSA Book Series nr. 1) Soil Science, Madison, WI pp 370-438.
76. Seoane, S and Leiros, C. M. 2001. Acidification-Neutralization processes in a lignite Mine Spoil Amended with Fly Ash or Limestone. *J. Environ. Qual.* 30: 1420-1431.
77. Seth. R, Ghazi, A.M., 1997. Release of sorbed sulfate from iron oxy hydroxides precipitated from acid drainage associated with coal mining. *Environ. Sci. Technol*, 31. 2136-2140.
78. Sherman Hsu, C.P. 1997. Infrared Spectroscopy. In: *Handbook of instrumental techniques for analytical chemistry*, F.A Settle (Ed), Prentice-Hall Inc., New Jersey, Chapter 15, 247-283.

79. Shokarev, M. M., E.V. Margulis, F.I. Vershinina, L.I. Beisekeeva, and L.A. Savchenko. 1972. Infrared spectra of iron (III) hydroxide sulphates and hydroxides. *Russ. J. Inorg. Chem.* 17: 1293-1296.
80. Slatter P.T. 1999. The role of rheology in the pipelining of mineral slurries, *Min. Pro. Ext. Met. Rev.*, 20, 281-300.
81. Slatter P.T. and Chhabra R.P. 2003. The flow of non-Newtonian slurries and sludges. Course notes, Cape Technikon.
82. Soma Y. and Soma M. 1985. Raman spectroscopic analysis of coal fly ash particles. *Kokoritsu Kogai Kenkyusho Kenkyu Hokoku*, 79, 133-143.
83. Sullivan P.J., Yelton, J.L. and Reddy K.J. 1988. Solubility relationships of aluminum and iron minerals associated with acid mine drainage. *Environmental Geology and Water Sciences* 11, 283-287.
84. Sutter. B; J.B. Dalton; S.A. Ewing; R. Amundson, and C.P. McKay. 2005. Infrared spectroscopic analyses of sulfate, nitrate, and carbonate-bearing atacama desert soils: analogs for the interpretation of infrared spectra from the martian surface. *Lunar and Planetary Science XXXVI*.
85. Taylor, H.F.W. 1997. *Cement Chemistry 2rd Edition*. Thomas Telford, London.
86. Taylor, H.F.W. 1998. *Cement Chemistry 2rd Edition*. Thomas Telford, London.
87. Tessier, A., Campell, P.G.C. and Bison, M. 1979. Sequential extraction procedure for the speciation of particulate trace metals. *Anal. Chem.* 51: 844-850.
88. Tessier, A., F. Rapin, and R. Carigan. 1985. Trace metals in oxic lake sediments: possible adsorption onto iron (oxy) hydroxides. *Geochim. Cosmochim ACTA.* 49: 183-194.

89. Tseng W J and Lin K-C. 2003. Rheology and colloidal structure of aqueous TiO₂ nanoparticle suspensions. *Material Science and Engineering*. A355. 186 – 192.
90. USEPA (United States Environmental Protection Agency). The Class V underground injection control study: mining, sand, or other backfill wells. Office of Ground Water and Drinking Water, 1999, 10, 74 p.
91. Von Willert, J. Frank and Stehouwer C. Richard. 2003. Compost, limestone, and gypsum effects on calcium and aluminum transport in acidic mine spoil. *Soil Sci. Soc. Am. J.* 67: 778-786.
92. Warren C. J and Dudas M.J.1985. Formation of Secondary minerals in artificially weathered fly ash. *Journal of Environmental quality.*, vol 14, no 3.
93. Warren, C.J., and M.J. Dudas. 1984. Weathering processes in relation to leachate properties of alkaline fly ash. *J. Environ. Qual.* 13: 530-538.
94. Wolt J.D., N.V. Hue., and R.L. Fox. 1992. Solution Sulfate chemistry in three sulfur-retentive hydrandeps. *Soil Sci. Soc. Am. J.* 56: 89-95.
95. Yong, R.N., Yaacob, W.Z.W., Bentley, S.P., Harris, C and Tan, B.K. 2001. Partitioning of heavy metals on soil samples from column tests. *Engineering geology*. Vol 60, pp 307-3222.
96. Yu, P., Kirkpatrick, R.J., Poe, B., McMillan, P.F. and Cong, X. **1999**. Structure of Calcium Silicate Hydrate (C-S-H): Near-, Mid-, and Far-Infrared Spectroscopy. *Journal of American Ceramic Society*, 82(3), 742-748.
97. Zachara, J.M., Cowan, C.E. and Resch, C.T. 1991. Sorption of divalent metals on calcite. *Geochim. Cosmochim. Acta* 55, 1549-1562.

Appendix A. Revised WRC deliverables compared to Coaltech2020 and original WRC deliverables

Coaltech Deliverables	WRC Deliverables	Revised WRC Deliverables
<p>Optimise large scale process parameters: Perform an engineering study of the requirements for large scale utilisation of fly ash as an ameliorant for acid mine drainage. Treat acid mine drainage on a large scale and recover water in order to neutralise acid water and replace current expensive treatment plants. Due Date: 01/03/2005 Total cost: R200 000</p>	<p>Preliminary planning and consultation: Preliminary planning and consultation for large scale studies including, neutralisation, ash walling, ash lining, water recovery, irrigation, mineralogical studies 2005/5/31 R 200 000</p>	<p>Preliminary planning and consultation: Preliminary planning and consultation for large scale studies including, neutralisation, ash walling, ash lining, water recovery, irrigation, mineralogical studies 2005/5/31 R200 000</p>
<p>Process variables and assessment of requirements for successful underground placement: Place and monitor at pilot scale the solid residues derived from the full scale neutralisation process as chemically stable backfill material in order to prevent subsidence of mined out areas. Due Date: 31/06/2005 Total cost: R200 000</p>	<p>Evaluation: Evaluation of progress, planning for next year, report writing, integration of research findings, scoping for implementation 2006/01/31 R 50 000</p>	<p>Historical ash placement studies: Negotiate access and determine the mineralogical and other environmental impacts and changes associated with historical placements of ash previously used as fill materials 2005/05/31 R50 000</p>
<p>Assess suitability of neutralisation solid residues as backfill material and necessary requirements for long term stability: Determine solid residues' overall suitability for extending the life of coal mines and increasing the amount of extractable coal from each mine. Due Date: 30/09/2005 Total cost: R200 000</p>	<p>Placement of co-disposed residues: Perform a pilot scale placement of co-disposed residues either as fill material or as soil ameliorant and compare the fill material characteristics with ash and/or with additional hardening agents. 2006/03/31 R150 000</p>	<p>Logistical studies: Determine logistical parameters for application of fly ash as ameliorant for treatment of acid mine drainage 2005/06/31 R50 000</p>
<p>Assess suitability of using fly ash as a walling material at a large scale: Control surface acid mine drainage by employment of fly ash as ash walls within coal mine spoil heaps. Due Date: 31/01/2006</p>	<p>Environmental impact assessment: Perform an environmental impact assessment of large scale utilisation of ash for remediation of acid mine drainage.</p>	<p>Engineering study of requirements for full scale co-disposal: Perform an engineering study of the requirements for large scale co-disposal utilizing flyash as treatment for acid mine drainage</p>

Total cost: R200 000	2006/06/30 R150 000	2005/08/30 R100 000
Assess suitability of recovered water for agricultural irrigation: Determine whether water recovered from the large scale co-disposal process is suitable for agricultural irrigation. Due Date: 30/03/2006 Total cost: R200 000	Ash utilisation as liner for containment areas: Development of adequate assessment tools for utilisation of ash liner for containments areas for storage of mine spoils that may leach acidic water 2066/06/30 R100 000	Long term monitoring of on site backfill placements: Establish requirements of long term monitoring of on site pilot scale backfill placements using co-disposed residues derived from the neutralization of acid mine drainage with fly ash 2005/09/30 R50 000
Assess suitability of ash as a liner for spoil heaps to contain seepage of acid mine drainage: Perform a larger scale study of ash used as a spoils containment liner to prevent acid mine drainage seepage from spoil heaps. Due Date: 30/06/2006 Total cost: R50 000	Recovery of water: Recover water from the co-disposal process and perform smaller scale testing for application as irrigation water. 2006/06/30 R50 000	Technoeconomic study: Perform a technoeconomic study of the Co-disposal process for treatment of acid mine drainage as replacement for current limestone treatment options 2005/12/31 R100 000
Assess the potential benefits or problems of ash placement underground: Perform a mineralogical study of historical ash placements underground in order to understand the long term behaviour of fly ash underground. Due Date: 31/09/2006 Total cost: R150 000	Treatment of acid mine drainage: Full scale treatment of acid mine drainage and comparative study with liming process currently utilised. 2006/12/31 R150 000	Large scale ashwalling study: Place a ashwall on site in coal mine spoil at larger scale and monitor its performance as an in-situ barrier for passive treatment of acid mine drainage flows 2005/12/31 R100 000
Final report: Large scale utilization of coal-fired power station fly ash in order to prevent the continued growth of unsightly and environmentally damaging fly ash dumps and ash dams. Due Date: 31/12/2006 Total cost: R65 400	Final report: Drafting of final report 2006/03/31 R50 000	Final report: Drafting of final report 2007/03/31 R50 000

Appendix B. Academic and Industrial Interactions

Preliminary meetings

Several preliminary meetings were held to determine the feasibility of utilizing the current limestone treatment plants and facilities for implementing the neutralization of AMD with ash. These included:

09/11/2004: D. Surender (ESKOM) and O. Etchebers (UWC) Visit to Navigation plant Limestone treatment plant active since 1996, using lime (CaO) & limestone (CaCO₃) mixed since 2001 and limestone only since 2003. Amount of water treated: 8 ML/day at Navigation and 14 ML/day at Kromdraai.

03/12/2004: D. Surender (ESKOM) and O. Etchebers (UWC) met with Dr. J. Maree from CSIR. Presentation of pilot plant project: FA treatment of AMD (alkalinity of FA, acidity of AMD, time of reaction, properties of process water, volumes and flows). In comparison to limestone treatment plant requirements may need adaptation as there is a larger amount of FA than limestone and a clarifier may not be required with FA, because of better settling rates. J. Maree visited a mine in Germany where they treat AMD with FA.

03/12/2004: D. Surender (ESKOM) and O. Etchebers (UWC) met with Dr. H. Ilgner from CSIR

- Backfilling is already applied in gold mines, at depth, with FA or tailings. Often it is blended with 6 % cement.
- It is important to minimise water and binder in the matrix. Yet, the slurry must flow. Tests must be run to compare pumpability and flowability vs. the amount of water in the slurry.
- Marsh cone tests will help to determine what slurry is pumpable, and what slurry can flow between boreholes when backfilling.
- Chemistry can also affect flowability. It is important to check the effects of the amount of cement, lime, etc.
- FA applied underground, around coal pillars, gives quite a good strength. Even if the pillars are crushed, they are thus stabilised and do not expand. FA adds pozzolanic effect, but not enough for underground filling. Cement is needed.
- Consideration is necessary of adding the binder just before putting the material into the borehole, so that the slurry remains flowable between the plant and the backfill site. It is necessary to optimise the composition and amount of binder.
- The amount of water also affects the strength of the material. Lime can also add strength. It has already been applied before with different kind of limes.
- Results of strength testing: a 0.8 MPa unconfined compressive strength would be sufficient for the envisaged application as this project aims to operate in confinement and open cast mining. For open cast mining, 0.5 MPa could be enough.
- Most important is the permeability of the backfill material. Legislation will not accept a permeable material. Permeability is enhanced by adding cement: to be tested. Conduct long-term permeability tests.
- In this case, making a paste is not the point. Paste is made at the top of a borehole and gravitationally placed underground. For this study it would add costs (thickeners to be added to the material, etc)
- When presenting the project to DWAF for permission to continue, it is necessary to highlight that this is a pilot test made in an already highly contaminated area.

Meetings at project start up

After several telephonic discussions with P. Gunther about the matter of setting up the pilot plant at Anglo, the following meetings were held

29/03/2005: L. Petrik (UWC), and Eskom representatives including D. Surender met with DWAF. Presentation by Leslie Petrik: Ash utilization for co-disposal and backfill. Discussion about licensing requirements

22/04/2005: L. Petrik and R. Vadapalli (UWC) met P. Gunther and F. Nkosi (Anglo) at Landau colliery

- Peter Gunther discussed the cost of the fly ash pilot plant and Anglo's responsibilities.
- L. Petrik explained the advantages of fly ash system over the limestone plant and detailed different designs of ash lining in pyrite mine spoil to control AMD generation. Mr Gunther undertook to pursue the matter of setting up the pilot plant at Anglo with his company and the authorities.
- Inspected the liming and sulphate reduction plant with Patrick Hlabela (CSIR) in order that the fly ash pilot plant could be designed in a similar way. The limestone treatment plant treats both mine water and toe seep water. The equipment that was used for pilot scale biological treatment plant that was decommissioned at Anglo was investigated to determine the possibility of using the equipment for components of the pilot plant. Further enquiry revealed that this equipment is already earmarked for other applications.
- A silo, with a volume of 105m³ and a screw feeder is available at Landau for use in the pilot plant. It has not been determined whether the silo is in working condition.

10/06/05: R. Vadapalli (UWC) met with Dr. J. Maree (CSIR) at CSIR

- Met initially with an engineer, Jacobs Clifford of Steel Utilities at CSIR.
- Briefed Mr Clifford about possible plant designs with and without a slurry mixing tank as per sketch plan by M. Ndaba (UWC).
- Discussed the options concerning a cemented slab vs. a settling tank.
- Discussed the importance of the design of the impeller and requested suggestions.
- Formulated design parameters for the 2 designs.
- Dr Maree suggested that the design without a slurry tank is feasible for our study.
- Requested 3 estimated quotes from Mr Clifford for a fly ash treatment pilot plant at Navigation treating different amounts of toeseep water, i.e. 24 000, 120 000 and 1 000 000 L per day. Size of pilot plant to be finalised.

Meetings for the cost analysis

Meeting with Jannie Maree (CSIR)

Ravi Vadapalli of UWC and Damini Surender of Eskom met Jannie Maree of CSIR to finalize the cost analysis based on the alkalinity experiments that were made at UWC (16/09/2005):

- Ravi Vadapalli explained to Jannie Maree how the alkalinity experiments of Hendrina, Arnot and Kriel FA and Navigation limestone were made.
- Ravi Vadapalli and Damini Surender reminded Jannie Maree that when making the cost analysis of limestone, cost of additives such as flocculants should be added.

- Based on the results, three separate cost entities were calculated and compared between limestone and different fly ash types:
 - II. Cost incurred to reach a pH of 7
 - III. Cost incurred to reach a pH of 10 or higher
 - IV. Cost incurred to reduce the sulphate concentrations to as low as 500 mg/L.
- Three options were given for the treatment process:
 - I. Use of limestone for the primary AMD treatment and sulphate reduction
 - II. Use of limestone for primary AMD treatment and use of FA for the sulphate reduction
 - III. Use of FA for both primary AMD treatment and sulphate reduction.
- Although option II looks to be economically viable, it was thought that it is not practically feasible and hence the total cost for option I and option II was compared. It was noticed that option III (FA treatment for both primary and sulphate reduction processes) is 0.38 R/m³ cheaper when compared to option I treatment process.
- It has been thought that if one can make use of returning trucks or train(s) which carry coal to the power stations and fill them with FA on their way back to the mines, this could greatly bring down the cost of the transportation of FA and thereby reduce the cost involved in the FA treatment process.

Meeting with Peter Gunther (Anglo)

Leslie Petrik of UWC and Damini Surender of Eskom met Peter Günther of Anglo to discuss the alkalinity experiments (19/10/2005):

- Leslie Petrik explained to Peter Günther about the alkalinity experiments and results achieved.
- Suggestions were made to firstly reduce the SO₄²⁻ concentrations to 2g/L using FA or CaCO₃ and then treat the water again to bring down the SO₄²⁻ concentrations to as low as 0.5g/L using lime and biological treatment or FA.
- Peter Günther suggested assessing the amount of sludge that will be produced in each case and compare with H.D.S. process.
- It was thought that to achieve the desired SO₄²⁻ concentrations more flocculants are needed for limestone treatment and higher amounts of neutralising agents are needed for FA treatment.
- Peter Günther wanted a document showing all the benefits of FA treatment along with a table that explained costs of SO₄²⁻, Fe, Mn removal for both FA and CaCO₃ in R/kg.
- Peter Günther also wanted a flow diagram of the plant design to be included in the document.
- Peter Günther suggested using a hopper with daily loads (and a conveyer/screw feeder to the mixing tank) instead of going straight from the ash tank to the mixing tank.

Meeting with Francis Nkosi (Anglo)

Olivier Etchebers of UWC and Damini Surender of Eskom met with Francis Nkosi of Anglo to fully understand the limestone treatment process (01/11/2005):

- Francis Nkosi showed the diagram of all the water dams, sources and treatment plants at Navigation.
- Schoongezicht water comes from old underground mining and Navigation water comes from old underground mining, different overflows and water from the top of the dumps.

- The pH of Schoongezicht AMD is 2.5. The sulphate concentration is approximately 2.5 g/L and acidity is around 0.55 g/L.
- Schoongezicht and Navigation waters are pumped to the 'acid dam', and from there to the Primary Liming Plant (PLP) where they are neutralised with limestone. The process water is pumped to the 'raw dam'.
- Toe seep water comes from the bottom of the dumps and it is the most contaminated water, with sulphate concentrations varying from 18 to 21g/L and acidity from 14 to 18 g/L.
- Toe seep water is pumped to the 'Toe Seep Plant' (TSP), where it is neutralised with limestone. The process water is pumped to the 'raw dam'. Some water from the 'raw dam' is pumped to the 'Sulphate Reduction Plant' (SRP), where sulphate is removed by using a treatment combining lime and bacteria.
- Effluents from PLP, TSP and SRP are mixed in the raw dam, which allows lowering the saturation index.
- This mixture has sulphate concentrations of around 0.9 g/L, and is used in the 'Coal Processing Plant' (CPP).
- Toe seep water which has acidity of more than 16 g/L is not treated.
- In the PLP, mixing and aeration tanks work continuously, with a capacity of 250 m³/h and 45 minutes residence time. In the TSP also, mixing and aeration tanks work continuously with a capacity of 40 m³/h and 4 hours residence time.
- In the PLP three steps are involved:
 1. Mixing with an agitator, for homogenisation of the slurry, during a few minutes
 2. Aeration with an agitator, for oxidation and air inflow, during 45 minutes
 3. Settling with flocculants, for separation of solids and liquid, during 2 hours.
- Apart from the treatment process, Francis Nkosi explained the problems they have been encountering:
 1. The solubility of the residual sludge obtained from CaCO₃ treatment is high.
 2. Precipitation occurs in the raw dam so that it must be cleaned and purged once a year. This is proving to be very costly.
 3. Sulphate concentrations tend to increase with time in toe seep and Schoongezicht waters.

Meetings on the hydraulic transport of the slurry

Meeting with Flow Process Research Centre, CPUT-I

Leslie Petrik, Ravi Vadapalli, Olivier Etchebers, Wilson Gitari and Mzoli Ndaba of UWC met Paul Slatter of Cape Peninsula University of Technology to discuss about a possible collaboration to assess the requirements for transport and underground placement of FA and solid residues (20/09/2005):

- Leslie Petrik briefly explained the research activities of the Environmental Remediation Group.
- Leslie Petrik explained the objective of placing underground the solid residues derived from FA/AMD treatment, in the form of slurry. The transport of FA to the AMD reaction tank should also involve the making of slurry. Leslie Petrik emphasized the need for understanding the slurry properties before proceeding further and discussed the possibility of a collaborative study between UWC and Cape Peninsula University of Technology.

- Paul Slatter said that the slurry study using this kind of material (solid residues from FA/AMD) is not new to them and that he could remember doing similar kinds of experiments using FA.
- Paul Slatter said that they could perhaps use a rheometer for the study if the material is not fast settling. If the material settles fast, then they will need larger volumes of sample to test it in a piping loop.
- Paul Slatter also discussed about the distance that is required to transport the slurry. It was mentioned that it could vary from a few meters to a few kilometres, depending on the usage of solids.
- It was thought of designing a slurry testing loop on site, at Anglo.
- Leslie Petrik wanted Cape Peninsula University of Technology to be involved in the design of the pilot plant.
- It was orally accepted that UWC and Cape Peninsula University of Technology would become involved in a collaborative programme on these aspects.
- UWC had to formulate research questions and based on them Cape Peninsula University of Technology would make a project proposal and take it further from there.
- It was also thought to send somebody from UWC for the study.

Meeting with Flow Process Research Centre, CPUT-II

Ravi Vadapalli, Olivier Etchebers and Mzoli Ndaba of UWC met Dr. Rainer Haldenwang and Gervais Sery of Cape Peninsula University of Technology to discuss the slurry testing experiments (05/10/2005):

- Ravi Vadapalli briefly explained to Dr. Rainer Haldenwang the ongoing research at the Environmental Remediation Group and a possible collaboration with Cape Peninsula University of Technology.
- Ravi Vadapalli and Olivier Etchebers explained that they are looking at the properties of the slurry, which is made up of different combinations of FA and AMD with different ratios.
- Ravi Vadapalli and Olivier Etchebers also said that they are looking at FA slurry properties and would like to compare it with the solid residues.
- Gervais Sery mentioned that he would like to have an initial look at the samples so that they can decide whether to go for rheometry or piping loop tests.
- It was agreed that UWC will supply samples for the study as soon as possible.

Meeting with Flow Process Research Centre, CPUT-III

L.Petrik, Ravi Vadapalli and Olivier Etchebers met Prof. Paul Slatter, Dr. Rainer Haldenwang, Dr. Veruscha Fester and Mr. Gervais Sery of Cape Peninsula University of Technology (CPUT) in 2005. A further meeting to discuss requirements and further strengthening of the collaboration programme on hydraulic transport of the residual slurry was held on 12/12/2005 at which meeting:

- Ravi Vadapalli initiated the meeting by asking some questions regarding the first set of results that was given by CPUT.
- Gervais Sery explained the various technical points that are involved in the study.
- He mentioned that looking at the first set of results for the residual solids and tap water mixture, a 50% (w/w) mixture can be suitable for pumping. For the FA and tap

water mixture, a concentration up to 65% (w/w) can be required. At these ratios the solids settle slowly.

- Some thoughts were given on mixing the FA either with process water or with fresh water, and then add the slurry to the reaction tank for the neutralisation process. But, it was again thought that if FA slurry is made then it must be a continuous process, otherwise there is a possibility of settling in the slurry tank and there is no advantage in making FA slurry unless the neutralisation works better than using dry FA.
- It is also agreed that UWC will give CPUT a list of properties of FA that change during the time in order to assess their influence on rheology.
- The impeller design was highlighted as an important parameter. It was thought that using a turbulator has an advantage, as it can be coupled with an O₂ input device.
- It was agreed that CPUT will advise UWC on mixing FA and AMD in such way that it works out in an efficient way.
- It was also agreed by CPUT that, if necessary, they could bring the testing apparatus on site.
- There are two important issues that have to be kept in mind while making the slurry experiments and that will probably have an influence on the transport properties. They are: 1) the FA:AMD ratio and 2) the amount of overflow extracted and amount of water remaining in the underflow.
- It was agreed that CPUT would give a detailed project proposal by 20/01/2006

Meeting with Flow Process Research Centre, CPUT-IV

L.Petrik, Ravi Vadapalli and Olivier Etchebers met Prof. Paul Slatter, Dr. Rainer Haldenwang, Dr. Veruscha Fester and Mr. Gervais Sery of Cape Peninsula University of Technology (CPUT) in 2005. A further meeting to discuss requirements and further strengthening of the collaboration programme on hydraulic transport of the residual slurry was held on 12/12/2005 at which meeting:

Results obtained from the initial rheometer studies on the Fly Ash and Residual solids have been discussed. Some thoughts on the influence of the design of the impeller/turbulator on the neutralization capacity while mixing have been exchanged. It was agreed that CPUT will advise UWC on the impeller and tank design. CPUT was ready to bring the testing apparatus onsite to perform the large scale rheological studies and promised to give a detailed project proposal by the 20th January, 2006.

Large Scale Rheological Studies at Eskom (CR&D)

Ravi Vadapalli of ENS along with Veruscha Fester, Gervais Sery and Rainer of CPUT were at Eskom-Rosherville from 5th June, 2006 to 9th June, 2006 to carry out rheological studies of FA-AMD sludge. The equipment (BBTV) was transported from Cape Town to Eskom-Rosherville. Large volumes of sludge were prepared using the pilot scale mixing rig at Eskom. Unfortunately, due to unforeseen problems at Eskom and since the equipment was damaged during transport, the experiments were postponed. However, laboratory scale rheometer studies were carried out.

Meeting with Flow Process Research Centre, CPUT-V

L.Petrik, O.Etchebers and VRK.Vadapalli met with Prof.Paul Slatter, Dr.Rainer Haldenwang, Dr. Veruscha Fester and Mr. Gervais Sery of CPUT on 22nd of June, 2006 to discuss about the difficulties faced during the experimental trails at Eskom, Johannesburg. CPUT agreed to build new testing equipment and redo the tests again. Everybody in the meeting felt that design of the mixing tank has to be changed before going to the other set of experiments. CPUT will assist ENS in designing the mixing rig. Moreover, it was decided to look at the influence of particle size of the FA on the rheological properties of the FA-AMD slurry. It was decided to carry on these experiments at CPUT as soon as possible

Meetings for building a pilot scale neutralization plant at Middleburg mine

L.Petrik , VRK Vadapalli from UWC and D.Surender from Eskom met with bhpbilliton officials during Oct and again in Nov 2006 to discuss building a pilot scale active neutralization plant at Middleberg Mine. The response was positive.

L.Petrik, VRK.Vadapalli and Damini Surender of UWC met with officials including Vik Cogho on 6 Dec 2006 to finalize the issue of building a pilot scale plant at Middleberg mine. BHPBilliton has indicated that they are happy to assist in building the plant and asked UWC for a revised project proposal.

Appendix C. Budget capital project cost estimate

The main components of the Fly-ash Handling and Dosing system for 1 and 5 cubic meter/h neutralisation pilot plant are the following:

Item	Size/Capacity	
	1 m ³ /h	5 m ³ /h
Concrete slab with side-walls	15 x 5 m	15 x 10 m
Fly-ash storage silo for 5 day storage capacity	20 m ³	100 m ³
Screw feeder (MS) with variable speed motor	166 kg/h	830 kg/h
Feed water pump	1 m ³ /h	5 m ³ /h
Reaction tank (MS) for a six hour retention time	6 m ³	30 m ³
Reaction water transfer pump	1 m ³ /h	5 m ³ /h
Cyclone (MS)	-	-
Sedimentation /Clarifying tank (MS)	1 m dia	1.5 m dia
Slurry pump	250 ℓ/h	1250 ℓ/h
Clean water pump	750 ℓ/h	3750 ℓ/h

Project cost estimate

Stage 1

Item	Amount
Design Fees	R 55 000
Project management Fees	R 15 000
Detailed Drawings	R 25 000
TOTAL Stage 1 (Excl. VAT)	R 95 000

Stage 2

The **budget** capital project cost estimate, is as follows:

Item	Amount	
	1 m3/h	5 m3/h
<i>Mechanical</i>		
Silo	R 45 000	R 150 000
Screw Conveyor/Feeder	R 60 000	R 60 000
Reaction Tank	R 70 000	R 150 000
Mixer	R 30 000	R 40 000
Cyclone	R 60 000	R 60 000
Sedimentation tank	R 35 000	R 70 000
Sludge Pump (2 off)	R 15 000	R 25 000
Process water feed pump	R 20 000	R 25 000
Reaction water transfer pump	R 20 000	R 25 000
Final effluent pump	R 5 000	R 8 000
<i>Electrical</i>		
Switches and Controls	R 30 000	R 30 000
pH Meter (2 off)	R 10 000	R 10 000
Level controller	R 10 000	R 10 000
Density meter	R 30 000	R 30 000
Conductivity	R 10 000	R 10 000
In-line flow meter	R 15 000	R 15 000
Site lighting	R 10 000	R 10 000
<i>Civil</i>		
Earthworks and Construction of concrete slab	R 50 000	R 90 000
Pipe work & Automatic valves	R 50 000	R 60 000
Subtotal	R 575 000	R 878 000
Contingencies (15%)	R 86 250	R 131 700
Subtotal	R 661 250	R 1 009 700
P & G's (20%)	R 132 250	R 201 940
Subtotal	R 793 500	R 1 211 640
Commissioning	R 20 000	R 20 001
Total Stage 2 (Excl. VAT)	R 813 500	R 1 231 641

Item list

The main components of the Fly-ash Handling and Dosing system and neutralisation plant (1Mℓ/d) are the following:

Item	1 Mℓ/d (41.6 m ³ /h)
Concrete slab with side-walls	25 x 20 m
Fly-ash storage silo for 5 day storage capacity	816.7 m ³
Screw feeder (MS) with variable speed motor	6 806 kg/h
Feed water pump	41.6 m ³ /h
Reaction tank (MS) for a six hour retention time	249.6 m ³
Reaction water transfer pump	41.6 m ³ /h
Cyclone (MS)	-
Sedimentation /Clarifying tank (MS)	4 m dia
Slurry pump	10 400 ℓ/h
Clean water pump	31 200 ℓ/h
Fly-ash usage	6806 kg/h

Project cost estimate

Stage 1

Item	Amount
Design Fees	R 85 000
Project management Fees	R 35 000
Detailed Drawings	R 55 000
TOTAL Stage 1 (Excl. VAT)	R 175 000

Stage 2

The **budget** capital project cost estimate, is as follows:

Item	1 Mℓ/d
<i>Mechanical</i>	
Silo (4 x 200 m ³)	R 1 040 000
Screw Conveyor/Feeder (4 off)	R 240 000
Reaction Tank (2 x 125 m ³)	R 360 000
Mixer (2 off)	R 200 000
Cyclone (2 off)	R 180 000
Sedimentation tank	R 260 000
Sludge Pump (2 off)	R 40 000
Process water feed pump	R 33 000
Reaction water transfer pump	R 33 000
Final effluent pump	R 23 000
<i>Electrical</i>	
Switches and Controls	R 80 000
pH Meter (4 off)	R 20 000
Level controller (2 off)	R 20 000
Density meter (2 off)	R 60 000
Conductivity (2 off)	R 20 000
In-line flow meter	R 15 000
Site lighting	R 15 000
<i>Civil</i>	
Earthworks and Construction of concrete slab	R 200 000
Pipe work & Automatic valves	R 80 000
Subtotal	R 2 919 000
Contingencies (15%)	R 437 850
Subtotal	R 3 356 850
P & G's (20%)	R 671 370
Subtotal	R 4 028 220
Commissioning	R 35 000
Total Stage 2 (Excl. VAT)	R 4 063 220

Appendix D1. Cost analysis of lime, Limestone and Fly Ash treatments (Phase I)

Neutralisation of AMD and sulphate removal in 3 steps

	SRP	Lime	Limestone	Arnot FA	Hendrina FA	Kriel FA
CaCO ₃ content (%)		0	90.4	0	0	0
CaO content (%)		87	0	6.87	9.40	8.55
Alkalinity (% as CaCO ₃)		155	90	12.3	16.8	15.3
Material price (R/t)		770	170	55	55	55
<hr/>						
Step 1: raise pH to 7	Acidity of Navigation toe seep AMD (g/L as CaCO ₃)	15	15	15	15	15
	Target acidity (g/L as CaCO ₃)	0	0	0	0	0
	Dosage required (g/L)	9.7	16.6	121.7	89.4	98.2
	Flocculants cost (R/m ³)	0.03	0.03	0	0	0
	Cost for step 1 (R/m ³)	7.46	2.85	6.70	4.91	5.40
<hr/>						
Step 2: raise pH to 10 for removal of Mg, Mn and SO ₄ ²⁻ partially	Acidity of process water at pH 7 (g/L as CaCO ₃)	0		0	0	0
	Target alkalinity (g/L as CaCO ₃)	1.5		1.5	1.5	1.5
	Dosage required (g/L)	1.0		12.2	8.9	9.8
	Cost for step 2 (R/m ³)	0.74		0.67	0.49	0.54
<hr/>						
Step 3a: remove sulphate with FA	Dosage required (g/L)			40	40	40
	Cost for step 3a (R/m ³)			2.20	2.20	2.20
	Buthanol cost (R/m ³)	2.88				
Step 3b: remove sulphate with biological SRP	Urea cost (R/m ³)	0.13				
	H ₃ PO ₄ cost (R/m ³)	0.19				
	FeCl ₃ cost (R/m ³)	0.08				
	Na ₂ CO ₃ cost (R/m ³)	0.03				
	Flocculants cost (R/m ³)	0.15				
Cost for step 3b (R/m ³)	3.47					

Appendix D2. Utilisation of Fly Ash to Neutralize and Remediate Acid Mine Drainage at Navigation

Objectives

The objective of this study is to demonstrate the large scale feasibility of utilising power utility Fly Ash (FA) to neutralise and remediate Acid Mine Drainage (AMD) specifically the toe seep generated at Navigation Plant.

Background

Laboratory (1 L AMD) and larger studies (250 L AMD) have proved that by mixing FA with AMD to a pre-determined pH endpoint, FA simultaneously neutralises the AMD and reduces the sulphate, iron and metal load, resulting in an improved water quality. For more information please contact the authors for detailed reports.

Current practice

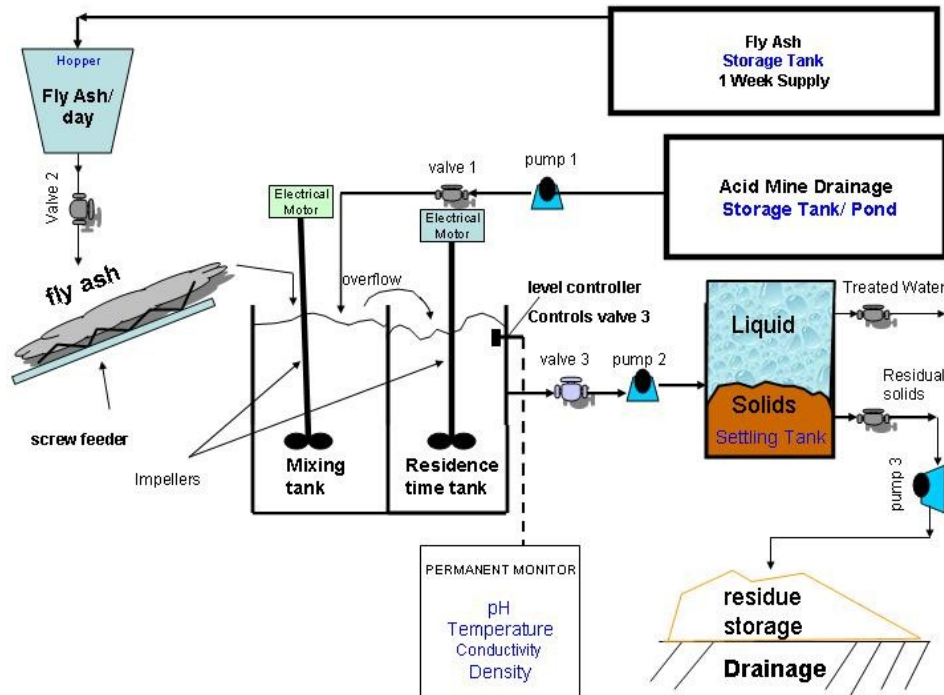
The current AMD treatment, using limestone as a neutralising agent, has several drawbacks.

- Limestone cannot be stored in a silo due to its high moisture content. It needs to be dosed in slurry form. It is abrasive and contains stones which cause blockage in pipes.
- In the primary liming plant (PLP), only neutralisation of AMD takes place at a cost of R 405 000 per annum (limestone cost only). Only a moderate sulphate removal is achieved (from 2 650 mg/L to 2 350 mg/L), without reduction of toxic elements content.
- The recovered water is separated from solids using flocculants, with a considerable expenditure: R 539 136 per annum for flocculants purchase.
- The sludge (“yellow boy”) that settles down after treatment is pumped to a discard dump. Storage costs R 2 724 400 per annum according to documentation provided by Anglocoal. The neutralised water needs to be further treated in the sulphate reduction plant (SRP), where sulphate concentration is reduced to 250 mg/L. A pre-treatment is required, using a costly agent: lime. The biological process of the SRP is energy and carbon feed (ethanol) consuming. It is very sensitive to temperature and pH fluctuations. As it may result in toxic H₂S releases, the redox reactions must be carefully controlled. The overall SRP costs R 5 757 500 per annum.
- The wastewater from the density medium separation plant (DMSP) is mixed with mine spoil, resulting in a highly acidic seepage with a sulphate concentration >16 000 mg/L. This effluent must be treated separately in the toe seep plant (TSP), adding further costs. After treatment in TSP, the water still has a sulphate concentration >3000 mg/L and is not suitable for industrial activities unless it is further treated with the biological SRP, introducing additional costs. Only after the treatment by the Biological plant that further reduces the saturation index of gypsum, is a suitable water for industrial purposes produced

Proposed design

The proposed design is based on treating 5 m³/h of Navigation toe seep AMD (highly contaminated effluent). FA is fed to the mixing tank on a continuous basis, either with the help of a screw conveyor or from a coal hopper. The residence time in the reaction tank is 4-6 hours. The FA settling rate is expected to be sufficiently high to allow for efficient separation of the solid and liquid phases by gravity.

Three different mixing tank sizes were considered (1 m³, 5 m³ and 2*125 m³). The surface area occupied by a 1m³ plant is 15 x 5 m; by a 5m³ plant is 15 x 10 m. In each case the surface area can be doubled to ensure sufficient capacity in terms of storage, delivery, etc. The energy input for impeller mixing is 37 152 kWhr per annum in the mixing tank and 164 160 kWhr per annum in the reaction tank. This is not expected to change if FA replaces limestone, unless the slurry take-up method is changed. The design below is a draft and the more detailed final design will be developed by Steel Utilities.



Volume of the mixing tank (m ³)	Volume of AMD treated (L/day)	Cost for the set up (R)
1	24 000	908 500
5	120 000	1 326 641
2*125	1 000 000	4 238 220

Cost comparison: limestone vs. fly ash for neutralisation of toe seep AMD

The current liming plants (PLP and TSP) do not result in water suitable for industrial applications because of high residual sulphate and toxic element content. After the PLP and TSP it is still necessary to implement the biological SRP for further removal of this residual sulphate and of toxic elements, whereas FA has proven to be an efficient material for neutralisation, sulphate precipitation and toxic element removal in one step, when used under the correct conditions, thus eliminating the need for the biological SRP step.

The treatment of toe seep AMD using limestone and FA was tested (Appendix D2-I) to obtain a circum neutral pH. The simulated scenario in Appendix D2-I does not include the additional costs of the biological SRP.

According to the current operational capacity of the TSP liming process - without considering additional costs of biological SRP, the figures presented in Appendix D2-I show that:

- In the case of FA a larger mass is used because of the lower alkaline material content of FA.

- This simulation used only enough FA to bring water to a comparable pH as could be achieved with limestone.
- A pH of about 7.5 is the maximum that can be attained using limestone, whereas FA can increase pH to higher levels as required, depending on the quantity used and the contact time, as was previously proven.
- The simulation study (Appendix D2-I) only achieved neutralisation of AMD after 6 hours for limestone. The restricted amount of FA used in this simulation allowed neutralisation in a similar or shorter time scale. The residual acidity and sulphate loads are still high in all cases at the pH attained.
- A limestone dosage of 25 kg/m³ (test 1) led to a similar decrease in acidity and sulphate load to FA used at higher dosages: 143 kg/m³ for Kriel FA (test 2), 250 kg/m³ for Hendrina and Arnot FA (tests 5 & 7).
- Kriel FA used at 250 kg/m³ (test 3) allowed for a more significant decrease in acidity and sulphate load, because of its higher alkalinity. Higher FA dosages or longer reaction times would achieve a complete neutralisation of AMD, but may not be applicable in the current plant as the limits of pumpability of the sludge may be reached, because of high solid contents.
- Kriel FA had the capacity to completely neutralise toe seep AMD, provided the reaction time was extended to over 20 h (test 10) without addition of more FA.
- Acidity (mg/L as CaCO₃) was reduced to 28 when using Kriel FA over 20h at a dosage of 143 kg/m³ of AMD (test 10) or to 3 740 at a dosage of 100 kg/m³ of AMD (test 8); with limestone the acidity was only reduced to 5120 mg/L as CaCO₃ (test 1). It shows that the FA treatment can be more efficient than limestone for reducing acidity load at an equivalent removal cost.
- The simulation shows that limestone is somewhat efficient as neutralising agent but does not achieve high sulphate removal from toe seep AMD. For a similar cost of about 0.6 R/kg SO₄ removed, Kriel FA was able to remove 9200 to 12200 mg/L of sulphate after over 20 hours, (tests 8, 9 & 10) while limestone only removed 7400 mg/L (test 1).
- The extension of the contact time to over 20 h allows a significant reduction of the amount of ash to be used. The test using 100 kg of Kriel FA per m³ of AMD (test 8) over 20h had a higher efficiency than that using 143 kg of Kriel FA per m³ of AMD (test 2) over 5 h.
- In the simulated study a reduction of about 40 % of the usual efficiency of neutralisation was observed in the case of limestone, compared to that currently obtained at the current Navigation TSP. This loss of efficiency is likely caused by the conditions applied in the simulated study.
- It is therefore expected that the results of the simulation given here using FA show a similar reduction in efficiency. Thus the FA neutralisation capacity can be expected to increase proportionately, and the corresponding cost reduced, when comparison is made in the current full scale TSP system.
- The sludge obtained after limestone treatment had to settle for 2 hours before the overflow could be extracted, while 1 hour was sufficient in the case of FA, indicating a quicker processing time.
- As FA sludge settles fast, it is expected that flocculants will not be necessary, whereas in the case of limestone these are routinely used.
- Limestone utilisation produced 10 kg of sludge per kg of material used, while with FA the sludge produced amounted to only 2.3 - 2.5 kg per kg of material used, since dewatering was more effective.

- The sludge obtained after limestone treatment only contained 12 % solids, while the FA sludge contained 42 – 45 % solids. Because of a better separation of phases after treatment with FA, a higher proportion of treated water could be recovered.
- Limestone needs to be mined, crushed and purchased at R 97.6 per ton, unlike FA. Eskom offers to supply free FA from Arnot, Hendrina or Kriel power station, where it is readily available in large quantities and in proximity to Navigation plant.
- Limestone needs to be transported for long distances at R 72.4 per ton. The transport cost for FA is estimated at R 55 per ton by truck. This transport cost was obtained for Arnot FA; it can be lowered if Hendrina or Kriel FA is used as distances are shorter. Alternative ways of transport, such as by train or by return after coal delivery, should be considered to reduce costs.
- The utilisation of FA for AMD treatment will reduce the costs associated with long term storage of FA (storage in large dumps, remediation of storage leachate). It would be a better use of ash than the potentially dubious use of ash dumps as a salt sink.

Other applications for fly ash

As Schoongezicht AMD is less contaminated than toe seep AMD, its treatment would require lower amounts of FA. Studies are in progress in order to compare Schoongezicht AMD neutralisation with limestone and FA. Other, less contaminated waters have already successfully been treated with ESKOM FA in various recently performed small pilot studies.

The current liming plants (PLP and TSP) do not result in water suitable for industrial applications after recovery, and an additional treatment (SRP) is required for sulphate removal after limestone based neutralization. This additional and costly treatment step could be eliminated by use of FA, with a longer contact time

The overall process using FA should provide water of good quality, which would become available for other applications. This water could be reintroduced in the industrial process or used for irrigation of agricultural fields in the region of the colliery.

The solid residues obtained from the process using FA could be used as a backfill option and provide an answer to the issue of preventing AMD generation.

- After neutralisation the solid residues recovered from the FA treatment option are available as fill in bulk on site, and thus no further purchasing or transport and importation of fill material would be required.
- The use of FA thus avoids the costly and hazardous long-term waste storage of the “yellow boy” sludge currently remaining after limestone treatment.
- Solid residues recovered from the FA treatment option are suitable fill materials, because of the following properties: durability, stability, development of strength over time, and are environmental benign.
- Solid residues have a good residual neutralising capacity and can be pumped in slurry or paste form as void fill material to mined out areas. This utilisation is expected to minimise the amount of AMD to be treated in the long term, by neutralising AMD at the site of formation and by preventing ingress of air.
- Solid residues utilisation as backfill material will add to the economic lifetime of mines, by allowing both a greater degree of extraction of coal and a geological and hydrological stabilisation of the worked out sites.

The solid residues can be transformed into zeolite adsorbents as shown by studies at UWC. Zeolites are excellent at removing toxic elements from water, representing another saving

opportunity by reducing the cost of maintenance and replacement of reverse osmosis or reverse electro dialysis systems by minimizing the salt and toxic load before the effluent stream enters these systems. Zeolites represent value added materials, and their manufacture from FA or solid residues and sale would represent a source of income.

Appendix D2-I: Comparison of limestone and fly ash neutralization treatments of toe seep AMD

NOTE: This cost comparison does not consider the additional costs of the biological SRP needed after limestone treatment

Test number		1	2	3	4	5	6	7	8	9	10
Toe seep water quality	pH	2.8	2.7	2.7	2.8	2.8	2.7	2.7	2.6	2.3	2.4
	Acidity (mg/L as CaCO ₃)	12 300	12 300	12 300	12 300	12 300	12 300	12 300	12 300	12 300	12 300
	Sulphate concentration (mg/L)	17 100	17 100	17 100	17 100	17 100	17 100	17 100	17 100	17 100	17 100
Neutralisation	Neutralising material	Limestone	Kriel FA	Kriel FA	Hendrina FA	Hendrina FA	Arnot FA	Arnot FA	Kriel FA	Kriel FA	Kriel FA
	Alkalinity (% as CaCO ₃)	98	18	18	13	13	13	13	18	18	18
	Reaction time (h)	6.0	4.7	4.7	6.0	6.0	5.0	5.0	23.0	22.2	21.0
Material usage (kg/m ³ of AMD)		25	143	250	143	250	143	250	100	125	143
Recovered water	pH	6.1	5.4	6.4	5.3	5.5	5.4	5.9	5.3	5.6	7.2
	Acidity (mg/L as CaCO ₃)	5 120	5 700	1 850	6 880	3 070	7 100	4 330	3739	1628	28
	Sulphate concentration (mg/L)	9 680	9 850	5 820	11 560	9 220	12 720	9 530	7890	5930	4850
Residual sludge	Settling time (h)	1.8	0.8	1.0	1.1	0.9	1.0	1.1	2.3	3.2	1.8
	Mass recovered (kg/kg material used)	10	2.5	2.5	2.4	2.3	2.5	2.4	3.1	3.3	2.3
	Solid content (%)	12	45	45	42	44	43	45	35	36	56
Costs	Neutralising material price (R/t)	97.60	0	0	0	0	0	0	0	0	0
	Flocculant cost (R/kg sludge)	0.0007	0	0	0	0	0	0	0	0	0
	Neutralisation cost (R/m ³ of AMD) excluding transport	2.62	0	0	0	0	0	0	0	0	0
	Transport cost (R/t)	72.40	55	55	55	55	55	55	55	55	55
	Neutralisation cost (R/m ³ of AMD) including transport	4.43	7.86	13.75	7.86	13.75	7.86	13.75	5.50	6.88	7.86
	Acidity removal cost (R/kg as CaCO ₃) including transport	0.62	1.19	1.32	1.45	1.49	1.51	1.73	0.64	0.64	0.64
	Sulphate removal cost (R/kg) including transport	0.60	1.08	1.22	1.42	1.50	1.79	1.82	0.60	0.62	0.64

Appendix E. Column leachate concentration for elements
(analyzed with drainage volume (mg/L) (n=4))

Table E1. Analytical results for fly ash solid core

FA core element	drainage 1		drainage 2		drainage3		drainage4		drainage 5		drainage6		drainage7		drainage8	
	ave	SD	ave	SD	ave	SD	ave	SD	ave	SD	ave	SD	ave	SD	ave	SD
B	7.0674	1.8557	0.8574	0.5558	0.7273	0.4591	1.6012	0.1714	2.7532	0.5029	3.9601	0.6362	5.6466	0.2170	5.8206	2.6734
Na	118.2698	9.7266	51.5786	1.2157	53.5169	0.3220	42.9099	1.3052	36.8938	0.9194	28.9214	0.8708	22.2097	0.2775	35.2795	13.0306
Mg	0.0494	0.0073	6.7123	6.6119	8.2259	1.9158	20.7984	11.2136	45.4523	25.9647	76.4975	43.1354	119.6805	36.6399	171.5821	35.1073
Al	0.0529	0.0210	0.1890		9.0892	0.0122	9.3289	0.0351	0.1851	0.0936	0.5992	0.3536	3.1191	2.9036	27.7867	27.2199
Si	0.3808	0.1141	2.7602	0.1090	4.5712	0.0049	3.6212	0.0217	2.4736	0.4284	2.3761	0.1310	2.6697	0.5362	1.5201	0.7229
K	33.8033	6.3454	22.3686	6.4599	24.6490	1.0385	29.3176	2.6001	35.0059	2.5130	32.5926	0.2978	29.8925	0.0032	34.3381	0.9028
Ca	791.0666	47.3456	461.9414	16.8327	450.6306	11.6440	454.0242	7.0622	560.3429	14.8058	611.2601	9.2169	578.2663	13.2110	561.4901	22.9370
V	0.0108	0.0017	0.0485	0.0196	0.1166	0.0119	0.1292	0.0005	0.0744	0.0662	0.0572	0.0559	0.0512	0.0501	0.1166	0.0593
Cr	1.5773	0.6567	2.6357	0.6507	2.1065	0.8260	1.5367	0.4767	0.5425	0.3227	0.5440		0.3750	0.0000	0.1740	
Mn	0.0017	0.0008	0.0370		0.0089	0.0075	0.0074	0.0046	2.2433	2.2330	7.6037	7.5584	15.8426	15.4205	19.7041	17.4608
Fe	1.9703	0.2235	1.2690	0.1387	1.7055	0.1020	2.0999	0.1580	1.3125	0.1451	13.9875	12.3649	55.5168	54.0827	27.3181	25.4650
Ni	0.0109	0.0003	0.0076	0.0006	0.0040		0.0092	0.0025	0.0318	0.0000	0.0241	0.0136	0.0712	0.0630	0.6700	0.0000
Co	0.0012	0.0001	0.0005	0.0000	0.0012	0.0003	0.0011	0.0002	0.0022	0.0008	0.0124	0.0109	0.0267	0.0252	0.0670	0.0641
Cu	0.0144	0.0005	0.0089	0.0055	0.0178	0.0066	0.0106	0.0035	0.0135	0.0010	0.0209	0.0021	0.0189	0.0041	1.4805	1.4450
Zn	0.0636	0.0044	0.0681	0.0022	0.0685	0.0052	0.0730	0.0049	0.0711	0.0073	0.0735	0.0171	0.1159	0.0450	1.1548	1.0644
As	0.0016	0.0005	0.0020		0.0014	0.0003	0.0026	0.0003	0.0021	0.0005	0.0020	0.0012	0.0017	0.0006	0.0215	0.0177
Se	0.7001	0.1726	0.4983	0.0273	0.5911	0.0298	0.5546	0.0051	0.4913	0.0357	0.4417	0.0316	0.3744	0.0770	0.4651	0.0920
Sr	38.4559	3.6289	34.3746	0.5153	35.6963	0.4203	34.7508	0.9017	34.9391	0.8984	33.8694	0.0101	30.9578	0.3562	28.7975	0.8088
Mo	1.7171	0.0945	1.9618	0.3797	1.8231	0.1795	1.3855	0.0386	0.8460	0.0305	0.4211	0.1695	0.2850	0.1543	0.3080	0.0659
Cd	0.0031	0.0002	0.0036	0.0006	0.0037	0.0001	0.0039	0.0013	0.0018	0.0002	0.0014	0.0004	0.0011	0.0000	0.0024	0.0007
Ba	0.1010	0.0546	0.0132	0.0042	0.0171	0.0022	0.0084	0.0047	0.0407	0.0364	0.0689	0.0206	0.1006	0.0258	0.0850	
Pb	0.0260	0.0156	0.0000	0.0000	0.0000		0.0010		0.0008	0.0001	0.0002	0.0000	0.0006	0.0002	0.2847	0.2787
SO4	2070.5000	226.0000	1478.7500	101.7500	1674.3900	10.9100	1446.0600	74.6400	1485.1150	132.4350	2042.8750	512.1250	2015.2400	102.2600	2610.1250	176.1250
Cl	33.2500	12.2500	12.2500	0.2500	19.3300	8.0200	138.3550	1.0450	239.5200	1.0100	331.2650	71.2350	268.6050	0.1450	256.5000	11.5000
NO3	271.0000	7.5000	ND	0.0000	74.5000	38.0000	113.5500	12.8500	75.1000	3.0000	63.6000	13.9000	28.1000	27.5000	70.6250	10.6250
PO4	ND		ND		ND		22.8500	1.3500	ND		ND		ND		14.3750	
alkalinity HCO3 (mg/L)	1479.6138	262.5000	297.4481	181.2500	137.2838	12.5000	75.5061	6.8750	50.3374	3.7500	38.1344	25.0000	74.7434		64.0658	
pH	12.0150	0.0150	10.0750	1.1950	9.1850	1.6150	9.1300	1.2200	8.6200	0.3600	6.6800	1.0800	6.2250	1.5150	6.5750	1.7550

Table E1 continued....

FA core element	drainage9		drainage10		drainage11		drainage 12		drainage13		drainage 14		drainage 15		drainage 16	
	ave	SD	ave	SD	ave	SD	ave	SD	ave	SD	ave	SD	ave	SD	ave	SD
B	12.860	1.131	17.735	2.090	15.411	12.527	18.664	3.300	24.175	0.996	26.194	0.479	15.387	0.867	12.048	9.996
Na	40.591	19.931	50.734	22.590	18.903	2.552	25.933	3.396	20.907	1.183	14.812	0.523	7.682	0.023	10.793	2.488
Mg	233.398	21.762	452.920	75.434	431.184	430.181	835.691	249.570	972.306	272.521	1222.741	191.172	993.974	80.504	1077.433	170.529
Al	5.943	5.595	5.172	4.953	0.091	0.057	18.109	15.968	34.012	22.227	77.968	46.807	83.347	52.136	290.826	
Si	3.587	1.797	1.038		1.249		2.979		2.570	0.518	6.231	1.128	6.718	1.247	5.051	4.489
K	30.257	3.363	20.523	10.037	22.463		11.505	1.138	22.487	0.012	21.308	0.902	4.300	2.849	BDL	
Ca	602.275	0.178	672.794	71.731	589.840		516.068	121.109	513.253	9.898	499.495	8.138	283.119	2.907	394.137	104.232
V	0.037	0.025	0.068	0.063	BDL		0.026	0.011	0.018	0.002	0.016		0.008	0.006	0.050	
Cr	0.130	0.050	0.000		BDL		BDL		BDL		BDL		BDL		BDL	
Mn	24.051	19.356	37.461	18.117	27.333	27.270	96.369	13.885	154.109	52.085	224.539	58.388	198.307	44.368	309.925	2.429
Fe	42.576	40.663	35.699	34.386	1.355	0.237	186.979	116.231	280.005	30.464	739.554	95.732	705.520	36.978	2378.258	909.831
Ni	2.095	2.016	0.277	0.250	0.088	0.048	0.382	0.112	0.384	0.088	0.727	0.180	0.654	0.149	1.717	0.151
Co	0.036	0.033	0.050	0.042	0.012	0.010	0.140	0.055	0.202	0.027	0.419	0.044	0.391	0.014	0.880	0.103
Cu	0.059	0.053	0.269	0.261	0.023	0.021	0.060	0.033	0.151	0.095	0.128	0.026	0.110	0.025	0.496	0.031
Zn	0.084	0.000	0.273	0.169	0.167	0.037	0.353	0.100	0.481	0.125	0.702	0.270	0.630	0.229	0.945	0.531
As	0.004	0.000	0.027	0.025	0.001	0.000	0.056	0.052	0.008	0.001	0.001	0.001	0.016	0.010	0.015	0.011
Se	0.254	0.073	0.234	0.081	0.190	0.076	0.145	0.008	0.294	0.012	0.098	0.015	0.181	0.007	0.241	0.203
Sr	27.584	2.437	26.118	2.376	10.687	10.557	23.246	2.148	20.966	0.446	20.286	1.221	12.515	0.727	21.434	2.021
Mo	0.299	0.029	0.303	0.013	0.107	0.101	0.061	0.040	0.023	0.013	0.065	0.040	0.030	0.015	0.082	0.027
Cd	0.002	0.001	0.003	0.001	0.001	0.000	0.003	0.000	0.003	0.001	0.007	0.002	0.011	0.000	0.011	0.007
Ba	0.089	0.054	0.101	0.007	0.154	0.058	0.354	0.280	0.101	0.004	BDL		BDL		BDL	
Pb		0.000	0.026	0.025	0.004	0.004	0.013	0.001	0.003	0.000	BDL		BDL		BDL	
SO4	2724.250	73.250	3113.125	161.875	5360.625	2569.375	4999.250	376.750	4194.500	189.500	9318.500	569.500	11357.500	57.500	15878.750	1103.750
Cl	343.000	37.000	173.750	7.500	119.375	25.625	85.750	18.250	ND		ND		ND		ND	
NO3	51.250	1.250	140.625	6.875	395.000	152.500	309.625	8.375	1328.500	332.500	410.000	0.000	368.000	31.000	453.750	21.250
PO4	ND		ND		ND		ND		ND		ND		ND		ND	
alkalinity HCO3 (mg/L)	91.523		112.878		45.761		ND		ND		ND		ND		ND	
pH	6.485	1.545	6.430	1.220	6.300	0.850	4.810	0.450	4.335	0.115	4.125	0.155	4.035	0.145	3.540	0.070

Table E2. Analytical results for solid residue core

SR core element	drainage 1		drainage 2		drainage 3		drainage 4		drainage 5		drainage 6		drainage 7		drainage 8	
	ave	SD														
B	1.990	0.092	2.004	0.097	2.012	0.073	2.116	0.007	2.475	0.106	3.630	0.092	5.647	0.128	17.477	0.067
Na	271.717	6.743	61.336	4.272	25.015	0.934	19.054	0.439	16.116	0.263	13.843	0.264	22.210	0.253	12.210	0.273
Mg	4.590	1.202	3.993	1.315	5.059	0.278	4.356	0.123	4.692	0.069	9.644	0.920	119.680	5.203	291.843	6.408
Al	0.782	0.070	8.921	0.010	9.059	0.170	4.872	2.125	0.787	0.075	0.838	0.030	3.119	0.357	0.825	0.031
Si	1.667	0.232	1.249	0.110	1.092	0.098	1.192	0.085	1.190	0.050	1.153	0.015	2.670	0.031	1.662	0.035
K	107.688	0.502	85.317	2.267	55.475	2.961	42.639	1.420	36.355	0.931	31.174	1.229	29.892	0.203	28.530	2.085
Ca	381.444	5.340	449.615	3.411	458.928	7.553	483.103	24.251	544.198	3.046	565.381	17.668	578.266	16.711	542.301	13.801
V	0.029	0.007	0.027	0.005	0.025	0.000	0.027	0.001	0.028	0.001	0.031	0.002	0.051	0.001	0.021	0.000
Cr	0.805	0.020	0.593	0.018	0.397	0.029	0.217	0.009	0.074	0.028	0.038	0.007	0.375	0.004	0.029	0.008
Mn	0.031	0.017	0.020	0.008	0.010	0.001	0.008	0.000	0.009	0.001	0.008	0.003	15.843	0.000	0.031	0.005
Fe	1.145	0.018	1.590	0.072	1.727	0.015	1.355	0.083	1.216	0.102	1.605	0.039	55.517	0.046	1.480	0.122
Ni	0.012	0.000	0.019	0.013	0.002	0.000	0.019	0.005	0.026	0.001	0.005	0.000	0.071	0.000	0.929	0.145
Co	0.001	0.000	0.001	0.000	0.001	0.000	0.001	0.000	0.001	0.000	0.001	0.000	0.027	0.000	0.001	0.000
Cu	0.023	0.003	0.008	0.001	0.009	0.002	0.014	0.002	0.018	0.005	0.028	0.001	0.019	0.006	0.019	0.002
Zn	0.086	0.004	0.149	0.103	0.058	0.002	0.055	0.003	0.067	0.002	0.059	0.007	0.116	0.004	0.160	0.029
As	0.003	0.001	0.002	0.001	0.002	0.001	0.001	0.000	0.002	0.000	0.002	0.001	0.002	0.000	0.003	0.000
Se	0.139	0.004	0.084	0.009	0.068	0.009	0.053	0.006	0.028	0.006	0.007	0.006	0.374	0.004	0.020	0.001
Sr	20.148	0.218	26.794	0.301	28.329	0.081	29.167	0.100	30.429	0.186	31.501	0.548	30.958	0.093	31.350	0.312
Mo	1.346	0.015	0.441	0.012	0.300	0.012	0.248	0.003	0.230	0.004	0.227	0.001	0.285	0.002	0.235	0.001
Cd	0.003	0.000	0.001	0.000	0.001	0.000	0.001	0.000	0.001	0.000	0.001	0.000	0.001	0.000	0.001	0.000
Ba	0.108	0.012	0.116	0.003	0.130	0.002	0.138	0.003	0.135	0.003	0.143	0.009	0.101	0.001	0.113	0.007
Pb	0.009	0.006	0.004	0.004	0.002	0.002	0.002	0.001	0.002	0.001	0.002	0.000	0.001	0.001	0.007	0.000
SO4	2040.500	18.500	1504.250	6.750	1486.645	37.685	1292.800	38.880	1323.000	54.130	1372.250	15.160	1766.810	37.030	5714.375	550.625
Cl	27.250	4.750	8.750	0.750	5.270	0.270	88.220	2.310	249.710	9.390	263.705	6.945	272.305	9.075	635.625	256.875
NO3	235.000	5.500	BDL		379.000	3.500	426.450	8.050	16.500	5.500	BDL		0.900		189.375	171.875
PO4	BDL		3.000		BDL		10.500	1.600	BDL		6.500		2.300		BDL	
alkalinity HCO3 (mg/L)	56.250	18.750	50.000	12.500	43.750	18.750	33.750	1.250	34.375	1.875	35.000		50.625	0.625	71.875	8.125
pH	8.325	0.095	8.065	0.475	8.030	0.490	8.055	0.285	8.025	0.235	8.240	0.420	8.090	0.410	8.225	0.105

Table E2: continued....

SR core	drainage 9		drainage 10		drainage 11		drainage 12		drainage 13		drainage 14		drainage15		drainage 16	
	ave	SD	ave	SD	ave	SD	ave	SD	ave	SD	ave	SD	ave	SD	ave	SD
B	28.686	0.555	38.571	2.239	31.172	12.223	28.586	1.341	17.238	0.996	13.961	0.151	5.486	0.080	9.336	4.927
Na	11.353	0.185	12.115	0.565	18.552	6.869	15.177	0.121	12.920	1.183	9.467	0.233	5.822	0.389	10.066	0.139
Mg	527.324	24.277	1501.890	27.164	1466.064	505.891	1654.894	0.862	1150.077	272.521	1025.209	54.105	791.299	10.620	1098.584	141.107
Al	0.277	0.029	0.225	0.021	0.044	0.018	0.274	0.250	0.113	22.227	0.102	0.039	0.277	0.127	44.630	44.353
Si	1.889	0.090	2.353	0.138	2.341	0.601	1.264	0.416	4.724	0.518	9.821	1.566	4.479	0.059	2.469	0.621
K	19.565	0.840	16.589	1.591	41.027	19.803	12.929	0.898	9.715	0.012	13.728	1.267	BDL		BDL	
Ca	483.466	8.436	531.054	45.101	239.315	78.538	326.920	7.431	437.173	9.898	427.489	4.663	265.704	39.516	365.297	7.177
V	0.019	0.000	0.017	0.003	0.028	0.025	0.026	0.001	0.021	0.002	0.004	0.001	0.024		0.011	
Cr	0.028	0.014	0.002	0.002	0.531		BDL		BDL		BDL		BDL		BDL	
Mn	0.245	0.217	4.450	1.955	78.019	7.176	374.150	21.324	439.348	52.085	380.505	2.590	232.735	2.105	341.700	23.593
Fe	1.717	0.278	1.211	0.144	3.611	1.433	494.170	70.009	1201.318	30.464	2122.404	131.316	1888.943	148.626	2687.094	804.525
Ni	0.132	0.031	0.012	0.000	0.092	0.073	0.287	0.039	0.340	0.088	0.592	0.079	0.641	0.146	1.760	0.112
Co	0.001	0.000	0.001	0.001	0.018	0.001	0.169	0.029	0.350	0.027	0.628	0.000	0.542	0.003	0.953	0.016
Cu	0.004	0.000	0.008	0.002	0.066	0.058	0.088	0.028	0.091	0.095	0.161	0.095	0.113	0.034	0.550	0.234
Zn	0.118	0.003	0.166	0.008	0.223	0.008	0.341	0.020	0.399	0.125	0.472	0.081	0.363	0.021	0.658	0.036
As	0.004	0.000	0.005	0.000	0.006	0.003	0.008	0.005	0.008	0.001	0.010		0.028	0.024	0.025	
Se	0.011	0.001	0.015	0.009	0.051	0.047	0.110	0.023	0.153	0.012	0.088	0.014	0.103	0.012	BDL	
Sr	27.853	0.312	26.260	0.158	22.720	8.338	29.357	0.310	26.158	0.446	25.579	0.076	14.649	0.476	20.222	0.565
Mo	0.219	0.001	0.178	0.008	0.088	0.052	0.001	0.000	0.004	0.013	0.010	0.001	0.010	0.002	0.063	0.027
Cd	0.001	0.000	0.001	0.000	0.001	0.000	0.001	0.001	0.002	0.001	0.002	0.000	0.003	0.001	0.009	0.006
Ba	0.120	0.031	0.018		0.059	0.035	0.122	0.044	0.090	0.004	BDL		BDL		BDL	
Pb	BDL		0.001		0.005	0.004	0.008	0.002	0.001	0.000	0.000		BDL		BDL	
SO4	4084.500	118.500	5788.750	377.500	6929.375	166.875	9246.000	200.000	5711.000	156.000	12617.000	559.000	14549.000	120.000	14737.500	172.500
Cl	324.500	2.500	210.000	18.750	95.000	6.250	100.000	4.000	BDL		BDL		BDL		BDL	
NO3	5.000		55.000	1.250	210.000	3.750	292.000	24.000	1008.500	135.500	395.500	14.500	379.000	1.000	386.250	41.250
PO4	BDL		BDL		3.750		10.000	2.000	BDL		BDL		BDL		BDL	
alkalinity																
HCO3 (mg/L)	114.375	5.625	189.375	11.875	73.750	52.500	BDL		BDL		BDL		BDL		BDL	
pH	8.295	0.125	8.205	0.075	6.985	0.235	4.315	0.055	3.835	0.045	3.590	0.010	3.525	0.035	3.180	0.070

Table E3. Analytical results for solid residue (SR) + 5 % FA core

SR + 5 % FA element	drainage 1		drainage 2		drainage 3		drainage 4		drainage 5		drainage 6		drainage 7		Drainage 8	
	ave	SD	ave	SD	ave	SD	ave	SD								
B	3.361	0.078	3.189	0.064	2.795	0.073	2.739	0.094	2.689	1.161	3.476	0.388	5.647	0.066	10.974	0.231
Na	304.161	3.179	79.426	3.975	27.982	0.934	21.256	0.843	16.484	74.182	15.670	1.406	22.210	0.017	12.850	0.161
Mg	15.393	1.058	7.179	0.846	6.969	0.278	6.600	1.258	6.143	5.259	7.076	2.064	119.680	0.649	144.393	0.351
Al	0.790	0.182	9.046	0.018	9.266	0.170	0.521	0.085	0.494		0.728	0.053	3.119	0.032	0.709	0.050
Si	0.812	0.295	0.991	0.011	0.755	0.098	1.018	0.141	0.789	2.008	1.054	0.024	2.670	0.121	1.125	0.156
K	107.138	1.749	96.203	0.948	58.469	2.961	47.554	2.667	34.665	69.301	30.952	1.602	29.892	1.129	26.076	0.264
Ca	388.810	3.378	464.349	5.160	439.634	7.553	540.829	17.984	464.683	171.838	591.299	36.215	578.266	6.816	635.995	26.392
V	0.017	0.013	0.017	0.006	0.026	0.000	0.028	0.002	0.026	0.049	0.029	0.003	0.051	0.002	0.022	0.002
Cr	1.464	0.035	0.994	0.095	0.815	0.029	0.518	0.016	0.236	0.938	0.139	0.022	0.375	0.026	0.053	0.019
Mn	0.058	0.032	0.046	0.015	0.019	0.001	0.009	0.005	0.011		0.007	0.005	15.843	0.002	0.014	0.007
Fe	2.305	1.131	1.823	0.008	1.713	0.015	1.236	0.025	1.116	0.562	1.680	0.308	55.517	0.297	1.215	0.038
Ni	0.011	0.003	0.004	0.001	0.009	0.000	0.025	0.003	0.026		0.006	0.000	0.071	0.000	0.528	0.008
Co	0.001	0.000	0.001	0.000	0.001	0.000	0.001	0.000	0.001	0.000	0.001	0.000	0.027	0.000	0.001	0.000
Cu	0.014	0.004	0.009	0.002	0.013	0.002	0.015	0.001	0.016	0.007	0.033	0.002	0.019	0.002	0.006	0.002
Zn	0.110	0.019	0.067	0.003	0.057	0.002	0.056	0.002	0.059	0.026	0.068	0.008	0.116	0.004	0.079	0.002
As	0.003	0.002	0.002	0.001	0.001	0.001	0.002	0.001	0.002		0.002	0.001	0.002	0.000	0.002	0.000
Se	0.169	0.008	0.132	0.006	0.128	0.009	0.123	0.010	0.082	0.160	0.039	0.003	0.374	0.000	0.030	0.002
Sr	18.017	0.377	26.111	0.086	27.997	0.081	29.569	0.968	27.903	12.210	31.614	1.054	30.958	0.362	32.661	0.153
Mo	1.500	0.021	0.625	0.009	0.386	0.012	0.298	0.001	0.227	0.564	0.241	0.000	0.285	0.007	0.241	0.002
Cd	0.003	0.000	0.002	0.000	0.001	0.000	0.001	0.000	0.001	0.001	0.001	0.000	0.001	0.000	0.001	0.000
Ba	0.111	0.011	0.127	0.010	0.129	0.002	0.134	0.005	0.124	0.056	0.153	0.016	0.101	0.007	0.129	0.005
Pb	0.001	0.001	0.001	0.000	BDL	0.002	0.001	0.000	0.001		0.004	0.001	0.001	0.000	0.003	0.001
SO4	2222.750	24.750	1550.500	12.000	1538.810	54.590	1378.190	10.190	1346.300	24.000	1301.890	20.880	1552.930	16.950	15857.500	6270.000
Cl	27.000	2.000	10.250	0.250	5.890	1.710	96.205	5.115	245.175	6.065	254.870	5.280	284.065	7.845	388.125	58.125
NO3	229.250	0.750	BDL		386.250	2.750	438.400	14.600	23.550	1.850	BDL		BDL		381.875	
PO4	BDL		BDL		BDL		BDL		3.350		BDL		69.750	58.950	BDL	
alkalinity HCO3 (mg/L)	50.000		56.250	6.250	43.750	6.250	35.625	0.625	30.625	3.125	30.625	0.625	43.750	1.250	53.125	5.625
pH	7.275	0.025	7.050	0.090	7.830	0.880	7.610	0.250	7.875	0.205	7.480	0.050	7.550	0.100	7.950	0.210

Table E3: continued.....

SR + 5 % FA	drainage 9		drainage 10		drainage 11		Drainage 12		Drainage 13		Drainage 14		Drainage 15		Drainage 16	
	ave	SD	ave	SD	ave	SD	ave	SD	ave	SD	ave	SD	ave	SD	ave	SD
B	20.647	0.100	32.324	1.987	15.411	1.155	43.046	1.341	32.982	0.631	24.550	0.074	9.289	0.518	7.192	0.446
Na	12.826	0.644	15.002	0.579	18.903	0.451	13.979	0.121	15.804	0.745	10.712	0.596	5.825	0.181	9.974	0.340
Mg	313.999	11.119	924.756	135.504	431.184	6.300	1994.335	0.862	1762.116	53.468	1463.652	49.240	978.176	25.373	1137.902	56.550
Al	0.409	0.041	0.224	0.015	0.091	6.496	0.059	0.250	BDL		0.110		BDL		0.614	
Si	1.522	0.043	1.942	0.280	1.249	0.194	2.678	0.416	1.353	0.126	1.668	0.053	3.102	0.067	1.011	0.753
K	21.998	1.174	20.320	0.542	22.463	0.828	20.837	0.898	27.915	0.273	55.653	34.749	DBL		BDL	
Ca	510.931	15.778	627.034	56.918	589.840	8.283	334.336	7.431	473.059	25.363	448.258	4.053	259.013	5.545	336.750	22.808
V	0.019	0.001	0.019	0.001	BDL	0.000	0.005	0.001	0.023	0.004	0.034	0.025	0.007	0.001	0.046	
Cr	0.048	0.007	0.015	0.010	BDL		0.003		BDL		0.283		BDL		BDL	
Mn	0.017	0.002	0.179	0.124	27.333	1.393	45.809	21.324	172.512	50.756	288.603	58.868	253.880	9.391	376.629	15.440
Fe	1.899	0.145	1.116	0.230	1.355	0.100	2.086	70.009	97.122		485.790	260.041	686.660	94.167	1795.538	157.627
Ni	0.094	0.003	0.016	0.003	0.088	0.002	0.018	0.039	0.080	0.020	0.300	0.073	0.370	0.024	1.511	0.126
Co	0.001	0.000	0.001	0.000	0.012	0.000	0.012	0.029	0.058	0.028	0.229	0.084	0.330	0.005	0.896	0.027
Cu	0.003	0.002	0.017	0.003	0.023	0.001	0.014	0.028	0.060	0.001	0.070	0.002	0.058	0.009	0.429	0.078
Zn	0.098	0.005	0.154	0.003	0.167	0.004	0.255	0.020	0.309	0.047	0.227	0.022	0.197	0.016	0.438	0.104
As	0.003	0.000	0.005	0.001	0.001	0.000	0.005	0.005	0.007	0.001	0.007	0.004	0.010	0.004	0.017	0.006
Se	0.031	0.008	0.018	0.003	0.190	0.001	0.019	0.023	0.112	0.036	0.069	0.000	0.208	0.043	0.124	0.096
Sr	28.555	0.601	28.096	1.558	10.687	0.523	27.438	0.310	29.306	0.078	27.682	0.734	15.982	0.675	22.097	1.057
Mo	0.227	0.010	0.229	0.025	0.107	0.036	0.171	0.000	0.056	0.043	0.006	0.002	0.004	0.000	0.023	0.005
Cd	0.001	0.000	0.001	0.000	0.001	0.000	0.001	0.001	0.001	0.000	0.004	0.001	0.003	0.002	0.011	0.005
Ba	0.126	0.004	0.096	0.007	0.154	0.014	0.073	0.044	0.035	0.002	BDL		BDL		BDL	
Pb	0.001	BDL	0.003	0.001	0.004	0.001	0.001	0.002	0.003		BDL		BDL		BDL	
SO4	2878.000	66.000	3825.000	470.000	7966.875	809.375	7299.000	137.000	4876.000	349.000	10962.000	874.000	10974.000	0.000	14655.000	117.500
Cl	334.500	9.500	268.750	6.250	117.500	1.250	122.000	16.000	BDL		BDL		BDL		BDL	
NO3	BDL		26.875	14.375	220.000	160.000	203.000	83.000	960.500	319.500	365.000	38.000	257.000	0.000	338.750	58.750
PO4	BDL	3.750		4.375		15.000	3.000		BDL		BDL		BDL		BDL	
alkalinity																
HCO3 (mg/L)	76.875	4.375	144.375	25.625	250.000	41.250	221.250	48.750	91.250		BDL		BDL		BDL	
pH	8.250	0.210	8.060		8.230	0.020	7.745	0.295	6.170	0.690	4.655	0.255	4.185	0.085	3.560	0.170

Table E4. Analytical results for solid residue (SR) + 25 % FA core

SR + 25 % FA	drainage 1		drainage 2		drainage 3		drainage 4		drainage 5		drainage 6		drainage 7		drainage 8	
element	ave	SD	ave	SD	ave	SD	ave	SD	ave	SD	ave	SD	ave	SD	ave	SD
B	2.773		2.694	0.181	1.645	0.000	1.488	0.028	1.703	0.166	2.490	0.144	4.414	0.235	8.000	0.015
Na	188.078		171.811	2.505	40.015	2.936	28.240	1.451	20.952	1.136	17.777	0.303	15.159	1.070	15.137	0.423
Mg	2.820		0.765	0.072	1.304	0.352	7.473	5.176	7.080	3.635	19.733	9.467	56.932	15.585	109.510	14.829
Al	0.225		8.962	0.020	9.211	0.015	0.638	0.001	0.646	0.045	0.634	0.079	0.452	0.057	0.397	0.146
Si	1.022		3.252	0.033	2.743	0.215	2.909	0.116	2.461	0.091	2.326	0.187	2.079	0.398	2.003	0.281
K	104.179		121.904	6.647	61.752	2.899	51.360	2.626	40.106	2.427	30.108	0.130	28.002	2.341	27.134	0.012
Ca	206.070		441.530	5.139	436.508	15.481	551.874	10.251	585.420	12.411	564.714	21.879	583.043	25.532	542.170	13.003
V	0.004		0.138	0.009	0.119	0.005	0.121	0.002	0.107	0.001	0.099	0.006	0.070	0.018	0.041	0.037
Cr	1.102		2.944	0.089	2.315	0.077	1.947	0.043	1.187	0.044	0.596	0.019	0.352	0.106	0.352	
Mn	0.209		0.011	0.002	0.003	0.000	0.002	0.000	0.002	0.001	0.007	0.004	1.671	1.668	3.758	3.711
Fe	0.455		1.769	0.159	1.730	0.330	1.357	0.174	1.388	0.537	1.477	0.071	1.612	0.171	1.350	0.061
Ni	0.010		0.003	0.000	0.010	0.000	0.027	0.001	0.019	0.010	0.005	0.001	0.003	0.001	0.560	0.049
Co	0.001		0.001	0.000	0.001	0.000	0.001	0.000	0.001	0.000	0.001	0.000	0.001	0.000	0.003	0.003
Cu	0.054		0.017	0.007	0.012	0.001	0.015	0.000	0.016	0.000	0.024	0.010	0.004	0.000	0.006	0.002
Zn	0.075		0.072	0.000	0.057	0.003	0.066	0.005	0.064	0.001	0.059	0.000	0.058	0.004	0.332	0.239
As	0.001		0.003	0.001	0.002	0.000	0.002	0.000	0.002	0.000	0.002	0.000	0.002	0.001	0.002	0.000
Se	0.131		0.314	0.014	0.347	0.001	0.341	0.003	0.241	0.005	0.140	0.002	0.090	0.001	0.084	0.024
Sr	8.528		30.098	0.016	35.313	1.580	37.716	1.132	36.397	0.886	33.544	1.077	33.555	1.079	32.231	0.672
Mo	0.992		1.404	0.034	0.794	0.021	0.557	0.014	0.421	0.001	0.339	0.007	0.318	0.019	0.282	0.024
Cd	0.002		0.003	0.000	0.002	0.000	0.001	0.000	0.001	0.000	0.001	0.000	0.001	0.000	0.001	0.000
Ba	0.074		0.176	0.039	0.161	0.005	0.173	0.000	0.157	0.017	0.183	0.016	0.166	0.033	0.143	0.040
Pb	BDL		0.000	0.000	0.000	0.000	0.000	0.000	0.000	0.000	0.001	0.000	0.001	0.000	0.002	0.000
SO4	2472.000		909.000	864.500	1536.905	25.895	1363.455	14.115	1320.205	7.185	1398.990	41.280	1596.175	18.805	5647.250	1794.250
Cl	51.500		8.750	5.250	15.225	7.055	102.205	3.845	249.135	12.345	272.855	3.445	273.790	4.300	444.750	90.250
NO3	47.500		BDL		320.500		419.000	2.400	49.200	3.800	1308.500	1296.500	7.550	1.850	2.000	
PO4	BDL		BDL		BDL		4.800		BDL		2.550		5.000		BDL	
alkalinity HCO3 (mg/L)	NA		112.500	12.500	62.500		55.000	1.250	53.125	6.875	48.125	3.125	55.000		48.125	18.125
pH	8.060		8.490	0.110	8.495	0.115	8.560	0.040	8.845	0.035	8.545	0.125	8.545	0.215	7.955	0.505

Table E4: continued...

SR + 25 % FA	drainage 9		drainage 10		drainage 11		Drainage 12		drainage 13		drainage 14		drainage 15		drainage 16	
	ave	SD	ave	SD	ave	SD	ave	SD	ave	SD	ave	SD	ave	SD	ave	SD
B	14.507	0.927	26.110	3.401	29.214	8.638	39.840	1.581	32.420	0.365	31.296	2.082	12.147	1.184	10.910	2.341
Na	14.815	0.032	17.994	2.728	21.408	5.187	14.822	2.446	14.651	0.879	10.938	1.011	5.379	0.096	8.612	0.100
Mg	194.986	10.068	574.082	156.364	760.769	205.781	1401.220	134.799	1444.825	2.194	1548.809	110.759	1032.668	30.394	1186.640	22.290
Al	0.363	0.083	0.284	0.078	0.086	0.043	0.107	BDL	0.071	BDL	0.086	BDL	0.313	0.056	2.959	0.392
Si	1.836	0.069	1.415	0.161	1.473	0.489	1.379	1.111	9.700	8.124	3.316	0.423	1.329	0.105	1.538	
K	24.343	0.715	23.075	2.769	25.009	2.036	10.451	4.757	77.339	59.245	6.629	1.847	BDL	BDL	BDL	BDL
Ca	535.422	5.887	653.103	41.946	368.985	93.776	371.747	61.569	435.283	33.007	459.416	21.863	238.508	8.959	345.562	13.010
V	0.039	0.019	0.020	0.011	0.005	0.001	0.013	0.012	0.049	0.041	0.005	0.004	0.002	BDL	0.017	0.008
Cr	0.158	0.077	0.160	0.010	0.087		0.026	BDL	0.843	BDL	0.005	BDL	BDL	BDL	BDL	BDL
Mn	5.486	5.354	5.395	0.221	15.795	11.506	50.769	26.999	102.736	3.215	217.636	17.965	207.198	5.121	364.697	1.684
Fe	2.748	0.788	1.407	0.137	1.070	0.141	47.589	46.286	120.560	116.383	471.498	279.055	672.747	238.326	1888.486	208.529
Ni	0.048	0.014	0.014	0.000	0.024	0.006	0.052	0.037	0.146	0.044	0.382	0.094	0.437	0.049	1.447	0.018
Co	0.003	0.003	0.002	0.000	0.007	0.005	0.037	0.034	0.108	0.032	0.266	0.028	0.340	0.011	0.914	0.076
Cu	0.003	0.001	0.011	0.002	0.033	0.010	0.049	0.040	0.109	0.037	0.193	0.006	0.044	0.000	0.330	0.148
Zn	0.091	0.004	0.116	0.007	0.131	0.013	0.235	0.027	0.354	0.184	0.262	0.046	0.197	0.001	0.496	0.153
As	0.002	0.001	0.002	0.001	0.003	0.002	0.005	0.003	0.016	0.009	0.021	BDL	0.003	0.000	0.007	BDL
Se	0.093	0.017	0.099	0.012	0.077	0.034	0.163	0.068	0.100	0.003	0.059	0.028	0.131	0.026	0.177	0.082
Sr	28.907	0.215	29.475	0.681	22.397	2.119	23.387	1.677	23.144	2.238	26.473	1.045	14.883	0.722	22.409	1.302
Mo	0.251	0.015	0.264	0.021	0.207	0.054	0.096	0.073	0.083	0.051	0.060	0.053	0.003	0.001	0.011	0.004
Cd	0.001	0.000	0.001	0.000	0.001	0.000	0.001	0.000	0.002	0.002	0.001	0.000	0.002	0.000	0.008	0.002
Ba	0.134	0.012	0.126	0.009	0.091	0.012	0.074	0.007	BDL		BDL		BDL		BDL	
Pb	BDL		0.002	0.000	0.001	0.001	0.002	BDL	BDL		BDL		BDL		BDL	
SO4	2321.500	59.500	2871.250	510.000	3252.500	848.750	6223.000	177.000	4158.000	97.000	10793.500	272.500	12363.500	788.500	13815.000	82.500
Cl	324.500	14.500	274.375	30.625	113.750		98.000	2.000	BDL		BDL		BDL		BDL	
NO3	5.000		46.250	8.750	208.125	18.125	180.000	16.000	418.500	173.500	339.500	10.500	315.000	9.000	263.750	6.250
PO4	BDL		5.000		15.625	8.125	4.375		21.000	1.000	BDL		BDL		BDL	
alkalinity																
HCO3 (mg/L)	67.500	16.250	93.125	16.875	135.000	91.250	221.250		83.750		BDL		BDL		BDL	
pH	8.095	0.335	8.115	0.125	7.665	0.335	6.690	1.190	5.935	0.745	5.010	0.590	4.310	0.200	3.450	0.290

Table E5. Analytical results for solid residue (SR) + 40 % FA core

SR + 40 % FA element	drainage 2		drainage 3		drainage 4		drainage 5		drainage 6		drainage 7		drainage 8		drainage 9	
	ave	SD	ave	SD	ave	SD	ave	SD	ave	SD	ave	SD	ave	SD	ave	SD
B	0.909	0.050	0.681	0.015	0.684	0.026	0.861	0.008	1.301	0.003	2.190	0.006	4.481	0.193	9.385	0.680
Na	239.196	1.275	48.859	0.727	30.648	0.128	23.035	0.013	19.738	0.198	16.466	1.176	16.456	0.309	15.076	0.772
Mg	0.753	0.015	0.763	0.130	2.890	0.718	2.483	0.301	6.212	1.341	19.472	4.316	45.770	21.820	112.014	23.320
Al	8.865	0.035	9.241	0.026	0.582	0.093	0.671	0.022	0.782	0.027	0.627	0.123	0.670	0.063	0.476	0.014
Si	6.857	0.140	4.291	0.233	3.307	0.179	2.993	0.104	2.830	0.051	2.746	0.266	2.447	0.079	1.755	0.242
K	137.988	12.587	67.913	6.737	51.272	3.741	41.862	1.842	34.229	0.989	30.201	2.364	30.020	0.193	25.631	2.162
Ca	403.108	6.806	413.690	20.010	543.446	15.995	523.445	16.548	554.399	10.984	562.253	5.918	682.079	11.213	543.601	31.904
V	0.226	0.009	0.173	0.005	0.169	0.004	0.153	0.001	0.145	0.002	0.129	0.007	0.119	0.000	0.083	0.003
Cr	4.357	0.007	3.364	0.110	2.895	0.156	1.721	0.209	0.760	0.102	0.350	0.058	0.304	0.013	0.255	0.025
Mn	0.003	0.000	0.005		0.030	0.024	0.002	0.001	0.007	0.001	0.004	0.002	0.011	0.000	1.450	1.419
Fe	1.642	0.100	1.754	0.284	0.868	0.212	1.051	0.099	1.602	0.053	1.395	0.054	1.405	0.076	1.799	0.408
Ni	0.007		0.007	0.004	0.028	0.001	0.027	0.000	0.006	0.000	0.126	0.123	0.687	0.009	0.034	0.001
Co	0.001	0.000	0.001	0.000	0.001	0.000	0.001	0.000	0.001	0.000	0.001	0.000	0.001	0.000	0.001	0.000
Cu	0.013	0.004	0.011	0.001	0.008	0.000	0.014	0.001	0.028	0.003	0.006	0.001	0.010	0.002	0.002	0.001
Zn	0.077	0.002	0.057	0.004	0.052	0.005	0.060	0.006	0.060	0.004	0.048	0.000	0.077	0.005	0.065	0.009
As	0.006	0.001	0.003	0.000	0.002	0.000	0.003	0.000	0.002	0.000	0.002	0.000	0.003	0.000	0.003	0.000
Se	0.225	0.039	0.265	0.046	0.400	0.095	0.214	0.036	0.094	0.009	0.066	0.012	0.071	0.019	0.072	0.011
Sr	33.358	1.372	40.010	3.507	41.309	2.683	38.461	2.629	36.428	1.169	35.945	1.361	34.690	1.832	30.174	2.794
Mo	1.947	0.026	1.177	0.060	0.824	0.042	0.569	0.042	0.479	0.008	0.441	0.007	0.417	0.002	0.347	0.021
Cd	0.004	0.000	0.002	0.000	0.002	0.000	0.007	0.006	0.001	0.000	0.001	0.000	0.001	0.000	0.001	0.000
Ba	0.118	0.030	0.147	0.015	0.106	0.020	0.106	0.045	0.207	0.046	0.169	0.021	0.097	0.021	0.141	0.005
Pb	0.000	0.000	BDL		0.003	0.002	0.001	0.000	0.001	0.000	0.002	0.001	0.003	0.001	BDL	
SO4	1959.500	9.000	1546.915	32.665	1289.230	33.260	1264.270	47.180	1304.980	69.670	1487.520	14.570	1512.250	180.750	1931.000	99.000
Cl	22.000	2.500	8.425	2.845	98.560	9.450	253.230	5.260	258.925	3.925	294.340	9.810	108.750	0.750	307.500	11.500
NO3	BDL	158.500	22.500	333.850	5.050	45.600	17.100	6240.000	2212.500	24.000	12.200		BDL		25.000	15.000
PO4	BDL		BDL		3.800		3.800		BDL		22.350	6.150	2.500		BDL	
alkalinity HCO3 (mg/L)	256.250	43.750	75.000		46.875	1.875	56.250	2.500	51.875	0.625	51.875	1.875	56.250	2.500	66.875	3.125
pH	10.780	0.020	9.580	0.880	9.545	0.745	9.945	0.705	9.360	0.560	8.570	0.050	8.860	0.190	8.750	0.250

Table E5: continued.....

SR + 40 % FA element	drainage 10		drainage 11		drainage 12		drainage 13		drainage 14		drainage 15		drainage 16	
	ave	SD	ave	SD	ave	SD	ave	SD	ave	SD	ave	SD	ave	SD
B	22.1	1.7	26.1	0.9	30.5	3.7	34.9	1.0	36.4	0.9	21.3	1.8	21.7	2.6
Na	39.4	23.3	22.2	7.3	15.9	2.5	15.7	1.2	12.0	0.8	6.0	0.0	9.3	0.2
Mg	332.6	35.1	447.0	96.5	804.4	106.9	957.6	272.5	1154.0	193.6	1040.7	51.6	1253.5	28.8
Al	0.740	0.090	0.618	0.273	BDL		0.399	22.227	0.420		7.301	3.423	3.431	0.188
Si	1.21		1.34		1.43		4.19	0.52	2.68	0.61	5.56	0.81	1.89	
K	62.0	39.4	18.1	5.8	14.2	4.9	59.6	0.0	7.4	0.9	3.7		BDL	
Ca	535.2	62.9	475.4	35.4	444.5	60.9	502.7	9.9	440.9	0.2	264.8	5.1	349.1	27.5
V	0.061	0.004	0.026	0.004	0.002	0.001	0.046	0.002	BDL		0.009	0.004	0.008	
Cr	0.719	0.462	0.124		BDL		0.174		BDL		BDL		BDL	
Mn	19.3	13.0	37.2	26.5	76.8	15.4	97.8	52.1	135.6	17.0	137.7	23.9	291.2	26.0
Fe	17.2	15.8	45.7	44.4	109.6	106.4	206.5	30.5	487.5	190.4	430.8	58.3	1320.0	155.3
Ni	0.292	0.281	0.056	0.046	0.065	0.031	0.148	0.088	0.289	0.032	0.319	0.008	1.032	0.022
Co	0.006	0.005	0.023	0.020	0.059	0.033	0.126	0.027	0.212	0.023	0.245	0.014	0.627	0.087
Cu	0.098	0.091	0.075	0.063	0.020	0.015	0.170	0.095	0.093	0.060	0.070	0.011	0.725	0.369
Zn	0.427	0.349	0.147	0.050	0.176	0.039	0.154	0.125	0.191	0.004	0.210	0.003	0.313	0.022
As	0.023	0.020	0.009	0.006	0.005	0.005	0.014	0.001	0.008	0.001	0.014	0.007	0.009	
Se	0.257	0.132	0.082	0.043	0.122	0.023	0.096	0.012	0.170	0.061	0.021	0.006	0.170	0.105
Sr	30.151	0.828	27.887	1.798	25.335	1.234	24.027	0.446	23.461	0.629	14.821	0.571	22.476	1.098
Mo	0.225	0.081	0.154	0.120	0.083	0.071	0.025	0.013	0.031	0.004	0.044	0.013	0.006	0.004
Cd	0.002	0.001	0.001	0.000	0.001	0.001	0.002	0.001	0.001	0.000	0.004	0.000	0.009	0.000
Ba	0.121	0.004	0.180	0.076	0.082	0.011	BDL	0.004	BDL		BDL		BDL	
Pb	0.105	0.105	0.002	0.001	0.001		BDL	0.000	BDL		BDL		BDL	
SO4	2356.3		5570.0	3133.8	4108.8	347.5	3644.5	114.5	9819.5	121.5	10832.5	949.5	10370.0	7032.5
Cl	232.5		125.0	16.3	56.9	0.6	BDL		BDL		24.0		BDL	
NO3	123.1	45.6	246.3	8.8	330.6	16.9	695.5	81.5	443.5	5.5	365.0	25.0	1211.3	743.8
PO4	BDL		3.125		BDL		BDL		BDL		BDL		BDL	
alkalinity HCO3 (mg/L)	80.00		77.50		57.50		72.50		BDL		BDL		BDL	
pH	7.52	0.98	6.80	1.40	5.63	0.96	5.03	0.58	4.68	0.62	3.78	0.74	3.90	0.04

Table E6. Analytical results for solid residue (SR) + 6 % FA core

SR + 6 % OPC element	drainage 1		drainage 2		drainage 3		drainage 4		drainage 5		drainage 6		drainage 7		drainage 8	
	ave	SD	ave	SD	ave	SD	ave	SD	ave	SD	ave	SD	ave	SD	ave	SD
B	0.336	0.091	0.091	0.058	0.140	0.097	0.170	0.121	2.770	2.770	2.384	0.367	67.153		NS	NS
Na	465.1	29.4	131.0	1.8	83.7	5.1	34.7	33.1	42.0	42.0	36.2	0.8	76.6	2.1	67.0	0.5
Mg	0.5	0.0	0.4	0.1	6.8	6.7	5.3	3.0	149.6	149.6	131.8	32.5	161.6	23.2	191.9	15.5
Al	0.91	0.06	9.01	0.02	9.33	0.05	0.08	0.03	0.72	0.72	10.30	10.17	82.88	32.57	129.41	35.90
Si	10.04	1.04	10.20	0.33	6.70	2.20	3.22	2.71	6.92	6.92	7.81	1.28	97.11	6.38	22.69	7.63
K	632.91	47.88	334.94	7.11	221.84	12.60	87.65	86.47	109.69	109.69	88.36	1.31	141.34		136.08	
Ca	360.00	0.02	392.31	1.27	409.47	9.71	248.85	240.98	411.28	411.28	495.88	61.66	401.49	28.84	619.99	32.97
V	0.06	0.01	0.04	0.00	0.03	0.01	0.01	0.01	0.00	0.00	0.00	0.00	0.17	0.03	0.12	0.06
Cr	1.46	0.13	0.35	0.03	0.23	0.01	0.08	0.03	0.04	0.04	BDL		0.57		0.44	
Mn	0.01	0.01	0.00	0.00	0.00	0.00	0.36	0.35	60.39	60.39	57.28	12.03	67.87	12.09	77.04	13.55
Fe	1.18	0.32	1.36	0.03	1.92	0.35	2.08	0.95	441.47	441.47	452.21	121.40	608.80	114.68	561.38	183.58
Ni	0.010	0.000	0.004	0.001	0.002	0.000	0.019	0.008	0.662	0.662	0.594	0.216	45.319	14.743	105.389	6.185
Co	0.001	0.000	0.001	0.000	0.001	0.000	0.001	0.000	0.123	0.123	0.117	0.035	0.162	0.010	0.214	0.030
Cu	0.015	0.002	0.013	0.008	0.012	0.001	0.052	0.043	0.023	0.023	0.042	0.007	14.490	6.715	5.400	0.316
Zn	0.125	0.010	0.079	0.005	0.080	0.001	0.059	0.011	0.370	0.370	0.438	0.282	8.255	3.258	2.621	0.205
As	0.002	0.001	0.001	0.001	0.001	0.001	0.001	0.000	0.001	0.001	0.002	0.001	0.063	0.013	0.031	0.006
Se	0.139	0.003	0.047	0.003	0.021	0.004	0.016	0.010	0.024	0.024	0.011	0.005	0.659	0.129	0.764	0.077
Sr	19.43	0.28	31.84	0.35	38.59	1.55	20.06	19.45	32.11	32.11	33.39	1.48	29.89	2.14	32.38	0.86
Mo	1.680	0.021	0.417	0.008	0.287	0.024	0.115	0.114	0.011	0.011	0.020	0.009	0.092	0.019	0.076	0.001
Cd	0.003	0.000	0.001	0.000	0.001	0.000	0.000	0.000	0.001	0.001	0.001	0.001	0.004	0.002	0.011	0.005
Ba	0.109	0.001	0.219	0.058	0.153	0.004	0.092	0.087	0.055	0.055	0.061	0.000	0.473		0.148	
Pb	0.001	0.000	0.001	0.000	0.001	0.000	0.001		0.000	0.000	0.004	0.000	0.545	0.149	0.596	0.018
SO4	2875.75	35.25	1906.00	2.00	1854.65	89.62	1767.48	135.02	7537.50	1530.00	2531.25	1.25	4002.50	31.25	4471.88	420.63
Cl	39.3	0.3	12.5	1.0	42.5	12.1	136.7	13.3	556.3	3.8	281.3	6.3	251.3	32.5	764.4	9.4
NO3	123.3	2.8	BDL		52.5	4.5	21.5	3.4	10.0		7.5		20.6	10.6	70.6	9.4
PO4	BDL		BDL		BDL		6.0		23.8	1.3	BDL		63.8	51.3	BDL	
alkalinity HCO3 (mg/L)	156.3	6.3	381.3	143.8	137.5	50.0	75.0									
pH	11.3	0.2	10.8	0.4	11.2	0.2	8.1	3.0	5.3	0.2	4.3	0.2	3.9	0.2	3.8	0.1

Table E6: continued

SR + 6 %														
OPC	drainage 9		drainage 11		drainage 12		drainage 13		drainage 14		drainage 15		drainage 16	
element	ave	SD	ave	SD	ave	SD	ave	SD	ave	SD	ave	SD	ave	SD
B	5.92	5.92	2.60	1.52	4.55	0.88	1.53	0.01	2.88	0.13	1.25	0.25	1.13	0.23
Na	65.22	65.22	46.61	3.37	32.29	0.02	25.31	1.47	21.39	0.12	10.87	1.12	17.23	1.74
Mg	161.96	161.96	134.48	0.50	140.53	12.36	136.19	1.84	177.14	9.78	126.62	11.45	206.68	29.17
Al	112.97	112.97	46.83	46.77	23.47	23.34	53.40	52.23	96.18	14.79	49.70	19.01	143.87	14.76
Si	5.27	5.27	4.89		3.92	3.05	8.35	3.09	7.02	1.69	3.79	1.32	31.49	19.60
K	17.60	17.60	16.62	3.73	25.37	0.84	85.15	80.17	16.08	1.79	1.55	0.12	129.32	
Ca	398.55	398.55	447.61	10.64	589.28	29.18	640.98	49.14	616.69	44.39	335.71	14.72	555.27	14.02
V	0.02	0.02	0.02	0.00	0.01		0.11	0.02	0.01	0.00	0.00	0.00	0.01	
Cr	0.17	0.17	BDL		BDL		0.70	0.21	BDL		BDL		2.32	
Mn	70.22	70.22	42.08	29.88	55.29	8.04	46.26	9.37	61.83	7.21	38.90	9.40	89.93	12.95
Fe	496.15	496.15	325.36	325.05	237.63	108.84	283.12	183.28	520.60	115.13	293.80	118.71	628.51	109.57
Ni	4.20	4.20	0.28	0.16	0.22	0.02	0.30	0.07	0.37	0.03	0.34	0.03	1.48	0.10
Co	0.15	0.15	0.06	0.05	0.08	0.01	0.08	0.02	0.13	0.02	0.09	0.02	0.18	0.02
Cu	0.47	0.47	0.10	0.07	0.09	0.02	0.21	0.04	0.10	0.03	0.10	0.01	0.35	0.10
Zn	0.91	0.91	0.37	0.29	0.42	0.11	0.34	0.13	0.61	0.10	0.58	0.10	0.91	0.12
As	0.01	0.01	0.01	0.00	0.01	0.00	0.03	0.01	0.01	0.00	0.01	0.00	0.04	0.03
Se	0.41	0.41	0.05	0.02	0.21	0.05	0.11	0.01	0.05	0.02	0.08	0.04	0.27	0.07
Sr	30.81	30.81	28.63	0.48	29.39	1.40	27.18	2.13	27.90	2.69	15.21	0.73	22.85	0.24
Mo	0.05	0.05	0.04	0.02	0.02	0.01	0.02	0.01	0.03	0.00	0.02	0.00	0.14	0.01
Cd	0.006	0.006	0.001	0.001	0.001	0.000	0.002	0.000	0.002	0.000	0.003	0.000	0.004	0.002
Ba	BDL		0.096	0.014	0.081	0.027	BDL		BDL		BDL		0.048	
Pb	1.01	1.01	0.04		0.03		0.02		BDL		BDL		0.02	0.00
SO4	4677.50		3333.75	1597.50	2712.50	533.75	2365.00	326.00	4726.50	526.50	5602.50	615.50	6862.50	865.00
Cl	367.50		215.63	1.88	117.50	8.75	BDL		23.00	4.00	83.50	62.50	BDL	
NO3			91.25	71.25	133.75	22.50	239.00	209.00	348.00	8.00	435.00	87.00	255.00	67.50
PO4														
alkalinity HCO3 (mg/L)														
pH	3.75		4.41	0.66	4.37	0.34	4.07	0.33	4.15	0.04	3.85	0.07	3.36	0.00

Saturation indices calculated using PHREEQC and WATEQ4 database for the column solid cores leachates are presented in Tables E7-E12 below

Table E7: Summary of saturation indices (SI) for mineral phases controlling element concentration in leachates for fly ash (FA) solid core.

Phase		drainage1	drainage2	drainage 3	drainage 4	drainage5	drainage6	drainage7	drainage8	drainage9	drainage10	drainage11	drainage12	drainage13	drainage 14	drainage 15	drainage 16
Al(OH)3(a)	Al(OH)3	-5.79	-3.26	-0.75	-0.75	-1.95	0.39	1.18	2.15	1.49	1.43	-0.38	-1.51	-2.22	-3.2	-3.63	-4.62
Alunite		-26.82	-13.6	-3.48	-3.55	-5.58	7.43	11.25	13.2	11.5	11.28	6.79	7.32	5.34	4.98	3.57	
Anhydrite	CaSO4	-0.27	-0.39	-0.33	-0.36	-0.3	-0.2	-0.24	0.29	-0.18	-0.16	-0.07	-0.21	-0.9	-0.13	-0.31	-0.16
Aragonite		2.93	2.34	1.43	-248.03	0.98	-0.97			-1.04	-0.9	-1.47					
Basaluminite		-27.77	-13.95	-2.23	-2.69	-6.48	6.86	11.46	14.66	12	11.85	5.13	3.47	1.18	-1.55	-2.91	-5.86
Boehmite	AlOOH	-3.59	-1.05	1.46	1.46	0.26	2.6	3.38	4.36	3.7	3.64	1.82	0.7	-0.02	-1	-1.42	-2.42
Diaspore	AlOOH	-1.85	0.68	3.19	3.17	1.98	4.32	5.12	6.09	5.42	5.36	3.55	2.42	1.72	0.73	0.31	-0.68
Ettringite		3.66	-3.54	-3.24	-3.2	-8.18	-14.91	-16.6	-9.48	-14.16	-14.42	-19.16	-30.75	-36.94	-38.57	-41.47	-45.64
Fe(OH)3(a)	Fe(OH)3	2.36	4.08	4.85	4.84	4.86	3.84	3.05	3.76	3.67	3.42	1.49	-0.78	-4.78	-2.35	-2.72	-3.7
Ferrihydrite	FeOOH	0.47	2.19	2.96	2.95	2.97	1.95	1.16	1.87	1.78	1.53	-0.4	-2.67	-6.67	-4.24	-4.61	-5.59
Gibbsite	Al(OH)3	-3.06	-0.54	1.97	1.95	0.76	3.09	3.9	4.87	4.2	4.14	2.33	1.2	0.51	-0.49	-0.91	-1.9
Goethite	FeOOH	3.82	5.56	6.33	6.39	6.41	5.39	4.53	5.24	5.19	4.93	3.01	0.74	-3.33	-0.86	-1.23	-2.21
Gypsum	CaSO4.2H2O	-0.04	-0.16	-0.1	-0.14	-0.07	0.02	0	0.52	0.05	0.07	0.16	0.02	-0.67	0.09	-0.09	0.07
Hematite	Fe2O3	14.42	17.92	19.46	19.58	19.62	17.57	15.85	17.27	17.17	16.66	12.81	8.27	0.13	5.07	4.34	2.38
Jarosite(ss)		-19.37	-8.13	-3.06	-3	-1.32	2.01	1.05	2.13	2.26	1.51	-3.31	-5.83	-17.81	-7.79	-8.86	
Jarosite-K		-18.57	-7.68	-2.77	-2.56	-0.97	1.97	0.76	1.91	2.1	1.29	-3.54	-6.43	-18.56	-8.52	-9.76	
Jarosite-Na		-21.77	-11.05	-6.16	-6.11	-4.65	-1.79	-3.1	-1.83	-1.49	-2.03	-7.32	-9.79	-22.33	-12.39	-13.21	-14.46
JarositeH		-31.46	-18.36	-12.66	-12.37	-10.34	-5.42	-6.26	-5.49	-5.11	-5.69	-10.4	-11.52	-23.59	-13.2	-13.64	-14.53
Jurbanite	AlOHSO4	-17.68	-11.29	-7.08	-7.18	-7.38	-1.05	0.77	1.06	0.58	0.62	-0.66	1.05	0.55	0.98	0.88	0.91
Portlandite	Ca(OH)2	-1.55	-5.51	-7.15	-7.08	-8.01	-11.9	-12.98	-11.78	-12.42	-12.49	-12.94	-15.92	-16.83		-17.98	-18.85
Rhodochrosite	MnCO3	-1.47	0	-0.89	-250.14	1.14	-0.22				0.22	0.5	-0.13				
Siderite	FeCO3	-13.62	-6.48	-4.16	-253.54	-3.07	-0.22				0.21	0.23	-1.69				
Sillimanite	Al2SiO5	-12.34	-4.69	0.87	0.52	-1.97	2.72	4.62	6.32	5.23	4.58	1.04	-0.84	-2.09	-3.8	-4.61	-6.71
SiO2(a)		-4.71	-2.02	-1.47	-1.58	-1.69	-1.67	-1.6	-1.85	-1.48	-2.02	-1.93	-1.55	-1.6	-1.22	-1.18	-1.29
Pyrolusite	MnO2	4.34	-1.48	-4.75	-4.43	-4.1	-11.29	-13.09	-11.63	-11.77	-11.81	-12.58	-17.94		-20.53	-21.01	-22.82
Barite	BaSO4	0.94	0.06	0.19		0.49	0.76		1.27		0.94	1.22		-0.99			
Brucite	Mg(OH)2	0.32	-1.13	-2.69	-2.24	-2.92	-6.63	-7.46	-6.1	-6.64	-6.47	-6.89	-9.52	-10.32	-10.88	-11.24	-12.22
Magnetite	Fe3O4	8.94	16.17	19.32	19.54	20.09	18.97	16.87	18.64	18.58	17.87	12.22	6.9	-3.32			
Manganite	MnOOH	5.03	1.06	-1.37				-6.73				-5.81		-10.32			
Ni(OH)2		0.62	-1.15	-1.86	0.66	-1.61	-4.37	-4.55	-2.66	-2.78	-3.8		-6.86		-7.79	-8	-8.31
Nsutite	MnO2	3.83	-2.15	-5.41	-5.39	-5.06	-12.25	-13.72		-12.57	-12.61	-13.38	-18.73	-20.02	-21.21	-21.69	-23.5
Pyrochroite	Mn(OH)2	-0.84	-2.81	-4.42	-4.29	-2.94	-6.24	-6.81	-6.05	-6.17	-6.1	-6.62	-8.99	-9.33	-10.09	-10.4	-11.22
Quartz		-3.42	-0.73	-0.18	-0.3	-0.41	-0.39	-0.31	-0.56	-0.2	-0.73	-0.65	-0.27	-0.31	0.07	0.11	-0.01
Sepiolite	Mg2Si3O7.5OH.3H2O	-3.37	1.74	0.27	0.67	-0.99	-8.37	-9.67	-7.69	-7.74	-9.01	-9.6	-13.72				
Calcite	CaCO3	3.08	2.49	1.57	-247.88	1.13	-0.83		-250.7	-0.89	-0.75	-1.32					
Celestite	SrSO4	0.47	0.47	0.52	0.46	0.44	0.48	0.44	0.94	0.42	0.37	0.13	0.39				
Cu(OH)2		-1.8	-1.93	-1.63					-0.32			-2.03					
CuCO3		-10.32	-7.05	-6.03	-255.64	-5.61	-4.6										
Smithsonite	ZnCO3	-6.91	-2.88	-2.18		0.39	-1.62				-3.54	-2.93	-3.7				
Strontianite	SrCO3	2.36	1.87	0.95						-1.76	-1.7	-2.6					
Pb(OH)2		0	-2.2		0.16	-1.66	-4.81	-5.12	-1.66				-6.81				

Table E8: Summary of saturation indices (SI) for mineral phases controlling element concentration in leachates for solid residue (SR) core.

Phase		drainage1	drainage2	drainage 3	drainage 4	drainage5	drainage6	drainage7	drainage8	drainage9	drainage10	drainage11	drainage12	drainage13	drainage14	drainage15	drainage16
Al(OH)3(a)	Al(OH)3	-0.88	0.35	0.4	0.1	-0.65	-0.84	-0.12	-0.08	-1.4	-0.22	-0.49	-5.07	-6.64	-7.86	-7.77	-6.5
Alunite		-0.37	3.58	3.63	2.41	0.2	-1.06	1.63	-0.14	-2.46	-2.38	3.32	-1.44	-5.32	-7.33		
Aragonite		0.62	-248.37	-250.42	-0.73	0.35	0.55		0.53	0.87	0.97	-0.94					
Anhydrite	CaSO4	-0.37	-0.34	-0.37	-0.4	-0.32	-0.3	-0.23	-0.35	-0.21	-2.72	1.72	-0.33	-0.35	-0.15	-0.31	-0.2
Basaluminate	Al4(OH)10SO4	-0.37	4.21	4.6	3.3	0.35	-0.82	2.4	1.34	-2.82	0.79	1.27	-9.39	-14.97	-18.96	-18.35	-12.66
Boehmite	AlOOH	1.31	2.55	2.6	2.31	1.55	1.36	2.08	3.08	0.81	2.53	3	-2.87	-4.44	-5.66	-5.57	-4.3
Diaspore	AlOOH	3.07	4.28	4.33	4.04	3.28	3.1	3.81	5.1	2.54	5.01	3.93	-1.13	-2.71	-3.92	-3.83	-2.57
Fe(OH)3(a)	Fe(OH)3	5.11	5.1	5.16	5.06	5.01	5.13	6.67	3.21	5.15	3.12	2.04	-1.95	-2.92	-3.57	-3.88	-4.72
Ferrihydrite	FeOOH	3.22	3.21	3.27	3.17	3.12	3.24	4.78	1.86	3.26	1.31	1.78	-3.84	-4.81	-5.46	-5.77	-6.61
Gibbsite	Al(OH)3	1.86	3.06	3.12	2.82	2.07	1.88	2.6	6.58	1.32	6.5	5.41	-2.35	-3.93	-5.14	-5.05	-3.78
Goethite	FeOOH	6.52	6.6	6.65	6.55	6.5	6.61	8.16	0.15	6.64	0.01	-0.26	-0.47	-1.44	-2.08	-2.39	-3.23
Gypsum	CaSO4.2H2O	-0.13	-0.11	-0.14	-0.17	-0.09	-0.07	0	19.96	0.02	19.79	17.62	-0.1	-0.12	0.08	-0.08	0.03
Hematite	Fe2O3	19.82	20	20.09	19.88	19.79	20.02	23.11	1.54	20.07	0.75	1.95	5.86	3.92	2.63	2.02	0.33
Jarosite(ss)		1.14	1.62	1.71	1.08	1	0.63	5.85	1.66	1.02	0.82	1.85	-7.41	-9.35	-9.64		
Jarosite-K		1.2	1.85	1.86	1.21	1.12	0.77	5.96	-2.42	1.12	-3.04	-2.21	-8.16	-10.22	-10.53		
Jarosite-Na		-2.15	-2.02	-2.22	-2.87	-2.97	-3.31	2.1	-7.27	-2.84	-7.87	-6	-11.8	-13.81	-14.39	-15.12	-16.51
JarositeH		-8.59	-7.44	-7.23	-7.79	-7.79	-8.28	-2.92	-4.87	-7.74	-5.6	-2.56	-12.82	-14.29	-14.47	-14.9	-16.2
Jurbanite	AlOHSO4	-5.28	-3.83	-3.7	-4.12	-4.8	-5.41	-4.33	-9.22	-5.73	-9.19	-12.02	-1.29	-2.14	-2.48	-2.14	-0.26
Portlandite	Ca(OH)2	-9.14	-9.31	-9.43	-9.33	-9.33	-8.89	-9.18	-1.07	-9.03	1.45	1.24	-17.27	-18.01	-18.69	-19.09	-19.6
Rhodochrosite	MnCO3	-0.87	-249.93	-252.09	-2.87	-1.82	-1.68		-1.77	0.14	1.45	1.24					
Siderite	FeCO3	-1.97	-250.39	-252.25	-2.78	-1.72	-2.07		0.3	-1.64	-0.64	0.31					
Sillimanite	Al2SiO5	0.55	2.51	2.63	2.08	0.57	0.17	1.97	-1.81	-0.72	-1.66	-1.65	-8.21	-10.79	-12.9	-13.05	-10.77
SiO2(a)		-1.81	-1.95	-2	-1.96	-1.97	-1.98		-1.62	-1.77			-1.91	-1.34	-1.01	-1.35	-1.61
Pyrolusite	MnO2	-7.81	-8.35	-8.69	-9.02	-9.1	-8.29	-5.36	-8.03	-6.81	-5.95	-9.52	-19.85	-21.32	-22.52	-23.05	-24.23
Brucite	Mg(OH)2	-4.83	-5.18	-5.18	-5.18	-5.19	-4.46	-3.68	-3.3	-2.79	-2.53	-5.04	-10.37	-11.38	-12.11	-12.42	-12.93
Barite	BaSO4	1.05	1.01	1.04	1.02	1.03	1.06	0.95	1.11	1.09	0.24	0.8	1.14	0.91			
Magnetite	Fe3O4	21.43	21.09	20.97		25.89	21.03	21.13	20.79	18.76		1.37	3.79	1.37	-0.33	-1.19	-3.37
Manganite	MnOOH	-3.22	-3.94	-4.17	-4.52	-4.57	-3.97	-0.89	-3.7	-2.55	-1.6	-3.95	-11.31	-12.59	-13.55	-14.02	-14.85
Ni(OH)2		-1.86	-1.62	-2.16	-2.64	-0.35	-0.67	-1.64	-2.96	-3.34		-8.8	-8.01	-8.8	-9.22	-9.38	-9.59
Nsutite	MnO2	-9.36	-9.69	-9.77	-8.95	-6.02	-8.7	-7.48	-6.62	-10.19		-21.98	-20.22	-21.98	-23.18	-23.72	-24.89
Pb(OH)2		-0.52	-1.25	-1.86	-1.69	-0.74	-1.45		-2.67	-3.24		-9.83	-8.17	-9.83	-11.03		
Pyrochroite	Mn(OH)2	-5.41	-5.86	-6.06	-6.43	-6.45	-6.07	-2.84	-5.78	-4.71	-3.66	-4.8	-9.48	-10.29	-11	-11.4	-11.89
Quartz		-0.5	-0.66	-0.71	-0.67	-0.68	-0.69	-0.33	-0.52	-0.48	-0.37	-0.36	-0.62	-0.05	0.28	-0.06	-0.32
Sepiolite	Mg2Si3O7.5OH.3H2O	-6.32	-6.2	-6.24	-4.81	-2.15	-1.99	-0.83	0.01	-4.97	-16.41	-16.72	-16.41	-16.72	-17.21	-18.85	-20.62
Calcite	CaCO3	0.76	-248.23	-250.27	-0.58				0.68	1.01	1.12	-0.8					
Celestite	SrSO4	0.3	0.38	0.36	0.32	0.37	0.39	0.43	0.63	0.49	0.42	0.43					
Cu(OH)2		-1.63	-1.94	-1.91	-1.74	-1.66	-1.44	-1.6	-1.62	-2.3	-2.03	-1.81	-6.78				
CuCO3		-4.92	-253.96	-255.88	-6.11	-4.94	-4.98		-4.84	-5.37	-4.84	-3.7					
Smithsonite	ZnCO3	-252.56	-3.32	-2.27	-2.2	-252.85	-1.82	-1.7	-1.53	-2.66	-9.99	-21.62	-9.99				
Strontianite	SrCO3	-251.01	-1.33	-0.28	-0.09	-251.31	-0.08	0.25	0.29	-1.35	-9.29	-10.74	-9.29				

Table E9: Summary of saturation indices (SI) for mineral phases controlling element concentration in leachates for SR + 5 % FA core.

phase		drainage1	drainage2	drainage3	drainage4	drainage5	drainage6	drainage7	drainage8	drainage9	drainage10	drainage11	drainage12	drainage13	drainage14	drainage15	drainage16
Al(OH)3(a)	Al(OH)3	0.16	1.34	0.6	-0.44	-0.75	-0.19	0.36	-0.71	-1.22	-1.31	-1.88	-1.58		-4.5		-7.22
Alumite	KAl3(SO4)2(OH)6	5.97	9.69	4.87	2.18	0.3	3	4.49	1.66	-2.05	-1.87	-3.2	-1.41		-0.02		
Anhydrite	CaSO4	-0.35	-0.32	-0.37	-0.35	-0.37	-0.3	-0.3	0.12	-0.23	-0.2	0	-0.39	-0.39	-0.14	-0.35	-0.22
Basaluminite	Al4(OH)10SO4	5.93	10.29	5.77	1.99	-0.04	2.93	5.04	0.83	-2.47	-2.47	-4.64	-2.76		-8.02		-16.49
Boehmite	AlOOH	2.36	3.55	2.8	1.77	1.46	2.01	2.57	1.49	0.99	0.9	0.33	0.62		-2.29		-5.02
Diaspore	AlOOH	4.11	5.28	4.53	3.5	3.18	3.74	4.29	3.22	2.71	2.62	2.05	2.35		-0.57		-3.29
Ettringite		-13.75	-11.67	-8.77	-11.76	-10.79	-11.51	-10.06	-10.04	-9.32	-10.3	-10.58	-14.49		-38.08		-51
Fe(OH)3(a)	Fe(OH)3	4.61	4.04	5.12	4.88	4.89	4.87	6.45	4.94	5.12	4.9	4.98	5.11	3.03	-0.97	-2.26	-3.76
Ferrihydrite	FeOOH	2.72	2.14	3.23	2.99	3	2.98	4.56	3.05	3.23	3.01	3.09	3.22	1.14	-2.86	-4.15	-5.65
Gibbsite	Al(OH)3	2.9	4.06	3.32	2.28	1.96	2.51	3.07	1.99	1.49	1.4	0.83	1.12		-1.8		-4.51
Goethite	FeOOH	6.02	5.53	6.62	6.37	6.42	6.4	7.98	6.47	6.65	6.43	6.51	6.64	4.56	0.56	-0.73	-2.24
Gypsum	CaSO4·2H2O	-0.11	-0.09	-0.14	-0.12	-0.14	-0.07	-0.08	0.34	-0.01	0.03	0.23	-0.17	-0.17	0.08	-0.12	0.01
Hematite	Fe2O3	18.82	17.86	20.03	19.54	19.64	19.59	22.76	19.73	20.11	19.66	19.83	20.08	15.92	7.93	5.34	2.31
Jarosite(ss)		3.06	1.72	2.28	2.02	1.16	2.21	6.78	2.59	0.9	0.72	1.32	2.71	1.18	-4.85		
Jarosite-K		2.92	1.74	2.41	2.09	1.33	2.3	6.87	2.72	1.1	0.87	1.5	2.79	0.98	-5.29		
Jarosite-Na		-0.38	-2.07	-1.64	-1.99	-2.71	-1.71	3.02	-1.26	-2.84	-2.97	-2.27	-1.08	-2.97	-9.7	-12.3	-14.63
JarositeH		-5.82	-6.59	-6.49	-6.5	-7.33	-5.92	-1.4	-5.74	-7.71	-7.7	-7.24	-5.45	-5.82	-10.84	-12.7	-14.65
Jurbanite	AlOHSO4	-2.1	-0.78	-3.09	-3.77	-4.65	-3.36	-2.91	-3.89	-5.66	-5.41	-5.87	-4.87		-1.37		-1.75
Portlandite	Ca(OH)2	-11.26	-11.35	-9.84	-10.17	-9.61	-10.29	-10.17	-9.86	-8.94	-9.24	-9.15	-10.25	-13.18	-16.42	-17.63	-18.84
Rhodochrosite	MnCO3	-1.61	-3.03	-251.71	-2.16	-1.84	-2.45		-1.97	-1.12			2.15	0.89			
Siderite	FeCO3	-0.37	-1.75	-251.5	-0.96	-1.57	-0.82		-1.49	-1.76			-0.31	0.39			
Aragonite	CaCO3	-0.46	-1.71	-250.25	-0.02	0.13	-0.16		0	0.76			0.41	-1.32			
Sillimanite	Al2SiO5	2.33	4.44	2.85	0.91	0.03	1.27	2.79	0.3	-0.63	-0.68	-2.01	-1.08		-7.12		-12.71
SiO2(a)		-2.1	-2.04	-2.16	-2.03	-2.15	-2.02	-1.62	-1.96	-1.87	-1.76	-1.95	-1.6	-1.89	-1.8	-1.53	-2
Pyrolusite	MnO2	-11.71	-12.21	-9.28	-10.73	-9.38	-11.16	-7.52	-9.47	-7.87	-7.55	-4.89	-6.57	-12.17	-18.16	-20.13	-22.56
Brucite	Mg(OH)2	-6.43	-6.97	-5.44	-5.88	-5.31	-6.02	-4.67	-4.33	-2.97	-2.88	-3.11	-3.29	-6.41	-9.73	-10.88	-12.13
Barite	BaSO4	1.07	1.05	1.04	1.01	0.99	1.05	0.88	1.24	1.06	0.91	1.25	0.84	0.42			
Magnetite	Fe3O4	20.3	19.05	21.53	21.02	20.88	21.21	25.89	20.95	21.21	20.73	20.81	21.68	17.01	6.54	3.13	-0.79
Manganite	MnOOH	-6.06	-6.75	-4.58	-5.81	-4.9	-6.28	-2.71	-5.06	-3.75	-3.25	-0.76	-1.95	-5.98	-10.46	-11.95	-13.69
Ni(OH)2		-3.51	-4.16	-1.66	-2.75	-2.44	-3.59	-1.94	-1.28	-1.77	-1.72	-0.85	-3.46	-4.9	-7.46	-8.34	-8.98
Nsutite	MnO2	-12.01	-12.92	-9.98	-11.43	-10.25	-12.02	-8.39	-10.34	-8.73	-8.41	-5.75	-7.43	-13.04	-19.02	-20.99	-23.35
Pb(OH)2		-3.4	-3.31		-2.98	-2.4	-2.17	-2.38	-2.08	-2.24	-0.99	-0.78	-3.5	-4.76			
Pyrochroite	Mn(OH)2	-7.2	-7.66	-6.27	-7.28	-6.63	-7.62	-4.12	-6.87	-5.86	-5.17	-2.85	-3.56	-6.01	-8.97	-10	-11.11
Quartz		-0.8	-0.75	-0.87	-0.74	-0.87	-0.74	-0.34	-0.68	-0.59	-0.47	-0.66	-0.32	-0.61	-0.51	-0.25	-0.72
Sepiolite	Mg2Si3O7·5OH·3H2O	-8.94	-10.04	-7.33	-7.82	-7.12	-8.17	-4.25	-4.6	-1.6	-1.09	-2.11	-1.43	-8.55	-14.89	-16.4	-20.28
Calcite	CaCO3	-0.31	-1.56	-250.1	0.13	0.28	-0.02		0.14	0.9							
Celestite	SrSO4	0.27	0.37	0.37	0.33	0.35	0.37	0.37	0.77	0.46	0.39	0.2	0.46	0.34	0.59	0.38	0.54
Cu(OH)2		-2.13	-2.28	-1.75	-1.81	-1.69	-1.46	-1.62	-2.1	-2.33	-1.6	-1.46	-1.93	-3.17	-6.2	-7.26	-7.69
CuCO3		-4.38	-5.6	-255.13	-4.62	-4.88	-4.27		-5.18	-5.57			-4.21				
Smithsonite	ZnCO3	-2.68	-4.16	-252.48	-2.66	-2.44	-2.73		-2.78	-1.81			-1.51	-3.14			
Strontianite	SrCO3	-1.16	-2.34	-250.82	-0.67	-0.48	-0.82		-0.68	0.12			-0.07	-1.92			

Table E10: Summary of saturation indices (SI) for mineral phases controlling element concentration in leachates for SR + 25 % FA core.

Phase		drainage1	drainage2	drainage3	drainage4	drainage5	drainage6	drainage7	drainage8	drainage9	drainage10	drainage11	drainage12	drainage13	drainage14	drainage15	drainage16
Al(OH)3(a)	Al(OH)3	-1.15	0.04	-0.09	-1.36	-1.47	-1.2	-1.33	-0.82	-0.98	-1.28	-1.19	-0.26	-0.89	-3.69	-5.38	-6.95
Alunite		-0.12		0.8	-3.54	-4.54	-3.03	-3.24	1.03	-0.67	-2.05	0.02	5.71	6.43	0.61		
Anhydrite	CaSO4	-0.55	-0.5	-0.37	-0.35	-0.31	-0.41	-0.27	-0.06	-0.24	-0.21	-0.43	-0.33	-0.41	-0.14	-0.37	-0.22
Basaluminit	Al4(OH)10SO4	-0.78	2.63	1.53	-4.03	-3.98	-2.32	-2.75	0.99	-0.33	-2.68	-0.3	5.56	4.05	-4.84	-10.08	-14.66
Boehmite	AlOOH	1.05	2.23	2.12	0.86	0.73	1	0.87	1.38	1.21	0.93	1	1.93	1.31	-1.49	-3.18	-4.75
Diaspore	AlOOH	2.8	3.98	3.84	2.57	2.48	2.75	2.62	3.13	2.97	2.65	2.76	3.68	3.05	0.25	-1.44	-3.01
Fe(OH)3(a)	Fe(OH)3	4.72	5.28	5.07	4.89	4.33	5.19	5.23	5.17	5.5	4.97	4.93	4.13	2.4	0.04	-1.97	-4.09
Ferrihydrite	FeOOH	2.83	3.39	3.18	3	3.19	3.3	3.34	3.28	3.61	3.08	3.04	2.24	0.51	-1.85	-3.86	-5.98
Gibbsite	Al(OH)3	1.59	2.78	2.62	1.35	1.27	1.54	1.41	1.92	1.76	1.43	1.55	2.48	1.84	-0.96	-2.65	-4.22
Goethite	FeOOH	6.12	6.69	6.59	6.44	6.49	6.6	6.64	6.58	6.91	6.52	6.34	5.53	3.84	1.48	-0.53	-2.65
Gypsum	CaSO4·2H2O	-0.31	-0.26	-0.15	-0.12	-0.07	-0.17	-0.03	0.18	-0.01	0.01	-0.19	-0.1	-0.17	0.1	-0.13	0.01
Hematite	Fe2O3	19.03	20.16	19.97	19.68	19.75	19.98	20.05	19.94	20.6	19.83	19.46	17.85	14.47	9.76	5.73	1.5
Jarosite(ss)		1.07	-2.98	0.03	-1	-1.41	-0.28	0.01	2.7	2.46	0.66	2.16	2.94	0.36	-3.69		
Jarosite-K		1.08	-9.41	0.34	-0.61	-1.3	-0.27	0.02	2.59	2.37	0.88	1.98	2.48	0.03	-4.46		
Jarosite-Na		-2.42		-3.57	-4.58	-5.34	-4.25	-4	-1.41	-1.6	-2.93	-1.84	-1.12	-4.43	-7.96	-11.97	-15.59
JarositeH		-8.43		-9.21	-10.08	-11.2	-9.72	-9.42	-6.19	-6.54	-7.78	-6.5	-4.62	-7.14	-9.59	-12.57	-15.54
Jurbanite	AlOHSO4	-4.88	-5.03	-5.15	-6.7	-7.12	-6.28	-6.31	-4.1	-4.94	-5.59	-4.27	-1.2	-0.62	-1.11	-1.28	-1.16
Portlandite	Ca(OH)2	-10	-8.61	-8.46	-8.14	-7.83	-8.5	-8.46	-9.94	-9.46	-9.03	-10.52	-12.57	-13.84	-15.88	-17.63	-19.18
Rhodochrosite	MnCO3		-1.07	-2.66	-1.9	-1.73	-1.46	1.02	0.63	1.23	1.34	1.54	1.21	0.42			
Siderite	FeCO3		-2.11	-3.53	-2.77	-3.2	-2.47	-2.37	-1.24	-1.06	-1.58	-0.44	0.92	0.23			
Aragonite	CaCO3		1.01	-0.22	1.06	1.25	0.89	1	0.12	0.59	0.83	0.29	-0.58	-1.61			
Sillimanite	Al2SiO5	-0.2	2.66	1.93	-0.71	-0.49	0.05	-0.26	0.77	0.4	-0.84	-0.11	1.73	1.18	-4.87	-8.65	-11.71
SiO2(a)		-2.01	-1.52	-1.62	-1.61	-1.67	-1.67	-1.72	-1.71	-1.76	-1.9	-1.84	-1.86	-1.02	-1.48	-1.87	-1.8
Pyrolusite	MnO2	-8.03	-7.55	-7.5	-7.48	-6.97	-7.62	-5.2	-7.37	-6.48	-5.8	-7.78	-11.25	-13.7	-17.24	-20.13	-23.31
Brucite	Mg(OH)2	-5.64	-5.14	-4.8	-3.83	-3.52	-3.72	-3.24	-4.42	-3.67	-2.91	-3.97	-5.76	-7.09	-9.13	-10.79	-12.43
Barite	BaSO4	0.94	1.13	1.13	1.09	1.13	1.14	1.18	1.27	1.13	1	0.95	0.92				
Magnetite	Fe3O4	19.83	21.09	20.77	20.24	20.13	20.77	20.88	21.3	22.15	20.93	20.87	19.43	15.1	8.96	3.62	-1.87
Manganite	MnOOH	-3.17	-3.12	-3.57	-3.77	-2.89	-3.24	-0.82	-2.4	-1.66	-1.65	-2.53	-5.02	-6.88	-9.5	-11.69	-14.01
Ni(OH)2		-1.66	-2.64	-1.37	-1.9	-1.33	-2.21	-2.46	-0.92	-1.92	-2.85	-2.99	-4.09	-4.87	-6.45	-7.86	-9.04
Nsutite	MnO2	-8.33	-7.86	-8.3	-7.27	-7.92	-5.5	-7.67	-6.79	-6.75	-8.09	-11.55	-14.16	-17.71	-20.6	-23.78	
Pb(OH)2			-2.51	-1.37	-2.85	-1.7	-2.13	-2.28		-2.19	-3.17	-4.39					
Pyrochroite	Mn(OH)2	-5.09	-5.47	-5.92	-6.19	-5.59	-5.65	-3.22	-4.22	-3.61	-3.62	-4.05	-5.57	-6.67	-8.37	-9.86	-11.32
Quartz		-0.71	-0.22	-0.34	-0.33	-0.36	-0.36	-0.41	-0.41	-0.45	-0.62	-0.54	-0.56	0.27	-0.18	-0.58	-0.51
Sepiolite	Mg2Si3O7·5OH·3H2O	-2.01	-4.62	-4.49	-2.58	-1.81	-2.2	-1.4	-3.73	-2.37	-1.62	-3.24	-6.87	-7.11	-12.55	-17.04	-20.12
Calcite	CaCO3	-6.1	1.15	-0.07	1.21	1.39	1.04	1.15	0.27		0.98	0.44	-0.43	-1.46			
Celestite	SrSO4	0.01	0.28	0.48	0.43	0.43	0.31	0.43	0.67	0.44	0.38	0.3	0.41	0.26	0.57	0.38	0.54
Cu(OH)2		-1.24	-1.76	-1.77	-1.65	-1.76	-1.59	-2.35	-2.22	-2.48	-1.82	-1.65	-2.65	-3.43	-5.14	-7.25	-8.08
Smithsonite			-1.84	-2.88	-1.9	-2.04	-2.07	-2.02	-1.86	-1.97	-1.74	-1.91	-2.49	-3.34			
Strontianite			0.47	-0.7	0.5	0.67	0.3	0.4	-0.47	-0.04	0.1	-0.29	-1.14	-2.26			

Table E11: Summary of saturation indices (SI) for mineral phases controlling element concentration in leachates for SR + 40 % FA core.

phase		drainage1	drainage2	drainage 3	drainage 4	drainage5	drainage6	drainage7	drainage8	drainage9	drainage10	drainage11	drainage12	drainage 13	drainage 14	drainage 15	drainage16
Al(OH)3(a)	Al(OH)3	N/A	-2.27	-1.08	-2.29	-2.66	-1.97	-1.32	-1.5	-1.58	-0.13	0.42		-2.52	-4.02	-5.57	-5.34
Alunite			-11.77	-5.15	-9.14	-11.59	-7.77	-3.48	-4.81	-4.65	3.84	7.84		4.18	0.7	-1.41	
Anhydrite	CaSO4		-0.39	-0.38	-0.36	-0.36	-0.33	-0.29	-0.23	-0.26	-0.29	-0.15	-0.31	-0.34	-0.15	-0.34	-0.28
Basaluminite	Al4(OH)10SO4		-10.83	-3.95	-9.12	-11.66	-7.47	-3.49	-4.3	-4.56	3.96	7.99		-0.57	-5.4	-9.73	-9.44
Boehmite	AlOOH		-0.07	1.12	-0.09	-0.45	0.23	0.89	0.7	0.62	2.06	2.62		-0.32	-1.82	-3.37	-3.14
Diaspore	AlOOH		1.68	2.87	1.65	1.28	1.97	2.62	2.45	2.36	3.81	4.36		1.42	-0.07	-1.62	-1.4
Ettringite			2.25	-2.05	-4.01	-2.15	-4.33	-7.46	-6.02	-7.21	-12.06	-15.61		-32.25	-37.55	-47.41	-45.35
Fe(OH)3(a)	Fe(OH)3		3.63	4.7	4.34	4.02	4.75	4.98	5.03	5.11	5.97	4.43		-0.11	-0.95	-3.75	-2.83
Ferrihydrite	FeOOH		1.74	2.81	2.45	2.13	2.86	3.09	3.14	3.22	4.08	2.54	1.43	-2	-2.84	-5.64	-4.72
Gibbsite	Al(OH)3		0.47	1.66	0.44	0.06	0.76	1.4	1.24	1.14	2.6	3.15	-0.47	0.21	-1.29	-2.83	-2.62
Goethite	FeOOH		5.03	6.13	5.81	5.52	6.21	6.49	6.46	6.57	7.4	5.86		1.32	0.48	-2.31	-1.36
Gypsum	CaSO4:2H2O		-0.15	-0.14	-0.13	-0.13	-0.1	-0.06	0.01	-0.03	-0.05	0.08	2.89	-0.11	0.08	-0.11	-0.05
Hematite	Fe2O3		16.85	19.05	18.41	17.84	19.22	19.77	19.71	19.94	21.59	18.51	-0.08	9.44	7.74	2.16	4.07
Jarosite(ss)			-11.08	-4.48	-5.8	-8.1	-4.11	-0.82	-1.67	-0.91	5.92	3.92	12.58	-4.31	-5.56	-11.15	
Jarosite-K			-10.49	-4.13	-5.4	-7.56	-3.77	-0.58	-1.52	-0.73	5.85	3.59	-1.89	-4.88	-6.4	-12.25	
Jarosite-Na			-14.01	-8.02	-9.36	-11.54	-7.75	-4.56	-5.53	-4.7	1.91	-0.06	-2.4	-9.2	-9.92	-15.76	-13.32
JarositeH			-22.85	-14.94	-16	-18.42	-14.02	-9.91	-11.27	-10.23	-2.85	-3.81	-6.08	-11.04	-11.27	-15.9	-13.72
Jurbanite	AlOHSO4		-11.57	-8.13	-9.47	-10.69	-8.76	-6.55	-7.21	-7.02	-3.04	-0.67	-8.48	-0.41	-0.75	-0.43	-0.62
Portlandite	Ca(OH)2		-4.26	-6.49	-6.34	-5.47	-6.7	-8.21	-7.69	-7.98	-10.55	-12.23	-14.42	-15.62	-16.59	-18.65	-18.16
Rhodochrosite	MnCO3		-1.09	-1.42	-0.37	-1.51	-1.03	-1.6		1.1	1.3	0.75	-0.14	-0.56			
Siderite	FeCO3		-9.19	-5.92	-5.78	-7.17	-4.86	-2.72		-2.93	0.62	0.57	-0.25	-0.5			
Aragonite	CaCO3		2.22	0.95	1.5	1.65	1.48	1.03	1.16	0.1	-0.82	-2.05	-2.51				
Sillimanite	Al2SiO5		-2.61	0.28	-2.38	-3.49	-1.75	-0.48	-0.65	-1.09	1.82	2.98		-2.4	-5.58	-8.36	-8.5
SiO2(a)			-2.18	-1.59	-1.7	-1.95	-1.71	-1.63	-1.68	-1.82	-1.94	-1.88	-1.87	-1.39	-1.57	-1.25	-1.72
Pyrolusite	MnO2		0.14	-3.49	-2.82	-2.36	-4.18	-7.31	-5.87	-4.23	-8.09	-10.86	-14.97	-17.41	-18.84	-22.47	-21.45
Brucite	Mg(OH)2		-0.76	-3.01	-2.41	-1.6	-2.44	-3.47	-2.64	-2.46	-4.53	-6.04	-7.96	-9.12	-9.95	-11.84	-11.4
Barite	BaSO4		1.08	1.14	0.91	0.91	1.22	1.14	0.91	1.1	1.04	1.33	0.89				
Magnetite	Fe3O4		13.83	18.33	17.39	16.12	18.79	20.39	20.04	20.48	24.2	20.31	12.56	8.46	6.27	-1.2	1.53
Manganite	MnOOH		2.28	-0.27	0.27	0.17	-0.9	-3.41	-1.93	-0.34	-2.81	-4.85	-7.95	-9.63	-10.71	-13.44	-12.71
Ni(OH)2			0.46	-0.23	-0.22	0.32	-1.2	-1.08	1.84	-1.4	-1.9	-3.78	-5.9	-6.63	-7.22	-9.01	-8.29
Nsutite	MnO2		-0.16	-3.91	-3.41	-3.11	-4.76	-8.06	-6.29	-4.82	-8.51	-11.28	-15.55	-17.83	-19.26	-22.89	-22.04
Pb(OH)2			-0.46		0.06	-0.15	-0.56	-1.47	0.12		-1.13	-4.03	-6.33				
Pyrochroite	Mn(OH)2		-2.36	-3.71	-3.13	-3.63	-4.12	-5.84	-4.65	-2.95	-4.19	-5.5	-7.44	-8.51	-9.24	-11.07	-10.46
Quartz			-0.57	-0.09	-0.27	-0.66	-0.42	-0.34	-0.38	-0.53	-0.64	-0.58	-0.57	-0.09	-0.27	0.05	-0.43
Sepiolite	Mg2Si3O7.5OH:3H2O		2.17	-0.61	0.17	0.95	0.08	-1.82	-0.14	-0.29	-4.7	-7.56	-11.42	-12.21	-14.44	-17.26	-17.87
Calcite	CaCO3		2.37	1.09	1.65	1.8	1.62	1.18	1.3	0.25	-0.68	-1.9	-2.37				
Celestite	SrSO4		0.51	0.55	0.46	0.46	0.43	0.46	0.42	0.43	0.41	0.56	0.39	0.28	0.52	0.36	0.47
Cu(OH)2			-1.86	-1.89	-2.02	-1.72	-1.45	-2.09	-1.94	-2.63	-1.15	-2.12	-4.74	-5.04	-6.14	-8.1	-6.75
Smithsonite	ZnCO3		-4.22	-3.27	-2.85	-3.4	-2.52	-2.07		-1.98	-1.69	-3.04	-4.1	-4.67			
Strontianite	SrCO3		1.81	0.56	1.01	1.14	0.92	0.45		0.52	-0.52	-1.42	-2.67	-3.21			

Table E12: Summary of saturation indices (SI) for mineral phases controlling element concentration in leachates for SR + 6 % OPC core.

phase		drainage1	drainage2	drainage3	drainage4	drainage5	drainage6	drainage7	drainage8	drainage9	drainage11	drainage12	drainage13	drainage14	drainage15	drainage16
Al(OH)3(a)	Al(OH)3	-3.83	-2.35	-2.7	-1.77	-1.98	-1.57	-3.53	-3.69	-4	-1.56	-2.6	-3.12	-2.92	-4.3	-5.18
Alunite		-17.26	-11.8	-14.21	-2.59	6.19	7.75		4.9	3.43		5.56	5.29	5.47	1.52	2.1
Anhydrite	CaSO4	-0.36	-0.44	-0.35	-0.52	-0.15	-0.29	-0.3	-0.13	-0.27	-1.56	-0.2	-0.23	-0.1	-0.28	-0.08
Aragonite		1.73	2.44	1.14	0.44											
Basaluminit	Al4(OH)10SO4	-18.08	-11.75	-13.94	-4.45	1.24	3.3	-2.57	-3.01	-4.05	2.79	0.13	-1.2	-0.26	-5.03	-8.1
Boehmite	AlOOH	-1.64	-0.15	-0.5	0.44	0.22	0.63	-1.32	-1.49	-1.8	0.64	-0.39	-0.93	-0.72	-2.1	-2.97
Diaspore	AlOOH	0.12	1.59	1.23	2.16	1.95	2.37	0.41	0.24	-0.07	2.38	1.34	0.82	1.02	-0.36	-1.24
Ettringite		2.27	2.2	4.38	-13.11	-29.79	-30.96	-40.83	-40.85	-42.86	-36.9	-35.28	-38.27	-37.4	-43.59	-46.61
Fe(OH)3(a)	Fe(OH)3	2.92	3.37	3.15	5.14	0.79	-0.27	-2.92	-3.33	-3.57	-4.59	-1.93	-2.76	-2.36	-3.6	-4.7
Ferrihydrite	FeOOH	1.03	1.48	1.26	3.24	-1.1	-2.16	-4.81	-5.22	-5.46	-6.48	-3.82	-4.65	-4.25	-5.49	-6.59
Gibbsite	Al(OH)3	-1.09	0.37	0.02	0.94	0.74	1.15	-0.81	-0.97	-1.28	1.16	0.12	-0.39	-0.19	-1.57	-2.47
Goethite	FeOOH	4.32	4.85	4.64	6.69	2.27	1.21	-1.44	-1.85	-2.09	-3.11	-0.45	-1.32	-0.92	-2.16	-3.19
Gypsum	CaSO4·2H2O	-0.13	-0.21	-0.12	-0.3	0.08	-0.06	-0.07	0.1	-0.03	-1.32	0.04	0	0.14	-0.05	0.15
Hematite	Fe2O3	15.43	16.5	16.07	20.17	11.33	9.2	3.91	3.1	2.61	0.56	5.89	4.15	4.94	2.47	0.43
Jarosite(ss)		-14.26	-11.57	-13.61	1.98	-1.22	-3.98		-9.46	-10.51		-7.85	-9.18	-8.27	-11.5	-11.77
Jarosite-K		-13.42	-10.72	-12.71	2.32	-1.59	-4.45		-10.1	-11.37		-8.54	-9.87	-9.12	-12.64	-12.42
Jarosite-Na		-17.31	-14.86	-16.86	-1.79	-5.73	-8.57	-13.17	-14.13	-14.52	-22.93	-12.16	-14.14	-12.73	-15.52	-17
JarositeH		-26.99	-23.33	-25.52	-6.89	-8.14	-10.53	-14.55	-15.32	-15.65	-24.59	-13.62	-15.24	-13.82	-16	-17.09
Jurbanite	AlOHSO4	-14.13	-11.8	-12.93	-5.89	0.05	0.86	0.87	0.93	0.82	0.33	0.78	0.83	1.15	0.53	0.49
Portlandite	Ca(OH)2	-3.24	-4.15	-3.28	-9.54	-15.35	-15.88	-17.85	-17.91	-18.24	-16.6	-16.73	-17.35	-17.33	-18.28	-18.89
Rhodochrosite	MnCO3	-0.82	-0.89	-2.8	0.18											
Siderite	FeCO3	-11.97	-9.22	-11.97	-1.25											
Sillimanite	Al2SiO5	-6.11	-2.93	-4.17	-1.47	-1.28	-0.42	-3.23	-4.19	-5.45	-0.6	-2.77	-3.36	-3.02	-6.05	-7.15
SiO2(a)		-2.56	-2.06	-2.59	-1.55	-1.18	-1.14	-0.04	-0.67	-1.3	-1.34	-1.43	-1.1	-1.17	-1.43	-0.53
Pyrolusite	MnO2	3.04	0.43	1.42	-7.17	-16.63	-18.17	-21.77	-22.21	-22.49	-18.95	-20.01	-21.44	-21.1	-22.59	-23.87
Brucite	Mg(OH)2	0.09	-0.92	1.09	-5.05	-9.59	-7.49	-12.05	-12.22	-12.44	-10.9	-11.15	-11.8	-11.65	-12.49	-13.13
Barite	BaSO4	1.08	1.3	1.16	0.93	0.83	0.74	1.68	1.17							0.72
Magnetite	Fe3O4	11.15	13.28	12.27	21.49		8.3					3.79	1.49	2.59	-0.81	-3.41
Manganite	MnOOH	4.62		2.83	-2.97	-9.31	-10.4					-11.79	-12.75	-12.5	-13.68	-14.8
Ni(OH)2		1.23	-0.41	0.49	-2.83	-5.79	-6.46		-6.34			-7.81	-8.18	-8.05	-8.78	-9.27
Nsutite	MnO2	2.74	-0.23	0.76	-8.13	-17.26	-18.8	-22.4	-22.84	-23.12		-20.65	-21.91	-21.57	-23.06	-24.67
Pb(OH)2		-0.42	-0.33	-0.28	-2.54	-7.69	-7.21	-6.95	-7.18	-7.11		-7.18	-8.1			-9.6
Pyrochroite	Mn(OH)2	-0.58	-2.43	-2.18		-8.43	-9.09	-10.89		-11.26		-10.02	-10.68	-10.51	-11.39	-12.01
Quartz		-1.26	-0.77	-1.3	-0.27	0.11	0.16	1.25	0.63	-0.01	-0.05	-0.14	0.2	0.13	-0.14	0.76
Sepiolite	Mg2Si3O7·5OH·3H2O	2.74	2.03	4.45	-4.84	-12.65	-13.85	-14.14	-16.37	-18.71	-15.74	-16.53	-16.74	-16.66	-19.14	-17.87
Calcite	CaCO3	1.88	2.58	1.29	0.58											
Celestite	SrSO4	0.33	0.47	0.57								0.34	0.51	0.32	0.48	
Cu(OH)2		-1.8	-1.76				-1.16				-30.96		-5.28			-7.21
Smithsonite	ZnCO3	-5.72	-3.94													
Strontianite	SrCO3	1.11														

XRD spectra of solid cores with depth compared to the fly ash are presented in figures E1-E4 below

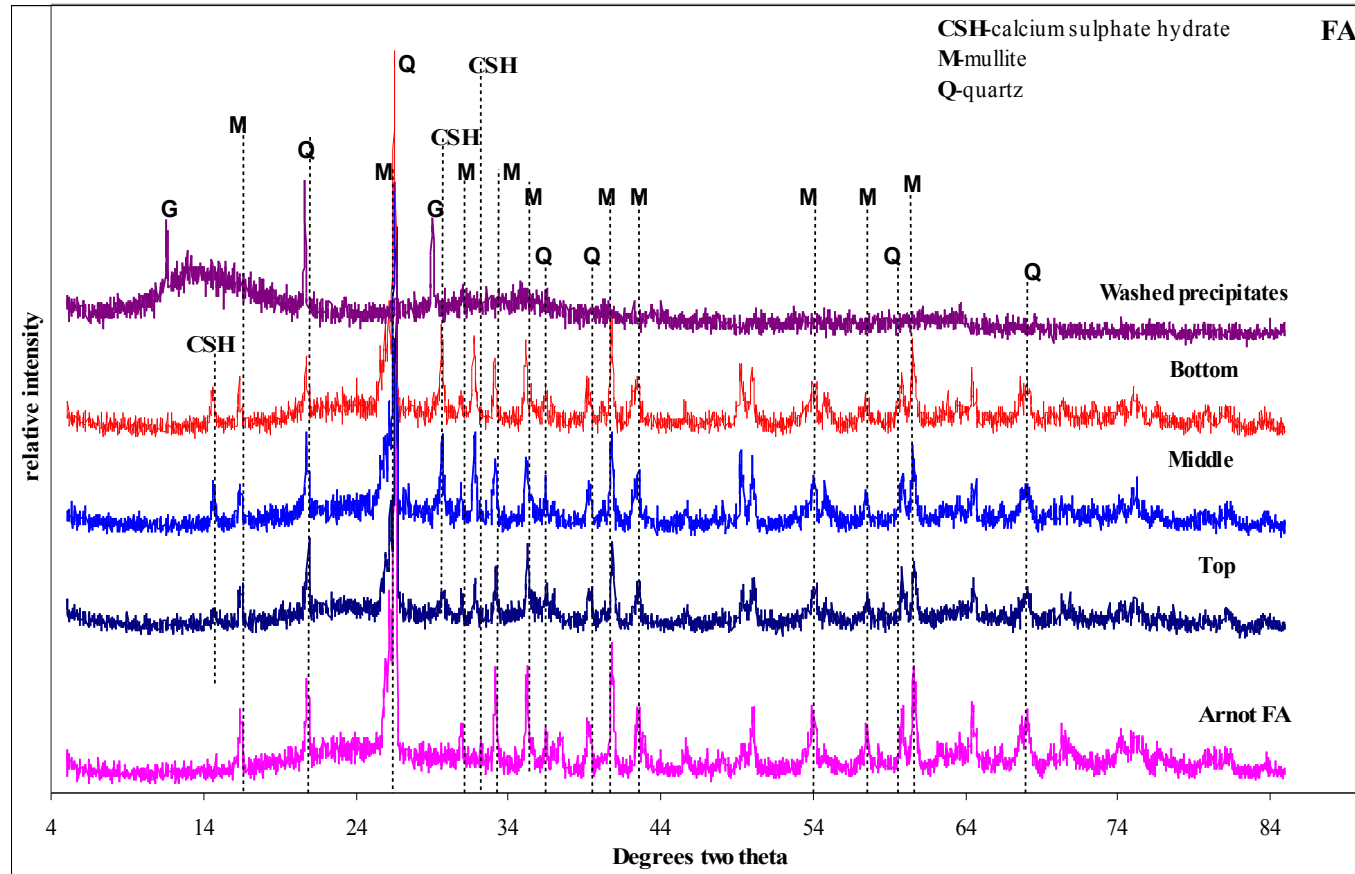


Figure E1: XRD spectra of FA solid core sections with spectra for precipitates washed down the solid core (G-gypsum).

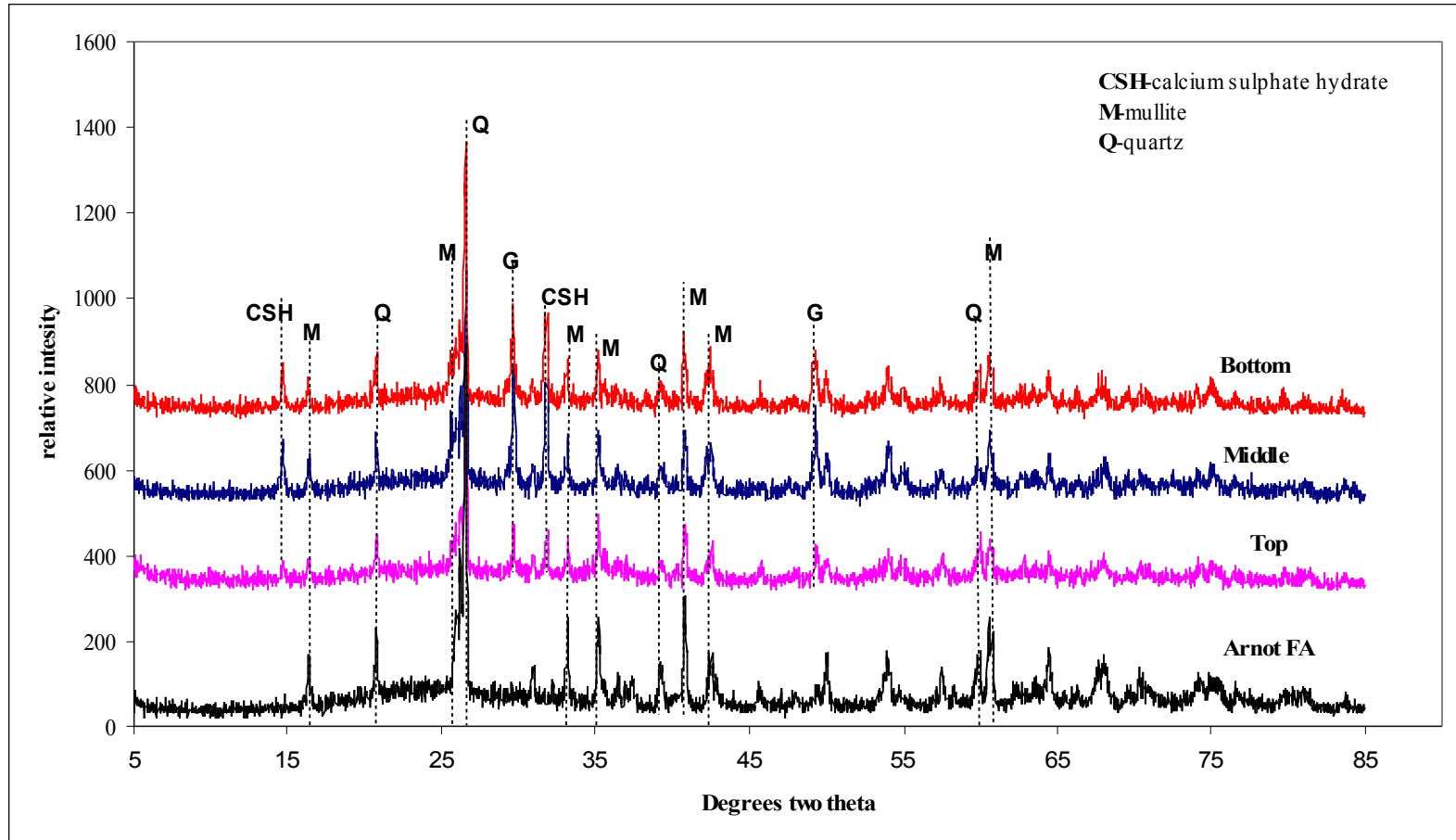


Figure E2: XRD spectra of solid residue core sections (G-gypsum)

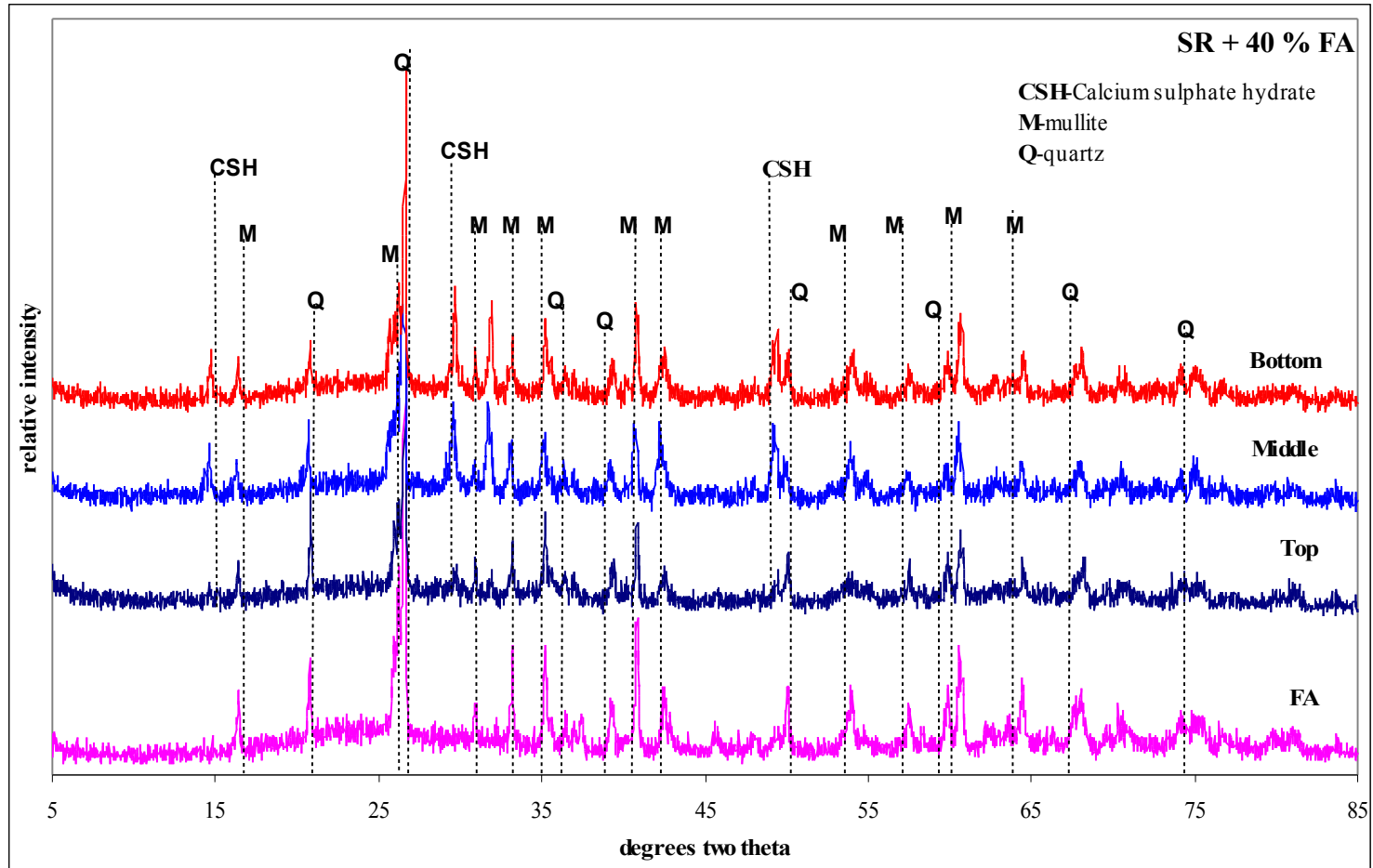


Figure E3: XRD spectra of solid residue (SR) + 40 % FA core sections (G-gypsum)

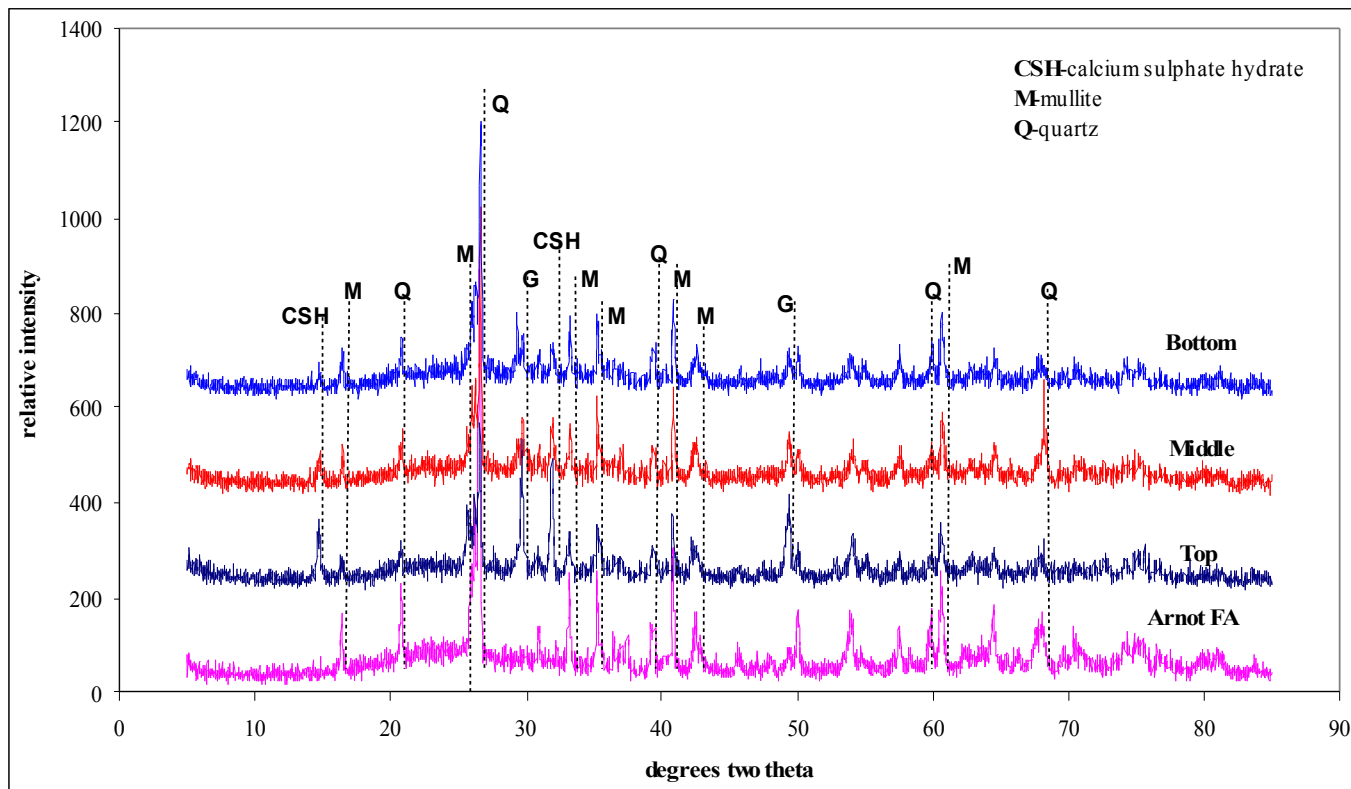


Figure E4: XRD spectra of solid residue (SR) + 6 % OPC core sections (G-gypsum)

Appendix F. Influence of Particle Size Distribution (PSD) of FA on the Neutralization Reaction Kinetics

Introduction

Fly Ash (FA) from South African power stations was successfully used to treat Acid Mine Drainage (AMD) and the insoluble solid residues (SR) that were obtained as a result of the reaction between FA and AMD proved suitable as a backfill material to stabilize mines (Petrik et al., 2005). Particle Size Distribution (PSD) of FA varies from time to time depending on the coal burning conditions in the power station. Such variability in PSD of FA could influence its capability to neutralize AMD. An attempt has been made to study the influence of variability of PSD on the reaction kinetics while neutralizing AMD with FA.

Materials and Methods

The FA from Arnot power station in South Africa was used for this study. PSD analysis showed that the FA particle size distribution was <25 μm (38%), 25-75 μm (42%) and 75-150 μm (14%). The % of fine and coarse particles (in the context of this study) could influence the neutralization capacity of FA. Therefore the original FA was compared to samples that were prepared by fine or coarse particle addition to have double % with respect to either the >25 μm or the 75-150 μm fractions. Thus the AMD from Landau mine was reacted with un-altered (original) FA and two altered FA that were doubled with respect to their fine and coarse fractions. The pH and EC of each reaction was monitored for every half an hour until the reaction reaches an alkaline pH. The original AMD and process waters recovered from different reactions were analyzed for metal and sulphate concentrations using ICP-MS. The original FA, two altered FA and solid residues recovered from the reactions were examined for major oxides using XRF. Table 1 shows % of fine and % coarse particles in different FA.

Table 1: Table showing % of fine and % coarse particles in different FA

FA	% of Fine and % Coarse
Normal	38% and 14%
FA doubled with Fines	76% and 5.4%
FA doubled with coarse	31.8% and 28%

Results and Discussions

pH and EC trends

The Arnot FA and Landau AMD were used for the experiments. They were mixed in 1:3 ratio (FA:AMD) for all the reactions. Figure 1 shows the pH and EC trends for the reaction that used Normal (Unaltered FA) to neutralize Landau AMD. It can be seen from Fig 1 that there was an immediate increase in the pH of the solution as soon as the FA was added to the system. This can be attributed to the dissolution of glassy phases that were present in the FA. This increasing trend continued for one and half hour and afterwards there was a long plateau observed at a pH of 6 for about 5 hours. According to Robbins et al. (1999) and Webster et al. (1998), most of the metals precipitate out of the solution between pH 4 to 6.5. It was observed that during the precipitation of metals the pH of the reaction mixture remains same.

The same principle can be applied to the above mentioned plateau. It can be also observed that there was a rapid decrease in the EC values during the first one and half hours of reaction which very well corresponds with the pH trend. But, unlike the pH, the EC values gradually decreased as the reaction went on. It approximately took 7.5 hrs for the reaction to reach to alkaline pH.

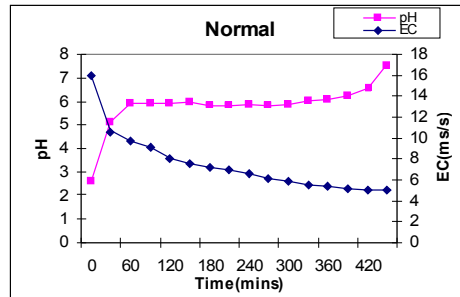


Figure 1: Graph showing pH and EC trends of the neutralization reaction that used normal FA

Figure 2 shows the pH and EC trends of the neutralization reaction in which the FA doubled with percentage of fines was used. The pH and EC trends were similar to the trends that were observed during the reaction that used normal FA. The only distinguishable feature was the time taken for the reaction to reach alkaline pH. The reaction was much quicker when compared to the previous reaction and it approximately took 5.30 hrs to reach a pH of 8.45.

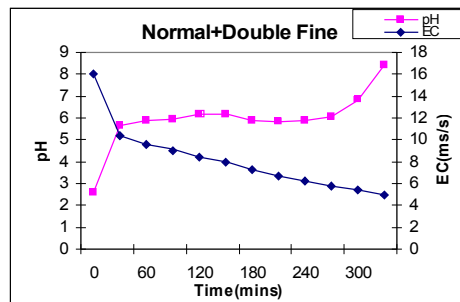


Figure 2: Graph showing pH and EC trends of the neutralization reaction that used FA doubled with % of fine particles

The neutralization reaction using FA that was doubled with % of coarse particles took longer time than other two reactions. Figure 3 shows the pH and EC trends of the reaction and it took nearly 11.5 hrs to reach a neutral pH.

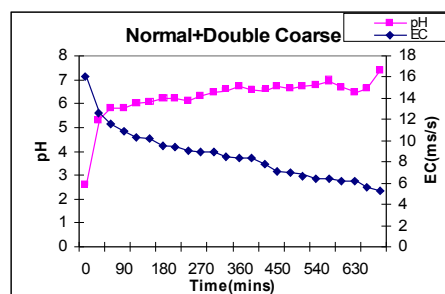


Figure 3: Graph showing pH and EC trends of the neutralization reaction that used FA doubled with % of coarse particles

Figure 4 gives a clear indication of pH and EC trends of different neutralization reactions. Although no significant difference observed in the EC values between the three reactions, it

is quite apparent from Fig 5 that the reaction that used % double fines was the quickest to reach alkaline pH, followed by the reactions that used normal FA and coarse FA.

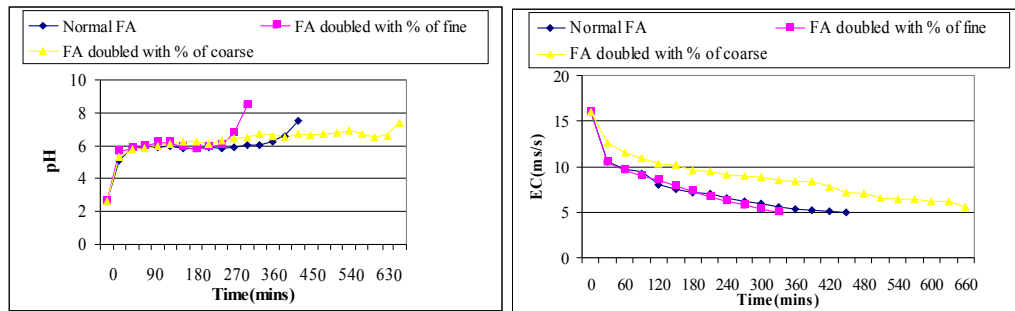


Figure 4: Graphs showing pH and EC trends of different neutralization reactions that used different FA

ICP-MS and XRF results

Table 2 shows the XRF analysis of the unaltered Arnot FA; altered Arnot FA doubled with % of fine and coarse particles and solid residues recovered from the different neutralization reactions that used the above mentioned FA.

Table 2: XRF analysis for different FA and SR recovered from different reactions

Oxide	Arnot FA	SR-Arnot FA	Arnot FA+DF	SR-DF	Arnot FA+DC	SR-DC
SiO ₂	53.69	49.792	53.811	49.123	53.861	51.254
Al ₂ O ₃	25.55	24.298	27.193	25.18	25.093	24.486
CaO	6.641	6.047	6.682	5.969	6.502	6.197
Cr ₂ O ₃	0.053	0.048	0.063	0.061	0.046	0.045
Fe ₂ O ₃	3.837	0.048	3.947	5.153	3.751	5.252
K ₂ O	0.587	0.559	0.615	0.555	0.603	0.565
MgO	2.6	2.201	2.668	2.421	2.565	2.271
MnO	0.055	0.11	0.05	0.129	0.057	0.114
Na ₂ O	0.00	0.00	0.00	0.00	0.00	0.00
NiO	0.01	0.009	0.011	0.012	0.008	0.009
P ₂ O ₅	0.302	0.274	0.36	0.328	0.28	0.281
TiO ₂	1.61	1.468	1.742	1.547	1.577	1.506

- SR-Arnot FA: Solid residues obtained from the reaction between un-altered FA and AMD
- SR-DF: Solid residues obtained from the reaction between FA doubled with fines and AMD
- SR-DC: Solid residues obtained from the reaction between FA doubled with Coarse and AMD

Although the difference is very low, it is evident from the above table that percentage of the most of the major oxides such as Al₂O₃, CaO, Cr₂O₃, Fe₂O₃, K₂O, MgO and TiO₂ is more in the FA that is doubled with % of fine particles when compared to the normal FA and FA doubled with % of coarse particles. The enrichment of Fe in the solid residues doubled with % of fines and coarse particles indicate their efficiency to remove iron from the AMD. It can be also noticed that minor amounts of major oxides such as SiO₂, Al₂O₃ and CaO were also utilized during the neutralization reactions. It also indicates that the main mechanisms that control the neutralization of AMD using FA are ion adsorption and precipitation. Table 3 gives a clear picture of the efficiency of each FA to remove toxic elements from AMD.

Figure 5 is a graphical representation and comparison of the efficiency of different FA to remove toxic elements and sulphate from AMD.

Table 3: ICP analysis of raw AMD and process waters recovered from different reactions

Element	Landau AMD	Process Water-NF	Process Water-DF	Process Water-DC
Zn	2.100	0.008	0.000	0.007
Pb	0.211	<0.010	<0.010	<0.010
Ni	0.373	0.173	0.002	0.060
Mn	238.788	127.850	14.828	98.742
Fe	6540.295	0.594	0.092	0.127
Co	0.637	0.324	0.008	0.106
Cd	0.001	0.001	0.001	0.001
As	<0.006	<0.006	<0.006	<0.006
Al	693.934	0.100	0.693	0.031
Ag	<0.005	<0.005	<0.005	<0.005
SO ₄ ²⁻	16452.000	5158.000	4401.000	5244.000

- Process Water-DF: Water recovered from the neutralization Reaction with FA doubled with fines
- Process Water-DC: Water recovered from the neutralization Reaction with FA doubled with coarse
- Process Water-NF: Water recovered from the neutralization Reaction with unaltered FA

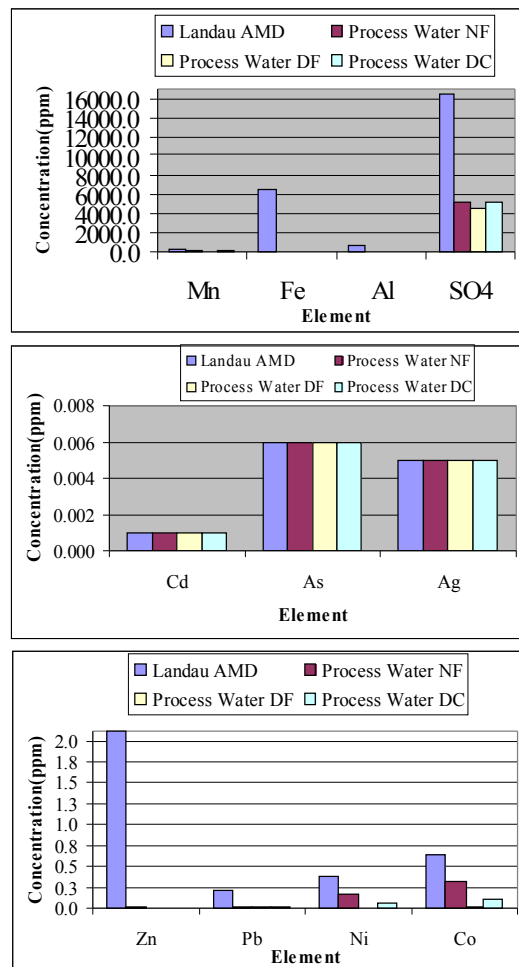


Figure 5: Graphs comparing toxic element removal efficiencies of different FA

It can be clearly noticed that the reaction that used FA doubled with % of fines was more efficient in removing toxic elements and sulphate concentrations from AMD. Especially, elements like Ni, Mn, Fe and Co were greatly removed when compared to the other reactions. This can be attributed to the higher surface area of fine particles which has greater reactive surface. This also indicates that neutralization kinetics is influenced by the particle size.

Conclusions

It can be concluded that the PSD of FA has an influence on the neutralization reaction time and also on the removal efficiency of toxic element and sulphate concentrations. The higher the % of fines in the FA the lower the time taken to neutralize the AMD. It was also noticed that the reaction that used FA with double % of fines was more efficient in removing the toxic metals.

References

1. Petrik L., Burgers C., Gitari W., Surender, D., Reynolds K., Ellendt A., Etchebers O., Vadapalli R., Key D., Iwuoha E. 2005. Stability and neutralization capacity of potential mine backfill material formed by neutralisation of fly ash and acid mine drainage. Water Research Commission, final report K5/1458.
2. Robbins EI, Cravotta CA, Savella CE and Nord Jr. GL (1999) Hydrobiogeochemical Interactions in Anoxic Limestone Drains for Neutralization of Acid Mine Drainage. *Fuel* **78**(2) 259-270.
3. Webster JG, Swedlund PJ and Webster KS (1998) Trace Metal Adsorption onto Acid Mine Drainage Iron (III) Oxy Hydroxy Sulphate. *Environ. Sci. Technol.* **32** (10) 1361-1368.

Appendix G. IR vibration modes of Matla fly ash and various layers of Matla fly ash columns

Matla FA	OH (ν_1, ν_2)			H ₂ O (ν_2)			Al/Si-O-Si (ν_3)			Al-O-Si (ν_1)			Si-O-Si (ν_4)		
	3436, 2342			1622			1096			560			460		
Column layer	bottom	middle	top	bottom	middle	top	bottom	middle	top	bottom	middle	top	bottom	middle	top
1.5 m column	3564 2342	3422 2342	3606 2342	1614	1618	1622	1078	1078	1152	562	562	562 660	460	460	460 600
1 m column	3420 2342	3384 2342	3608 2342	1618	1618	1618	1084	1094	1152	558	558	558 660	458	458	458 602
0.5 m column	3394 2342	3610 2342	3606 2342	-	1618	1620	1078	1152	1152	562	562	562 660	460	460	460 600
0.25 m column	3476 2342	3458 2342	3608 2342	1622	1620	1620	1152	1152	1152	562	560	560 660	450	456	462 600

- ν_1 : symmetric stretching
- ν_2 : symmetric bending
- ν_3 : asymmetric stretching
- ν_4 : asymmetric bending

Appendix H. Capacity Development and Technology Transfer

The project was carried out at the Environmental & Nano Sciences Group, Department of Chemistry, University of the Western Cape.

The submitting organisation, University of the Western Cape (UWC), is a previously disadvantaged institution. The execution of the research project has contributed to a significant improvement in the research capacity of this organisation and, as a result, to higher quality teaching programmes.

PROJECT PARTICIPANTS

Project leaders: L. Petrik (UWC); J. Beukes (Coaltech2020); M. Du Plessis (WRC).

Students

This programme in environmental remediation of acid mine drainage, has allowed 5 students to proceed with higher degrees, supported three postdoctoral students, and provided work study to 2 students and research experience to three MSc graduates.

2004-2007: Drs O. Etchebers (completed in August 2006), VRK. Vadapalli and W.Gitari (Post docs)

Students graduated in 2006 on previous associated project WRC K5/1458: N.Hendricks (MSc) and W. Gitari (PhD)

Graduating in 2006-7: T. Sonqishe (MSc pt), D. Surender (MSc pt); K. Reynolds (PhD pt) (Eskom, UWC)

Workstudy and internships 2005-2007: M.Ndaba (completed in 2006) and M.Antonie (Pentech)

Research assistants: C. Burgers (MSc, completed in 2006), A. Ellendt (MSc, completed in 2006) and S.Akinyemi (MSc)

This list includes: 12 people of which 6 are women and 10 are historically disadvantaged.

Student interaction

Part time students and ESKOM employees K. Reynolds, D. Surender spent time at UWC laboratories in 2005 and 2006 and presented their progress to their supervisors.

Kelley Reynolds and Damini Surender visited the following colleagues at USA institutions during the period 8-27 April 2005: University of Southern Illinois: Carbondale: John Mead, Sanjeev Kumar, Shashi Marikunte, Anna Harrington, Tomasz Wiltowski, Prof Yoginder Chung; University of North Dakota: Debbie Plughhoff-Hassett, Dave Hassett, Bruce Dokter, Loreal Heebrink, Tera Buckley, Eric Zacher, Oscar Manz; Ohio State University: Prof Tarunjit Butalia; Frostburg State University/ Garrett College: Peter Skylstad, Gary Reeves, Jason Litten

Industrial partnership

Eskom site specific study at Middleberg Mine (Optimization of Large Scale plant, Zeolite synthesis, Slurry pumping tests): 2007-2009, Damini Surender

L.Petrik, BHPBilliton. Utilization of Fly Ash to Neutralize and Remediate Acid Mine Drainage at Middleburg mine. 2007-2009.

L.Petrik, Coaltech 2020. Brine Treatment and Disposal. 2006-2008.

L.Petrik, Sasol-Eskom. The Chemistry And Mineralogy Of Sustainable Salt Sinks Relating To The Co-Disposal Of Brines Within Inland Ash Dams.2006-2008

L. Petrik, COALTECH 2020. Stability and neutralisation capacity of potential mine backfill material formed by co-disposal of fly ash and acid mine drainage (WRC662. 2005-2007.

L.Petrik, WRC: Toxic Element Removal From Water With Electrosorption Using Zeolite Adsorbents Made From Co-Disposal Residues. 2005.

Eskom site specific study at Arnot: 2003 2005 Damini Surender

Eskom leaching and ash walling study; 2003 -2005 Kelly Reynolds

Summary of Academic and Industrial Interactions

A summary of academic and industrial interactions is provided in Appendix-B.

Consultancy

2002-2006 L. Petrik continued to act as consultant at Eskom CR&D, and currently serves on the Ash Applications Committee, Resources and Strategy Group, C R&D: Water and Applied Chemistry Dept. Eskom, Cleveland, Johannesburg, RSA

Site visits

09/11/2004: D. Surender (ESKOM) and O. Etchebers (UWC) Visit to Navigation plant

22/04/2005: L. Petrik and R. Vadapalli (UWC) met P. Gunther and F. Nkosi (Anglo) at Landau colliery

19/10/2005: Leslie Petrik of UWC and Damini Surender of Eskom met Peter Günther of Anglo to discuss the alkalinity experiments

01/11/2005: Olivier Etchebers of UWC and Damini Surender of Eskom met with Francis Nkosi of Anglo to fully understand the limestone treatment process

05/06/2006: Ravi Vadapalli of ENS along with Veruscha Fester, Gervais Sery and Rainer of CPUT were at Eskom-Rosherville from 5th June, 2006 to 9th June, 2006 to carry out rheological studies of FA-AMD sludge.

International collaboration

Prof. S.Liao, College of Chemistry, South China University of Technology, Guangzhou 510641, China

SAFeWATER SA French Bilateral programme

L.Petrik (UWC) was an invited participant to First Workshop. South African- French Centre for Water Sciences and technologies (SAFe WATER), 30, 31 May and 1 June 2005 held between WRC and Institut de Recherche pour le developpement (IRD) France. The theme Salinity and Sanitation was addressed and opportunities for future collaboration were discussed. The outcome of this interaction were joint proposals via the NRF/WRC Protea programme for 2006 and via the SAFeWATER SA French Bilateral programme - both proposals were successfully funded in 2006.

Research partners in 2006 on the SAFeWATER programme are:

Chris Buckley and Katherine Foxon. Pollution Research Group, School of Chemical Engineering University of KwaZulu-Natal (UKZN)

Leslie Petrik, Department of Chemistry, University of Western Cape (UWC)

Donald Cowan. Department of Biotechnology, University of Western Cape

Maggy Ndombo Benteke. Department of Water Care. Tshwane University of Technology

Leslie K.C. Strachan, Water Geoscience Unit, Council for Geoscience (CGS)

Marc Heran, Université Montpellier II (UM2/LGPEB)

Ligia BARNA, Laboratoire d'Ingénierie des Procédés de l'Environnement

INSA Toulouse (INSA/LIPE-Toulouse)

Jean-Jacques GODON, Laboratoire de Biotechnologie de l'Environnement, INRA (INRA/LBE-Narbonne)

Odile BRUNEEL, Laboratoire Hydrosociences Montpellier (HSM) CNRS – IRD – Universités Montpellier

Yann Itard, Ressources Minérales (REM) BRGM (BRGM/REM), Orléans

Lachassagne Patrick, Service EAU:BRGM, Montpellier

EXPOSURE TO INDUSTRY

The project has promoted significant interaction between academia and industry. The team led by L. Petrik at UWC is collaborating with:

Eskom

Eskom site specific study at Arnot, R 182 000 in 2005, R100 000 in 2006 D. Surender

Eskom leaching and ash walling study, R 100 000 in 2005, R 100 000 in 2006 K. Reynolds

V.R. Kumar Vadapalli ran experiments at Eskom from 5 to 9 June 2006 with the help of CPUT staff.

DWAF

L. Petrik gave a presentation of the progress made on the overall programme at DWAF on 29 March 2005.

Sasol

Meetings of Eskom-Sasol project team at Johannesburg were attended on 14 June, and 17 Aug 2006.

L.Petrik, V.R.Kumar Vadapalli, W.Gitari, O.Fatoba and M.Antonie of ENS, K.Reynolds from Eskom, K. Surridge from University of Pretoria and C. Pretorius from Sasol met at UWC, Cape Town to discuss about the core drilling at Tutuka and Sasol on the 21st of June, 2006.

L.Petrik of ENS, C.Buckley of KWZN, B.Usher of UFS, K.Reynolds of Eskom and C.Pretorius of Sasol met at Johannesburg on 28 June, 2006 to further discuss the work plan that will be adopted for the Eskom-Sasol Brine project.

On the 26 July 2006, K.Reynolds, L.Petrik and C.Pretorius met for the poster preparation for presentation at ASHES, FROM POWER GENERATION, 13th International Conference, November 6 - 8, 2006, "Sympozjum" Hotel, Cracow, Poland

L. Petrik, O. Etchebers, W. Gitari, and O. Fatoba visited Secunda (Sasol) and Tutuka (Eskom) industrial sites on 24/04/2006.

L. Petrik, O. Etchebers, W. Gitari, and O. Fatoba attended the knowledge sharing workshop organised for the Eskom-Sasol research co-operation on co-disposal of brines and ash project on 25-26/04/2006 in Johannesburg.

L. Petrik, O. Etchebers, W. Gitari, and O. Fatoba visited Secunda (Sasol) industrial site on 24/04/2006.

O. Etchebers visited Tutuka (Eskom) industrial site on 06/06/2006 and Secunda (Sasol) industrial site on 06-07/06/2006.

O. Etchebers, W. Gitari, O. Fatoba and A. Nyamhingura visited Tutuka (Eskom) industrial site on 10-11/07/2006.

O. Etchebers, W. Gitari, O. Fatoba and A. Nyamhingura visited Secunda (Sasol) industrial site on 12-13-14/07/2006

W.Gitari, S.Akinyemi, J.Nel, K.Reynolds and H.Soloman were on a field trip to Tutuka for sampling of ash dams and toe drains from 16th of October to 18th of October.

J.Nel, H.Soloman and K.Reynolds were involved in Geophysics resistivity mapping at Tutuka power station from 23rd of October to 25th of October.

J.Nel, R.Vadapalli, Ojo Fatoba and W.Gitari were involved in core drilling at Tutuka from 30 October to 3 November 2006

Workshops attended in 2006

"Fundamentals of groundwater chemistry" Workshop on the 3rd and 4th of July, 2006, Department of Earth Sciences, UWC organized a 2 day workshop on the 3rd and 4th of July'06 presented by W Kelley of USA. L.Petrik, VRK.Vadapalli, W.Gitari and O.Fatoba from ENS attended the course.

"Estimation of Evaporation" Workshop held at the University of KWZN, Pietermaritzburg from 17 -21 July 2006. This workshop focused on teaching various techniques that are used to measure evaporation in the environment. C.Pretorius (Sasol), and VRK Vadapalli, W.Gitari and O.Fatoba of ENS (UWC) attended

"Geochemical and Reactive Transport Modelling" Workshop held at on the 27th of November 2006 to 1st of December 2006, Department of Earth Sciences. This workshop

focussed on understanding the basics of geochemical as well as solute and reactive transport modelling, and application of state-of-the-art models to real world water quality problems using tools such as MODFLOW, MT3DMS, PHREEQC-2 etc. PHREEQC, MT3DMS and PHT3D” VRK Vadapalli, W.Gitari, O.Fatoba, A.Nyamingura of ENS (UWC) attended.

“X-Ray Diffraction techniques”. Work shop at iThemba labs, Faure, Somerset West
O. Etchebers, VRK. Vadapalli, W.Gitari, A.Ellendt, O.Fatoba, M.Antonie and M.Ndaba of ENS attended a on the 17th of March, 2006 at ithemba labs at Cape Town. This workshop focused on latest developments in X-ray diffraction techniques and current XRD facilities and future plans of iThemba labs.

W.Gitari and B.Hendry attended WISA conference in Randfontein, Johannesburg from 19th of October to 20th of October.

PUBLICATIONS

Industrial reports

L.Petrik, O.Etchebers and V.R.Kumar Vadapalli, 2007. Towards the development of Sustainable Salt Sinks: Fundamental Studies on the Co-Disposal of brines within Inland ash dams. 3rd Interim report to Eskom and Sasol

L.Petrik, O.Etchebers and V.R.Kumar Vadapalli, 2006. Towards the development of Sustainable Salt Sinks: Fundamental Studies on the Co-Disposal of brines within Inland ash dams. 2nd Interim report to Eskom and Sasol

L.Petrik, O.Etchebers and V.R.Kumar Vadapalli, 2006. Towards the development of Sustainable Salt Sinks: Fundamental Studies on the Co-Disposal of brines within Inland ash dams. 1st Interim report to Eskom and Sasol.

L. Petrik, V.R. Kumar Vadapalli and O. Etchebers. 2006: Large Scale Stability and Neutralization Capacity of Potential Mine Backfill Material Formed by Neutralization of Fly Ash and Acid Mine Drainage. WRC Research Project Proposal number 8757275, Reference K8/662, 4th interim report

L. Petrik, V.R. Kumar Vadapalli and O. Etchebers. 2006: Large Scale Stability and Neutralization Capacity of Potential Mine Backfill Material Formed by Neutralization of Fly Ash and Acid Mine Drainage. WRC Research Project Proposal number 8757275, Reference K8/662, 3rd interim report

L. Petrik, N. Hendricks, A. Ellendt, C. Burgers, O. Etchebers, D. Key and E. Iwuoha. 2006. Toxic element removal from water using zeolite adsorbents made from solid residues from the reaction between FA and AMD. WRC Research Project No K1546, final report.

L. Petrik, V.R. Kumar Vadapalli and O. Etchebers. 2005: Large Scale Stability and Neutralization Capacity of Potential Mine Backfill Material Formed by Neutralization of Fly Ash and Acid Mine Drainage. WRC research project proposal number 8757275, reference K8/662, 2nd interim report

L. Petrik, C. Burgers, O. Etchebers and R. Vadapalli. 2005: Large Scale Stability and Neutralization Capacity of Potential Mine Backfill Material Formed by Neutralization of Fly Ash and Acid Mine Drainage. WRC research project proposal number 8757275, reference K8/662, 1st interim report.

L. Petrik, N. Hendricks, A. Ellendt, C. Burgers, O. Etchebers, D. Key and E. Iwuoha. 2006: Toxic element removal from water using zeolite adsorbents made from solid residues from the reaction between FA and AMD. WRC Research Project No K1546, final report.

L. Petrik, C. Burgers, W. Gitari, D. Surender, K. Reynolds, A. Ellendt, O. Etchebers, R. Vadapalli, D. Key and E.I. Iwuoha. 2005: Stability and neutralisation capacity of potential mine backfill material formed by neutralisation of fly ash and acid mine drainage. WRC research project No K5/1458, in collaboration with Coaltech 2020 (Task 6.1.6), final report.

K. Reynolds. 2004: The Use of Fly Ash For Ash Walling of Acid Mine Drainage. Eskom Technology Services International. Project No: 7760T105R. Report No: RES/RR/02/19247.

L. Petrik and S. Mavundla. 2004: Characteristics of Classified and Unclassified Ash. Ash Resources (Pty) Ltd, Randburg, Gauteng. Report 1.

L. Petrik and D. Surender. 2004: Development of a site specific co-disposal protocol for the neutralisation and amelioration of Arnot AMD and fly ash. The co-disposal and neutralisation of AMD with Fly Ash. Eskom Resources & Strategy-Research Development and Demonstration. Project No: R1263. Progress Reports 1-2: RES/RR/03/21911.

K. Reynolds and L. Petrik. 2004: Acid Precipitation Tests Conducted on Kendal Ash. Eskom Technology Services International. Task No: 9RE-000049; Project No.: R0089; Generic Contract No.: UWESC001. Report 2.

L.F. Petrik, R. White, M. Klink, V. Somerset, D. Key, E. Iwuoha, C. Burgers and M.V. Fey. 2004: Utilization of fly ash for acid mine drainage remediation. Water Research Commission (WRC) research project No K5/1242, in collaboration with Coaltech 2020 (Task 6.1.4). Final Report.

L. Petrik. 2004: Simultaneous water recovery and utilization of two harmful effluents, fly ash and acid mine drainage, for production of high capacity inorganic ion exchange material useful for water beneficiation. Coaltech2020 Task 6.1.4(b), in collaboration with WRC (project No K5/1242). Final Report.

Thesis

Gitari, W. 2006: Leachate chemistry and contaminants attenuation in Acid Mine Drainage by Fly Ash and its derivatives. PhD Thesis, University of the Western Cape, South Africa.

Hendricks, N.R. 2006: The Application Of High Capacity Ion Exchange Adsorbent Material, Synthesised From Fly Ash And Acid Mine Drainage, For The Removal Of Heavy And Trace Metals From Secondary Co-Disposed Process Waters. MSc Thesis, University of the Western Cape, South Africa.

Klink, M.J., 2004: The potential use of South African coal fly ash as a neutralisation treatment option for acid mine drainage. MSc Thesis, University of the Western Cape, South Africa.

Somerset V. Sept. 2003. The preparation and characterization of high capacity ion exchange adsorbents made by co-disposal of fly ash and acid mine drainage, and their use in electrochemical systems for water purification. M.Sc. Thesis, University of the Western Cape, South Africa.

Burgers C. 2002. Synthesis and characterisation of sesquioxidic precipitates formed by the reaction of acid mine drainage with fly ash leachate. M.Sc. Thesis, University of Stellenbosch, South Africa.

Refereed Journals

In Press:

1. Rong-fang Wang, Jun-min Liu, Shi-jun Liao, L.F. Petrik. 2006 High Methanol Tolerance Of Pd-Cu/C Electrocatalysts For Oxygen Reduction Reaction. *Catalysis Letters* (Submitted)
2. Shijun Liao, Junmin Liu, Shan Ji, Xuelian Zhang, LF Petrik. 2006.High Surface Area Acid Catalysts SO₄²⁻/Zr-HMS Prepared by Sulfating Mesoporous Zr-HMS (Submitted)
3. M.J. Klink, L.F. Petrik, V.R. Kumar Vadapalli, O. Etchebers, R.A.White, D. Key and E. Iwuoha. 2006. A Case Study on Utilization of South African Fly Ashes to Neutralize Acid Mine Drainage. (Submitted).
4. O. Etchebers, M.A.M. Kedziorek and A.C.M. Bourg. 2006. Soil water chemistry as an indicator of the reproducibility of artificially contaminated soil mesocosms. *Water, Air, & Soil Pollution* (In press).
5. M.W. Gitari, L.F. Petrik, O. Etchebers, D.L Key, E. Iwuoha and C. Okujeni. 2006. Utilization of fly ash for remediation of coal mines waste water: solubility controls on major inorganic contaminants (Under review); *Journal of Environmental quality*. Manuscript Ref No: Q06-0172.
6. S.E. Mavundla, V.S. Somerset, L.F. Petrik, M.J. Klink, P. Baker and E. Iwuoha. 2006. Electrochemical and Spectroscopic Properties of Fly Ash-Polyaniline Matrix Nanorod Composites. *Microchimica Acta* (In press).

Published:

1. Emmanuel I. Iwuoha;, Siphon E. Mavundla, Vernon S. Somerset, Leslie F. Petrik, Michael J. Klink, Mantoa Sekota, and Priscilla Bakers. Electrochemical and Spectroscopic Properties of Fly Ash–Polyaniline Matrix Nanorod Composites *Microchim Acta* 155, 453–458 (2006)

2. Gitari M.W., Petrik L.F., Etchebers O, Key D.L, Iwuoha E, Okujeni C. Treatment of acid mine drainage with fly ash: removal of major contaminants and trace elements. *J Environ Sci Health A Tox Hazard Subst Environ Eng.* 2006;41(8):1729-47
3. Dong-Gen Huang; Shi-Jun Liao; Jun-Min Liu; Zhi Dang; Leslie Petrik. Preparation of visible-light responsive N–F-codoped TiO₂ photocatalyst by a sol–gel-solvothermal method. *Journal of Photochemistry and Photobiology A: Chemistry* Volume 184, Issue 3 , 15 December 2006, Pages 282-288
4. Jun-min Liu; Shi-jun Liao; Guo-dong Jiang; Xue-lian Zhang; Leslie Petrik. Preparation, characterization and catalytic activity of Zr embedded MSU-V with high thermal and hydrothermal stability. *Microporous and Mesoporous Materials* Volume 95, Issues 1-3 , 18 October 2006, Pages 306-311
5. V.S. Somerset, L.F. Petrik, R.A. White, M.J. Klink, D. Key and E.I. Iwuoha. 2005: Alkaline hydrothermal zeolites synthesized from high SiO₂ and Al₂O₃ co-disposal fly ash filtrates. *Fuel*, 84, 2324–2329.
6. Somerset, L. Petrik, M. Klink, O. Etchebers, R. White, D. Key and E. Iwuoha. 2005: Acid mine drainage transformation of fly ash into zeolitic crystalline phases. *Fresenius Environmental Bulletin*, 14 (11), 1074-1076.
7. Somerset, L. Petrik and E. Iwuoha. 2005: Alkaline Hydrothermal Conversion of Fly Ash Filtrates Into Zeolites 2: Utilization in Wastewater Treatment. *Journal of Environmental Science and Health*, 40 (8), 1627-1636.
8. V.S. Somerset, L. Petrik, R.A. White, M.J. Klink, D. Key and E. Iwuoha. 2004: The use of X-ray fluorescence (XRF) analysis in predicting the alkaline hydrothermal conversion of fly ash precipitates into zeolites. *Talanta - special issue: Southern and Eastern Africa Network for Analytical Chemists*, 64 (1), 109-114.

Articles in Magazines

1. L. Petrik. 2005: Eskom as capacity builder fuel cells, fuels and chemicals. *Reach. Eskom*, November 2005, 5-7.
2. L. Petrik. 2004: Utilisation of fly ash for the neutralisation of acid mine drainage. *ESI Africa*, Issue 2.

Conference Proceedings

1. L.F.Petrik, D.Surender, A.A.Ellendt, N.R.Hendricks. The application of zeolites prepared using solid waste residues recovered from the neutralization of acid mine drainage with fly ash for toxic element removal. *World of Coal Ash (WOCA Northern Kentucky Convention Center, Kentucky, USA May 7-10, 2007. (Accepted)*
2. D Surender, L.F Petrik, A.A Ellendt, N.R Hendricks The application of zeolites synthesized from solid waste residues recovered from the neutralization of acid mine drainage with fly ash for toxic element removal. *IWA Specialist Conference *Facing Sludge Diversities: Challenges, Risks and Opportunities* Antalya, Turkey, 28-30 March, 2007(Accepted).*

3. W. M. Gitari, L. F Petrik, O. Etchebers, D. L Key, E.Iwuoha and C. Okujeni (2007). Acidity attenuation in acid mine drainage by fly ash and its derivatives: A column leaching study International Water Association (IWA) Specialist conference "Facing sludge diversities challenges, risks, and opportunities. 28-30 march 2007 Belek -Antalya, Turkey
4. KA Reynolds, L Petrik and VR Kumar Vadapalli. Mineralogy of ash columns after exposure to AMD. World of Coal Ash (WOCA Northern Kentucky Convention Cent, Kentucky, USA May 7-10, 2007. (Accepted)
5. K Reynolds, C Pretorius, L Petrik, C Buckley, B Usher, G Gericke, D Roux. Sustainability of inland ash disposal facilities as salt sinks. World of Coal Ash (WOCA) Northern Kentucky Convention Centre, Kentucky, USA, May 7-10, 2007 (Accepted)
6. VR Kumar Vadapalli, L.F. Petrik, Veruscha Fester, Paul Slatter and Gervais Sery. Effect of Fly Ash particle size on its capacity to neutralize Acid Mine Drainage and influence on the rheological behaviour of residual solids. World of Coal Ash (WOCA Northern Kentucky Convention Center, Kentucky, USA May 7-10, 2007. (Accepted)
7. M. Nel, M de Klerk, K Reynolds, L.F. Petrik, Y Xu, O Batelaan. The use of electrical resistivity to map water flow paths through ash dumps and the underlying fractured aquifers, Mpumalanga, South Africa. World of Coal Ash (WOCA) 2007. (Accepted)
8. L.F. Petrik, D.Surender, VR Kumar Vadapalli, O.Etchebers. Fly Ash as an alternative to limestone in active acid mine drainage treatment systems. World of Coal Ash (WOCA) Northern Kentucky Convention Center, Kentucky, USA, May 7-10, 2007 (Accepted)
9. L.F.Petrik, C.A. Pineda-Vargas, E.Iwuoha. Novel Platinum And Iridium Nanophase Composite Gas Diffusion Electrodes. The 38th National Convention of the South African Chemical Institute (SACI), Durban, South Africa 3 - 8 December 2006
10. O.Fatoba, W., L.F. Petrik, W. M. Gitari and O. Etchebers. Chemical compositions and leaching behaviour of fly ash. The 38th National Convention of the South African Chemical Institute (SACI), Durban, South Africa 3 - 8 December 2006
11. L.Petrik, M.W.Gitari, V.R.Kumar Vadapalli, O.Etchebers, A.Ellendt, K.Reynolds, D.Surender, N.Hendricks, M.J.Klink, V.S.Somerset, R.A.White, C.Burgers, D.L.Key and E.I.Iwuoha. 2006: Applications of ash and its derivatives: water treatment, mine backfilling, lining and walling. 13th International Conference Ashes from Power Generation, 6-8 November, Krakow, Poland.
12. K. Reynolds, C. Pretorius, L. Petrik, C. Buckley, B. Usher, G. Gericke and D. Roux. Sustainability of inland ash disposal facilities as salt sinks. 13th International Conference on Ashes from Power Generation, Krakow, Poland, 6-8 November 2006.

13. K.Reynolds and L.F. Petrik. The Utilization of an Ash Wall for the Treatment and Control of Acid Mine Drainage. International Conference on Coal Ash. CSIR International Convention Centre, Pretoria, South Africa 2-4 Oct 2006
14. W. M. Gitari, L.F. Petrik, O. Etchebers, D.L Key, E. Iwuoha and C. Okujeni Passive Treatment of Acid Mine Drainage with Fly Ash Blended Solid Residues: An Insight into the Contaminants-attenuating Mechanisms and Strength Development. International Conference on Coal Ash. CSIR International Convention Centre, Pretoria, South Africa 2-4 Oct 2006
15. L.F. Petrik, D.Surender, V.R. Kumar Vadapalli, O.Etchebers. A Cost Comparison of Fly Ash and Limestone for the Amendment of Acid Mine Drainage. International Conference on Coal Ash. CSIR International Convention Centre, Pretoria, South Africa 2-4 Oct 2006
16. Ellendt and L. Petrik. 2006. Monitoring of evolution of species during the synthesis of zeolite using Fourier transformed infrared spectroscopy. 1st Southern African Conference on Rheology (SACOR), Cape Town, 24-27 September 2006.
17. L. Petrik, A. Ellendt and O. Etchebers. 2006: Treatment of mine effluent with zeolite synthesised from solid residues resulting from the neutralization of acid mine drainage with fly ash. Submitted to the International Symposium on Zeolites and Microporous Crystals (ZMPC2006), [Yonago](#), [Tottori Prefecture](#), Japan, 30 July – 2 August 2006.
18. L. Petrik, A. Ellendt, N. Hendricks and O. Etchebers. 2006: Synthesis of zeolite at low and high temperature using solid residues resulting from the neutralization of acid mine drainage with fly ash. Submitted to the International Symposium on Zeolites and Microporous Crystals (ZMPC2006), [Yonago](#), [Tottori Prefecture](#), Japan, 30 July – 2 August 2006.
19. D. Surender, O. Etchebers, V.R. Kumar Vadapalli and L. Petrik. 2006: Remediation of acidic mine drainage with fly ash. Submitted to EnviroWater, International Conference and Exhibition on Water in the Environment, Stellenbosch, South Africa, 20–22 February 2006.
20. W. Gitari and L. Petrik. 2005: Contaminant mobility in fly ash amended acid mine drainage/fly ash solid residues: a column leaching study. Oral presentation. East and Southern Africa Environmental Chemistry Workshop (ESAECW) and the 6th Theoretical Chemistry Workshop in Africa (TCWA), Windhoek, Namibia, 5-9 December 2005.
21. L.F. Petrik, N. Hendricks, V.R. Kumar Vadapalli, O. Etchebers, V.S. Somerset, A. Ellendt, D. Key and E.I. Iwuoha. 2005: Zeolite synthesis from solid waste residues: a case study from the treatment of acid mine drainage with fly ash. Oral Presentation WISA Conference on The Management of Residues Emanating From Water And Wastewater Treatment, Sandton Convention Centre, Johannesburg, South Africa, 9-12 August 2005.

22. L.F. Petrik, M.W. Gitari, .O. Etchebers, V.R. Kumar Vadapalli, D. Key and E.I. Iwuoha. 2005: Utilisation of fly ash for remediation of coal mines wastewater: reaction on AMD and possible backfilling with residual solids. Oral Presentation. The South African Institute of Mining and Metallurgy (SAIMM) Colloquium: Sustainable development in the life of coal mining in South Africa, Carnival City, Boksburg, South Africa, 13 July 2005.
23. M.W. Gitari, V.S. Somerset, L.F. Petrik, D. Key, E.I. Iwuoha and C. Okujeni. 2005: Mineralogy and trace element partitioning in coal fly ash/acid mine drainage co-disposed solid residues. Full paper. The World of Coal Ash 2005, incorporating International Ash Utilization Symposium of the UK CAER, the ACAA's 16th International Symposium and meeting of the U.S. Office of Surface Mining, Lexington, Kentucky, USA, 11-15 April 2005.
24. M.W. Gitari, V.S. Somerset, L.F. Petrik, D. Key, E.I. Iwuoha and C. Okujeni. 2005: Treatment of acid mine drainage with fly ash: Removal of major, minor elements, SO₄ and utilization of the solid residues for wastewater treatment. Full paper. The World of Coal Ash 2005, incorporating International Ash Utilization Symposium of the UK CAER, the ACAA's 16th International Symposium and meeting of the U.S. Office of Surface Mining, Lexington, Kentucky, USA, 11-15 April 2005.
25. K. Reynolds. 2005: The utilisation of an ash wall for the treatment and control of acid mine drainage. Full paper. The World of Coal Ash 2005, incorporating International Ash Utilization Symposium of the UK CAER, the ACAA's 16th International Symposium and meeting of the U.S. Office of Surface Mining, Lexington, Kentucky, USA, 11-15 April 2005.
26. D. Surender and L. Petrik. 2005: Development of a co-disposal protocol for the neutralization and amelioration of acid mine drainage with fly ash. Full paper. The World of Coal Ash 2005, incorporating International Ash Utilization Symposium of the UK CAER, the ACAA's 16th International Symposium and meeting of the U.S. Office of Surface Mining, Lexington, Kentucky, USA, 11-15 April 2005.
27. M.W. Gitari, L.F. Petrik., D. Key. and C. Okujeni. 2004: Neutralization of acid mine drainage with fly ash: A laboratory investigation of metal and SO₄²⁻ removal in the process waters. Poster presentation. 37th National Convention of the South African Chemical Institute (SACI), Pretoria, South Africa, 4-9 July 2004.
28. S.E. Mavundla, V. Somerset, L. Petrik, P. Baker and E.I. Iwuoha. 2004: Fly ash-conducting polymer matrix composites: structural and electrochemical impedance characterisation. ENVIROMIN2004, Environmental and Health Aspects of Mining, Refining and Related Industries, Mowana Safari Lodge, Kasane, Botswana, 28 June - 2 July 2004.
29. K. Reynolds. 2004: The utilisation of a fly ash wall of the treatment and control of acid mine drainage. Oral presentation. Sustainability of Coal Colloquium, Secunda, South Africa, 18 June 2004.

30. V.S. Somerset, L.F. Petrik, R.A. White, M.J. Klink, D. Key and E. Iwuoha. 2004: Alkaline hydrothermal zeolites synthesized from fly ash SiO_2 and Al_2O_3 . Poster presentation. WISA Biennial Conference, Cape Town, South Africa, 2-5 May 2004.
31. K. Reynolds. 2004: The utilisation of an ash wall for the treatment and control of Acid Mine Drainage. WISA Biennial Conference, Cape Town, South Africa, 2-5 May 2004.

PATENTS

1. Leslie Felicia PETRIK, Wilson Mugeru GITARI, Viswanath Ravi Kumar VADAPALLI, Olivier Christian Albert ETCHEBERS, Annabelle Anne Marie ELLENDT, Kelley Anne REYNOLDS, Damini SURENDER, Nicolette Rebecca HENDRICKS, Michael John KLINK, Vernon Sydwill SOMERSET, Colleen Lucie BURGERS. 2006. Fly Ash and Its Derivatives. South African Patent filed on 2nd November, 2006. DRG Ref No: 655414.
2. Leslie Felicia PETRIK, Annabelle Anne Marie ELLENDT, Nicolette Rebecca HENDRICKS, Vernon Sydwill SOMERSET, Damini SURENDER, Emmanuel Iheanyichukwu IWUOHA, 2006. Synthesis of zeolites. South African Patent filed on 13th September 2006. Ref No: 2006/07650